Loughborough University

This item was submitted to Loughborough University as a PhD thesis by the author and is made available in the Institutional Repository (https://dspace.lboro.ac.uk/) under the following Creative Commons Licence conditions.

creative commons
COMMONS DEED

Attribution-NonCommercial-NoDerivs 2.5

You are free:

- to copy, distribute, display, and perform the work

Under the following conditions:

Attribution. You must attribute the work in the manner specified by the author or licensor.

Noncommercial. You may not use this work for commercial purposes.

No Derivative Works. You may not alter, transform, or build upon this work.

- For any reuse or distribution, you must make clear to others the license terms of this work.
- Any of these conditions can be waived if you get permission from the copyright holder.

Your fair use and other rights are in no way affected by the above.

This is a human-readable summary of the Legal Code (the full license).

Disclaimer

For the full text of this licence, please go to:
http://creativecommons.org/licenses/by-nc-nd/2.5/

LOUGHBOROUGH
UNIVERSITY OF TECHNOLOGY
LIBRARY

AUTHOR/FILING TITLE
WALSH, FC

ACCESSION/COPY NO.
043839/02

VOL. NO.
CLASS MARK

date due:-
~~3 JUL 1983~~
~~LOAN 1 MTH + 2~~
~~UNLESS RECALLED~~
date due
for return:-
18 JULY 1983
No Renewal
BASEL

- 6 OCT 2000

LOAN COPY

0043839 02

Vol I

ELECTRODEPOSITION OF METALS IN A ROTATING CYLINDER ELECTRODE REACTOR

by

Francis Charles Walsh
B.Sc.(CNAA), M.Sc.(Loughborough),
M.I.Corr.T., M.I.M.F., C.Chem.,
M.R.S.C..

A Doctoral thesis submitted in fulfilment
of the requirements for the award of
Doctor of Philosophy of the Loughborough
University of Technology, 1981.

Supervisor: Dr. D. R. Gabe
Department of Materials
Engineering and Design

ⓒ by F. C. Walsh, 1981

VOLUME ONE

THEORETICAL PRINCIPLES AND LITERATURE REVIEW

(Chapters I-7)

Loughborough University
of Technology Library
Date Dec 81
Class
Acc. No. 043839/02

To Pamela and my parents.

" If only there was as much science in politics as there is

politics in science "

SYNOPSIS

Following a brief introduction to outline the relevance and scope of the thesis (Chapter 1), the initial half of this work (Chapters 2-7) concerns original and compiled information regarding theoretical aspects and literature review. The second half of the thesis (Chapters 8-12) involves novel studies at both laboratory (Chapters 8 and 10) and pilot plant (Chapters 9 and 11) scale.

The academic and technical literature is critically reviewed with regard to the rotating cylinder as a reactor geometry. Particular attention is paid to the electrodeposition of metals, in powder form, in a rotating cylinder electrode reactor (R.C.E.R).

In an overall attempt to present and characterise the R.C.E.R, hydrodynamics (Chapter 2) and mass transport (Chapter 3) are extensively reviewed and discussed. In order to place the R.C.E.R. in relation to other reactor geometries, mass transport to various electrode types (Chapter 4) is reviewed, and novel/important electrochemical reactors are featured (Chapter 5).

One of the major parts of the thesis (Chapter 6) presents fundamental design equations and an extensive review of laboratory and commercial cell/reactor design. Applications of the R.C.E.R. are also discussed in Chapter 6, with particular regard to electrodeposition.

The concluding section on literature and theoretical aspects (Chapter 7) briefly covers the production, use and properties of metal powders, especially those produced by electrodeposition.

The experimental work at laboratory scale is aimed at the study of mass transport to smooth, developing and developed roughness at a rotating cylinder electrode. Copper deposition is used not only as the mass transport indicator reaction, but also as the means of roughness development. Comparison is made with roughness produced by knurling. The development of roughness is studied by a variety of techniques including electrochemical measurements (polarisation and mass transport), surface profilometry and scanning electron microscopy.

The effect of roughness development on reactor performance is especially studied with respect to scale-up and sizing.

The R.C.E.R. is investigated as a means of separating a noble metal from multi-metal solutions, under potentiostatic control. Here again, roughness development may enhance reactor performance. Both simple, synthetic bimetallic/acid solutions and complex multimetal cyanidic industrial liquors are examined, as are reactor operating conditions.

Pilot Plant studies involve the performance of novel R.C.E.R's for mass transport controlled deposition of copper powder, the controlled potential separation of cadmium from a zinc hydrometallurgical liquor , and multiple cathode compartment, cascade reactors. The data from previous reactors, both the single cathode and cascade type, is analysed and reviewed.

It is shown that the R.C.E.R. is an efficient and high performance device, which may be utilised for high rate production of a single metal in powder form, or for selective deposition of a noble metal. Potentiostatic control of the electrode near limiting current conditions assures mass transport controlled deposition with high current efficiency.

The development of powdery, rough metal deposits under such conditions is seen to markedly enhance mass transport, due to an improvement in real surface area and in hydrodynamic shear. The resultant reactor performance in simple batch, batch recirculation and single pass modes of operation is greatly increased.

The overall conversion in a single R.C.E.R. may be increased by the use of multiple catholyte compartments in a hydraulic series. Such 'cascade' reactors are capable of treating relatively high volumetric throughputs, while discharging low concentrations of metal (p.p.m.). Metal may be periodically removed as substantially pure powder.

Selective deposition of a nobler metal from a multimetal solution is facilitated by uncomplexed acid electrolytes and a wide separation in reduction potentials. Cu may be successfully removed from Cu/Zn or Cu/Ni in sulphuric acid, and Ag from Ag/Cu in nitric acid. Heavily complexed solutions raise problems including the deposition of smooth metal and reduced selectivity.

Acknowledgements

I would like to thank all the people, both colleagues and friends, who have helped in any way during the research for this thesis.

In particular, I am indebted to my research supervisor Dr. D.R. Gabe for his patience, help and guidance. Thanks are also due to my fellow research students, both in the Department of Materials Engineering and Design and in Dr. N.A. Hampson's electrochemistry research group in the Department of Chemistry, for informal and informative discussion.

I would also like to thank the staff of Ecological Engineering Limited, Macclesfield, Cheshire, especially Mr. N.A. Gardner and Dr. F.S. Holland for their cooperation during my periods of industrial research.

I would like to acknowledge provision of a two-year 'CASE' award grant by the Science Research Council, and provision of laboratory facilities by Prof. I.A. Menzies.

Finally, I would like to thank Mrs. S. Hart for typing this thesis.

A NOTE ON PRESENTATION OF FIGURES

Certain of the figures relating to chapter 6 have been necessarily reproduced from poor-quality copies from the patent literature. The author apologises for the lack of definition in these cases.

PAGE NO.

1. INTRODUCTION 1

2. FLUID FLOW 6

2.1 General Considerations 6

2.2 Flow Regime and Stability 6

2.3 Velocity Distribution 9

2.4 The Rotating Cylinder Geometry 13

2.4.1 General 13

2.4.2 The Laminar to Turbulent Transition 15

2.4.3 Velocity Profiles 18

2.4.4 Drag and Friction Factors 19

2.4.5 Effect of Axial Flow 21

2.4.6 Power Requirements 27

3. ELECTROCHEMICAL MASS TRANSFER 32

3.1 General Considerations 33

3.1.1 Electrode Processes 33

3.1.2 Types of Polarisation 34

3.1.3 Polarisation Curves 35

3.2 Transport Porcesses 36

3.2.1 Introduction 36

3.2.2 The Diffusion Layer 39

3.2.3 Convective Diffusion 41

3.3 Boundary Layer Theory 43

3.4 Dimensionless Group Analysis 44

3.5 Mass, Heat and Momentum Transfer Analogy. 47

3.6 Electrochemical Mass Transfer Reactions 49

3.7 Mass Transfer Correlations and Data Treatment 57

3.8 Measurement of Mass Transfer 61

3.8.1 Direct Methods 61

3.8.2 Indirect Methods 63

PAGE NO.

4. MASS TRANSFER AND ELECTRODE GEOMETRY 66

4.1 General 67

4.2 Static, Bulk Electrodes 68

4.2.1 Parallel Plates 68

4.2.2 Annulus 72

4.3 Porous Electrodes 73

4.4 Fluidised Bed Electrodes 78

4.5 Dynamic, Bulk Electrodes 80

4.6 The Rotating Cylinder Electrode 84

4.6.1 Introduction 84

4.6.2 Theoretical Aspects 85

4.6.3 Experimental Work 87

4.7 Surface Roughness 99

4.8 Gas Evolution 102

4.8.1 Introduction 102

4.8.2 Academic Studies 105

4.8.3 Practical Studies 107

4.9 Miscellaneous Methods of Mass Transfer Enhancement 109

4.9.1 Ultrasonics and Vibration 109

4.9.2 Abrasion and Wiping/Scraping 111

5. ELECTROCHEMICAL REACTORS 112

5.1 Introduction 113

5.2 Design Equations 122

5.2.1 Plug Flow Reactors 123

5.2.2 Continuously Stirred Tank Reactors 126

5.2.3 Batch Recycle Mode 132

5.3 Control and Characteristics of Electrochemical Reactors 136

5.3.1 Electrical Control 136

5.3.2 Potential and Current Density 139

5.3.3 Duty and Performance 144

5.4 Comparison of Reactor Configurations 148

PAGE NO.

7.3 Fundamental Aspects 24I

7.3.I Conditions Favouring Powder Deposition 24I

7.3.2 Properties of Metal Powders 242

7.4 Theories of Powder Formation 242

7.4.I Hydrogen Evolution 243

7.4.2 Oxide Formation 243

7.4.3 Discharge of Complex Ions 243

7.4.4 Colloidal Substances 244

7.4.5 Ion Depletion in the Cathode Layer 244

7.4.6 Quantum Mechanical Tunnelling 244

7.5 Apparatus 245

7.6 Operating Variables and the Transition from Compact to Powdery Deposits 246

7.7 Closure 248

LIST OF TABLES

1.1 Mine Production of Metals (1974)

2.1 Critical Reynolds Number for the Laminar to Turbulent Flow Transition for Various Gases

2.2 Friction Factor Expressions for Various Geometries

2.3 Possible Flow Combinations for a Concentric Cylindrical Geometry

2.4 Comparison of Rotating Disc and Rotating Cylinder

3.1 Limiting Current Density and Equivalent Thickness of Diffusion Layer for Various Hydrodynamic Systems

3.2 Dimensionless Groups Commonly Used in Electrochemical Mass Transfer Studies

3.3 Asymptotic Forms of Some Commonly Used Heat and Mass Transfer Correlations

3.4 Mass Transport Studies Involving the Ferrocyanide/Ferricyanide Redox Reaction

3.5 Mass Transport Studies Involving the Cathodic Deposition of Copper

4.1 Mass Transfer Correlations for the Parallel Plate Geometry

4.2 Mass Transfer Correlations for Laminar Flow in an Annular Geometry

4.3 Mass Transfer Correlations for Porous and Packed Bed Electrodes

4.4 Comparison of Mass Transfer Studies for the Fluidised Bed Electrode

4.5 Mass Transfer Correlations for Smooth Rotating Electrodes

5.1 Influence of Electrode Size on Limiting Current Density

5.2 Influence of Peripheral Velocity on Mass Transfer to Rotating Electrodes

5.3 Comparison of Reactor Design in Terms of Space Time Yield and Electrode Area per Unit Cell Volume

5.4 Importance of Space-Time Yield, Chemical Yield and Ease of Control on Reactor Performance

5.5 Commercially Developed Fluidised Bed Electrode Reactors

6.1 Effect of Flow Rate on the Fractional Conversion of a R.C.E.R.

6.2 Possible Scale-up of 'Eco-Cells' (maintaining the mass transfer coefficient)

6.3 Possible Scale-up of 'Eco-Cells' (maintaining the peripheral velocity)

6.4 Idealised 'Eco-Cell' Volume as a Function of Reactor Size

6.5 Nominal Residence time as a Function of Flow Rate for an Idealised Eco-Cell

6.6 Comparison of Rotating Bipolar Electrode and Cascade Eco-Cell Reactors

6.7 Comparison of Laboratory R.C.E. Cells Regarding Design and Construction

6.8 Patended R.C.E. Cells

6.9 Comparison of Patented R.C.E. Cells for Electrodeposition of Metals

6.10 Performance of Hypothetical 'Eco-Cascade Cell'

7.1 Reviews of Electrolytic Metal Powder Deposition

7.2 Use of Metal Powders

7.3 Use of Copper and Copper Base Powders

7.4 Electrodeposition of Alloy Powders

List of Figures

1.1 Pathways of Toxic Metals from the Environment to Man.

2.1 Pressure Gradient as a Function of Reynolds Number for Pipe Flow.

2.2 Friction Factor as a Function of Reynolds Number for Pipe Flow.

2.3 Friction Factor as a Function of Reynolds Number for Pipe Flow (showing the effect of roughness).

2.4 Velocity Profiles for Pipe Flow.

2.5 Model of Turbulence Damping Near a Solid Wall.

2.6 Tangential Fluid Motion for the Laminar Regime around a Rotating Cylinder.

2.7 Taylor Vortices around a Rotating Cylinder.

2.8 Friction Factor as a Function of Reynolds Number for a Rotating Cylinder.

2.9 Torque as a Function of Reynolds Numberfor a Rotating Cylinder.

2.10 Secondary Flows around a Rotating Cylinder in the Turbulent Regime.

2.11 Velocity Profiles in the Annular Gap Between a Rotating Cylinder and a Stationary Concentric Outer Cylinder.

2.12 Friction Factor as a Function of Reynolds Number for a Rotating Cylinder (showing the limits of stability).

2.13a Friction Factor as a Function of Reynolds Number for a Rotating Cylinder (showing the effect of saturated roughness).

2.13b Friction Factor as a Function of Reynolds Number for a Rotating Cylinder (showing the effect of unsaturated roughness).

2.14 Development of a Tangential Velocity Profile around a Rotating Cylinder.

2.15 Schematic Representation of Domains of Flow Regimes around a Rotating Cylinder.

2.16 Axial Reynolds Number as a Function of Taylor Number for a Rotating Cylinder.

2.17 Tangential Stres as a Function of Axial Reynolds Number for a Rotating Cylinder.

3.1 Schematic Polarisation Curve for Copper Deposition from Acid Sulphate Solutions (showing the limiting current plateau).

3.2 Schematic Polarisation Curves for Copper Deposition from Acid Sulphate Solutions (showing the effectof agitation).

3.3a Concentration Profile Near an Electrode.

3.3b Velocity Profile Near an Electrode.

3.4 Schematic Polarisation Curves for Copper Deposition (showing ill-defined limiting current plateaux).

4.1 Configurations for Flow-Through, Porous Electrodes.

4.2 Classification of Rotating Electrodes.

5.1 Modes of Operation of Electrochemical Reactors.

5.2 Operational Sketch for Plug Flow Reactors.

5.3 Operational Sketch for an Annular Plug Flow Reactor.

5.4 Operational Sketch for a Continuously stirred Tank Reactor.

5.5 Sketch of an Experimental C.S.T.R.

5.6. Operational Sketch for an Electrochemical Reactor in the "Batch Recycle" Mode.

5.7 Agitated Vessel for Electrochemical Mass Transport Studies.

5.8 Schematic Polarisation Curves for Copper Deposition from Acid Sulphate Solutions (controlled current operation).

5.9 Schematic Polarisation Curve for the Idealised Deposition of a Series of Metals.

5.10 Nemstian Plot for Selected Metal Cations, 25° C.

5.11 Current Density Distribution for Unbounded Parallel Plate Electrodes.

5.12 Current Density Distribution for Bounded Parallel Plate Electrodes.

5.13 Schematic Representation of Current and Equipotential Lines for a Parallel Plate Electrode.

5.14 Current Density Distribution for the Rotating Disc Electrode.

5.15 Sketch of a Rotating Cylinder Electrode Reactor (showing area and volume relationships).

5.16 Sketch of a Rotating Disc Electrode Reactor.

5.17 Classification of Electrochemical Reactors.

5.18 The Electrochemical Pump Cell.

5.19 The "Swiss Roll" Cell.

5.20 Planar, Side by Side Fluidised Bed Electrode Reactor (C.J.B.)

5.21 Tube,Fluidised Bed Electrode Reactor (AkZO).

5.22 Planar Fluidised Bed Electrode Cell (The "Chemelec" Cell - ECRC).

6.1 Definition Sketch for a Batch Rotating Cylinder Electrode Reactor.

6.2 Conversion as a Function of Time for a Theoretical Batch R.C.E.R.

6.3 Definition Sketch for a Single Pass Rotating Cylinder Electrode Reactor.

6.4a Definition Sketch for a Rotating Cylinder Electrode Reactor with Recycle.

6.4b Process Schematic of a R.C.E.R. with Recycle and Fixed Inlet and Outlet Concentrations.

6.5 Electrode Connections for Potentiostatic Control of a Rotating Cylinder Electrode.

6.6 Laboratory Rotating Cylinder Electrode (Swalheim, 1944).

6.7 Laboratory Rotating Cylinder Electrode (Eisenberg et al., 1954).

6.8 Laboratory Rotating Cylinder Electrode (Arvia et al., 1962).

6.9 Laboratory Rotating Cylinder Electrode (Krishna et al., 1965).

6.10 Laboratory Rotating Cylinder Electrode (Kappesser et al., 1971).

6.11 Laboratory Rotating Cylinder Electrode (Edwards and Wall, 1966).

6.12 Laboratory Rotating Cylinder Electrode (Robinson and Gabe, 1970).

6.13 Laboratory Rotating Cylinder Electrode (Postlethwaite et al., 1971).

6.14 Laboratory Rotating Cylinder Electrode (Sedahmed et al., 1977).

6.15 Laboratory Rotating Tripolar Electrode Cell (Nadebaum and Fahidy, 1973).

6.16 Industrial Rotating Bipolar Electrode Reactor (Nadebaum and Fahidy).

6.17 Undivided Laboratory Rotating Cylinder Electrode for Precious Metal Recovery (Walsh, Ecological Engineering Ltd.)

6.18 Divided Laboratory Rotating Cylinder Electrode Reactor (Ecological Engineering Ltd.)
6.19 Laboratory Rotating Cylinder Electrode (Chin et al., 1977).
6.20 Experimental Rotating Cylinder Electrode Cell for Controlled Potential Coulometric Analysis (Johansson, 1965).
6.21 Amalgamated Rotating Cylinder Electrode Reactor for Synthesis of Salicylaldehyde (Udupa et al., 1963).
6.22 Wiped Rotating Cylinder Electrode Cell for Synthesis of Sodium Dithionite (Spencer et al., 1969).
6.23 Patented Bipolar Rotating Cylinder Electrode for Removal of Ions from an Ionised Liquid (Benner, 1969).
6.24 Patented Rotating Cylinder Electrode for Electrolysis of Metallic Solutions (Lacroix, 1912).
6.25 Patented Rotating Cylinder Electrode for Deposition of Iron (Cowper-Coles, 1915).
6.26 Patented Rotating Cylinder Electrode for Coating of Metal Articles (Schaefer, 1945).
6.27 Patented Rotating Cylinder Electrode for Metal Winning from Ores. (Campbell et al., 1974)
6.28 Patented Rotating Cylinder Electrode for Recovering Silver from Photographic Solutions (Fulweiler, 1971).
6.29 Patented Rotating Cylinder Electrode for Recovering Silver from Photographic Solutions (Fisher, 1972).
6.30 Patented Rotating Cylinder Electrode for Metal Recovery (Goold et al., 1975).
6.31 Patented Rotating Cylinder Electrode for Copper Production (Julien, 1925).
6.32 Patented Rotating Cylinder Electrode for Metal Recovery (Cooley, 1970)
6.33 Patented Rotating Cylinder Electrode for Metal Removal (Arigo Pini S.p.A 1966).

6.34 Patented Rotating Cylinder Electrode for Cupro-Lead Powder Production (Societe Industrielle des Cousinets, 1961).

6.35 Patented Rotating Cylinder Electrode for Metal Recovery (Prunet and Guillen, 1962).

6.36 Patented Rotating Cylinder Electrode for Copper Recovery from Its Ores (Gordy, 1970).

6.37 Patented Rotating Cylinder Electrode for the Production of Zinc Dust (Johnson, 1939).

6.38 Patented Rotating Cylinder Electrode for Deposition of Metals (Cleave, 1925).

6.39 Patented Rotating Cylinder Electrode for Producing Nickel Flakes (Nordblom, 1968).

6.40 Patented "Eco-Cell" for Recovery and Production of Metal as Powder (Holland, 1977).

6.41 Flow Schematic of a Typical "Eco-Cell" Process.

6.42 A Cascade of R.C.E.R's in Hydraulic Series.

6.43 A Six-Element"Cascade Eco-Cell"(divided, with internal distribution of current).

6.44 A Six-Element "Cascade Eco-Cell" (undivided with external resistive distribution of current).

GLOSSARY OF TERMS

Symbol	Meaning	Units	Page first used
η	dynamic viscosity	$g\ cm^{-I} s^{-I}$	6
τ_s	shear	$g\ cm^{-I} s^{-2}$	6
U	velocity	$cm\ s^{-I}$	6
y	distance	cm	6
ϵ	eddy viscosity	$cm^2 s^{-I}$	6
ρ	fluid density	$g\ cm^{-3}$	6
(Re)	Reynolds Number	—	6
ν	kinematic viscosity	$cm^2 s^{-I}$	6
x	characteristic dimension	cm	7
P	pressure drop	$g\ cm^{-I} s^{-2}$	7
l	length	cm	7
F	friction	$g\ cm\ s^{-2}$	8
g	acceleration due to gravity	$cm\ s^{-2}$	8
$f/2$	friction factor	—	8
n	integer	—	8
$d/$	relative roughness (= diameter/roughness)	—	9
r	radius (of pipe, disc or cylinder)	cm	I0
L	friction length	cm	II
ϵ	roughness	cm	9
U_r	friction velocity	$cm\ s^{-I}$	II
u	local velocity coefficient	$cm\ s^{-I}$	I2
(Ta)	Taylor Number	—	I6
r_O, r_I	outside and inside radiae	cm	I6
ω	angular velocity	$rad\ s^{-I}$	I6
G	torque	$g\ cm\ s^{-2}$	I9
(Sc)	Schmidt Number	—	26

GLOSSARY OF TERMS (Cont'd)

Symbol	Meaning	Units	Page first used
D_G	drag	$g\ cm\ s^{-2}$	28
A	surface area	cm^2	28
q	dynamic pressure	$g\ cm^{-I}\ s^{-2}$	28
M	angular momentum / radius	g cm	28
W	power	watts	28
h	height (of cylinder)	cm	28
RPM	rotation rate	$rev\ (min)^{-I}$	30
e^-	electron	——	33
M	metal	——	33
z	charge of ion	——	33
E_o	equilibrium potential	V	34
E	applied electrode potential	V	34
η	polarisation, overpotential	V	34
R	Gas Constant	$J\ K^{-I} mol^{-I}$	34
T	Absolute Temperature	K	34
F	Faraday constant	$(= 96480\ Coulomb\ mol^{-I})$	34
i_o	exchange current density at the equilibrium potential	$mA\ cm^{-2}$	34
i	observed cell current density	$mA\ cm^{-2}$	34
i_L	limiting current density	$mA\ cm^{-2}$	35
D	diffusion coefficient	$cm^2\ s^{-I}$	37
C	concentration	$mol\ cm^{-3}$ also $mg\ dm^{-3}$	37
u	mobility	——	37
ϕ	electrostatic potential	V	37
N_F	total flux	$mol\ cm^{-3} s^{-I}$	37
U	fluid velocity	$cm\ s^{-I}$	37
∇	Laplace Operator	——	37

GLOSSARY OF TERMS (Cont'd)

Symbol	Meaning	Units	Page first used
R_i'	heterogeneous rate constant for production of species	mol $cm^{-3} s^{-I}$	37
μ	electrochemical potential	V	38
j	mass transfer rate	mol $cm^{-2} s^{-I}$	40
δ_N	(Nernstian) diffusion layer thickness	cm	40
K_L	mass transfer coefficient	cm s^{-I}	4I
δ_{Pr}	(Prandtl) hydrodynamic boundary layer thickness	cm	43
(Sh)	Sherwood Number	———	45
(St)	Stanton Number	———	45
d_e	equivalent diameter	cm	54
L	length of electrode	cm	54
ΔL	promoter spacing	cm	70
j_D	Chilton Colburn factor	———	7I
H	hydrodynamic entrance length	cm	72
(Pe)	Peclet Number	———	87
β	a constant in Eqn. 4.I5	———	87
j_D'	Modified Chilton Colburn factor	———	92
v	gas evolution rate	$cm^3 s^{-I}$	I05
I	current	A	I23
N	volumetric flow rate	$cm^3 s^{-I}$	I23
f_R	fractional conversion	———	I23
C_{IN}, C_{OUT}	inlet and outlet concentration	mg dm^{-3}	I23
I_L	limiting current	A	I24
R	recycle ratio	———	I24
C_t	concentration at time t	mg dm^{-3}	I26
C_o	initial concentration	mg dm^{-3}	I26
t	time	s	I26

GLOSSARY OF TERMS (Cont'd)

Symbol	Meaning	Units	Page first used
$V_{reactor}$	volume of reactor	cm^3	I26
V_{RES}	volume of reservoir	cm^3	I32
τ	residence time	s	I33
(Nu)	Nusselt Number	——	I35
(Pr)	Prandtl Number	——	I35
j_H	heat transfer factor	——	I35
Y_{ST}	space time yield	mol cm^{-} hr^{-I}	I44
A_s	'specific' surface area	cm^{-I}	I44
p	Faradaic amount of product per A hr	mol	I44
θ	current efficiency	——	I44
Y_E	chemical yield	——	I45
V_{cell}	cell voltage	V	I45
m	mass of product	g,kg	I45
k	apparent first order rate constant	s^{-I}	I70
γ	dimensionless current density $= i/i_L$	——	I72
P_E	electrolytic power consumption	W	I77
P_{rot}	rotational power requirement	W	I8I
l	length of R.C.E.	cm	I97
$(f_R)_n$	overall fractional conversion	——	230
n	number of elements in cascade	——	230
t_p	initiation time for powder formation	s	247

INTRODUCTION

The routine and essential extraction and use of metals has created two severe problems: not only is our environment being polluted with toxic metals, but there is a depletion in world resources of metal ores, necessitating the working of increasingly dilute ore deposits. Table 1.1[1] indicates the annual production rate of various metals, this being a measure of the rate at which localised deposits of ores become dispersed.

The above situation has created the need to remove and recover metals from dilute industrial process solutions, for financial/commercial reasons (regarding metal or water value) or in order to comply with effluent legislation. Recent years have seen increasing costs of both metals and water, while effluent and water pollution laws continue to become more severe, and more stringently applied by water authorities.

Sources of dilute solutions include the great majority of manufacturing industries in addition to primary ore and mine dump leachings, industrial effluents, liberator cells in electrowinning, and naturally occurring waterways. Indeed, such solutions tend to be found wherever metals are produced or processed.

Dilute metal solutions are commonly treated, if at all, by chemical precipitation, yielding a metal-containing sludge which is normally disposed of by spreading onto selected areas of land. This method of treatment is quite unfortunate; not only is the metal value lost and the disposal costly, but also an environmental hazard is created. Fig.1 indicates in a schematic fashion, the major pathways of toxic metals from the environment to man. It can be seen that toxic metals spread on land can reach man via leaching by surface streams which lead to rivers and lakes being polluted, or crop production may result in toxic plants or animals being eaten by animals, including man. In addition, pollution of the sea can lead more directly to toxic poisoning, via ingestion of marine life.

Toxic metals may be divided into two categories, according to their degree of toxicity. Most hazardous are those which are at present considered inherent toxins, e.g. cadmium, mercury, lead and arsenic. The remaining category comprises metals which are toxic at low concentrations over an extended time, and includes copper, nickel, zinc and tin. It may be noted that the above metals form the bulk of those encountered in the field of metals production and treatment.

Various techniques of recovery and regeneration such as reverse osmosis, ion exchange and evaporative recovery may often be successfully applied to concentrate the dilute metal solution, while providing for possible re-use of water. If the concentrate cannot be used within the industry concerned however, the problem of disposal remains. Clearly, in the majority of cases, it is desirable to recover the metal directly for re-use or resale, producing water which may either be recycled or which is acceptable to the receiving water treatment authorities. The cleanest, most direct and most convenient method of achieving this aim is often by electrodeposition of the metal.

Dilute solutions, however, present several possible problems to this technique. Firstly, in order to operate selectively at high current efficiency, side reactions should be minimised and secondly, electrodeposition must occur at a high rate in order to quickly and conomically remove the metal in a compact plant. Finally, electrodeposition should be capable of being carried out on a continuous basis, in order to minimise labour and downtime, and facilitate automation. The first two problems result in the need for a controlled potential, high mass transfer process, while the third indicates the requirement for continuous removal of metal product.

One reactor geometry which meets the above requirements particularly well is the concentric rotating cylinder electrode reactor, (abbreviated in this thesis to R.C.E.R.). A commercial reactor employing such an electrode has been developed over the past eight years by Ecological Engineering Limited, Macclesfield.

It is the general object of this Thesis to present and review the R.C.E.R. in the context of other electrochemical reactors, both academic and industrial, and to offer experimental work, at both laboratory and pilot plant/commercial scale to illustrate its performance and application to the removal of metals from dilute solutions, typically of metal concentration 1 to 1,000 mg dm^{-3}.

... oOo ...

CHAPTER TWO

FLUID FLOW

A prior knowledge of electrolyte fluid flow behaviour is essential for the design and scaleup of electrochemical reactors, with regard to the prediction of solid-liquid heat and mass transfer, mixing characteristics within the reactor, and removal of gas from the electrodes and the reactor.

Following a general introduction to fluid flow, using pipe flow as a model, this chapter concentrates on turbulent flow due to its relevance to high rates of mass transfer, and on the rotating cylinder geometry in particular, due to its relevance to the theme of this thesis.

2. FLUID FLOW

2.1 General Conditions.

Aqueous solutions, including electrolytes, are generally both incompressible and Newtonian in nature, i.e. one can relate the dynamic viscosity[+], η, of the fluid to the shear between its adjacent layers, τ_s, and the interfacial velocity gradient dU/dy by

$$\tau_s = \eta \frac{dU}{dy} \qquad \text{Equation 2.1}$$

for laminar flow.

For turbulent flow, an apparent eddy viscosity, e, is involved, which enhances the effective overall viscosity, η_{TURB}

$$\eta_{TURB} = \eta + \rho\epsilon \qquad \text{Equation 2.2}$$

where ρ is the fluid density. This results in a non-linear relationship between dU/dy and τ_s.

2.2 Flow Regime and Stability.

A fluid may be considered stable if laminar (streamline) flow persists, but unstable if chaotic eddies reinforce turbulent flow. Reynolds[3] examined the transition between these two distinct types of flow, finding that a fluid became unstable above a critical Reynolds Number, (Re) where

---

[+] the dynamic viscosity, η should not be confused with the kinematic viscosity, ν , the two being related by the fluid density, ρ

$$\nu = \eta/\rho$$

$$(Re) = \frac{Ux}{\nu} \qquad \text{Equation 2.3}$$

Here, U is the fluid velocity, x is a characteristic dimension, and ν is the kinematic viscosity of the fluid.

The nature of the flow regime depends upon the drag or frictional forces operating at the solid walls of the system. Thus a low drag is associated with laminar flow, while turbulence is achieved when high drag forces are operative. The Renolds Number can be seen as representing the ratio of inertial to viscous forces

$$(Re) = \frac{\rho x^2 U^2}{\eta x U} = \frac{\rho x U}{\eta} = \frac{Ux}{\nu} \qquad \text{Equation 2.4}$$

For a given type of geometry, reactors of different size are found to have similar fluid flow properties if (Re) is maintained constant, according to the 'principle of dynamic similarity'.

The importance of flow regime can perhaps be best understood by considering a geometrically simple but practically important system, flow through a circular section straight pipe. In this case, U is the linear fluid velocity, and x, the characteristic dimension, is the internal diameter of the pipe, d.

Experimentally, one can relate the drag force at the pipe wall to measurements of the pressure drop, ΔP over unit length of tube, l, according to an equation

$$\frac{\Delta P}{l} = \frac{F\rho}{l} = \frac{4f}{d}\,\frac{U^2}{2g}$$ Equation 2.5

where

F is the friction loss due to drag,
g is acceleration due to gravity,
f is the (Fanning) friction factor.

f ?

If the pressure gradient, $\Delta P/l$, is plotted against (Re) on log-log axes, as in Fig. 2.1, two distinct flow regions are seen as straight lines, with a transition region between. Thus

$$\frac{\Delta P}{l} = \text{constant}\ U^n$$ Equation 2.6

and

$$\mathrm{LOG}_{10}\left\{\frac{\Delta P}{l}\right\} = \mathrm{LOG}_{10}\ \text{constant} + n\ \mathrm{LOG}_{10}\ U$$ Equation 2.7

n, the slope of Fig. 2.1 is 1.0 for laminar flow at low (Re), and 1.5-2 for turbulent flow at higher (Re), the exact value depending upon roughness at the pipe wall. The critical Reynolds Number is about 2000.

It is more usual to present Fig. 2.1 as a log-log plot of the friction factor, $\frac{f}{2}$ against (Re), as in Fig. 2.2 where the friction factor may be related to the pressure gradient by equation 2.5

Again, the laminar and turbulent regions are represented, separated by an unstable transition region. The laminar region may be described by the approximate relationship due to Poiseuille[4]

$$\frac{f}{2} = \frac{8}{(Re)}$$ Equation 2.8

while the turbulent region may be approximately described by the Blasius Equation[5]

$$\frac{f}{2} = 0.0396\ (Re)^{-0.25} \qquad \text{Equation 2.9}$$

The above picture is, in practice, more complicated; the friction factor is better expressed in turbulent flow by a formula of the von Karman type (see Appendix 1) due to Nikuradse[6] and others

$$\frac{1}{\sqrt{f/2}} = -0.40 + 4.00 \log_{10} (Re) \sqrt{f/2} \qquad \text{Equation 2.10}$$

Also, it is found (Fig. 2.3, after Moody[7]) that after a second critical (Re), the friction factor becomes independent of (Re), being a function of the relative roughness, d/e only

$$\frac{1}{\sqrt{f/2}} = 3.46 + 4.00 \log_{10} \frac{d/2}{e} \qquad \text{Equation 2.11}$$

As seen in Fig. 2.3, this second critical (Re) is lower for increased values of the relative roughness.

2.3 Velocity Distribution.

The velocity profile within the pipe is quite different for each regime. For both regimes the velocity is zero at the wall due to friction and a maximum at the centre of the pipe section. In laminar flow there is a smooth (parabolic) change in velocity across the pipe, while in turbulent flow there is a laminar region adjacent to the wall, but considerable eddying away from the wall, giving rise to the flattened profiles shown in Fig. 2.4.

For laminar flow, the velocity profile is described by

$$U_x = U_{max} (1 - r_x^2/r^2) \qquad \text{Equation 2.12}$$

where U_x and U_{max} are the local and maximum velocities respectively, and r_x and r are the local and pipe radiae. For turbulent flow,

$$\frac{U_{max} - U_{mean}}{(\tau/\rho)^{\frac{1}{2}}} = 5.75 \log_{10} \left\{\frac{r_2}{r}\right\} \qquad \text{Equation 2.13}$$

where U is the mean velocity

r_2 is the distance from the pipe wall.

Following a treatment by Prandl[4] and von Karman[8], the turbulent zone may be subdivided into three layers; (Fig. 2.5)

1. a laminar boundary layer adjacent to the wall where all mass transfer is due to molecular effects

2. a viscous sublayer, acting as a buffer region, where molecular viscosity tends to damp out eddies, and

3. a fully developed turbulent layer where all mass transfer is due to eddy effects.

Levich[8a] has discussed the addition of an additional turbulent sublayer. A mathematical summary of von Karman's approach is given in Appendix 1, after Theodorsen and Regier[9], and it may be noted that an equation of the following general form is attained

$$\frac{U_{max}}{U_r} = \text{constant} + \frac{1}{\text{constant}^1} \log_{10} \frac{r}{L} \qquad \text{Equation 2.14}$$

known as a universal velocity distribution, where U_r is friction velocity, defined by

$$U_r = \sqrt{\frac{\tau}{\rho}} \qquad \text{Equation 21.5}$$

and the corresponding friction length, L is given by

$$L = \frac{\nu}{U_r} \qquad \text{Equation 2.16}$$

The effect of surface roughness may also be treated in a similar manner. If the roughness to friction length ratio, e/L is less than 3.3, there is no effect. For $e/L > 3.3$, however, U_{max}/U_r becomes independent of L for saturated roughness, and equation 12 becomes

$$\frac{U_{max}}{U_r} = \text{constant} + \frac{1}{\text{constant}^1} \log 3.3 \frac{r}{e} \qquad \text{Equation 2.17}$$

$$\frac{U_{max}}{U_r} = \text{constant}^{11} + \frac{1}{\text{constant}^1} \log \frac{r}{e} \qquad \text{Equation 2.18}$$

The velocity distribution is effectively as if a laminar layer of thickness 3.5 e was present, or as if the friction length was e/3.3. The physical significance of this is that the laminar layer is of the order of three to four times that of the surface irregularities giving rise to roughness.

This von Karman-Prandl theory for turbulent flow is based on two assumptions:

1. the ratio of the velocity defficiency, $(U_{max}-U)/U_r$ to the friction velocity, L is a function of geometric parameters only, and

2. adjacent to the wall, but beyond the laminar sublayer, the slope of the curve representing this ratio is inversely proportional to distance from the wall, where the proportionality constant is a universal one.

The von Karman-Prandl treatment may be extended to other geometries with caution; in particular the geometrical configuration must be described by a single parameter.

To return to the three layer concept, specific expressions may be written for each layer, involving u^+ and y^+, the dimensionless velocity and distance. For the laminar boundary layer,

$$u^+ = y^+ \qquad \text{Equation 2.19}$$

for $y^+ < 5$.

For the buffer layer,

$$u^+ = 3.05 + 11.52 \log_{10} y^+ \qquad \text{Equation 2.20}$$

for $5 < y^+ < 30$.

and for the turbulent core,

$$u^+ = 5.5 + 5.76 \log_{10} y \qquad \text{Equation 2.21}$$

for $y^+ > 30$.

For rough wall pipes of saturated roughness,

$$u^{+} = 8.5 + 5.76 \log_{10} \frac{y}{e} \qquad \text{Equation 2.22}$$

$$\text{for } y^{+} > 30.$$

In the above equations,

$$u^{+} = \frac{U}{U_r} = \frac{\text{local velocity}}{\text{friction velocity}} \qquad \text{Equation 2.23}$$

$$y^{+} = \frac{yU_r}{\nu} = \frac{y}{L} \qquad \text{Equation 2.24}$$

where y is the distance from the pipe wall.

2.4 The Rotating Cylinder Geometry.

2.4.1 General

Aside from its direct relevance to the subject matter of this thesis, fluid flow in the concentric rotating cylinder geometry is of considerable importance in severl other situations including

i) measurement of viscosity,

ii) heat transfer in rotating mechanical and electrical machines,

iii) corrosion of rotating parts,

iv) rotating cylinder extraction columns,

v) cyclone chamber efficiency and

vi) journal bearing operation.

Flow in the annulus of a concentric rotating cylinder system has also proved to be an interesting academic system, where the geometry would appear relatively simple, and certainly uniform, while the actual fluid flow behaviour is rather complex. It is possible to consider various cases also, e.g. the inner cylinder, outer cylinder or both may be rotated with or without a superimposed axial flow. In the case of axial flow without rotation, the system is effectively flow through an annulus.

It is noteworthy that Newman[10] has used the inner rotating cylinder system as a model for the explanation of both fluid flow and mass transfer behaviour, while the early work of Taylor[11], using an inner rotating cylinder provided an insight into the nature of turbulent flow in general, and the transition from laminar to turbulent flow in particular.

In addition to direct applications of rotating cylinder fluid flow studies to practical systems, the rotating cylinder system has also provided useful information for indirectly related problems including the flow around a continuously moving strip. Due to its compactness, and convenience, it often presents a model system for studies involving reproducible turbulent flow conditions.

2.4.2 The laminar to turbulent transition

As has been noted previously, the first successful treatment was by Taylor[11] who studied the concentric rotating cylinder system with the inner system rotated, and no axial flow. Three general zones of behaviour exist, depending on the speed of rotation.

At very low rotational speeds, the fluid flows in a straightforward manner, in concentric circles around the inner cylinder as in Fig. 2.6, i.e. the flow is tangential and laminar.

On increasing the rotational speed, this simple flow pattern becomes unstable, and a cellular motion is imposed upon the flow around the inner cylinder. The resulting toroidal Taylor vortices (Fig. 2.7) contain a radial component of velocity. Thus the flow is still laminar, but no longer tangential, as a radial and axial motion are superimposed.

At still higher rotational speed, flow becomes fully turbulent, as chaotic eddies increasingly break up any regular flow pattern. Flow is then characterised by rapid and random fluctuations of velocity and pressure, which include a fluctuating radial velocity component.

Regarding mass transfer to the inner cylinder (which will be fully treated in chapter 4), the tangential laminar flow requires the least torque to rotate the cylinder, but provides no marked enhancement of mass transfer. The Taylor vortex flow requires a higher torque and contributes to mass transfer, but far more important is fully turbulent flow, which requires the highest torque, but contributes most effectively to mass transfer, while also providing vigorous stirring in the annular gap.

Taylor[11-13] found that instability occurred when the Taylor number

$$(Ta) = (Re) \left\{\frac{r_o - r_I}{r_o + r_I}\right\}^{\frac{1}{2}} \qquad \text{Equation 2.25}$$

exceeded 29.3,

where r_o and r_I are the radiae of the outer and inner cylinders, and (Re) is defined in this case as

$$(Re) = \frac{r_I \ \omega \ (r_o - r_I)}{\nu} \qquad \text{Equation 2.26}$$

where ω is the angular velocity of the inner cylinder,

$$\omega = \frac{U}{r_I} \qquad \text{Equation 2.27}$$

and U is the peripheral velocity of the inner cylinder.

Schlichting[14] has defined a modified Taylor Number (Ta^1)

$$(Ta^1) = (Re) \left\{\frac{r_o - r_I}{r_I}\right\}^{\frac{1}{2}} \qquad \text{Equation 2.28}$$

and according to this definition, the critical value for fluid instability is 41.3.

The existence of the critical Taylor Number has been confirmed by the studies of Lin[15] and Flower et al.[16].

Taylor also showed that steady laminar flow could be maintained to higher (Re) if the outer cylinder only rotated (Fig. 2.8), a more difficult system experimentally.

The critical (Re) for instability is 200, corresponding to (Ta) = 29.3.

For (Ta) $>$ 400, true turbulent flow develops.

In contrast to the above, it is interesting to note that, following an extensive study of drag at an inner rotating cylinder, Theodersen and Regier[9] concluded that no distinct transition from laminar to turbulent flow existed, rather the flow had some essential turbulent character down to the smallest (Re).

Donnelly and coworkers[17-20], however, have also examined the stability of flow via measurements of torque, and their data strongly indicates a large transition region where discreet Taylor vortices are stable. Similar results have been obtained by Stuart[20a] (Fig. 2.9).

It should be appreciated that the Taylor analysis is strictly limited to the criterion of the annular gap being small compared to the mean radius.

$$(r_o - r_I) \ll \tfrac{1}{2} (r_o + r_I)$$

i.e. the case of a small annular gap, whereas Theodersen and Regier employed a vessel of undefined boundaries. The case of large gaps has been discussed by Chandrasekhar[21], whose results were confirmed by Donnelly et al.[17-20].

It is of interest to note that even in the turbulent regime, a stable secondary flow pattern has been observed by Pai[22] (Fig. 2.10) superimposed on the turbulent fluctuations.

2.4.3 Velocity Profiles

Following the discussion of velocity profiles in the case of flow through a pipe, earlier in this chapter, it is now of interest to examine the velocity distribution in the annular gap between a rotating inner cylinder and a static outer cylinder. This has been examined by various authors[22-24], and the general profiles for laminar and turbulent flow are as shown in Fig. 2.11. The laminar profile may be expressed by a parabolic relationship, e.g.

$$U = \frac{\text{constant } y^2}{(r_o - r_I)^2} \qquad \text{Equation 2.29}$$

where y is the distance measured in a radial direction.

This forms the basis for the determination of dynamic viscosity, n via measurements of the torque transmitted by an inner rotating cylinder to a fixed outer cylinder. Here, it may be shown[25] that, neglecting the submerged ends of the cylinder,

$$\omega = \frac{G}{4 \pi \eta l} \left\{ \frac{r_o^{2} - r_I^{2}}{r_o^{2} \; r_I^{2}} \right\} \qquad \text{Equation 2.30}$$

where l is the length of the cylinder and

G is the torque

In the case of turbulent flow, the profile is necessarily more complicated, an approximate form being

$$U = \text{constant} \left\{ \frac{\tau}{\rho} \right\}^{\frac{1}{2}} \log_{10} \frac{y}{r_o - r_I} \qquad \text{Equation 2.31}$$

cf. equation 2.11 for pipe flow.

2.4.4 Drag and Friction Factors

As in the case of pipe flow, the velocity distribution may be treated by a von Karman type approach yielding an equation for drag.

$$\frac{1}{\sqrt{f/2}} = -17.5 + 5.75 \log_{10} \frac{Re}{\sqrt{f/2}} \qquad \text{Equation 2.32}$$

in turbulent flow.

Such an equation was obtained by Theodersen and Regier[9] following their studies of oil, air and water as fluids*.

---

* In fact the original Theodersen and Regier equations have been rewritten here, as they involved a definition of (Re) based on radius rather than

For laminar flow

$$\frac{f}{2} = \frac{2}{(Re)} \qquad \text{Equation 2.33}$$

while for turbulent flow around a rotating cylinder of saturated roughness, e, at a Reynolds number greater than the second critical value,

$$\frac{1}{\sqrt{f/2}} = 1.25 + 5.76 \log_{10} \frac{d}{e} \qquad \text{Equation 2.34}$$

$(Re)_{crit}$ is approximately given by

$$(Re)_{crit} = \left\{11.8 \frac{d}{e}\right\}^{1.18} \qquad \text{Equation 2.35}$$

The results of Theodersen and Regier are summarised in Figs. 2.12 and 2.13 where the friction factor is plotted against the Reynolds number on log-log axes. The following points may be made:

1. there appears to be no distinct transition from laminar to turbulent flow, i.e. the critical (Re) for instability is not well defined, as previously noted (Fig. 2.12)

2. Fig. 2.13a involving saturated roughness shows that after the second critical (Re) is exceeded, the friction factor is invariant with (Re), depending only on the relative roughness e/d, according to equation 2.34.

3. the greater the relative roughness, the lower is the second critical (Re)

4. Fig. 2.13b refers to unsaturated roughness, where, in contrast to the above, the friction factor is influenced both by (Re) and the relative roughness.

It is instructive at this point to consider the similarity between drag relationships for three systems of both academic and commercial importance; the rotating disc, the rotating cylinder, and pipe flow. On one hand, pipe flow represents a normally turbulent regime in practice, as does the rotating cylinder. The rotating disc and rotating cylinder may be contrasted, the former normally giving rise to laminar flow (Table 2.1).

2.4.5 Effect of Axial Flow

Previous discussion has been limited to the case of zero axial flow, but in practice axial flow represents a more common situation as for example in the case of forced air flow through a rotating machine with an outer cover, or of more importance here, the case of a R.C.E.R. with continuous flow. Two questions arise, viz. what is the effect of the axial flow rate on the critical (Re) for instability, and what is the effect on the degree of mass transfer to the inner cylinder. The laminar and turbulent flow regimes may be discussed separately.

Table 2.3 indicates that a whole variety of flow patterns is possible for a rotating cylinder geometry, depending on which electrode is rotated, and whether axial flow is present.

The case of laminar flow has been reviewed[29]. It might be anticipated that an axial flow of sufficient magnitude might persuade the fluid around a rotating cylinder to follow a helical rather than a tangential path. The studies of Fage[26] and Cornish[27] have shown that both types of flow are possible, whereas the intermediate vortex flow apparently does not occur; the laminar-turbulent transition becoming more comparable to pipe flow.

Goldstein[28] analysed the stability of laminar flow concluding that the tangential laminar flow is increased slightly by axial flow superimposition.

For all superimposed axial velocity distributions the tangential velocity is subject to an axial entrance length, as in purely annular flow (Fig. 2.14)[29]. At the entrance, only fluid in contact with the rotating surface acquires a circumferential velocity, while the remaining fluid is swept downstream. With increasing axial distance, the tangential boundary layer thickens to eventually fill the gap. In a sufficiently long annulus, the tangential profile further develops an approach towards Couette flow, when the fully developed tangential velocity distribution is independent of the axial coordinate.

The effect of axial flow on the laminar regime has been analysed theoretically by Goldstein[28] (1937), Di Prima[30] (1960), Chandrasekhar[31,32], and Krueger & Di Prima (1964)[33]. Experimental studies have been conducted by Cornish (1933)[27], Fage (1938)[26], Kaye & Elger (1958)[34], Donnelly & Fultz (1960)[18], Yamada (1962)[35], Snyder (1962)[36], Astill (1961)[37], (1964)[38] and more recently by MacLeod & Shahbendrian (1969)[16], McLeod & Russ (1975)[39], and Coney et al.[55,56,66,67,124].

Four separate flow regimes may be realised (Fig. 2.15): laminary, laminar with vortices, turbulent and turbulent with vortices. In practice, however, the turbulent regimes are difficult to realise at low rotational speeds without a severe axial flow.

In contrast to the laminar flow case, it is rather surprising that there appears to be very little literature concerning the effect of axial flow on a turbulent core flow in a rotating cylinder annulus. This is a case which merits attention, as it represents for example the case of an electrochemical reactor with high mass transfer to the inner cylinder and good agitation; i.e. it approximates to the case of a flow through-continuously stirred tank reactor (CSTR), in chemical engineering terms (see chapters 5 and 6).

It might be anticipated that two extremes of behaviour could be observed: at low axial velocities, and high rotational speeds, the fluid behaviour would be as in the case of normal turbulent core rotating cylinder annulus; at high axial velocities and low rotational speeds, a tendency towards turbulent annular flow might be expected, with superposition of a helical flow. This latter case might destroy the CSTR approximation, giving a tendency towards plug flow.

In practice, however, it is the author's experience that at rotational speeds necessary to produce turbulence, the highly turbulent conditions in a rotating cylinder reactor are not affected to any great extent by relatively high axial flow rates.

One of the few available works is that of Kosterin et al.[40] who studied air flow in an annular channel of relative size $(r_o - r_I)/r_I = 0.271$ ($r_o = 24.4$ cm, $r_I = 19.2$ cm), in a long (ca. 2 metre) annulus. Pressure measurements were made over this length, and also radially, and velocity profiles were measured with a thermoanemometer. The (Ta) range was 0-700, where

$$(Ta) = \frac{\omega (r_o + r_I)^{\frac{1}{2}}}{2\,(r_o - r_I)^{3/2}} \qquad \text{Equation 2.36}$$

equivalent to a (Re) of 10^5, where

$$(Re) = \frac{\omega\, r_I\,(r_o - r_I)}{\nu} \qquad \text{Equation 2.37}$$

while the axial velocity range was equivalent to an axial (Re) of $0-10^3$,

where

$$(Re)_{axial} = \frac{U_{axial}\,(r_o - r_I)}{\nu} \qquad \text{Equation 2.38}$$

It was found that as a critical axial flow rate was approached, vortices appeared in the turbulent core, and the transition between the turbulent and turbulent plus vortices region is as shown in Fig. 2.16.

Measurements were also made, in the above study, of the effect of axial velocity on the tangential shear stress at the outer cylinder wall at constant rotational speed, and it was found that the stress steadily decreases with $(Re)_{axial}$ in the turbulent region, but became steady at a certain axial velocity, then increased with further increases in axial flow (see Fig. 2.17).

It should be noted that the above work involved air as a fluid; there is a marked scarcity of information on aqueous fluids under similar conditions.

It is interesting that the case of axial flow superimposed on rotational has been studied electrochemically as part of a heat transfer study[40A]. This work involved the laminar and Taylor vortex flow regimes, the main purpose being to observe the interrelation between axial vortex movement and periodically varying rates of mass transfer. The apparatus employed two concentric vertical, 38 cm long copper cylinders. The inner cylinder had diameter of 5.8 cm, while the diameter of the outer cylinder was 9.4 cm, giving an annular gap of 1.8 cm. The inner rotating cylinder served as an anode. The outer cylinder contained 36 0.4 cm diameter circular copper cathodes embedded at 4 mm axial intervals to investigate the case zero flow rate. A single 1.1 mm diameter cathode was embedded 28.4 cm from the bottom of the outer cylinder for the case of constant axial flow with varying rotational rates. In addition, three 1.1 mm diameter copper wire cathodes were inserted into the annular space, 28.4 cm from the bottom of the cell, and separated in arc by ca. 20^{0}. These micro cathodes had an active surface at ca. 2 mm from the outer cylinder, (the centre of the annulus), and 2 mm from the inner cylinder. These wire cathodes were very sensitive to velocity exponent perpendicular to the cathode surface, but not very sensitive to the axial component. The cathodic deposition of copper from acid copper sulphate was employed as a test reaction over the following ranges of experimental parameters, (Ta) 35-9200, (Re) 0-260, (Sc) 3×10^{3} to 8×10^{5}.

The results showed that the axial motion resulted in a damping effect on the formation of Taylor vortices, and a lowering of mass transfer. As in an earlier study[406], the vortices were found to move axially, in single file along the annulus of secondary flow. This axial movement is important, as it indicates that an electrochemical reactor would operate in the plug flow mode under these conditions.

2.4.6 Power Requirements

From an operational and economic standpoint, it must not be forgotten that fluid flow is attained by supply of energy; as pump pressure in the case of pumped flow through a pipe or via rotational power in the case of rotating cylinder or disc systems.

While turbulent flow is often desirable both for good mass transfer and effective stirring; these features are attained at the expense of increased power consumption in comparison with laminar flow.

In addition, the power required to rotate a rough cylinder or disc is markedly greater than that for a smooth electrode under comparable conditions, due to the increased drag.

Table 2.4 compares expressions for the torque and power requirements of rotating cylinders and discs, in terms of system parameters.

It has already been seen that measurement of torque at a rotating cylinder provides a means for measuring dynamic viscosity (Equation 2.29), and also a means of measuring the friction factor.

The torque for an inner rotating cylinder in a concentric geometry^{G}, may be related to the friction factor as follows

$$\frac{f}{2} = \frac{D_G}{qA} = \frac{G}{2\, r_I\, Aq} \qquad \text{Equation 2.39}$$

where D_G is the drag coefficient, A is the circumferential surface area, and q is the dynamic pressure.

For a RCE, $q = \frac{1}{2}\rho\, \omega^2 r_I{}^2$ Equation 2.40

where ω is the angular velocity $= \frac{U}{r_I}$

As $D_G = \frac{M}{r_I}$ Equation 2.41

where M = angular momentum divided by the radius,

$$\frac{f}{2} = \frac{M}{q\, A\, r_I} \qquad \text{Equation 2.42}$$

$$M = \frac{f}{2}\, q\, A\, r_I \qquad \text{Equation 2.43}$$

The rotational power may be expressed as the product of momentum and angular velocity.

$$P_{rot} = M\, \omega \qquad \text{Equation 2.44}$$

$$= \frac{f}{2}\, q\, A\, r_I\, \omega \qquad \text{Equation 2.45}$$

as $q = \frac{1}{2}\rho\, \omega^2 r_I{}^2$. Equation 2.40

$A = 2\pi\, r_I\, h$ Equation 2.46

and $\omega = \frac{U}{R}$ Equation 2.27

$$P_{rot} = \frac{f}{2} \cdot \pi \rho\, r_I h\, U^3 \qquad \text{Equation 2.47}$$

This last equation expresses the rotational power as a function of both geometrical and electrolyte properties. If the C.G.S. system of units is adopted, P_{rot} will be in watts if the last equation is multiplied by 10^{-7},

$$P_{rot} = \frac{f}{2} \cdot \pi \rho \, r_I \, h \, U^3 \times 10^{-7}$$ Equation 2.48

For the case of a rotating disc, a similar treatment may be adopted, and allowing for the change in surface area,

$$P_{rot} = \frac{f}{2} \cdot \frac{\pi}{2} \rho \, r_I^2 \, U^3 \times 10^{-7}$$ Equation 2.49

It can be seen that equations 2.48 and 2.49 differ only by the ratio of surface areas.

Thus

$$_{RCE}P_{rot} = {}_{RDE}P_{rot} \times \frac{2h}{r_I}$$ Equation 2.50

and the difference in the value of the friction factors, is considerable.

Note that the effect of the 'discs' at the top and bottom of the cylinder has been ignored.

Considering, for example, a rotating disc and rotating cylinder both of radius r_I = 10 cm, and a cylinder height $h = 2r_I$ = 20 cm, both rotating at a peripheral velocity, U of 100 cm s^{-1}. The rotation rate of the cylinder and disc is then given by

$$(RPM) = \frac{U \times 60}{2 \pi r_I} \qquad \text{Equation 2.51}$$

$$= 95.5$$

If the electrolyte has a kinematic viscosity of 0.01 cm^2 s^{-1}, the relevant Reynolds numbers are given by

$$(Re)_{CYL} = \frac{Ud}{\nu} = \frac{100 \times 20}{10^{-2}}$$

$$= 2 \times 10^5$$

$$(Re)_{DISC} = \frac{Ur}{\nu} = \frac{100 \times 10}{10^{-2}}$$

$$= 1 \times 10^5$$

Thus, the cylinder is in turbulent flow, while the disc is probably still in laminar flow.

Assuming both the disc and cylinder are smooth, $f/2$ is given for the cylinder by ;

$$1/\sqrt{\frac{f}{2}} = -17.5 + 5.75 \log_{10} Re \sqrt{\frac{f}{2}} \qquad \text{Equation 2.32}$$

which may be approximated by[57,58]

$$\frac{f}{2} = 0.079\ Re^{-0.30} \qquad \text{Equation 2.52}$$

$$\text{CYL} \quad \frac{f}{2} = 0.079\ (2 \times 10^{5})^{-0.30}$$

$$\text{CYL} \quad \frac{f}{2} = 2.03 \times 10^{-3}$$

and for the disc,

$$\frac{f}{2} = 0.62\ Re^{-0.5} \qquad \text{Equation 2.53}$$

$$= 0.62\ (10^{5})^{-0.5}$$

$$= 1.96 \times 10^{-3}$$

The surface areas are 3948 cm^2 and 314 cm^2 for the cylinder and disc respectively.

The above comparison is summarised in Table 2.4

CHAPTER THREE

ELECTROCHEMICAL MASS TRANSFER

This general subject is presented in some detail, to form a background for the understanding of the mass transport behaviour of electrodes in both laboratory cells and commercial reactors. Attention is drawn to the importance of electrochemical techniques of mass transfer measurement, and the choice of reaction system is discussed and reviewed.

3. ELECTROCHEMICAL MASS TRANSFER

A relatively concise account is offered here; for further discussion, the reader is referred to reviews by various other authors[8a,10,].

3.1 General Considerations.

3.1.1 Electrode Processes

An aqueous electrochemical process involves electron transfer between an electrode and a species in solution. Such a process may be represented by

$$\text{(OXIDISED)} + ze^- \rightleftharpoons \text{(REDUCED)} \qquad \text{Equation 3.1}$$

More specifically, for the electrodeposition of a metal M, via discharge of its ions of charge z, we may consider the forward reaction of

$$M^{z+} + ze^- \rightleftharpoons M \qquad \text{Equation 3.2}$$

Such an overall process comprises three consecutive steps:

i) mass transfer, i.e. the movement of the metal ions from the bulk solution to the electrode surface,

ii) charge transfer, i.e. neutralisation of the positively charged metal ions leading to neutral atoms on the electrode surface, and,

iii) crystallisation, in which the neutral metal atom diffuses along the surface to a nucleus and is subsequently incorporated into the lattice of the metal.

The overall reaction rate will be determined by the slowest of the above steps. While each of the above steps may be rate controlling, this thesis is mainly concerned with mass transfer control, when step i) is the important one.

3.1.2 Types of Polarisation

Considering equation 3.1, if the rates of the forward and reverse reactions are identical, the electrode is at its equilibrium potential, E_0, and the partial current densities for the forward and reverse reactions are equal, resulting in no net current flow. As the applied electrode potential, E, is increased, a point is reached where the rate of the reverse reaction may be neglected, and it is generally found that

$$\eta = (E - E_0) = \frac{RT}{zF} \ln\left\{\frac{i}{i_0}\right\} \qquad \text{Equation 3.3}$$

where i_0 is the exchange current density at the equilibrium potential and η is referred to as the polarisation, or overpotential. Equation 3.3 describes activation polarisation, where the electrode process is under charge transfer control, and is often referred to as the Tafel equation.

Further increase in the applied potential, and hence in the resulting overpotential gradually leads to a situation where the rate of charge transfer becomes fast compared to the rate of transfer of ions from solution to the electrode. The system is then said to be under mass transfer control, as concentration polarisation predominates. The observed cell current density, i, reaches a maximum level for complete mass transfer control known as the limiting current density, i_L, when the metal ion concentration at the electrode surface approaches zero. The limiting current density represents the maximum rate of reaction under given experimental conditions.

The above description of polarisation is deliberately oversimplified; the reader is referred elsewhere[48] for a detailed discussion.

3.1.3 Polarisation Curves

Cell current density/electrode potential curves may be obtained experimentally, the electrode potential normally being measured relative to a standard reference electrode. Fig. 3.1 shows a typical generalised curve for copper deposition from acidic sulphate solutions:

$$Cu^{2+} + 2e^- \longrightarrow Cu \qquad \text{Equation 3.4}$$

an idealised system often used in mass transfer studies. The plot shows the potential regions corresponding to charge transfer, mixed and mass transfer control, as the potential is increased from the equilibrium potential. The limiting current density, i_L, is exhibited as a plateau which extends to a certain potential, after which the observed current density increases. At this point, an additional reaction, hydrogen evoluation takes place at an increasing rate as the potential is raised further.

The limiting current, under given experimental conditions, may be increased by agitation of the electrode relative to the electrolyte (Fig. 3.2).

3.2 Transport Processes.

3.2.1 Introduction

Transport phenomena occur when the individual components of a system are not in equilibrium, giving rise to gradients. In particular, gradients in concentration, velocity and temperature give rise to diffusion, momentum transfer and heat transfer. A detailed discussion of transport phenomena is provided elsewhere[49], while reviews of transport in electrochemical systems are provided by Levich[8a] and Newman[10,50], the last author having stressed the importance of transport phenomena in the engineering design of electrochemical reactors,[51].

The laws governing transport in dilute electrolytic solutions have been known for many years[52].

In the case of mass transport, three processes exist:

i) diffusion, a molecular transport process due to movement under a concentration gradient,

ii) convection, in which the species is transported via a bulk hydrodynamic flow, and

iii) migration, where ions move under the influence of an electric potential gradient.

The flux of a species in solution is then described by :

∇ ?

Total Flux = Diffusional Flux + Convectional Flux + Migrational Flux

$$N_F = -D\nabla C + UC - zuFC\nabla\phi \qquad \text{Equation 3.5}$$

where D is the diffusion coefficient of the species of concentration C, u is the mobility, F is the Faraday constant, ϕ the electrostatic potential, and U the fluid velocity.

A material balance for a small volume element leads to the differential form of the law of conservation

$$\frac{dC}{dt} = -\nabla N_F + R' \qquad \text{Equation 3.6}$$

R' represents a bulk reaction term, the heterogeneous rate constant for production of species. In electrochemical systems, restriction of reaction to an electrode allows the neglect of R. To a good approximation, the electrolyte is electrically neutral,

$$\sum zC = 0 \qquad \text{Equation 3.7}$$

(neglecting the diffuse part of the double layer very near the electrode surface).

The current density in an electrolyte is due to the motion of charged species;

$$i = F \sum zN \qquad \text{Equation 3.8}$$

The flux relation involves the fluid velocity, which must be determined from the Navier-Stokes equation:

$$\rho\left\{\frac{dv}{dt} + U\nabla v\right\} = -\nabla p - \mu\nabla^2 U + \rho g \qquad \text{Equation 3.9}$$

where μ is the electrochemical potential, and the continuity equation

$$\nabla U = 0 \qquad \text{Equation 3.10}$$

Both experimentally and in practice, the electrolyte has an excess of an indifferent species. This has several consequences:

i) the physical properties of the electrolyte and pH are governed mainly by the nature and concentration of the indifferent electrolyte,

ii) the electrolyte conductivity is enhanced, and most important here,

iii) the contribution of migration to the mass transport of the main species may be neglected.

Indifferent electrolytes typically encountered in academic studies are potassium hydroxide for ferri-ferrocyanide systems and sulphuric acid for the copper sulphate system. Such conducting electrolytes are added in relatively high concentrations.

For the reaction of the species of interest, it is then permissible to neglect the contribution of ionic migration to the flux of reacting ions, and

Total Flux = Diffusional Flux + Convectional Flux

$$N = -D\nabla C + UC \qquad \text{Equation 3.11}$$

substituting into equation 3.6 yields

$$\frac{dC}{dt} + U\nabla C = D\nabla^2 C \qquad \text{Equation 3.12}$$

which is sometimes referred to as the equation of convection diffusion. Similar equations apply to convective heat transfer and mass transfer in non-electrolytic solutions, and since these fields have been studied in some detail, it is often possible to apply the results to electrochemical systems. Equally, electrochemical systems often provide an elegant instrument to test results which are too complex for precise analysis.

3.2.2 The Diffusion Layer

The concept of a diffusion layer is generally considered essential to the understanding of convective transport problems. Normally, due to a relatively small value of the diffusion coefficient, concentration differs from its bulk value in only a thin region near the electrode surface. In this region, known as the diffusion layer, fluid velocity is small, and diffusion is the predominant means of mass transport. In principle, there are as many diffusion layers as there are ions present, but discussion will be restricted only to the ions of interest, e.g. metal ions in the case of cathodic metal deposition.

Experimentally, it is found that the concentration increases approximately linearly over a substantial part of the diffusion. Following an approach by Nernst in 1904[53], it is sometimes assumed (as a first approximation) that this linearity extends to the outside of the diffusion layer, the slope $\frac{dC}{dy}$ remaining constant until a point is reached where the concentration is that of the bulk solution. The concentration profile is then represented by the dotted line of Fig. 3.3a which defines the fictitious Nernst diffusion layer, δ_N, which is typically tenths to thousandths of a millimetre. In reality, the concentration distribution is of the form indicated by the full line, which asymptotically approaches the bulk concentration, rendering the real diffusion layer thickness an ill-defined quantity.

According to the Nernst approach, an expression for the mass transfer rate may be written as

$$j = D\left\{\frac{dC}{dy}\right\}_S = \frac{D\{C_B - C_S\}}{\delta_N} \qquad \text{Equation 3.13}$$

and recalling equation 3.8, the mass transfer rate may be written in terms of a current density

$$j = \frac{i}{zF}(1-\eta_C) = \frac{D\{C_B - C_S\}}{\delta_N} \qquad \text{Equation 3.14}$$

This last equation indicates that the mass transfer rate is proportional to $C_B - C_S$ and inversely proportional to δ_N. The former term may be regarded as a driving force for diffusion, while δ_N is a form of resistance offered by the diffusion layer to mass transfer.

Thus, the Nernst model has the advantage of offering a compact explanation of diffusional mass transfer. The great weakness of the Nernst approach is that it offers no fundamental computation of δ_N from the general properties of the system under study. To accomplish this, a more rigorous approach is necessary involving a consideration of hydrodynamics and convective diffusion. A proportionality constant K_L may be defined

$$j = K_L (C_B - C_S) \qquad \text{Equation 3.15}$$

where K_L is generally known as the mass transfer coefficient+, a form of notation often used in chemical engineering.

3.2.3 Convective Diffusion

In practice, convection is always present in electrochemical systems, involving either free (natural) convection in the absence of artificial solution or electrode movement, or combined free and forced convection in its presence. The presence of a bulk, hydrodynamic flow due to convection results in a considerable enhancement in mass transfer (as measured by the limiting current density, i_L) with a consequent lowering in δ_N. Table 3.1 illustrates this by listing i_L and δ_N values for various hydrodynamic systems[46].

+ Ibl[54] has recommended that K_L be renamed the heterogeneous diffusion rate constant, an apt but rather unwieldy assignment.

Regarding the mathematical solution of mass transfer problems, the presence of hydrodynamic flow causes complications, as it renders the relevant differential equations non-linear, and less readily soluble, if at all.

A further complication is that the Navier-Stokes equation

$$U\nabla C = D\nabla^2 C - \frac{dC}{dt} \qquad \text{Equation 3.16}$$

applies strictly to laminar flow, but may be carefully applied to turbulent flow after subjection to an averaging process, yielding a pseudo steady state relation

$$U\nabla C = (D + D\text{turb})\nabla^2 C \qquad \text{Equation 3.17}$$

where Dturb represents an enhanced diffusion due to the random motion of eddies, and is itself dependent on fluid velocity.

In general, four methods are available for evaluating the rate of convective mass transfer, and these may be applied separately, or in combination:

i) exact solution of the Navier-Stokes equations together with a simultaneous solution of the convective diffusion mass transfer equation,

ii) solution of the hydrodynamic and mass transfer boundary layer equations.

iii) empirical correlation of experimental data, and

iv) analogy between mass, heat and momentum transfer.

The aim of the solution is to express the rate of mass transfer in terms of a mass transfer coefficient, which is related in turn to certain physical properties of the electrode/electrolyte system, (equation 3.15).

It has already been noted that method i) is beset with difficulties for practical systems, but the other methods will now be examined.

3.3 Boundary Layer Theory.

At the surface of a solid phase boundary, such as an electrode, the flow velocity is zero due to friction, but increases progressively with distance from the boundary until the value in bulk solution is reached (Fig. 3.3b). The zone near the phase boundary is referred to as the (Prandtl) hydrodynamic boundary layer, by analogy with the diffusion layer. In contrast to the latter, however, the hydrodynamic boundary layer of notional thickness δ_{Pr} extends much further from the electrode, as indicated in Fig. 3.3.

Boundary Layer Theory assumes that perpendicular to the boundary, both the above layers are very thin, allowing a considerable simplification of fundamental differential equations, facilitating their solution for simpler geometries and flow conditions. In fact, the theory is very restricted in that it provides a wholly satisfactory treatment only for laminar flow; the situation for turbulent flow becomes exceedingly complex.

In some cases, however, it is possible to adopt reasonable empirical relationships for velocity distribution. Care must be taken though not to apply the theory indiscriminately. In particular, it is sometimes not appreciated that the boundary layer equations, e.g. von Karman's integral approach -, are themselves simplifications of the Navier-Stokes equations for the very specific case of a surface in an unbounded free stream.

The extension of boundary layer theory to turbulent flow via von Karman equations must also be undertaken carefully, since once again a specific, idealised system, flow through a pipe, is employed to render complex differential equations determinate.

In practice, Boundary Layer Theory[14] has been successfully applied to simple systems including natural convection at vertical electrodes[55], and forced laminar convection along a plane electrode[56].

3.4 Dimensionless Group Analysis.

This generally forms the most satisfactory approach to practical problems, but in contrast to the boundary layer theory, it does not allow a complete calculation of the quantities of interest. A complete description of the theory of dimensionless group analysis is to be found elsewhere[21], but the relevant features will be summarised.

The approach starts from the premise that the mathematical relationship between the variables involved in the problem must be dimensionally correct, i.e. the relation does not depend on the fundamental units of measurement. It is then possible to combine the variables into dimensionless groups. This combination may involve the normal mathematical operations of division and multiplication, or the variables may be raised to some power. The actual formation and choice of dimensionless groups is somewhat arbirtrary, being governed largely by convenience.

This procedure considerably simplifies data treatment by reducing the number of variables to be handled. According to the π theorem of dimensional analysis*, the number of dimensionless groups is given by the number of original variables minus the number of fundamental dimensions.

Table 3.2 defines and lists the more common dimensionless groups used in electrochemical engineering. It may be noted that some of these groups are related, for example (Sh) = (St) (Re)/(Sc).

Dimensionless groups may be correlated by a least squares analysis

e.g. $(St) = a(Re)^b(Sc)^c$

where a, b and c are constants.

---

* This rule occasionally fails in exceptional cases.

Such an expression is referred to as a mass transfer correlation in dimensionless group format.

While some of the merits of the technique have already been mentioned, certain disadvantages arise. Firstly, the application of dimensionless group analysis presupposes that the number and nature of relevant variables is known initially. Secondly, a wide range is necessary for each of the variables, preferably over at least a decade, in order to achieve a mathematically sound correlation, and this is not always possible experimentally; e.g. the Schmidt Number, (Sc) may be changed by altering the temperature, but this has attendant experimental problems, and even so, a large change in temperature has a relatively small effect on (Sc). Thirdly, and related to the first point, the selection of a variable in forming a dimensionless group is not always obvious initially. For example, the characteristic dimension in the Reynolds number, (Re) may be an electrode height, length or indeed an interelectrode distance or other dimension. In the case of a concentric rotating cylinder system, with mass transfer to the inner cylinder, one may consider the inner cylinder diameter or the interelectrode distance to be characteristic lengths (see later), while for a parallel plate system, one may consider the interelectrode distance or the electrode length. In practice, the characteristic distance used is generally the same as that used in defining (Sh). It should also be realised that a dimensionless group correlation is by nature an averaged expression over a certain range of experimental conditions, hence extrapolation outside this range should be undertaken with caution. Related to this, an exact prediction of mass transfer under specific conditions should not be expected. Indeed, it is often considered that a good correlation will result in a predicted value ± 20% of the experimental value.

A review of the use of dimensionless group analysis in electrochemical systems is provided by reference 60.

3.5 Mass, Heat and Momentum Transfer Analogies.

Analogies between mass transfer and heat transfer or momentum transfer may provide useful guidelines for the development of electrochemical mass transfer correlations. Such analogies may be used, if valid, to predict temperature and concentration profiles, and therefore heat and mass transfer rates from measurements of friction factors (see later). Additionally, they may be used to extrapolate available data to new operating conditions, different boundary conditions, or different geometries, and to rationalise empirical expressions.

Unfortunately, many semi-empirical expressions for mass transfer conflict with each other, and are not fully supported by the often scant data.

The most well known analogy between mass transfer and momentum transfer is the empirical Chilton-Colburn[61] relation.

$$j = (St)\,(Sc)^{\frac{2}{3}} = \frac{f}{2} \qquad \text{Equation 3.18}$$

Like this relation, heat and mass transfer correlations derived from empirical, or semi-empirical models also have the form

$$j = (St)\,(f,Sc) \qquad \text{Equation 3.19}$$

Such functions are often complicated in their appearance, but always yield a simple asymptotic solution of the form

$$(St) = a\,f^{b}\,(Sc)^{c} \quad (\text{Limit}, (Sc) \rightarrow \infty) \qquad \text{Equation 3.20}$$

for large (Sc).

Table 3.3[62] lists the asymptotic form for some of the more commonly used of such expressions.

This table shows a great variance in the predicted value of mass transfer (as indexed by (Sh)). In particular, (Sh) varies either as $f/2$ or f, and as $(Sc)^{\frac{1}{3}}$ or $(Sc)^{\frac{1}{4}}$. These asymptotic expressions are related to the basic assumptions made in developing corresponding turbulence models for the viscosity (see previously). Thus an exponent of $\frac{1}{2}$ on f arises from the use of the von Karman hypothesis (Appendix 1) for velocity profiles, while the exponent on (Sc) follows from the assumption that eddy diffusivities will vary as the $\frac{1}{3}$ or $\frac{1}{4}$ power of distance from the electrode into the fluid.

Hubbard and Lightfoot[62] have shown that the Chilton-Colburn analogy is adequate for most practical purposes, and in fact this, or rather a modified version of it, has been successfully used to describe the R.C.E.

3.6 Electrochemical Mass Transfer Reactions.

In studies of mass transfer, electrochemical reactions present several advantages over purely chemical reactions (e.g. solids dissolution) including the following:

i) in the case of an electrochemical redox reaction, neither the solution composition nor the solid surface change appreciably

ii) the measurement of a limiting current avoids the necessity of tedious weighings

iii) in addition to providing a rapid evaluation of mass transfer, continuous monitoring is also possible.

While providing an accurate, convenient and reproducible technique for the elucidation of mass transport characteristics, electrochemical studies are somewhat constrained by the choice of reaction; the following criteria must normally be applied:

i) the reaction is diffusion controlled

ii) the reaction is well established

iii) the reaction is stoichiometric, and takes place at 100% current efficiency

iv) a limiting current density may be readily defined and measured experimentally

v) analytical control should be straightforward and the solution must be stable.

The above criteria are well met by a variety of reactions, but the two which have received most attention are:

i) the ferrocyanide/ferricyanide redox reaction

$$[\mathrm{Fe(CN)_6}]^{4-} \overset{e^-}{\rightleftharpoons} [\mathrm{Fe(CN)_6}]^{3-} \qquad \text{Equation 3.21}$$

and

ii) the cathodic deposition of copper

$$\mathrm{Cu^{2+}} + 2e^- \longrightarrow \mathrm{Cu} \qquad \text{Equation 3.4}$$

It has already been noted than an excess of indifferent electrolyte is desirable, and this is normally provided by sodium or potassium hydroxide (1 to 3 molar) in the case of the first reaction, and sulphuric acid (1 to 2 molar) in the second. Thus the redox reaction is stable in high pH media, while the copper deposition reaction is stable in low pH media.

The redox reaction is normally conducted on a platinum or fresh nickel electrode for good reversibility and reproducibility, although some workers[66] have misguidedly employed copper, a practice which has been criticised[100]. The copper deposition reaction is less critical regarding substrate, but is best carried out on a fresh copper surface. It is interesting that the reverse reaction viz. anodic dissolution of copper has not received more attention, although Robinson[68] has pointed to some problems with surface passivation and poorly defined limiting currents.

In the case of the ferrocyanide/ferricyanide redox reaction, oxygen is normally removed from solution, especially when using a nickel electrode, in order to avoid passivation, and also to avoid the possibility of oxygen reduction or evolution which might interfere with the primary reaction.

The ferrocyanide/ferricyanide system is somewhat prone to slow photolytic decompsotion[69,70]:

$$[\mathrm{Fe(CN)_6}]^{4-} + \mathrm{H_2O} \underset{\text{dark}}{\overset{\text{light}}{\rightleftharpoons}} [\mathrm{Fe(CN)_5}]^{3-} + \mathrm{CN^-} \qquad \text{Equation 3.22}$$

$$\mathrm{CN^-} + \mathrm{H_2O} \rightleftharpoons \mathrm{HCN} + \mathrm{OH^-} \qquad \text{Equation 3.23}$$

but in practice, the use of freshly prepared solutions stored in darkness eliminates this problem[71].

A fundamental practical difference between the two reactions for mass transfer studies is that in the redox reaction no change in electrode surface roughness is expected, rough deposits may develop at or near the limiting current, given sufficient time. Normally, such rough deposits are to be avoided, as they give rise to an enhanced mass transfer. As is demonstrated in this Thesis, however, the controlled deposition of metal powder on a rough electrode provides the basis for a powerful, high mass transfer reactor. A recent and interesting example of the disadvantage of roughness development is provided by Chin et al.[72], who studied a rotating cylinder with a skimmer plate, in order to simulate a continuous moving sheet electrode. These authors were forced to use a nickel electrode and a redox reaction, as in the initial copper deposition reaction, copper powder particles became detached and damaged the soft PTFE skimmer plate, resulting in electrode contamination.

Both the ferrocyanide/ferricyanide reaction and the copper deposition reaction have been employed in a whole variety of mass transfer investigations. Table 3.4 provides a compilation of examples of the former reaction, while Table 3.5 provides examples of the latter reaction. Where possible, the Schmidt Number has been calculated, and it may be seen that, in the absence of glycerol additions and varying only temperature and concentration, (Sc) varies within a small range. It may be noted that the majority of mass transport studies in Tables 3.4 and 3.5 have been carried out at or near room temperature, presumably for convenience.

It is also noteworthy that in the study by Viswanathan et al.[72] the concentration of indifferent electrolyte, potassium hydroxide, was kept relatively low, at 0.01M, to avoid chemical reaction with the glycerol which was, in some cases, present at rather high concentrations.

While the two reactions discussed above have been employed in by far the majority of electrochemical mass transport studies, other reactions have been satisfactorily used including:

i) cathodic deposition of silver from acid solutions[87,103]

$$Ag^+ + e^- \longrightarrow Ag \qquad \text{Equation 3.24}$$

ii) oxygen reduction on silver[78] or monel[88,89] electrodes

$$O_2 + 2H_2O + 4e^- \longrightarrow 4OH^- \qquad \text{Equation 3.25}$$

iii) quinone reduction at a silver electrode[78]

$$C_6H_4O_2 + 2H^+ + 2e^- \longrightarrow C_6H_4(OH)_2 \qquad \text{Equation 3.26}$$

iv) anodic dissolution of copper into phosphoric acid[68,90]

$$Cu - 2e^- \longrightarrow Cu^{2+} \qquad \text{Equation 3.27}$$

v) cathodic reduction of m-nitrosulphonic acid[93,94,99], and

vi) the iodine/iodide redox reaction[115,116]

$$I_2 + 2e^- \longrightarrow 2I^- \qquad \text{Equation 3.28}$$

It is obviously desirable to know the transport properties of an electrolyte for mass transfer studies, including the density, dynamic viscosity and diffusion coefficient of the electroactive species. Sources of such data exist in the literature for copper sulphate/sulphuric acid[106,108,109,101], ferro/ferricyanide/potassium hydroxide[111] and ferro/ferricyanide/sodium hydroxide[110].

The importance of choosing and having available correct physical properties of electrolytes is illustrated by the work of Wragg & Ross who studied ionic mass transfer for fully developed streamline flow in annuli[100,107]. Originally[100], these authors presented a correlation

$$(Sh) = 1.76 \quad (Re)(Sc) \quad d_e/L^{\,0.33} \qquad \text{Equation 3.29}$$

the experimental data thus falling some 10% below the values predicted by the theoretical relationship

$$(Sh) = 1.94 \quad (Re)(Sc) \quad d_e/L^{\,0.33} \qquad \text{Equation 3.30}$$

This discrepancy vanished[107] when more reliable values of D[106] were used.

French and Tobias[101] have presented an expression for cupric ion diffusion coefficients in the copper sulphate/sulphuric acid system, based upon previous data by Wilke et al.[112]. This expression gives the product of ν and D as a serial function of each component of concentration, but is thought by Arvia et al.[106] to give values which are too high, especially at elevated viscosity.

The latter authors determined the diffusion coefficient of cupric ions with a rotating disc electrode technique, and the viscosity, over a temperature range of 18-40°C. The following Einstein-Stokes relationship was found

$$\frac{D\eta}{T} = (2.23 \pm 0.37) \times 10^{-10} \mathrm{cm}^2 \text{ poise/s}^{0}\mathrm{K} \qquad \text{Equation 3.31}$$

With good approximation, the ratio was found to be independent of viscosity and temperature. A similar relationship was also found for the diffusion of ferro and ferricyanide ions in sodium hydroxide solutions[110].

Following the above discussion of ν and D, it is now relevant to briefly examine how these important parameters may be measured experimentally.

The determination of dynamic viscosity and fluid density are relatively straightforward, the former being via a U-tube or rotating cup viscometer and the latter via a standard density bottle.

Several possibilities exist, however, for the determination of D , which may be divided into:

1. optical methods[117], including Gouy Diffractometry, Wavefront, Schering and Hologram Interferometry,

2. porous diaphragm diffusion,

3. electrical conductivity,

4. electrochemical methods,[118] including
   - $it^{\frac{1}{2}}$ curves at constant potential,
   - ip measurement from peak voltammetry,
   - chronopotentiometry, and
   - i_L measurement at a R.D.E.

The last mentioned technique is generally considered to be the most satisfactory, in view not only of the convenience, but also the precision. A rigorous equation exists for the limiting current in terms of D and other parameters, allowing ± 1% or better accuracy.

3.7 Mass Transfer Correlations and Data Treatment.

Various possibilities exist for the treatment and presentation of mass transfer data. In the majority of cases, three dimensionless variables are involved, and to avoid a three dimensional plot, one of the variables may be plotted against a function of the other two. For example, in the case of the expression

$$(St) = a\ (Re)^b (Sc)^c \qquad \text{Equation 3.32}$$

rearranging

$$(St)(Sc)^c = a\ (Re)^b \qquad \text{Equation 3.33}$$

and taking logs,

$$LN\ (St)(Sc)^c = LN\ a + b\ LN\ (Re) \qquad \text{Equation 3.34}$$

If $(St(Sc)^c$ is plotted against (Re) on log-log axes, a straight line is obtained, of slope b.

Ideally, it may be considered that the most satisfactory way of arriving at a correlation of the above type, i.e. determining a, b and c, might be to perform a multiple regression on the dimensionless variables (see Appendix 1). This is only acceptable, however, if a sufficient range exists for each variable, and the experimental data is sufficiently precise. If only a small number of data sets is available, omission of just one of these may appreciably change the appearance of the computed correlation. The great advantage of this method, however, is that there is no prior assumption of the values of a, b or c, and a multiple regression will yield measures of the significance of, and confidence in the computed values of these constants.

A less satisfactory method of data treatment is to assume a given value of a, b or c and perform a simplified regression. For example, if in the above expression it is assumed that $a = 0.0791$,

$$(St)(Sc)^{c} = 0.0791(Re)^{b} \qquad \text{Equation 3.35}$$

or more severe, if it is also assumed that $c = 0.644$,

$$(St)(Sc)^{0.644} = 0.0791(Re)^{b} \qquad \text{Equation 3.36}$$

Here, the regression has been confined to two variables,(St) and(Re).

The above two techniques may yield quite different results, as is illustrated by the data of Robinson and Gabe concerning mass transfer of cupric ions to an inner rotating cylinder in a concentric geometry[68,83]. At first,[83] the 49 sets of data were regressed assuming a dependence on the form

$$(St) = a(Re)^{b}(Sc)^{-0.667} \qquad \text{Equation 3.37}$$

i.e. the value of c was assumed to be $-\frac{2}{3}$, according to a semi-theoretical analysis[68,113]. $(St)(Sc)^{0.667}$ was then used as a dependent variable against Re in a two dimensional least squares analysis. The resulting correlation

$$(St) = 0.169(Re)^{-0.34}(Sc)^{-0.67} \qquad \text{Equation 3.38}$$

may be contrasted with the one obtained by a three dimensional least squares regression of (St), (Re) and (Sc),

$$(St) = 0.0791(Re)^{-0.31}(Sc)^{-0.59} \qquad \text{Equation 3.39}$$

Similar occurences in the literature may be quoted. Thus Raja et al.[114] studied mass transfer of ferro/ferricyanide ions to an inner stationary copper[+] cylinder in the presence of a rotating outer cylinder. These authors assumed a relationship of the form

$$(St)(Sc)^{\frac{2}{3}} = a(Re)^{b}, \qquad \text{Equation 3.40}$$

the experimental data being fitted to

$$(St)(Sc)^{\frac{2}{3}} = 0.041(Re)^{-0.37} \qquad \text{Equation 3.41}$$

One of the most extensive mass transfer studies is provided by the work of Eisenberg, Tobias and Wilke[57,58] who studied mass transfer of ferro/ferricyanide ions to an inner rotating nickel cylinder. These authors employed a wide range of each of the variables (St), (Re) and (Sc), and the indices b and c could be obtained by crossplotting, on log-log axes, (St) and (Re) at constant (Sc), and (St) against (Sc) at constant (Re). The authors also studied chemical dissolution of organic acids, and computed an overall correlation

$$(St)(Sc)^{-0.644} = 0.0791(Re)^{-0.30} \qquad \text{Equation 3.42}$$

[+] The use of copper electrodes for investigations involving ferro/ferricyanide has already been criticised[100].

In contrast to this extensive study, the data of Krishna and Jagannadharaju[74] is most meagre, but an attempt was still made to correlate the results by an expression of the form

$$(St)(Sc)^{\frac{2}{3}} = a(Re)^{b}, \qquad \text{Equation 3.40}$$

resulting in

$$(St)(Sc)^{\frac{2}{3}} = 1.83(Re)^{-0.42} \qquad \text{Equation 3.43}$$

It is of interest to note that a series of articles[129] has recently been published describing a range of regression analyses relevant to mass transfer correlations. These analyses are performed by packages for a programmable desk top calculator, and include for the following cases:

$$Y = a_o + b_oF(X) \qquad \text{Equation 3.44}$$

$$Y = a_o + b_oX_1 + c_oX_2 \qquad \text{Equation 3.45}$$

$$Y = a_o + b_oX_1 + b_1 X_2 + b_2X_3 \qquad \text{Equation 3.46}$$

where Y is the dependent variable and X_1, X_2 and X_3 are independent. Of particular interest here is the programme concerning

$$Y = a_o + b_oX + c_oX2, \qquad \text{Equation 3.47}$$

as this is the form of equation obtained by taking logs of

$$(St) = a\ (Re)^{b}(Sc)^{c}$$

$$LN(St) = LNa + b\ LN(Re) + c\ LN(Sc) \qquad \text{Equation 3.48}$$

of $$Y = a_c + b_cLNX + c_oLN\ X_2, \qquad \text{Equation 3.49}$$

The programme referred to above has the advantage of offering correlation coefficients not only for the above case, but also

$$Y = d_o + d_1 X_1 \qquad \text{Equation 3.50}$$

$$Y = e_o + e_1 X_2 \qquad \text{Equation 3.51}$$

and provides a correlation coefficient for all of the above equations. The user can then determine which correlation is most suited to the experimental data.

3.8 Measurements of Mass Transfer.

It would be inappropriate to close a chapter on mass transfer without briefly describing methods of measuring it.

3.8.1 Direct Methods

The simplest measurement technique is to obtain a polarisation curve on the electrode geometry of interest, under controlled conditions and to read the limiting current density, i_L directly as the plateau, for a known reaction (see previously) in the presence of supporting electrolyte.

Problems arise, however, if the mass transfer rate is very high, the degree of mass transfer control is only partial, or the electrode does not experience a uniform current density. In such cases, the plateau is ill-defined (Fig. 3.4). Such results are often found in e.g. the fluidised bed electrode reactor.

An interesting compromise occurs in obtaining cathodic polarisation curves for metal deposition, in that the rate of increase in potential must be great enough to discourage significant roughness formation near the limiting current, but low enough to produce steady state values of current (sse Experimental work).

If it is desired to estimate limiting currents under a wide range of conditions, a useful technique is to set a controlled potential corresponding to the plateau and read the resulting steady state (limiting) current directly (see Experimental work).

If it is required to measure localised mass transfer rates or mass transfer distribution, two techniques are available:

1. point 'indicator' electrodes[205,206] may be used, mutually isolated, and the electrode of interest. These may be polarised to a predetermined point (as above) and the individual currents measured.

2. the electrode of interest may be segmented[104,236,237], and a similar approach adopted.

Both of the above techniques are extremely valuable for stationary electrodes, but for rotating assemblies, complications are caused by the need to insulate separate rotating electrodes, and to supply each with current.

By maintaining the potential of a bulk electrode at a fixed value, it is also possible to study the gradual transition in mass transfer with changing cell conditions such as concentration, electrode or solution movement, or electrode area (experimental work), i.e. the dynamic response of the cell.

A disadvantage of the use of probes is that the hydrodynamics at the probe tip may not be the same as at the bulk electrode. Indeed, unless care is exercised, the presence of the probe may even alter the hydrodynamics at the electrode.

Interferometry[238] and Brenner's freezing method[239] have also been used to measure mass transfer. Interferometric methods are based on the difference between the refractive index of the electrolyte in the diffusion layer and in the bulk solution, which gives rise to optical fringes. Brenner's freezing method involves sudden cooling of the electrolyte layer near the cathode, with subsequent chemical analysis of the solid.

While both of these methods provide valuable means of laboratory measurement, they require high skill, and complicated experimental arrangements.

3.8.2 Indirect Methods

It is possible to deliberately study a reaction above the limiting current when a secondary reaction, e.g. the hydrogen evolution reaction (HER) or deposition of a second metal takes place. If allowances are then made for the secondary reaction current, the limiting current may be calculated. For example, the amount of hydrogen liberated may be measured, or its separate polarisation curve obtained. This is fraught with error, however, as the HER is catalysed by impurities, and the partial currents for HER and metal deposition may not sum to the observed current. Additionally, it will be seen that gas evolution can provide an effective means of augmenting mass transfer.

The method developed by Ettel, Gendron and Tilak[180] was aimed at in situ determination of mass transfer coefficients in natural and forced convection electrowinning cells. It involves introduction of a noble metal tracer ion into the electroplating solution, e.g. silver and codeposition of the silver with the metal of interest, e.g. copper or nickel. The important assumption is that silver will plate out at its maximum (limiting) current density.

Chemical analysis of the resulting deposit gives a value for the limiting current density for silver via Faraday's laws. From this value and the known or measured concentration of silver ions in the electrolyte K_{Ag^+} may be calculated from

$$K_{Ag^+} = \frac{i_{L_{Ag^+}}}{FC_{Ag^+}} \qquad \text{Equation 3.52}$$

It is important to appreciate that the mass transfer has been measured under actual operating conditions which may be well below the limiting current for copper.

The assumption of mass transfer deposition of Ag^+ was verified by a rotating disc electrode study.

One problem is that chloride ions must be removed from the electrolyte, prior to applying the technique, due to the removal of silver from solution by insoluble silver chloride formation. Also, if the tracer concentration is very low, its value may change during an experiment. The presence of addition agents in concentrations (typically 10^{-3}M) greater than the silver also presents a problem with regard to complex formation and non-mass transfer controlled deposition.

The method also assumes uniform distribution of silver with increasing deposit thickness.

The method has been found useful for mapping of mass transfer distribution in commercial cells[180,182], where $K_{Cu^{2+}}$ may be derived from

$$K_{Cu^{2+}} = K_{Ag^+} \left\{\frac{D_{Cu}}{D_{Ag}}\right\}^n \qquad \text{Equation 3.53}$$

$n = \frac{2}{3}$ for turbulent flow and $\frac{3}{4}$ for natural convection. Hence the D value for both silver and copper must be known.

CHAPTER FOUR

MASS TRANSFER AND ELECTRODE GEOMETRY

The literature has been reviewed with respect to the effect of reactor geometry on electrochemical mass transport. Generalised correlations of data are provided for the various geometries, which may be broadly divided into static and dynamic electrode systems. Bulk and particulate electrodes are considered, and the relationships between the various geometries are discussed.

4. Mass Transfer and Electrode Geometry

4.1 General

A whole range of geometries has been studied in the literature, but only some of the more common and potentially useful ones will be considered here. It is interesting, philosophically, to note that several of the common geometries encountered are related. Consider, for example, the case of concentric cylinders. If axial flow is superimposed, annular flow results, and if the inner cylinder radius is negligible, there is effectively pipe flow. If, however, both radiae become infinite, the parallel plate goemetry exists. In addition, if one or both of the cylinders is rotated, the rotating cylinder electrode is the result. In the case of the parallel plate, employing circular discs, a specific example is provided by the rotating disc electrode. The example of a concentric rotating inner cylinder of very small diameter is effectively provided by rotating wire electrodes. Turning to particulate beds, a sufficient axial velocity may transform the packed bed electrode to the fluidised bed electrode, a situation which could be remedied by restraining the bed.

In addition to the above considerations, the electrode of interest may or may not be directly responsible for direct mass transfer enhancement, as in the case of rotating electrodes. Here the use of turbulence promoters or fluidised inert beads for flat plate electrodes could be quoted; the recently introduced static disc electrode in a uniformly rotating field (SDERF)[249] provides another example.

4.2 Static, Bulk Electrodes

This group includes annular geometry, and parallel plate electrodes, both systems having received a lot of attention in the literature.

4.2.1 Parallel Plates

The parallel plate geometry is a classical arrangement, whose origins are centuries old. The vertical arrangement of parallel plates, in absence of pumped flow, is used not only throughout industrial electroplating, but also in battery technology and in chlorine producing cells. Here, a multitude of plates are assembled in a 'filter press' arrangement, and the possibility arises of bipolar operation.

The general hydrodynamic treatment of widely spaced parallel plate cells is described by Ibl[42], Marchiano[119], and Pickett[120]. While widely spaced horizontal plates have been studied hydrodynamically[42,121,12 there would appear to be little industrial use of such geometry, due presumably to the problems of gas locking on the underside of the above electrode, and the difficulty in removing such electrodes from the cell.

Commonly, in electroplating for example, mass transfer at parallel plates in an open system is augmented by one or more of a series of techniques including reciprocating the cathode, air sparging and solution pumping. The enhancement of mass transfer by cathodic gas evolution and/or roughness is discussed in later sections(4.7 and 4.8).

The case of pumped flow through a parallel plate geometry has been extensively studied, and is a favourite with many electrochemists. Despite this background of knowledge, and its ease of construction, the geometry is of little interest commercially, with the important exception of the Monsanto process for the production of adiponitrile[123]. Mass transfer to these electrodes is complicated by such variables as gas scouring, leading edge effects, and high current density edge effects. The situation has been treated in detail by Pickett[120].

One special case of the narrow gap parallel plate geometry is provided by the capillary gap cell of Beck, which has a typical gap of $\geqslant 0.02$ cm. Such a geometry has been revived recently[223] in the academic literature, but it is difficult to foresee widespread large scale use of such cells in view of the severe mechanical requirement of creating and maintaining uniform capillary gaps over extensive areas.

One of the most satisfactory treatments of flow through parallel plate cells is provided by Eisenberg[125], who pointed out that flow is laminar in the majority of practical cases.

Another method of enhancing mass transfer at parallel plates is by means of turbulence promoters, these commonly taking the form of sheet plastic netting placed against or near the electrode surface. Such a promoter may also be utilised to act as a porous inter-electrode spacer.

The electrode itself may form its own turbulence promoter as in the case of metal mesh electrodes. One can also envisage a cell-dividing membrane acting in a similar fashion.

An interesting variation on parallel plate cells is provided by the 'Swiss Roll Cell' of Ibl and Robertson[126,127,128]. This is a long, thin parallel plate system which is coiled up on itself, with the anode and cathode separated by a sheet turbulence promoter. One cannot help noticing the similarity between this recent development and the older du Pont 'extended surface area' cell[130,131].

A recent study of the effect of turbulence promoters in rectangular section flow has been undertaken by Leitz & Marincic[76], who studied elevated promoters of rectangular, triangular and circular section. A series of such promoters was located at various positions on and away from the electrode surface. Separate mass transfer correlations were offered for each circumstance, taking the general form :

$$(Sh) = a(Sc)^{1/3}(Re) \left\{\frac{d_e}{\Delta l}\right\}^{c} \qquad \text{Equation 4.1}$$

where Δl is the promoter spacing.

The most favourable mass transfer promoter used was one of detached circular section.

Table 4.1 provides a summary of mass transfer correlations, in both laminar and turbulent flow, for parallel plate systems.

Practical parallel plate cells suffer from both a hydrodynamic and a mass transfer entrance effect; Pickett & Ong[99] have studied this situation experimentally and the following conclusions were drawn:

1. for fully developed laminar flow, the average mass transfer coefficient is well represented by an equation of the form

$$(Sh) = 2.54 \left[(Re)(Sc)\left\{\frac{d_e}{L}\right\} \right]^{0.3} \qquad \text{Equation 4.2}$$

2. for turbulent flow proper, fully developed mass transfer is obtained after about twelve equivalent diameters; the mass transfer may then be represented by

$$(Sh) = 0.023(Re)^{-0.8}(Sc)^{1/3} \qquad \text{Equation 4.3}$$

which may be rewritten in terms of the Chilton-Colburn analogy

$$j_D = \frac{(Sh)}{(Re)(Sc)^{1/3}} = 0.023(Re)^{-0.2} \qquad \text{Equation 4.4}$$

For shorter electrodes, with $0.10 < \left\{\frac{d_e}{L}\right\} < 5.95$

$$(Sh) = 0.125(Re)^{2/3}(Sc)^{1/3}\left\{\frac{d_e}{L}\right\}^{0.2} \qquad \text{Equation 4.5}$$

3. for developing laminar flow, an empirical equation is

$$j_D = 0.96(Re)^{-1/2}\left\{\frac{d_e}{L}\right\}^{-0.05}\left[1 - \left\{\frac{H}{X} + L\right\}^{3/4}\right]^{2/3} - \left\{1 + \frac{H}{L}\right\} \qquad \text{Equation 4.6}$$

Here the cell length, X = L + H and the Reynolds number is defined in terms of this; H = hydrodynamic entrance length.

4.2.2 Annulus

It has already been noted that one could regard a concentric cylindrical arrangement, with flow through the annular gap as a special sort of parallel plate reactor. In addition, this geometry represents the situation of flow through a rotating cylinder electrode reactor with the cylinder stationary. In common with the flat parallel plate system, the annular geometry also suffers from leading edge complications. Space restrictions will probably dictate that practical reactors based on these geometries will have an inherent leading edge section.

Therefore, flow is often introduced into such a reactor via a dispersion system, typically a perforated plate or porous frit, to encourage premature flow development.

Table 4.2 summarises mass transfer correlations obtained with an annular geometry.

In comparison with the flat parallel plate geometry, the annular geometry has the following specifications:

i) no edge effects are present, as at the edges of a flat plate,

ii) it can normally be assured that limiting conditions will occur on the inner cylinder.

The most extensive study of this geometry has been by Ross and Wragg[100], who considered mass transfer under various flow regimes, hydrodynamic and mass transfer entrance lengths, and annular radius ratios. The data from this study could be correlated by

$$(Sh) = 1.76 \left\{(Re)(Sc)\left\{\frac{d_e}{L}\right\}\right\}^{1/3} \qquad \text{Equation 4.7}$$

for turbulent flow.

The constant = 1.76 was slightly sensitive to the annular radius ratio.

4.3 Porous Electrodes

The term 'porous' is used here to describe electrodes which permit flow through their interstices, rather than merely over the surface as with 'bulk' electrodes.

Hydrodynamics and mass transfer characteristics of porous matrices have been extensively studied in the fields of geology and civil engineering, in addition to chemical engineering; much of the resultant information may be transferred to electrochemical engineering.

Porous electrodes may consist of a continuous physical surface, such as a metallic mesh or stack of meshes, or may comprise a 'packed bed' of discrete particles such as graphite flakes or metallic rods, spheres or chips. Additionally, an arrangement of filaments may be used, for example steel wool. Earlier electrodes comprised particles of a conducting material, but continued developments in the metallisation of polymers and ceramics have encouraged the adoption of a whole new range of matrices, including metallised polymer foams. Thus the porous electrode may be a regular array as, for example, in the case of expanded metal mesh or packed spheres, or a completely random three dimensional array such as a packed bed of carbon particles or a metallised foam.

Flow through porous electrodes are attractive because they provide intimate contact between the electrolyte and electrode, with an extensive electroactive area per unit volume. Their use has been somewhat restricted, however, by lack of available design information, the relatively large ohmic drop across the electrode (which renders uniform potential control difficult), and the possibility of blocking porous sites by metal or insoluble electrolyte impurities.

Recently, Newman and Tiedemann[133] have attempted to review the field of porous electrodes. Various cell configurations are possible with respect to both electrolyte and current flow, as indicated in Fig. 4.1.

Mass transfer to these electrodes is complicated by the nature and extent of porosity, which is often difficult to measure or reproduce. In practice, the geometry of a porous electrode is characterised by both porosity and shape factors. The inherent problems here may be readily seen when it is considered that even perfect spheres may pack differently, with a porosity of 0.260, 0.4 or 0.478 for close, random or simple cubic packing.

Dispersion, both axially and radially may also have a marked effect on mass transfer, and non-uniformity of geometry may lead to channelling.

The overwhelming advantages of flow through electrodes have been appreciated for some time. Thus Liebenow[134] (1897) showed how mass transfer could be enhanced by flow, while Heise[135] (1939) has discussed the application of flow through porous electrodes to inorganic and organic redox reactions, and metal recovery.

The development of theoretical models to describe porous electrodes has lagged behind experimental trials, and a whole variety of assumptions have been necessary in developing models, including

1. steady operation with uniform flow,
2. one dimensional geometry,
3. first order kinetics, with no side reactions,
4. negligible ohmic loss in the solid matrix,
5. constant electrolyte conductivity,
6. negligible diffusion and dispersion in the direction of fluid flow,
7. negligible mass transfer resistance within the pores.

Certain papers by Sioda[80,137-140] have shown an increeasing awareness that the overall reaction rate is determined more by electrode mass transfer limitations within the porous regions than by electrode kinetics.

Bennion and Newman[136] have emphasised the importance of mass transfer in a packed carbon bed used to treat dilute solutions of metal.

Potential distribution under limiting current conditions has been discussed by Bennion and Newman[136] and Sioda[139]. The distribution of electrode potential over a porous electrode not only influences electrode kinetics, but also determines the suitability of an electrode for operation within a narrow range of potential.

Sioda[141-143] and Wroblowa and Razumney[144] have extended previous analyses of electrode operation to include axial dispersion. In many practical cases, however, the axial flow rate is sufficiently high to justify ignoring the effect of axial dispersion.

Due to the large number of relevant parameters, and the difficulty in characterising the porous electrode and its hydrodynamics, there exists no single correlation to predict mass transfer.

Wilson and Geankoplis[145] have proposed⁺

$$\frac{\epsilon \, d_p K}{D} = 1.09 \left\{\frac{\nu d}{D}\right\}^{1/3} \qquad \text{Equation 4.8}$$

for $(Re) = \frac{U}{a\nu} = 5 \times 10^{-4}$ to 15

in the case of shallow packed beds, while Colquhoun-Lee and Stepanek[146] have proposed

$$\frac{K}{aD} = 0.62 \left\{\frac{\nu}{D}\right\}^{1/3} \left\{\frac{U}{a\nu}\right\}^{0.61} \qquad \text{Equation 4.9}$$

for $14 < Re < 1400$.

+ See Table 4.3 for a definition of terms.

Mass transfer to a metallised polyurethane foam 'macroreticular' electrode has been studied by Tentorio and Casolo-Ginelli[147]. While insufficient results were obtained to formulate an overall correlation, the following equations were derived for two types of resin. For 10 pores per inch,

$$(Sh) = 0.99(Sc)^{0.32}(Re)^{0.53} \qquad \text{Equation 4.10}$$

and for 20 pores per inch,

$$(Sh) = 0.95(Sc)^{0.33}(Re)^{0.49} \qquad \text{Equation 4.11}$$

Mass transfer correlations for various porous electrodes are summarised in Table 4.3.

4.4 Fluidised Bed Electrodes

If electrolyte flow through a particulate packed bed exceeds a certain value, the particle/electrolyte system behaves in a fluid-like manner, and the electrode is termed a fluidised bed. Such systems are widely used and are becoming well established in non-electrochemical fields, such as catalytic fluidised bed reactors in chemical processing, and fluidised coke furnaces in fuels technology.

As long as fluidisation is maintained by the use of a fluid velocity within a certain range, the result is an increase in mass transfer compared to a static bed, while the active electrode surface area is still relatively high. In addition, fluidisation may produce one or more of the following benefits:

1. removal of electrode gas,

2. alteration of the electrodeposit quality.

The particles of the bed may be conducting, e.g. metal spheres or graphite flakes, or inert as in the case of ballotini glass spheres or alumina particles. In addition, the properties of each are displayed by, for example, metal coated glass beads. In all cases, the particles are in intermittent contact with each other and the current feeders.

Pioneering work on fluidised bed electrodes (FBE's) was performed by Backhurst[148,149] and extended by Fleischmann et al.[150,153] and Goodridge et al.[154,155]. Early work resulted in the filing of a patent by the National Research & Development Corporation[156].

Further work has been performed by Kreysa et al.[87] who compared non-conducting and conducting beds, Carbin and Gabe[85,86] who studied mass transport and deposit morphology in a metallised glass bead bed and Walker and Wragg[157,158] who studied the FBE as an electrochemical reactor.

Bipolar (as opposed to monopolar) fluidised beds are a more recent development, their characteristics having been described by Goodridge[159].

In the case of monopolar beds, all particles behave in either a cathodic or anodic manner, whilst in the case of bipolar beds, each individual particle exhibits both anodic and cathodic sites.

As in the case of packed bed electrodes, various geometries are possible, as indicated in Table 4.13 which summarises mass transport studies using the FBE.

Commercial development of the FBE may be said to have been started by studies of Warren Spring Laboratory[164] and CJB Developments Ltd.[165], the latter workers having produced pilot plant evaluations.

Refinements and further investigations have given rise to the development of two markedly different FBE systems, the Chemelec cell[166] developed by the Electricity Council at Capenhurst, and the FBE reactor developed by AKZO[167] Zout Chemie at Hengelo, Netherlands. Both of these FBE designs will be discussed in the next chapter.

4.5 Dynamic, Bulk Electrodes

Previous sections have concerned the effect of electrolyte flow on mass transfer at continuous and porous electrodes (with the possibility of fluidisation). An obvious alternative method of mass transport enhancement is to employ a dynamic electrode, and the possibilities may be inclusive of reciprocating, vibrating or rotating the electrode in question, in any dimension.

In practice, the most useful dynamic electrode systems are those which have a regular geometry and a regular movement, giving rise to a uniformly accessible electroactive area and a reproducible, predictable mass transport. Foremost here are rotating electrodes, such as the rotating disc and cylinder, where mass transport to a given size electrode may be controlled by the rotational speed, and predicted by reliable mass transport correlations.

The use of rotating electrodes in specific fields has been reviewed by Narasimham and Udupa[255] in the case of electrodeposition of metals, and Deslouis and Epelboim[256] in the case of recent electrochemical kinetic studies.

Fig. 4.2 attempts to classify the various simple rotating electrode geometries and their developments.

Much of our present knowledge and understanding of hydrodynamics and mass transport has arisen from studies of rotating systems, notably the rotating disc electrode (RDE) geometry. Additionally, the use of small rotating electrodes such as the RDE has served to increase our appreciation of fundamental aspects of electrochemistry such as reaction kinetics and mechanisms.

The particular success and widespread use of the RDE as a powerful electrochemical tool may be ascribed to its merits.

1. It is one of the very few geometries for which an explicit version of the Navier-Stokes equation (Ch. 3) may be formulated.

2. There is uniform mass transport accessibility to the electrode.

3. The RDE provides a well defined laminar flow regime over a wide range of rotational velocity.

The success of the RDE is well illustrated by the number of papers and monographs/texts[59,250-253] devoted to it. More recently, the basic R.D.E. has been modified to provide more sophisticated geometries such as the rotating ring disc electrode[254] (R.R.D.E.). Here, a coaxial ring outside the central RDE is maintained at a constant independent potential.

The rotating disc geometry has also been extended by the use of multiple discs stacked on a common rotating shaft in a 'jukebox' fashion[81], and by the use of rotating disc cells employing capillary gaps and known as the "electrochemical pump cell" (Chapter 5).

While the RDE is undoubtedly a favourite geometry in electrochemical studies, other rotating systems including the wire[257], sphere[258], cone[259] and ring[260] have been employed, particularly for hydrodynamic voltammetry studies at solid electrodes[261,118]. Table 4.5 compares mass transfer correlations for various rotating geometries.

It is interesting to note that a rotational flow may be induced around an electrode by rotating either an impeller, the counter electrode, or the electrolyte vessel itself. Examples of impeller enhanced mass transfer are given in Chapter 5. Rotation of the counter electrode is illustrated in the case of the RDE by Matsuda et al.[249] and the monopolar electrochemical pump cell[223] (Chapter 5). Jordan[262] has described induced rotational flow at stationary disc and cone electrodes by movement of the containing vessel (the 'rotating bucket'). Matsuda[249] and Bucur and Bartes[264] have recently presented a stationary disc electrode in a uniformly rotating field (the S.D.E.R.F.).

There has been relatively little work on rough rotating disc electrodes; indeed, normally great care is taken to polish the electrode surface before use.

4.6 The Rotating Cylinder Electrode

4.6.1 Introduction

In marked contrast to the number of publications involving the RDE, there have been comparatively few concerning the RCE. There are several possible reasons for this discrepancy:

1. the RDE is essentially a laminar flow geometry over wide experimental ranges of rotation speed, and this is often considered to be preferable for electrokinetic studies,

2. there exists an exact and rigorous solution of mass transfer to the electrode, based on theoretical as well as experimental studies,

3. construction and preparation of a disc may be regarded as somewhat easier than that of a cylinder,

4. the relatively low mass transport to a RDE restricts current requirements to a low level, allowing the use of modest power supplies.

The RCE, however, is particularly well suited to high mass transfer or turbulent flow studies, and to studies involving metallographic examination of extensive surface areas. Unlike the RDE [10,315], the RCE has a substantially uniform primary and secondary current density distribution (Chapter 5), and is thus well suited to mass transport studies, especially those involving controlled potential.

Due to the relatively low value of the critical Reynolds number (Chapter 2), practical RCE's are invariably turbulent devices, and this provides very effective mixing inside the cell (Chapter 6).

It has already been noted (Chapter 2) that a wide variety of flow conditions are possible in a concentric geometry, depending on the rotation sense of each electrode, and the presence of axial flow. In practice, the most convenient geometry for metal deposition is a rotating inner cylinder and stationary (counter electrode) outer cylinder, with or without axial flow. Due to severe turbulence around the inner cylinder, practically encountered axial flows have negligible effect on mass transfer to the working electrode.

The general subject of mass transfer to the RCE geometry has been ably reviewed by Gabe[25] (1974), and the present discussion will attempt to update and extend this.

4.6.2 Theoretical Aspects

The derivation of a mass transport relation for the RCE normally begins with the definition of a velocity profile in the vicinity of the electrode, for a given flow regime. Normally, a parabolic profile is assumed in laminar flow (Chapter 2), while the profile in turbulent flow is considerably more complicated.

Three analyses have appeared for the laminar flow case[90,91,95], the first two[90,91] having assumed a linear velocity profile, while the third[95] is considerably more involved.

Gabe and Robinson[90] have derived the following relationship:

$$(Sh) = 0.64 \left[(Re)(Sc) \frac{r_I}{M} \left\{ \frac{(1 + r_I{}^2/r_0{}^2}{1 - r_1{}^2/r_2{}^2} \right\} \right]^{1/2} \qquad \text{Equation 4.12}$$

where $M = 2 \pi r_I$

Kimla and Strafelda[91] employed a somewhat different velocity profile to derive:

$$(Sh) = 0.38 \left[(Re)(Sc) \frac{r_I}{(1 - r_1{}^2/r_2{}^2)M} \right]^{\frac{1}{2}} \qquad \text{Equation 4.13}$$

Comparison of the two above equations reveals a similar dependence of (Sh) on (Re) and (Sc), although the empirical and geometrical constants are quite different.

Mohr and Newman[95] have attempted to treat the system using rotating cylindrical coordinates, rather than static cartesian ones, and have incorporated various refinements, leading to

$$(Sh) = 1.0174\,(Pe)^{1/3}\left[1+0.1966\left\{\frac{L}{r_I}\right\}(Pe)^{-1/3} + 0.618(Pe)^{-1/3} + 0.009949\left\{\frac{L}{r_I}\right\}^{2} - 0.1548\,(Pe)^{-2/3} + \text{---}\right] \qquad \text{Equation 4.14}$$

$$\text{where } (Pe) = \beta L^{2}/2D \qquad \text{Equation 4.15}$$

Comparison of equations 4.12 and 4.13 shows that the latter serves to apply a number of higher order 'correction' terms, which Mohr and Newman[95] consider to represent $\leqslant$6-7% error.

The absence of a rigorous, well established theoretical treatment of the velocity field for the rotating cylinder geometry may be contrasted with the case for the RDE, which has been amply documented[59].

Turbulent Flow

As has been pointed out in Chapter 2, the case of turbulent flow is much more difficult to treat. A three zone model (Chapter 2) is normally employed.

Gabe and Robinson[80] have attempted a simplified treatment, and applying a Deissler type eddy viscosity component:

$$(Sh) = (2b)^{1/3}\,(Re)^{2/3}\,(Sc)^{1/3} \qquad \text{Equation 4.16}$$

The treatment cannot yield a value for the constant $(2b)^{1/3}$, which is a function of cell geometry and surface roughness. Substitution of a relation due to Theodersen and Regier[9] in equation 4.16, however, yields a value of 0.079,[45] which has been confirmed experimentally[6,7,20,79].

4.6.3 Experimental Work

Early experimental work on the RCE was largely empirical, with little attempt being made to correlate the reaction rates with experimental parameters. In addition, the geometry of the RCE was not always well defined.

The effect of rotation speed upon mass transfer rate was first studied by Brunner[265] who found that the diffusion layer thickness decreased with the 2/3 power of rotational velocity. Only qualitative conclusions may be drawn, as the effects of electrolyte properties and rotor diameter were not considered.

Other workers[266-269] showed that the rotational velocity exponent had a value 0.67-0.70.

Much of the earlier work was confused by the study of non-mass transport (or only partially-mass transport) controlled reactions, or additional effects such as gas evolution, poorly defined flow, or development of surface roughness.

X

Roald and Beck[175] studied the dissolution of rotating magnesium rods in hydrochloric acid. At low acid concentration, n was 0.71 in the relationship

$$\text{rate} = \text{constant} \quad U^{n} \qquad \text{Equation 4.17}$$

but at higher acid concentrations, the rate of dissolution became independent of rotational speed. This effect was attributed by the authors to additional agitation by hydrogen gas.

Similar effects were obtained by King et al. who studied several corrosion and dissolution reactions[270-277]. It was later concluded that at high rotational speeds, chemical reaction control predominates over mass transport control, and reaction becomes independent of rotational speed.

King and Catheart[273] indicated that the mass transfer rate was proportional to the power of the diffusion species of the reactant raised to 0.7.

Early electrodeposition studies at a RCE have been reviewed by Narasimhan and Udupa[255].

1. Laminar and Laminar + Vortex Flow

The majority of experimental mass transfer studies have involved turbulent flow, but several authors have studied preturbulent regimes mainly by chemical rather than electrochemical techniques.

Flower, MaCleod and Shahbenderian[16] have examined mass transfer to the inner cylinder of a long annulus, for laminar + vortex flow with superimposed axial flow. Air was used as the medium ($(Sc) \approx 1$). MaCleod and Ruess[39] in a later (1975) paper, extended the previous study to a liquid medium ($(Sc) \simeq 2000$). In these studies, the mass transfer was found to be insensitive to axial velocity, over the experimental range of variables, i.e.

$$(Re)_{axial} = \frac{2(r_0 - r_I)\, U_{axial}}{\nu} = 33 \text{ to } 100 \qquad \text{Equation 4.18}$$

$$(Ta) = \frac{U\,(r_0 - r_I)^{3/2}}{\nu\ r_0^{\frac{1}{2}}} = 209 \text{ to } 680 \qquad \text{Equation 4.19}$$

In the studies involving air[16], the correlating expression involved $(Sh) \propto (Ta)^{0.52}$, but the later study[39] relating to liquid was consistent with $(Sh) = 1.91(Ta)^{0.7}$, which approximated to the Eisenberg et al. expression . In comparison to this last work, however, the annular gap was much smaller and the annulus much longer:

$$\frac{r_0 - r_I}{r_0} \simeq 0.238 \quad ; \quad \text{c.f. W.E.T., } 0.17\text{–}0.9$$

This agreement with Eisenberg et al's work is rather surprising, as the MaCleod et al. studied laminar+Vortex rather than the turbulent flow of the former!

MaCleod and Ruess[39] also noted that

1. the mass transfer coefficient at the outer (stationary) cylinder was higher than that at the inner (rotated) one, and,

2. the overall simultaneous mass transfer coefficient for both walls of the annulus was intermediate between that at the individual walls.

The correlating equation employed involved a dependence of (St) on both the annular radius ratio and the annular gap

$$(St) \propto (Re)^{-0.3} \left\{\frac{r_0}{r_I}\right\}^{-0.3} \left\{\frac{r_0 - r_I}{r_0}\right\}^{+0.05} \qquad \text{Equation 4.20}$$

Kataoka et al[278-281] have also studied mass transfer in an annular system with rotation of the inner electrode, the later studies employing electrochemical techniques. In particular, a recent study[278] has described the interrelation between axial movement of Taylor vortices and periodically varying rates of transfer at the outer fixed cylinder by localised mass transfer measurement. Copper deposition was employed as the mass transfer controlled reaction, at copper electrodes. It was shown that axial flow resulted in movement of the Taylor vortices, with subsequent damping of vortex formation, leading to a 30-50% lowering of the average mass transfer.

The first systematic mass transfer correlation was deduced by Eisenberg, Tobias and Wilke[57,58](1953). These authors studied several reactions at an inner rotating cylinder:

1. dissolution of benzoic acid in aqueous solutions
2. anodic oxidation of ferrocyanide ions
3. cathodic reduction of ferricyanide ions

and correlated their results by the empirical equation:

$$j_D' = (St)(Sc)^{0.644} = 0.079\,(Re)^{-0.30} \qquad \text{Equation 4.21}$$

Arvia, Carrozza and Marchiano[77] (1964) studied copper deposition from acid sulphate solutions and the ferro/ferricyanide reaction at an inner rotating cylinder, and chose to correlate their data by

$$(Sh) = 0.217(Re)^{3/5}(Sc)^{1/3} \qquad \text{Equation 4.22}$$

In an earlier study[82], (1962) Arvia and Carrozza studied copper deposition to a static outer cylinder, in which the inner, anodic cylinder rotated. The results could be correlated by

$$j_D' = 0.0791\,(Re)^{-0.\ 3} \left\{\frac{d_I}{d_0}\right\}^{-0.70} \qquad \text{Equation 4.23}$$

In the second study[77], the authors suggested that the above two equations could be resolved into a single correlation

$$(Sh) = 0.217\,(Re)^{3/5}(Sc)^{1/3} \left\{\frac{d_I}{d_0}\right\}^{2/5} \qquad \text{Equation 4.24}$$

Robinson and Gabe also studied deposition of copper to an inner rotating cylinder, and at first correlated their results by[68,83]:

$$(St) = 0.169(Re)^{-1/3}(Sc)^{-2/3} \qquad \text{Equation 4.25}$$

This equation was arrived at by assuming the exponents on (Re) and (Sc) to be -1/3 and -2/3. An improved treatment of the data via a three dimensional least squares regression gave[68,83]:

$$(St) = 0.079(Re)^{-0.31}(Sc)^{-0.59} \qquad \text{Equation 4.26}$$

showing the sensitivity of the empirical constant to the value of the (Re) and (Sc) exponents.

Matic, Lovrecek and Skansi,[282] have presented a paucity of data on ferricyanide reduction, choosing to correlate their results in a similar manner to Arvia et al.[77]. It should be noted that in this particular study geometry was not particularly well defined, and the rotational velocities used involve the laminar and vortex regime as well as turbulent flow.

Several authors have obtained results in accordance with the Eisenberg et al. correlation[57,58]. Ellison and Schmeal[283] studied corrosion of a mild steel rotating cylinder in concentrated sulphuric acid, finding that the reaction rate could generally be expressed by this equation.

Postlethwaite et al.[284] studied cathodic reduction of m-nitrobenzene sulphonic acid to metalinic acid at a turbulent inner rotating cylinder. It was found that the data were in reasonable agreement with the Eisenberg et al equation, but were correlated better by

$$j_D' = (St)(Sc)^{0.644} = 0.21(Re)^{-0.4} \qquad \text{Equation 4.27}$$

Kar et al.[285] studied the corrosion of a rotating copper cylinder in saline solution, and obtained results in keeping with the Eisenberg et al. equation.

Krishna et al.[286] studied the ferro/ferricyanide redox reaction, and chose to correlate their results by

$$(Sh) = 1.83(Re)^{0.58}(Sc)^{1/3} \qquad \text{Equation 4.28}$$

Ramaraju et al.[287] studied the cathodic reduction of ferricyanide at a stationary copper cylinder lying coaxially outside a rotating copper anode. The results were described by:

$$j_D' = (St)(Sc)^{2/3} = 0.041 \left\{\frac{d_o U}{\nu}\right\}^{-0.37} \qquad \text{Equation 4.29}$$

There has been relatively little work published in the literature on mass transfer to rough rotating cylinders, although such electrodes may achieve particularly high rates of reaction. In addition, the study of rough electrodes is relevant to corrosion and chemical dissolution and to electrochemical production of metal powders.

Theodorsen and Regier[9] studied the effect of surface roughness on cylinders and discs revolving in air, and their results have been described in Chapter 2. It was found that for turbulent flow above a certain critical Reynolds Number and in the presence of saturated roughness, the drag on a cylinder could be independant of (Re), and a function of relative roughness, e/d,

$$\frac{1}{\sqrt{f/2}} = 1.25 + 5.76 \log_{10}\left\{\frac{d}{e}\right\} \qquad \text{Equation 4.30}$$

for Reynolds numbers exceeding

$$(Re)_{crit} = (11.8\ d/e)^{1.18} \qquad \text{Equation 4.31}$$

Makrides and Hackerman[191] studied the corrosion of mild steel in 2N HCl solutions, with and without additions of $FeCl_3$ and organics, and obtained results in accordance with Equation 4-30. These authors attributed the results to developed roughness of the corroding specimens.

In an attempt to study the effect of well-defined, time independent roughness at rotating cylinders, Kappesser, Cornet and Greif[190] studied oxygen reduction at knurled monel cylinders in oxygenated saline solutions. Four cylinders were employed, a smooth one, $e = 3 \times 10^{-5}$ cm and three of differing peak to valley roughness, $e = 7.3 \times 10^{-3}$, 4.1×10^{-2} and 1.52×10^{-2} cm, which for the 6.35cm diameter cylinders gave d/e ratios of 72×10^{5}, 416, 156, and 87. The roughness took the form of staggered diamond knurls.

The results were in reasonable agreement with equation 4.30. Thus this equation has been tested by roughness produced by sandcasting[9], corrosion[191] and machining (knurling)[190] and by measurements of drag reduction in air[9], corrosion rates of steel in acid solutions[191], and oxygen reduction at a monel electrode in saline solution[190]. It is important to note that the equation is only valid for saturated roughness. Whereas sand casting, abrasion and corrosion produce a wide dispersion of roughness, difficult to measure experimentally and to reproduce, knurling offers a much more suitable means of producing a well-defined, measurable, uniform roughness.

While the Kappesser et al. study deliberately avoided the complications of time dependent roughness and characterisation of roughness, this is of importance in production of metal powder surfaces by electrodeposition, and has been studied in this Thesis.

A recent paper by Sedahmed et al.[317] has considered the effect of a non-saturated, bulk roughness viz. the effect of finning (or slotting). These authors chose the cathodic reduction of ferricyanide at a nickel plated copper cylinder. Six cylinders were used, a smooth one, and five finned. Fins were produced by cutting longitudinal rectangular grooves, such that the peak to valley height, e, was 0.0185, 0.026, 0.053, 0.059 and 0.075, giving d/e ratios of 54, 38.5, 18.9, 17 and 13.3 for the 1 cm. diameter, 9 cm. high electrodes. 28 grooves were machined in each electrode giving a common fin spacing of 0.5 mm, and a 0.5 mm. width.

Comparisons were made with the Eisenberg et al. equation for smooth cylinders, and a 30-140% increase in mass transfer was found depending on (Re) and fin height. The enhancement may be attributed to vortex promotion in the fin space, increase in electroactive area and the increase in hydrodynamic shear. The correlating equation (average deviation 5%) was

$$j_D' = (St)(Sc)^{0.644} = 0.714(Re)^{-0.39}\left\{\frac{e}{d}\right\}^{0.2} \qquad \text{Equation 4.32}$$

Thus this equation is in marked contrast to Kappesser et al's work [190] where a dependence of j_D' on Re disappeared after an initial value of (Re). In Sedahmed et al's work, however, the j_D' factor was dependent on (Re) even for (Re) greater than the value given by equation 4.31. This indicates the importance of the pattern of roughness as well as the relative value of roughness, the fin geometry representing a two dimensional roughness only. It would be interesting to see a study aimed at this aspect, attempting to take into account surface area changes.

While this Thesis concerns enhancement of mass transfer for the purpose of electrowinning and electrorecovery of metals, it is appropriate also to remember that mass transfer reduction is important, for example in controlling corrosion or chemical dissolution. It is interesting in this context to consider recent work on the R.C.E. by Sedahmed et al.[73] . These authors have studied electrochemical mass transfer controlled reactions in the presence of drag reducing polymers, typically 0-I00 ppm. polyethylene oxide ('polyox') at smooth cylinders in turbulent flow, finding:

$$(St)(Sc)^{0.644} = 0.0475\,(Re)^{-0.3} \qquad \text{Equation 4.33}$$

Nadebaum and Fahidy[290] have studied mass transfer to a R.C.E. with the electrode surface continuously wiped by spring loaded 'Teflon' skimmer blades. A theoretical analysis lead to :

$$(Sh) = \frac{2}{\pi}\left[\frac{w}{I-\frac{wx}{2\,r_I}}\,(Re)(Sc)\right]^{I/2} \qquad \text{Equation 4.34}$$

where w=number of wiper blades, each of thickness x, and (Sh) and (Re) were defined as :

$$(Sh) = 2\,i_L\,r_I/\,z\,F\,D\,C$$

$$(Re) = 2\,U\,r_I/\nu$$

An experimental investigation of the cathodic reduction of ferricyanide or oxygen in the range 820 > (Re) > 7I,000 yielded results in ± 5°/o agreement with the above for (Sc) > 200. The relative enhancement in mass transport compared to a simple rotating cylinder was given by :

$$\frac{K_L\ \text{wiped}}{K_L\ \text{unwiped}} = 8.05\ w\,(Re)^{-0.2}(Sc)^{0.I44}. \qquad \text{Equation 4.35}$$

when the thickness of wiper blades was small. This factor was typically 2 to 8 under the experimental conditions. At very high rotation rates, the factor

$\rightarrow 1$, and the wiper blades would offer negligible improvement in mass transport. An alternative method of enhancing performance would be an increase in rotation speed. For the particular cell studied, the limiting current density at 5 rad s^{-1} (wiped) could be attained at 50 rad s^{-1} (unwiped). The equivalent rotation rate required to achieve wiped mass transport rates was expressed as :

$$\frac{\omega'}{\omega} = 19.7\, w^{0.715} (Re)^{-0.286} (Sc)^{0.206} \qquad \text{Equation 4.36}$$

For the particular case $(Re) = 1250$ and $(Sc) = 1237$, equation 4.36 reduced to :

$$\omega' = 11.5\, w^{0.715} \omega^{0.714} \qquad \text{Equation 4.37}$$

indicating that the relative increase in rotation rate necessary (without blades) became smaller as the number of blades increased.

4.7 Surface Roughness

It has been known for some time that increased surface roughness of an electrode can appreciably enhance mass transfer. The effect is normally two-fold, being due both to an increase in the electroactive surface area, and to improved hydrodynamic shear at the electrode, the rough surface acting, in a sense, as its own turbulence promoter.

This two-sided effect presents problems to quantitative investigations,as it is often difficult to measure the true area.

As noted in an earlier chapter, surface roughness also lowers the critical Reynolds Number for the onset of turbulence, for a given set of conditions.

Rough electrodes may exhibit markedly different mass transfer behaviour to their smooth counterparts, as evidenced by different mass transfer correlations. A striking example is provided by the rotating cylinder electrode, where mass transfer to the smooth electrode may be described by, for example, the Eisenberg, Tobias and Wilke[57,58] correlation

$$(St) = 0.079\ (Re)^{-0.30}\ (Sc)^{-0.644} \qquad \text{Equation 4.23}$$

while mass transfer to a rough electrode may be described by

$$(St) = \left[1.25 + 5.76 \log_{10} \left\{\frac{d}{e}\right\}\right]^{-2} (Sc)^{-0.644} \qquad \text{Equation 4.11}$$

according to the work of Kappesser, Cornet and Grief[190], and also Makrides and Hackerman[191].

Here $\frac{d}{\varepsilon}$ is the relative roughness of the electrode i.e. the ratio of cylinder diameter to surface roughness.

It may be readily seen that the rough cylinder correlation describes the Stanton Number as independent of the Reynolds Number, and dependent only on the relative roughness, while the smooth cylinder correlation describes a Stanton Number which is quite strongly dependent on (Re), varying as $(Re)^{-0.30}$. It may be noted that for convenience, any area increase has been disregarded in the above correlation.

The characteristic surface roughness, ϵ, may be readily defined for uniform machined cylinders e.g. in the case of knurled surfaces it may be represented by the peak to valley height. Similarly, in the case of a cylinder close wrapped with wire, the pseudo-sinusoidal profile is uniform and a constant peak to valley height may be taken. Similar considerations apply in the case of a helical, screw thread profile. Less regular roughened surfaces present more of a problem, however, as not only the degree of roughness but also the spacing of irregularities may vary widely. Such a situation exists for abraded grit blasted or sand cast surfaces, electrodeposited metal powder surfaces or corroded metal electrodes. In such cases, it is also much more difficult to account for the increased true surface area. One possibility is to use the root mean square (RMS) surface roughness, as revealed by microsectioning or surface profile stylus instruments.

The effect of surface roughness on natural convection at vertical plate electrodes has been studied by Fouad and Zatout[192].

One of the earliest electrochemical studies of roughness was carried out by Ross and Badhwar[264] who used cylindrical depressions in a flow through tube.

Fouad et al.[188] have studied the interesting case of mutual enhancement of mass transfer by the combined effects of surface roughness and gas evolution. The effect of both hydrogen evolution and oxygen evolution on the rate of mass transport of ferricyanide and ferrocyanide ions to nickel electrodes was investigated. The electrodes used were of similar size, and roughened by horizontally machined parallel grooves, as in the above investigation[192]. Comparison was made with a smooth (mirror polished) electrode. The surface roughness was such that peak to valley height was 0.1, 0.25 and 0.45 mm., while the corresponding peak to peak width was 0.52, 1.03 and 1.03 mm. for the three rough electrodes. In the case of hydrogen evolution, the results showed that the increase in mass transfer due to roughness was higher than the increase in the surface area of the electrode, the extra effect being attributable to the projections giving rise to increased hydrodynamic shear, leading to an increase in the number of active sites for gas nucleation. In addition, as the surface roughness exceeded the mean diffusion layer thickness, the effective cross section for convective diffusion was increased, giving rise to possible turbulent wakes downstream of the projections due to separation of the hydrodynamic boundary layer. In the case of oxygen evolution, however, mass transfer decreased with increasing roughness except at low degrees of roughness and high gas discharge rate. This puzzling contradiction may perhaps be explained by gas bubbles obscuring the electrode by clinging to the lower side of protrusions. This effect is likely to be much higher for oxygen than for hydrogen, as the oxygen gas bubbles are large and the rate of increase of size with current density is greater than in the case of hydrogen.

The more practical case of rough metal powder deposits has been reviewed by Ibl[193]. Of particular relevance to the studies in this Thesis is the paper by Ibl and Schadegg[193] concerning the development of powdery copper deposits at rotating discs. This study, aside from this Thesis, represents one of the very few studies concerning roughness development at an initially smooth electrode.

4.8 Gas Evolution

4.8.1 Introduction

Mass transfer to an electrode may be appreciably enhanced by gas bubbles agitating the adjacent electrolyte. A well established example is the use of air sparging in electroplating baths for the production of smooth metal plate, which enables higher current densities to be employed, with correspondingly higher plating rates. Such sparging may also serve to enhance deposit quality, and thoroughly mix the bath, although the latter is not always a desirable feature if sediment is dispersed and entrained in the deposit. A further problem is the possibility of foaming. A great advantage of practical air sparging is that the necessary equipment and plumbing is 'low level technology' and may be readily added to an existing electroplating bath, whether this is in a metal finishing/electroforming installation or an electrowinning tankhouse. Indeed, Kuhn[168], and Houghton and Kuhn[169] have argued that the use of flat plate electrodes together with suitable air sparging should be satisfactory for the majority of high mass transfer metal recovery applications for some years to come. This rather simplistic notion takes no account, however, of other important considerations including:

i) the requirement of continuous metal production e.g. in powder form,

ii) the high floor space and extensive wiring and plumbing necessary with conventional parallel plate-in-tank cells,

iii) the large inventory of metal in the cells and in solution, which is especially important for precious metals,

iv) the need for an electrode geometry which facilitates selective metal deposition via the use of controllable electrode potential,

v) the lack of automation and the control possible when using an array of separate plate-in-tank cells.

One other attendant problem with air sparging is the risk of deleterious oxidation of species in the electrolyte, e.g. ferrous ions being oxidised to ferric, although this may be overcome, albeit at greater expense, by the use of an inert gas such as nitrogen.

While the introduction of gas into a cell may serve to enhance mass transfer, the effect of gas stirring is most strikingly seen in evolution of a gas actually at an electrode surface, as in the case of concurrent hydrogen evolution with metal deposition. Such a secondary reaction is indeed unavoidable to some extent, particularly in the case of highly acidic solutions or a cathode surface of low hydrogen overvoltage. In the case of copper deposition from acid sulphate solutions, however, a current efficiency of ca. 100% is normally possible for deposition by the judicious control of electrode potential. It is perhaps curious, therefore, to consider that some Faradaic energy could be deliberately wasted to evolve some hydrogen in order to increase the mass transfer. In practice, there are other considerations, apart from mass transfer enhancement. Hydrogen evolution may, for example:

i) increase the pH near the cathode, leading to e.g. codeposition of unwanted metal oxide/hydroxide

ii) cause hydrogen embrittlement of the deposit, or pitting

iii) alter the deposit morphology

iv) present an explosive or spray hazard, or cause electrolyte foaming

v) result in a lower production rate of metal, if the applied cell current is not increased

vi) dislodge metal product from the electrode

vii) lead to an increase in the effective electrolyte resistance

viii) obscure the cathode leading to an effective decrease in active surface area.

†

4.8.2. Academic Studies

The effect of gas evolution on the primary electrode reaction has been less well studied than in the case of pumped flow or rotational electrodes, but has been studied in the past 15 years by several authors including Ibl[42,175], Venczel[171], Janssen and Hoogland[172] and Fouad et al.[173] and Ibl and Venczel[174]. Ibl[170] has reviewed previous work, and formulated an expression for the mass transfer coefficient at a flat vertical plate

$$K_L = \text{constant } v^a \qquad \text{Equation 4.12}$$

where a is a constant $\triangleq 0.5$

and v is the gas evolution rate.

The same author has also compared the effects of hydrogen, oxygen and chlorine on mass transfer.

Relevant earlier studies were largely concerned with metallic corrosion via gas evolution rather than with mass transfer enhancement as such. For example, Roald and Beck[175] studied the rate of dissolution of rotating magnesium cylinders in acid solution, hydrogen being freely evolved. These authors reported that although the reaction rate depended upon $w^{0.71}$ for low acidity, it became independent of rotation speed (w) as the acidity increased and hydrogen bubbles contributed more strongly than rotation to the forced convection. Ibl and Venczel[174] also reported that in the case of hydrogen evolution at a rotating copper cylinder, the mass transfer coefficient was only markedly altered at a slowly rotating cylinder, there being little effect at the rapidly rotating cylinder.

In the case of gas sparging[42], Ibl has described the injection of gas via porous glass frit distributers at the bottom of concentric cylindrical cells. In such cells, it is interesting to note that pumping energy is governed almost entirely by the frit resistance, and hence it is independent of cell height. With such an arrangement it is perhaps strange that the pumping energy per unit electrode area may actually decrease with electrode height, until the electrolyte head presents a certain pressure drop. The use of such porous frits presents some practical problems, however, when the attendant high pumping energies and the possibility of frit blockage are considered.

One interesting and extreme effect of gas introduction in a cell is found in the case of 'gas lift' cells[176], where the buoyancy created by gas bubbles may be utilised to provide an autogenous source of pumping.

Aside from the promotion of mass transport by a foreign gas introduced into the cell or coevolution of a gas at an electrode, a third possibility is the enhancement by anodic gas bubbles[177-183], especially if anode and cathode are in close proximity. Recently, Mohanta and Fahidy[177] have studied this situation, concluding that the effect was modest, being 20% or less. Ettel and Gendron[178] have argued, however, that the effect may be substantial, averaging an increase of ca. 50% over a vertical electrode, this being particularly marked at the top of the electrode due to the rising gas wedge of anodic oxygen.

Mohanta and Fahidy[179] have produced a correlation to predict mass transfer enhancement. but this leads to a falsely low prediction[178], and is probably only of use for the one specific set of conditions pertaining to the study.

There are two current models of mass transfer at gas evolving electrodes, the hydrodynamic model of Janssen and Hoogland[172], and the penetration model of Ibl and Venczel[42,170,174]. According to recent papers by Janssen[184,185], the penetration model may be useful when coalescence of gas bubbles is a frequent occurence, while for the no-coalescence case, the hydrodynamic model is much more successful.

The combined effects of gas evolution and surface roughness may be mutually enhancing, as demonstrated in the work of Fouad and Sedahmed[188], which will be discussed in the next section.

Unlike the case of natural convection mass transfer or forced flow via pumping or electrode movement, mass transfer to gas evolving electrodes presents a newer and more difficult field of study, and this is reflected in the relatively few published papers. Very few dimensionless correlations of data exist aside from the ones mentioned above, althouoh it is understood that Vogt[189] has recently reviewed the field, deriving a theoretical, generalised, dimensionless mass transfer correlation which has been substantiated by experimental data.

4.8.3 Practical Studies

Much of the theoretical work outlined in the above section has been promoted by the need to develop gas stirred cells for the practical electrodeposition of metal, particularly for electrowinning operations, and the relevance of gas stirring to fuel cells and storage batteries.

In particular, the electrowinning of copper from acid sulphate solutions has been facilitated by both higher current density anodes and cathodes, as described by Ettel and coworkers[178,180-183]. Higher cathode current densities are now available, without powder formation, by the use of air sparging. Enhancement of natural convection mass transfer on the upper portions of vertical cathodes due to a rising anodic gas wedge (referred to in the above section) has led to improved cell design in an 'INCO'[+] copper electrowinning tankhouse[186], via the use of wedge shaped anodes, the top of the anode tapering towards the cathode with increasing vertical height.

Air sparged, vertical parallel plate arrays have also been suggested for silver recoverv from photofix solutions[187]. Problems may arise here however, due to

i) air depolarising of the silver cathode,
ii) reduction of effective electrode area by obscuring gas bubbles,
iii) foaming near the cell top, and
iv) air oxidation of the photographic fixer.

[+] INCO = International Nickel Company Ltd.

4.9 Miscellaneous Methods of Mass Transfer Enhancement

The major methods of enhancement involving electrode and/or solution movement have now been reviewed, and it remains to briefly mention others.

4.9.1 Ultrasonics and Vibration

While the application of ultrasound may appreciably increase mass transfer, it's main advantages in electrodeposition lie in the attainment of better physical and mechanical properties to deposits, including increased tensile strength, hardness and adhesion, and decreased porosity and stress[241].

The development of robust, reliable transducers has been spurred by other, sometimes related fields such as ultrasonic cleaning, but the problems of cost and noise pollution remain.

The application of ultrasonics in metal finishing has been comprehensively reviewed by Shenoi et al.[240], and Walker and Clements have reviewed electroplating aspects[241].

Unfortunately, the majority of literature in the field is not readily available, being restricted to Russian journals, although Kochergin and Vyaseleva[242] have reviewed some of this literature, and several contradictions and misconceptions are apparent.

Examples of the application of ultrasound to metal recovery problems include high current density electrowinning of copper[243], and the prevention of fluidised bed agglomeration by ultrasonic stimulation[157].

It may be noted that vibrating dropping mercury or platinum wire electrodes have been used for a long time in electroanalytical chemistry to yield reproducible polargrams.

The effect of vertical electrode vibration on copper deposition has been studied by Ismail et al. using wire electrodes at up to 48 Hz frequency and $\leqslant$8 mm. amplitude. Enhancements of up to 6x were found compared to a stationary electrode.

Longitudinal vibration at horizontal disc electrodes has been investigated by Podesta et al.[97], who powered their disc electrode with a loudspeaker voice coil. Similar enhancements of ca. 6x were found.

While no general mass transfer correlation is yet available, one has been attempted for the specific geometry of cylindrical electrodes under longitudinal vibration[245].

The effect of magnetic fields has been recently investigated in a series of articles by Mohanta and Fahidy[246]. The effect on mass transfer was only modest; a factor of ca. $\leqslant$1.25 using a magnetic field intensity of 7.95 Wb m^{-2} under natural convection conditions to vertical plates.

4.9.2 Abrasion, and Wiping/Scraping

Eisner[247] has described increase in mass transfer and deposit quality by mechanically abrading a working electrode with an abrasive belt. However, little has been heard of this patented[248] process since.

Wiped and scraped electrodes are reviewed in Chapter 6, with special reference to rotating cylinder electrodes.

5. ELECTROCHEMICAL REACTORS

This chapter reviews the subject of electrochemical reactor technology for metal deposition, with reference to the mode of operation, control and performance. Particular attention is paid to electrode geometry. Certain of the known and more novel reactor geometries are reviewed as a prelude to the presentation of the rotating cylinder electrode reactor in Chapter 6 and the remainder of this Thesis.

5. ELECTROCHEMICAL REACTORS

5.1 Introduction

Unlike chemical engineering, which has been an established discipline for almost a century, electrochemical engineering is a much younger science. This is evidenced by the widespread use of the term electrochemical 'cell' rather than the terminology of electrochemical 'reactor'. The latter implies that the cell has been designed and engineered to perform a definite duty, which may be energy production in the case of 'driving' cells, or production of material in the case of 'driven' cells. Examples of the former include batteries and fuel cells, while the latter cells are illustrated by electroplating baths and chlorine producing cells.

Electrochemical engineering is an interdisciplinary field, involving a combined consideration of the following aspects: electrochemical thermodynamics, electrode kinetics, transport phenomena, general chemical engineering, process engineering, materials engineering and design, and electrical engineering.

As with chemical engineering, it is important to consider the integration of unit processes. For example, the reactor may serve as a production unit which follows feed preparation and precedes product separation. Thus in the case of an electrochemical reactor used to produce metal powder from an acidic electrolyte, it may be necessary to control the acid strength to minimise hydrogen evolution or prevent codeposition of metal hydroxide prior to electrolysis. Following the reactor, separation of a three phase mixture of metal, gas and electrolyte may be necessary, together with further purification of the metal product or the electrolyte. As with chemical reactors, it is normally desirable to achieve as pure a product as possible and this may be encouraged by controlled potential electrolysis (as discussed later in this chapter).

The study of mass transport (Chapter 3) plays a very important part in reactor and process design, as the majority of reactions encountered in practice are mass transport controlled to some extent.

In order for electrochemical engineering to develop into a fully recognised discipline, it will be necessary to formulate generalised relationships to describe reactor design, and also to appreciate the wide spectrum of available and possible reactor types and their modes of operation.

Regarding generalised relationships, great progress has been made in the last two decades in the use of dimensionless mass transfer correlations (as described in Chapter 3), both by empirical analysis and from theoretical considerations. The best practical approach is invariably an empirical one (possibly guided by theory), however, as industrial electrolytes may behave in a very non ideal fashion due to e.g. a high degree of contamination. In addition, the use of mass transfer correlations necessitates prior knowledge or measurement of the viscosity and diffusion coefficient of the (metal) ion concerned. While the viscosity may be readily measured, data on diffusion coefficients for industrial process solutions is much more difficult to generate. Care should also be taken not to expect a mass transfer correlation to yield accurate predictions well outside the limit of variables used to formulate it in the first place.

Wagner[203] and Newmann[51] have stressed the importance also of current distribution relationships. It must be remembered, however, that reactor geometries are available where the current (and potential) distribution is substantially uniform thus avoiding the need for such complex relationships (see later).

Use of the term electrochemical engineering implies that a scale-up step is involved, perhaps from a laboratory cell through a pilot plant to a full sized industrial reactor. This also begs the question as to which particular reactor dimensions need to be increased during the scale-up operation. In general, scale-up will be a function of electrode size, surface area, and solution or electrode motion.

Table 5.1 indicates the influence of electrode size on the (average) mass transfer coefficient, according to known mass transfer correlations. It can be seen that in the case of natural convection at horizontal plates, the mass transfer is insensitive to electrode length, while in the case of turbulent rotating discs and laminar and turbulent rotating cylinders, a marked dependence on electrode radius occurs, especially for the turbulent rotating disc where k varies as $r^{0.8}$. The importance of flow regime here is readily demonstrated by the r^0 variation for a laminar rotating disc. The effect of surface roughness may also be very important, as evidenced by turbulent rotating cylinders, where the dependence on mass transfer changes from $d^{0.70}$ for a smooth cylinder, to d^0 for a cylinder of saturated roughness (see Chapter 3).

The influence of the peripheral velocity of a rotating electrode on mass transfer is also dependent on the electrode type, e.g. disc or cylinder, and on the surface roughness (Table 5.2).

There have been relatively few papers on generalised aspects of electrochemical reactor design, in contrast to chemical engineering where a whole spectrum of undergraduate and specialist texts is available. One of the few texts has been provided recently by Pickett[120]; while this provides a valuable collation of known data, the approach is perhaps unnecessarily over complicated and detailed. An excellent text on purely chemical reactor design is provided by the very readable book by Denbigh[196]; it is quite unfortunate that an analagous text is not available in the field of electrochemical engineering.

As with chemical reactors, electrochemical reactors may be divided into two distinct categories, namely continuous stirred tank reactors (CSTR) and plug flow reactors (PFR), and each of these may be employed in the batch mode or the continuous mode. In the batch mode, the reactor is charged with feed and then operated; following discharge of products this is repeated.

Advantages of this system include:

i) flexibility - the reactor conditions may be altered each time to suit various feeds or to achieve various products from the same feed, this is especially useful for a large number of small scale preparations, to avoid a multiplicity of reactors,

ii) capital cost may be much lower than that for a continuous process. For this reason, the batch system is especially useful for new and improved processes, which may then be changed over to a continuous reactor scheme at a more advanced stage of development.

Continuous processes, despite greater cost, are eventually adopted in almost all large scale industrial installations, however, as

i) labour costs may be minimised as routine charging, discharging, monitoring and control changes, may be more readily avoided due to

ii) the facility of automatic control. This in turn leads to

iii) greater constancy of reaction conditions and better quality product.

It is interesting that the choice between the above two modes is very dependent on work costs in relation to capital costs; the cost or provision of labour may be a deciding factor.

The routine electroplating of metals and plastics for decorative or protective purposes is a good illustration of a batch process, while the electroplating of wire or steel strip is a continuous process, the product of reaction (plated metal) being continuously removed from the reactor (plating bath).

There are very few truly continuous electrochemical reactors, especially in the case of the electrowinning of metal from industrial process streams. The above example of removal of metal onto plated wire and foil is unrealistic as a means of product removal, rather it is a means of obtaining the product in the required form, as in electroforming of sheet metal.

An alternative is to produce the electrodeposited metal in powder form, by judicious control of reactor feed and operating conditions. Such a product may be dislodged from the electrode by scraping, fluidised out of the reactor with the outlet electrolyte, and separated by conventional means such as centrifuge, settlement, filtration or cycloning. Alternatively, the powder product may be collected in the bottom of a suitably designed cell, and periodically withdrawn. This represents the interesting case of continuous electrochemical operation with intermittent product recovery.

The plug flow reactor is one through which there is a steady movement of the electrolyte in a given direction; no attempt is made to induce mixing, i.e. dispersion of electrolyte along the direction of flow. Examples of this type of reactor are provided by annular and rectangular channel geometries, with axial flow and flow through packed beds. The plug flow reactor results in a gradual concentration profile over the reactor, the inlet concentration profile tending progressively towards that of the outlet. Plug flow conditions are favoured by laminar flow through the reactor.

The continuously stirred tank reactor has perfect mixing of electrolyte in all directions, resulting in a completely uniform concentration within the reactor equal to the outlet concentration. Thus this extreme reactor may be viewed as a plug flow reactor with infinite dispersion in the direction of flow. The result is a stepwise change in concentration between the inlet manifold and the reactor itself. Approximations to this reactor type include vigorously agitated plate-in-tank reactors and the rotating cylinder electrode reactor (RCER). In both cases, the high degree of mixing is favoured by turbulent flow. The perfect mixing of a CSTR is destroyed by any bypassing loss: a given part of the inlet to the reactor may find its way directly into the outlet. This may be minimised in practice by judicious manifold design and positioning, together with severe agitation.

It is interesting to note that certain electrode geometry may be utilised as a PFR or CSTR depending on the electrolyte flow conditions. For example, laminar flow through an annulus approximates to PFR behaviour, as previously noted. If however, the inner cylindrical electrode is rotated, even at modest speeds, turbulence and very effective mixing ensues, and the system is transformed dramatically to CSTR behaviour. A further example is provided by flow through a packed bed electrode reactor. This PFR system will tend towards the CSTR model if the linear velocity becomes sufficient to cause fluidisation. In the case of this fluidised bed electrode reactor, however, behaviour is intermediate between that of PFR and CSTR models, (as with most reactors) and this renders mathematical modelling more difficult.

The desired reaction in an electrochemical reactor may be the anodic or cathodic one, or both. For example, in the case of the recovery of metal from industrial process streams, the important reaction is cathodic deposition of metal; the corresponding anode reaction may commonly be oxygen evolution and becomes comparable to a side reaction in a chemical reactor. In the case of metal refining, anodic dissolution of the metal to be recovered may be practised, either in the same reactor, or a preceding one. There are cases however, when the anodic reaction is beneficial here, e.g. oxygen evolution may increase the mass transfer to the cathode[177], or an unwanted, toxic species such as cyanide may be destroyed by oxidation, as described in a recent patent[197].

Often, the electrodes are separated by a membrane, which may take the form of a porous cloth, ceramic pot, or an impermeable membrane with or without ion exchange properties. Thin ion exchange membranes have a much lower resistance than thicker ceramic dividers, and are less sensitive to an increase in their thickness with scale-up. In addition they are not prone to brittle fracture like ceramics, and their ion exchange properties may be tailored, to an extent, to suit a given application. Ceramic dividers are only readily available in standard shapes and sizes which limits reactor design. Thin resin-impregnated cloth membranes, however, require adequate support and are prone to cracking on drying.

In general, the use of a cell dividing membrane may confer one or more of the following advantages:

i) choice of a separate anolyte/anode system is possible, allowing independent alteration of the catholyte, e.g. effluents containing different metals may be treated cathodically, while maintaining a constant acid anolyte,

ii) anode corrosion via aggressive catholyte species may be avoided,

iii) the products of reaction at the anode and cathode may be separated, e.g. for reasons of safety, cathodic hydrogen and anodic oxygen may be separately vented, or metal powder dislodged from the cathode may be prevented from anodic dissolution,

iv) the ion exchange properties of the membrane may be utilised for synthesis of a wanted product, or maintenance of a species, e.g. if hydrogen ions are lost at the cathode via hydrogen evolution, some degree of pH balance may be attained by the use of an acid anolyte and H^+ transfer through a cation exchange membrane to the catholyte.

It must be remembered, however, that the above advantages are gained at the expense of increased engineering complexity, increased cost of materials and increased power requirements due to the potential drop across the membrane.

5.2 Design Equations

It is important to establish the best mode of operation of a reactor. As indicated in Fig. 5.1, common examples of operation include:

i) simple batch,

ii) single pass,

iii) batch with recycle.

The characteristics of each may now be compared by considering the relationship between concentration, flow rate, time and current for both CSTR and PFR models.

5.2.1 Plug Flow Reactors

Consider the generalised plug flow reactor of Fig. 5.2a, where a steady volumetric flow rate N of electrolyte enters the reactor at a metal concentration C_{IN}, to emerge with a concentration C_{OUT}.

If the total current passed is I, an overall material balance yields

$$N\,(C_{IN} - C_{OUT}) = \frac{I}{zF} \qquad \text{Equation 5.1}$$

Ignoring dispersion due to longitudinal diffusion, the concentration may be expressed by the first order differential equation

$$\frac{dC}{dx} = -\frac{KA}{N}\,C \qquad \text{Equation 5.2}$$

which may be integrated to

$$C_{OUT} = C_{IN}\exp\left\{-\frac{KA}{N}\right\} \qquad \text{Equation 5.3}$$

where K is the averaged mass transfer coefficient. Rewriting as a ratio of the terminal concentrations

$$\frac{C_{OUT}}{C_{IN}} = \exp\left\{-\frac{KA}{N}\right\} \qquad \text{Equation 5.4}$$

and as a fractional conversion

$$f_R = \frac{C_{IN}-C_{OUT}}{C_{IN}} = 1 - \exp\left\{-\frac{KA}{N}\right\} \qquad \text{Equation 5.5}$$

The overall limiting current is given by combining equations 5.1 and 5.5

$$I_L = zFN\, C_{IN} \left[1 - \exp\left\{ \frac{-KA}{N} \right\} \right] \qquad \text{Equation 5.6}$$

Equation 5.5, for a single pass PFR, indicates that a high conversion may be achieved by the use of low throughputs. This in turn, however, results in diminishing mass transfer, especially if the flow regime changes from turbulent to laminar. A more suitable alternative is a high value of electrode area.

If, however, part of the outlet stream is recycled and mixed with fresh feed, it is possible to achieve the same degree of conversion as in single pass operation, but with higher mass transfer rates. Such a mode of operation has been considered by Pickett[198] and Wragg and Walker[199].

Fig. 5.2b shows the recycle mode, a flow rate N_R of exit solution being recycled to the inlet. The duty of the reactor is similar to single pass operation except that a greater volumetric flow rate $N + N_R$ flows through it, with a subsequently lowered inlet concentration C_R where:

$$C_R = \frac{C_{IN} + R\, C_{OUT}}{1 + R} \qquad \text{Equation 5.7}$$

and R is the recycle ratio $= \frac{N_R}{N}$

Equation 5.7 may be rewritten

$$C_{OUT} = C_R \exp\left[-\frac{K_R \quad A_R}{N + N_R}\right] \qquad \text{Equation 5.8}$$

where K_R and A_R are the modified average mass transfer coefficient and electrode surface area.

Comparison of the single pass and recycle electrode areas reveals that

$$\frac{A_R}{A} = \frac{K}{K_R} (1+R) \ln \frac{C_R}{C_{OUT}} \quad \ln \frac{C_{OUT}}{C_{IN}} \qquad \text{Equation 5.9}$$

If it is assumed that both modes operate in the same flow regime, and K is proportional to the flow rate raised to the same power β in both cases

$$\frac{A_R}{A} = (1+R)^{1-\beta} \ln \left\{\frac{C_{IN} + R\ C_{OUT}}{C_{IN} + R\ C_{IN}}\right\} \ln \frac{C_{OUT}}{C_{IN}} \qquad \text{Equation 5.10}$$

This equation indicates that A_R is appreciably lower than A for a given conversion.

Fig. 5.3 shows an annular plug flow reactor, for which equation 5.4 becomes

$$\frac{C_{OUT}}{C_{IN}} = \exp\left[-\frac{K.2\pi r_I h}{N}\right] \qquad \text{Equation 5.11}$$

5.2.2 Continuous Stirred Tank Reactors

Consider the operation of the batch CSTR shown in Fig. 5.4a where the electrode under study is the cathodic inner, rotating cylinder in the concentric geometry. The reactor has an electrolyte volume $V_{REACTOR}$ and initial concentration C_0.

If the reactor is operated under limiting current density conditions, the concentration will decay exponentially with time, so that at time t,

$$C_t = C_0 \exp\left[\frac{-K_L A}{V_{REACTOR}}\ t\right] \qquad \text{Equation 5.12}$$

The exponential term is equivalent to an apparent rate constant, for the first order process, k.

Fig. 5.4b shows a CSTR with a volumetric throughout N. According to the CSTR approximation, the outlet concentration C_{OUT} will be equal to that inside the reactor.

Under limiting current operation, a material balance across the reaction yields;

$$N\,(C_{IN} - C_{OUT}) = KA\ C_{OUT} \qquad \text{Equation 5.13}$$

and the terminal concentrations are related by

$$\frac{C_{OUT}}{C_{IN}} = \frac{1}{1 + KA/N} \qquad \text{Equation 5.14}$$

and the fractional conversion is given by

$$f_R = \frac{C_{IN} - C_{OUT}}{C_{IN}} = 1 - \frac{C_{OUT}}{C_{IN}}$$

$$= \frac{KA/N}{1 + KA/N} = 1 - \frac{1}{1 + KA/N} \qquad \text{Equation 5.15}$$

The corresponding limiting current is given by

$$I_L = NzF\ C_{IN}\ LN\ (1 + KA/N) \qquad \text{Equation 5.16}$$

Equations 5.14, 5.15 and 5.16 may be compared to the corresponding equations for a PFR, 5.4, 5.5 and 5.6. It becomes evident that a smaller fractional conversion is obtained with a CSTR than with a PFR for given values of KA and N. In addition, a high value of K may be maintained by vigorous agitation in a CSTR with a moderate reactor size, whereas PFR conditions may demand a large reactor to maintain the same K value.

One means of increasing the overall conversion with a CSTR is to operate several reactors in hydraulic series. Such a cascade of CSTR's is considered later for the case of a rotating cylinder electrode reactor.

The design equation for a rotating cylinder electrode reactor is particularly straightforward in that the value of K is invariant with electrode distance, both axially and circumferentially, due to the uniform current density distribution. The RCER is also an exceedingly good approximation to the CSTR model, as the very severe three dimensional turbulence around the inner electrode provides very effective mixing. Also, in practice, volumetric flow rates have no appreciable effect on mass transfer to the inner cylinder, as noted in Chapter 2, particularly if the inner cylinder is not long compared to its diameter, and the annular gap is relatively large.

The possibility of recycling part of the outlet of a CSTR may be considered, according to Fig. 5.4c, in order to achieve better performance than in the single pass mode.

Assuming limiting current density operation again, the inlet concentration is now C_R, which results from mixing fresh feed of concentration C_{IN} with product feed,

$$C_R = \frac{C_{IN} + R\,C_{OUT,R}}{1 + R} \qquad \text{Equation 5.17}$$

The terminal concentrations are related by

$$C_{OUT,R} = \frac{C_R}{1 + \frac{K_R A}{N}(1+R)} \qquad \text{Equation 5.18}$$

where K_R is the mass transfer coefficient under recycle conditions.

Combining equations 5.17 and 5.18, and simplifying gives

$$C_{OUT,R} = \frac{C_{IN}}{1 + K_R A/N} \qquad \text{Equation 5.19}$$

Comparing equations 5.19 and 5.14:

$$\frac{C_{OUT,R}}{C_{OUT}} = \frac{1 + KA/N}{1 + K_R A/N} \qquad \text{Equation 5.20}$$

which demonstrates the superiority of the recycle mode over single pass operation, as long as $K_R > K$.

If the increased flow rate on recycle has negligible effect on the mass transfer (i.e. the latter is largely determined by electrode movement as in a R.C.E.R.), $K_R \bumpeq K$ and for a given value of C_{IN},

$$\frac{C_{OUT,R}}{C_{OUT}} = \frac{C_R}{C_{IN}} \; \frac{\left\{1 + \frac{KA}{N}\right\}}{1 + \frac{KA}{N+N_R}} \qquad \text{Equation 5.21}$$

which is > 1.

The fractional conversion is given by

$$f_{R,R} = 1 - \frac{C_{OUT,R}}{C_{IN}} \qquad \text{Equation 5.22}$$

By manipulating equations 5.17 and 5.18

$$f_{R,R} = 1 - \frac{1}{\frac{KA}{N(1 + R)}} \qquad \text{Equation 5.23}$$

and a comparison of recycle and single pass conversions (equations 5.23 and 5.5) reveals

$$\frac{f_{R,R}}{f_R} = \frac{1 - KA/N}{1 - KA/N(1+R)} \qquad \text{Equation 5.24}$$

showing that $f_{R,R} < f_R$.

It should be noted that for a given C_{IN} and K, the increased C_{OUT} value will necessitate a higher current and a subsequently higher rate of product conversion, i.e. enhanced duty.

Despite the importance and simplicity of CSTR's, there have been relatively few relevant electrochemical studies.

Sudall[200,201] has considered theoretical aspects of electrochemical CSTR's and performed experimental work on a concentric, cylindrical, divided reactor using nickel mesh electrodes and the ferrocyanide/ferricyanide redox reaction (Fig. 5.5). The electrode under study was the anode, the anolyte being recycled. The outer catholyte was stationary, and separated by a porous ceramic cylinder from the anolyte. Electrode conditions were altered to produce hydrogen and oxygen evolution at the cathode and anode in addition to the redox reaction. Departure from true steady state behaviour was observed, as the anolyte composition changed with time, (despite the steady inlet concentration) due to migration of hydroxyl ions through to the anolyte. The conductivity of electrolyte in both compartments steadily increased, and under the applied constant cell voltage conditions, the reactor current increased, as did ferrocyanide oxidation. The above behaviour could have been avoided by flowing the catholyte, when both compartments would have acted as CSTR's, by use of a more selective membrane, or by potential control of the electrodes.

Krishna et al.[74,202] have produced a small amount of data on a stirred tank system, although this study was undertaken to evaluate mass transfer and flow regimes present at various positions in the tank, rather than the efficiency of the overall cell. The experimental arrangement comprised a copper ring electrode on a rotating shaft, and several copper ring counter electrodes lying flush on the cell bottom. Mass transfer was studied via the ferro/ferricyanide redox reaction, and it was found that the presence of an impeller on the bottom of the shaft, or provision of vertical baffles made no significant contribution. Mass transfer enhancement was observed when either the shaft diameter or the impeller - bottom of cell distance was increased.

The above authors[74] also studied mass transfer to each of several concentric rings in the bottom of the vessel, showing that two regions existed; one of increasing velocity from the centre radially outwards to a certain point, followed by one of decreasing velocity as the vessel wall was approached.

The work was extended[202] to obtain a better correlation for mass transfer to the radial rings, using extra rings and vessels of two sizes.

5.2.3 Batch Recycle Mode

Previously, PFR and CSTR operation has been considered both in the single pass and the recycle mode. A third mode of operation commonly used both in the laboratory and industrially is the 'Batch Recycle' mode (Fig. 5.6). Here a batch of electrolyte is continuously recirculated through the cell and back to a (stirred) reservoir, which effectively extends the volume of the electrolyte beyond the cell volume.

Such a system has been considered by several authors[164,207,208,120], and more recently by Walker & Wragg[199]. The system as a whole approximates to CSTR behaviour if the reservoir volume is much greater than that of the reactor, and the residence time is high. Unlike the previously considered systems, both the inlet and outlet concentrations of the reactor are time dependent.

A mass balance over the well mixed reservoir (of volume V_{RES}) gives

$$V_{RES} \frac{dC_{IN}}{dt} = N (C_{OUT} - C_{IN}) \qquad \text{Equation 5.25}$$

For a plug flow reactor, substitution for C_{OUT} from equation 5.4 into 5.25 and integration gives

$$C_{IN}(t) = C_{IN}(o) \quad \frac{-t}{\tau} \left[1 - \exp \left\{ \frac{-KA}{N} \right\} \right] \qquad \text{Equation 5.26}$$

where τ is the reservoir residence time = V_{RES}/N.

For a CSTR, substitution for C_{OUT} from equation 5.12 into 5.25 and integration gives

$$C_{IN}(t) = C_{IN}(o) \quad \exp \quad \frac{-t}{\tau} \left[1 - \frac{1}{1 + \frac{KA}{N}} \right] \qquad \text{Equation 5.27}$$

Equations 5.26 and 5.27 are approximate solutions[199], and are adequate for practical reactor modelling.

In the laboratory, a convenient mode of operation is batch recirculation with dosing of the reservoir by concentrated reactant. A negligible volume change occurs if the reservoir is of high capacity, and the reactor may be operated with continuous flow and product recovery.

The relevant limiting current history for equations 5.26 is given by :

$$I_L = zFC_{IN}N\left[1-\exp\left\{-\frac{KA}{N}\right\}\right] \times \exp\frac{-t}{\tau}\left[1-\exp\left\{-\frac{KA}{N}\right\}\right] \qquad \text{Equation 5.28}$$

for the batch recycled plug flow case, and

$$I_L = zFC_{IN,0}N \ln\left\{1+\frac{KA}{N}\right\} \times \exp\frac{-t}{\tau}\left[1-\left\{1+\frac{1}{KA/N}\right\}\right] \qquad \text{Equation 5.29}$$

for the batch recycled CSTR case, where τ is the residence time in the reservoir, $\tau = V_{reservoir}/N$.

Mizushina et al.[205,206] have made measurements of mass transfer in an agitated vessel employing the inner surface of a hollow cylinder as the cathode, and a flat disc at the bottom of the cell as anode (Fig. 5.7). An array of isolated point cathodes was let into the cathode proper, and individual polarisation of these enabled localised mass transfer coefficients to be studied. The above electrodes were made of copper, with an electrolyte of 0.001 M $CuSO_4$ and 2 M H_2SO_4.

Mass transfer measurements on the cathode yielded data which could be correlated by:

$$\frac{f}{2} = j_D = 0.15(Re)_d^{-1/3} \qquad \text{Equation 5.30}$$

where the Reynolds number was based on the diameter of the paddle-type impeller.

Chilton et al.[204] obtained the following equation for heat transfer in a paddle-impeller, agitated vessel

$$(Nu) = 0.36\ (Re)_d^{2/3}\ (Pr)^{1/3} \left\{\frac{\mu}{\mu_i}\right\}^{0.14} \qquad \text{Equation 5.31}$$

where μ_i is the interfacial viscosity.

Neglecting the correction term for viscosity, this may be translated into

$$j_H = 0.156\ Re_d^{-1/3} \qquad \text{Equation 5.32}$$

which tends to substantiate the mass/momentum/heat transfer analogy for this system.

In Mizushina et al.'s work, the vertical distribution of mass transfer was such that a maximum occurred around the impeller height. This peak became lower as the impeller width increased, eventually separating into two peaks. The peak effect was attributed to jet flow(s) from the impeller, the flatter distribution away from the impeller being attributed to rotating motion of the electrolyte. There was very little evidence of vertical flow in the above work.

The special case of a CSTR employing a cathodic rotating cylinder as an agitator forms the main subject matter of this Thesis, and will be considered in detail later.

5.3 Control & Characteristics of Electrochemical Reactors

5.3.1 Electrical Control

There are various possibilities for the mode of electrical control, and as in the electroanalytical technique of coulometry; three cases occur, which may be discussed with the aid of polarisation curves for copper deposition:

1. constant current (galvanostatic),
2. constant cell voltage, or
3. constant (working) electrode potential (potentiostatic).

The constant current mode is perhaps the most conventional one, and is commonly used when it is required to establish a constant rate of reaction. For example, in electroplating it is normally desirable to achieve a given thickness of deposit, and this is most easily done by passing a fixed current for a given time to a workpiece of known surface area.

The metal concentration of most plating baths is held at a high and reasonably constant level. If the same technique of controlled current is employed with dilute solutions with a high current, depletion takes place, and the potential of the electrode may rise (Fig. 5.8a), such that the limiting current is exceeded. The subsequent formation of hydrogen in the case of copper deposition, results in a progressive lowering of current efficiency.

A similar effect is seen if a decrease in electroactive surface area or mass transfer occurs during deposition. (Figs. 5.8b and 5.8c). If, on the other hand, the electroactive surface area increases (due to increasing roughness for example) or the mass transfer increases (due to greater electrode or solution movement), the maximum duty will not be attained in the reactor, as the control current lies below that of the new limiting current. In addition, the change in electrode potential may result in a significant change in deposit morphology.

In summary, if constant current is to be used, and the electrode potential must remain reasonably constant, then the concentration in the reactor must also remain at a fixed level. It is noteworthy that the inlet concentration to a reactor may be allowed to vary, within limits, and the reactor concentration maintained by altering the flow rate, a point which will be returned to in Chapter 6.

Constant cell voltage is often convenient in practice, as simple transformer/rectifier power supplies effectively operate in this mode, for a fixed load. While this method is generally less sensitive to reactor changes than the constant current mode, in order to achieve constant electrode potential, all the sources of polarisation in the system must remain constant, including anode polarisation, iR drop in the electrolyte and external iR drops e.g. across a brush and slip ring assembly in the case of a rotating cylinder electrode assembly.

X

The most satisfactory mode of control is often that of constant electrode potential, where a third (reference) electrode is employed, and the cell current alters so as to maintain the electrode potential. This situation may be achieved automatically using potentiostatic circuitry[225], which may be either solid state or electromechanical. Unfortunately, such sophisticated electronics is normally relatively expensive, and the requirement of a reliable reference electrode sensor is an additional consideration.

The control of electrode potential, however, may result in greatly enhanced selectivity of reaction and controlled deposit characteristics.

It has already been noted, however, that very few industrial reactors operate potentiostatically, probably due to the lack of large scale potentiostat devices, coupled with the previous scarcity of reactors which give rise to uniform potential across their electrode surfaces.

Both constant current and constant voltage techniques have been employed in cells utilised for silver recovery from photofix solutions. Potentiostatic control, however, has only recently been introduced[321].

5.3.2 Potential and Current Density

The control of electrode potential is of paramount importance to electrochemical reactor operation, in general, as it affects the specificity of reaction and hence the purity of product. An impure product may necessitate a difficult and expensive purification stage after the reactor.

Additionally, in the case of metal deposition, the potential can greatly affect the deposit quality. Thus the hard, smooth deposits obtained at low potential, as in metal finishing operations, progressively lead to darker, roughened powdery deposits at high potential.

In the case of deposition of a single noble metal, (such as copper from acidic solutions) the potential must be controlled below that at which hydrogen evolution occurs as a secondary reaction, in order to maintain 100% current efficiency (Fig. 5.8). Operation at such a potential also corresponds to the maximum current density and hence the maximum recovery rate of metal. Powdery deposits are still maintained if the potential is lowered somewhat, although the powder characteristics may change appreciably (Chapter 7).

In the case of a mixed metal electrolyte, the idealised cathodic polarisation curve may comprise a number of limiting current plateaux (cf. standard polarograms where the plateaux are regarded as polarographic waves) (Fig. 5.9). If the differences in standard potentials of the metals are sufficiently large, each of the metals (starting with the most noble) may be successively deposited in a selective manner.

Fig. 5.10 indicates the idealised, standard electrode potentials shown by certain metals over a wide activity range. It may be seen that while copper and silver, for example, have a wide separation, facilitating controlled potential electrolysis, nickel and tin are much closer.

Due to the Nernstian change in potential with activity, the separation in potential of a given pair of metals may appreciably alter if the concentration of either is changed.

Also, the presence of complexants such as cyanide or borates, commonly present in e.g. plating process solutions or metal cleaning solutions, may drastically shift the electrode potentials at which limiting current plateaux occur. In this case, observed plateaux may be associated with mass transfer decomposition of the complex rather than mass transfer controlled deposition of the metal.

By far the majority of work here is restricted to the electroanalytical literature[210,211,226,227], where miniature electrodes such as the dropping mercury electrode are used, the technique being referred to as polarography. In such cases, however, the electrolyte to be analysed is normally treated to allow an efficient separation to occur. Such a treatment may include complex removal steps (e.g. oxidation of cyanide), pH correction (by buffer addition), or concentration correction (e.g. by evaporation). This procedure is rarely possible in the treatment of industrial process solutions, as the chemical and equipment costs are prohibitive, and the process solution may be required, substantially unaltered, for reuse.

The use of the rotating cylinder electrode reactor for selective recovery of metal will be discussed later in this chapter.

One of the few pilot plant scale studies in the literature concerns the 'Swiss-Roll' cell of Robertson and Ibl[126], which is described later. Successful separation of copper from copper/zinc and copper/nickel solutions was obtained, using an initial metal concentration of 10^{-2} M for each metal, together with 10^{-2} M sulphuric acid. 99.9% of the copper was recovered, in each case, with no detectable change in the concentration of the second metal.

It is interesting to note that the problem of metals separation from industrial processing solutions such as pickling, plating and etching dragouts and rinses and hydrometallurgical streams is the converse of the problem of codepositing metals from a solution to produce an alloy for metal finishing purposes*.

---

322 346 357
* Brenner, Raub, Gorbunova.

The possibility of clean, selective separation and recovery of metals in the above manner is a strong advantage of electrolysis compared to other less discriminating means of metal removal from process streams.

Closely linked to potential distribution is the subsequent current density distribution over an electrode. In the idealised case, both distributions will be uniform, and the mass transfer coefficient will be spacially invariant. An approximation to this implies a uniform interelectrode spacing, which leads us to consider the parallel plate, annular and concentric spherical geometries.

Discussions of current distribution are to be found in works by Pickett[120] and Newman[10], but a simplified approach will be adopted here. Two limiting cases may be identified. When the current distribution over an electrode is determined by convection and diffusion, the 'primary' current density conditions exist and the current density is infinite or zero at the edges. On the other hand, if ohmic potential drop in the electrolyte and surface over-potentials are taken into account, the secondary current density distribution exists. The general effect of electrode polarisation is to render the current distribution more uniform than the primary one; infinite current density at electrode edges is eliminated.

Consider the parallel plate geometry, perhaps the simplest and most obvious one for an electrochemical reactor. Fig. 5.11 shows a definition sketch and the corresponding current distributions along an upper cathode. The primary curve is hyperbolic, the substantially uniform current density over the central portion of the electrode rapidly tending to an infinite value near the edges. The limiting current distribution continuously decreases from its initially infinite value at the leading edge to lower values with electrode distance.

If the parallel plates are bounded by the cell as in Fig. 5.12 which depicts free convection in a rectangular cell, the primary distribution becomes uniform, which is readily understood by comparing the corresponding current and equipotential lines (Fig. 5.13).

The rotating disc electrode has a uniform limiting current density distribution and a non-uniform primary one, while the rotating spherical electrode shows behaviour intermediate between a uniform primary distribution and mildly non-uniform limiting distribution (Fig. 5.14).

The non-uniform primary distribution on a rotating disc electrode is negligible for small laboratory electrodes, moderate rates of reaction and high conductivity solutions, but scale-up, fast reactions and low conductivity process solutions could each result in a substantially non-uniform distribution[10,315]. This situation could lead to a secondary reaction occurring at the edges of the disc, e.g. hydrogen evolution or deposition of a secondary metal, while the main reaction occurred under limiting current conditions over the main disc area.

The rotating cylinder electrode is unusual in that both the primary and limiting current density distributions are substantially uniform, only a negligibly small area being suspect at the top and bottom of the cylinder.

5.3.3 Duty and Performance

Design of an electrochemical reactor necessitates a compromise between capital and power costs; in addition, space is often at a premium and this may also prove an important restriction.

Rapidly increasing costs of electricity have recently focused more attention on process inefficiencies, and power consumption has become a major consideration. Exceptions always suggest themselves, and in the field of precious metals recovery, power costs are normally a secondary consideration.

In order to compare the performance of reactors, several 'figures of merit' may be invoked, many of these being interrelated.

One possibility is to define a space-time yield, Y_{ST}[212]

$$Y_{ST} = \frac{\text{amount product}}{\text{electrolysis time} \times \text{reactor volume}} \qquad \text{Equation 5.33}$$

$$Y_{ST} = A_S \quad i \quad p \quad \Theta$$

where

i is the current density

p is the Faradaic amount of product per Ahr.

θ is the current efficiency

p may be on a weight basis or (especially for gases) a volume basis

A_s is in itself a figure of merit:

$$A_s = \frac{\text{area electrode}}{\text{unit volume}} \qquad \text{Equation 5.34}$$

The denominator is normally the reactor volume, which will be reflected in increased capital costs, but a second A_s may be defined in terms of the electrode volume. This latter A_s is especially useful for expensive electrodes and three dimensional electrodes.

Chemical yield, Y_E is given by

$$Y_E = \frac{\text{amount product}}{\text{maximum possible amount product based on reactant conversion.}} \qquad \text{Equation 5.35}$$

If costs of electricity are considered in relation to the reactor product, power consumption figures are all important.

$$\text{Specific power consumption} = \frac{V_{cell} \times I \times t}{m} \qquad \text{Equation 5.36}$$

where V_{cell} is the total cell voltage, I the cell current and m the mass of product. Typical units would be KWhr kg^{-1}. In the case of treatment of a process stream with recycling of electrolyte, the recovery of a metal product may be secondary to the treatment of the stream, and a more suitable figure of merit is the power consumption per unit volume of effluent treated, stated, for example in terms of KWhr m^{-3}.

Kuhn and Houghton[169] have compared reactor performance using as an index the limiting current density in 0.01 M concentrated solutions, for a two electron reaction. Equally useful, and more familiar to chemical engineers is the mass transfer coefficient:

$$K_L = \frac{i_L}{zFC}$$

Table 5.3 compares estimated A_s and Y_{ST} values for a variety of reactor designs. A_s and Y_{ST} are an index of the compactness of a given design. It can be seen that particularly high values are obtained for reactors employing three dimensional electrodes such as packed and fluidised beds, and mesh electrodes, where A_s may be as high as 100 cm^{-1}. The A.C.E.R. (Fig. 5.15) has an area/volume ratio which approaches 1 cm s^{-1} for small gaps and large electrodes, while the A.D.E.R. (Fig. 5.16) has a value which is independant of electrode size In the case of the Swiss-roll cell, it is interesting to note that the electrode area per unit electrode volume (~ 200 cm^2 cm^{-3}) appreciably exceeds the electrode area per unit cell volume (~ 20-50 cm^2 cm^{-3}).

The importance of the effects of the above figures of merit to electrochemical reactor performance is summarised in Table 5.4.

Recalling equations 5.5 and 5.15 describing conversion over plug flow and CSTR electrochemical reactors,

$$f_R' = 1 - \exp\left[\frac{-KA}{N}\right] \qquad \text{Equation 5.5}$$

$$f_R = 1 - \frac{1}{1 + \frac{KA}{N}} \qquad \text{Equation 5.15}$$

it can be readily seen that for a given value of flow rate, N, i.e. a given reactor throughput, the conversion f_R may be increased by increasing either K, A or both.

Reactors such as the RCER may achieve high conversion efficiencies by virtue of high mass transfer, i.e. large K, while packed beds or the trickle tower achieve such conversions via a high electroactive surface area. Reactors employing fluidised bed electrodes or turbulence promoted parallel plate or mesh assemblies achieve a similar goal by a moderately high mass transfer and electroactive surface area.

If mass transfer rather than electroactive surface area is considered, the ratio $K_L/V_{reactor}$ becomes important. Devices such as the R.C.E.R. have a relatively high value of this index, indicating their relative compactness for a given duty.

From the above discussion, it is clearly misleading to compare electrochemical reactors according to a single figure of merit, rather several such indices must be used together to arrive at a suitable design.

It must also be remembered that other considerations may be of overriding importance in reactor selection, including ease of product removal, ease of maintenance, facility for control and automation, and specificity of reaction.

5.4 Comparison of Reactor Configurations

5.4.1 General

Various classifications are possible, but one of the most general is shown in Fig. 5.17 where reactor types are first divided into dynamic and stationary electrode reactors, each of which is in turn subdivided.

Mass transfer to various types of electrode geometry was discussed in Chapter 3, and it was noted that a number of interrelations occur as indicated in Fig. 5.17.

In recent years, a whole variety of new or improved reactor designs have been presented in the electrochemical literature. The novelty of some of these designs is questionable, however, as there is evidence that many designs have in fact been 'rediscovered'.

The majority of designs have been developed for either electro-organic synthesis or the removal of metals from dilute industrial process streams. In both cases, the problem is to find a reactor capable of high mass transfer and/or high electroactive surface area, in order to provide a reasonable duty from low concentration solutions.

It is possible to criticise the preoccupation of certain electrochemists with the possibility of novel designs. This has resulted, on one hand, in extensive investigations into rather obscure geometries, and on the other hand, specific geometries have been placed on a pedestal as possible 'universal' reactors. It is the author's opinion that a whole spectrum of reactor designs are now possible, and the main aim of the electrochemical engineer should be to choose the most suitable one for the job in hand.

A full discussion of reactor designs will not be attempted here, for reasons of space. Instead, some of the more recent or promising reactor designs will be briefly reviewed with special relevance to the cathodic removal of metal from dilute solutions.

Mass transfer and flow characteristics of the designs that follow (or similar ones) have been discussed previously, in Chapter 3.

5.4.2 Electrochemical Pump Cell

This reactor, which is an extension of the capillary gap cell of Beck[214], has been developed by Jansson, Fleischmann and coworkers at the University of Southampton and a patent application has been filed[215]. Like the capillary gap cell, interelectrode gaps are small, typically $\leqslant 0.5$ mm., yielding a low solution iR drop, but one of the electrodes is rotated.

Features of the design (Fig. 5.18) include[216]:

1. a high velocity gradient between the electrodes, encouraging high mass transport,
2. an inherent pumping action,
3. the possibility of the cell being self-cleaning,
4. the ability to treat or produce dispersions,
5. reasonable potential distribution,
6. the reactor may be adapted to continuous use, and the solution residence time controlled independently of the mass transfer rate, by controlling static pressure at the cell inlet.

Disadvantages of the reactor include:

1. the difficulty in fitting a diaphragm,
2. the requirement for precise engineering and dimensional and chemical stability of the electrodes.

Both mass transfer[217,218] and hydrodynamic characteristics[219-] of the pump cell have been studied, and studies of possible applications have concerned:

1. organic syntheses[220], including the hydrodimerisation of acrylonitrile, alkoxylation of furan and epoxidation of propylene,

2. inorganic synthesis including oxidation of bromide to hypobromite[221], and production of chlorate[222],

3. production of metal powders[224,216] (see Chapter 7).

The reactor may be operated in either the monopolar or bipolar mode (Fig. 5.19), the latter obviating the need for a rotating power feed to the rotor. A small commercial pump cell is available driven by a magnetically coupled pump[224].

Tracer experiments[222] have shown that thereactor behaves essentially according to the plug flow model, but within each radially expanding fluid element, excellent mixing is obtained due to tangential shear. Residence time within the reactor may be controlled by adjusting the mass flow, while mixing of species originating at the anode and cathode is mainly governed by rotational speed. This situation allows partial tailoring of the reactor environment to suit the needs of the electrochemical reactions and subsequent or consecutive chemical reactions.

In general, the reactor is said[220] to be suitable for the following kind of reactions:

1. fast electrode reactions such as metal deposition or redox reactions, where its high mass transfer may be utilised,
2. reactions with fast kinetics following the electrochemical reaction,
3. irreversible electrode reactions,
4. reactions requiring mixing of electrogenerated products,
5. reactions requiring a species generated at one electrode which is then to be oxidised or reduced at the other,
6. reactions of electrogenerated species with dispersions or emulsions of other phases.

The possibility of sealing the reactor facilitates treatment of toxic materials.

5.4.3 Extensive Surface Area Reactors

Several examples of high electroactive area cells have been referred to already, including the Swiss-roll cell, the Dupont Extended Area Cell and the HSA reactor.

The Swiss-roll cell has been developed and patented [128] by Ibl and Robertson's research group at the Swiss Federal Institute of Technology (ETH), Zurich. It is constructed[126,228] from an electrode sandwich (Fig. 5.19) consisting of electrode and separating layers, the assembly being spirally wound around an axis, and incorporated into a cylindrical container. The electrodes may be sheets or nets, while the separators may be individual or combined cloths, ion exchange membranes or porous non-woven materials. This results in a modular reactor of high surface area per unit volume and moderate mass transfer.

Mass transfer and hydrodynamic characteristics have already been referred to in Chapter 3, where the importance of turbulence promotion via the separator/electrode combination was noted.

Advantages of the Swiss-roll geometry include:

1. a divided cell enables anode corrosion by contaminated catholyte to be avoided,

2. the properties of the cell may be partially tailored by alteration of the electrode/separator combination, although this must be done on a modular basis,

3. the small interelectrode gap and monopolar construction result in a relatively low cell voltage and power consumption,

4. substantially uniform current density distribution,

5. high space-time yield,

6. high electroactive surface area (20-50 cm^{-1}) per cell volume.

Disadvantages include:

1. in the case of metal deposition, the product may not be removed continuously. Instead, intermittent operation is necessary with backwashing and chemical or anodic stripping. This is undesirable as a concentrated solution is obtained, rather than metal, and reversal of cell polarity may damage the expensive anodes,

2. the modular design means that electrode/separator changes must be made as a package change, with consequent loss of versatility,

3. the engineering design, while simple in concept, is rather complicated in practice,

4. due to metal accretion, the pressure drop over the reactor progressively increases; when the backpressure increases to a critically high value, operation must cease pending cleaning, or alternatively a second, standby reactor must be employed,

The Swiss-roll cell has been used for the removal of various metals from dilute solutions, including:

1. deposition of copper from acidic solutions, on a batch recycle basis, from 5×10^{-3} M Cu to 5.1×10^{-5} M Cu, at an overall current efficiency of 57%, and a cell voltage of $\leqslant 1.99$ V[228].

2. removal of silver from photographic fixing solutions, a 2 litre batch decaying from an initial concentration of ca. 0.05 M to a residual concentration below 0.1 ppm. in some 400 minutes.

3. removal of mercury from waste waters (4×10^{-3} M $Hg(NO_3)_2$) at a stainless cathode resulted in high end concentrations of 2 ppm. due to disproportionation or reoxidation of mercury. The use of an amalgamating cadmium cathode solved this problem, with a residual concentration ~ 0.01 ppm. (the Swiss legal limit)

4. removal of zinc from cyanide plating dragouts from 10^{-3} M Zn to $\leqslant 10^{-6}$ M Zn. It was found that indirect oxidation of cyanide, encouraged by Cl^- addition and subsequent anodic OCl^- formation, resulted in a faster deposition rate with lower end concentrations

5. selective removal of copper from copper-nickel and copper-zinc solutions[126], of 10^{-2} M in each metal and 10^{-2} M H_2SO_4. 99.9% of the copper was removed with no detectable change in the concentration of the second metal.

It has already been noted that metal product removal is a problem with the Swiss-roll cell. There are three possible stripping methods:

1. cell opening and mechanical removal,
2. chemical dissolution,
3. electrochemical (anodic) dissolution.

The first is messy, tedious and rather impractical for a full size reactor. Chemical dissolution is a fast and more convenient solution, but rather aggressive oxidising solutions such as nitric acid or sulphuric/hydrogen peroxide must be used. This raises corrosion and materials degradation problems, regarding both the electrodes and the reactor construction. In particular, damage could result to the expensive Ti/RuO_2 anodes.

Anodic stripping can be performed under milder solution conditions e.g. 1 M H_2SO_4, but Ti/RuO_2 anodes face serious damage due to reduction of RuO_2. Carbon felt and paper[126] have been suggested as alternative anode materials.

The metal holding capacity of the cell is illustrated by copper deposition where, theoretically, 2 g/cm^2 may be deposited. In practice lower loads can be tolerated.

Simultaneous with the development of the Swiss-roll cell, Dupont have independently developed a similar concept, the Extended Surface Electrolysis (or ESE) reactor,[131,229] which has also been patented[130]. Curiously, Dupont have referred to this cell as a 'jelly-roll'[131].

The electrode sandwich used would appear to be comparable with that of the Swiss-roll cell, but knitted stainless steel mesh (1 cm. thick) is employed rather than the thinner expanded titanium mesh or sheet of the latter. The electroactive cathode surface area per unit volume would appear to be similar at 30-50 cm^{-1}.

In addition to metal containing effluents, the ESE reactor has been examined with a view to treatment of hydrometallurgical process streams. Work has been described on copper, gold, silver, mercury and lead.

"DSA" anodes (Electrode Corporation, Chardon, Ohio) have been employed rather than the Ti/RuO_2 anodes of the Swiss-Roll cell.

Metal leaching of copper was carried out with 20% w/w HNO_3 to produce a concentrate of typical concentration ca. 20,000 p.p.m. Cu. H_2SO_4/H_2O_2 has also been employed, when the leaching step took 30 minutes (cf. 10-30 hours for deposition).

The stacking of ESE modules end to end has also been investigated, in order to achieve high overall conversions.

Scale-up has been accomplished through a 3 gal/min. pilot plant setup to a 100 gal/min. commercial scale. Although most of the development work used spiral wound sandwiches, consideration of fabrication ease and cost caused the sandwich to be unrolled and used in the planar configuration, with a fibre-reinforced polyester reactor body.

A third high surface area reactor has recently been developed, in addition to the above two. The patented[231] carbon fiber reactor of H.S.A. Reactors Ltd. (Toronto, Ontario, Canada) has been developed by Das Gupta and Fleet[232]. Its application to the treatment of metal containing effluents has been described by Kennedy and Das Gupta[230].

The carbon fibre cathode material is advantageous in:

1. having a high electrical and thermal conductivity,

2. being hard and light,

3. having a very low coefficient of thermal expansion,

4. having a high chemical inertness,

5. possessing high hydrogen and oxygen overpotentials,

6. exhibiting an enormous surface area, typically[230] 2.6×10^6 cm^2 per g. fibre, which results in a specific surface area several thousand times larger than with other particulate reactors. Indeed, such a value approaches that of heterogeneous catalytic reactors in chemical engineering.

This reactor, however, still faces the problem of product recovery, which again is discontinuous. Additionally, treatment of effluent streams containing significant concentrations of certain organics such as plating bath addition agents may serve to poison the carbon fibre surface by irreversible chemisorption.

5.4.4 Fluidised Bed Electrode Reactors (F.B.E.R.)

The fluidised bed electrode reactor, invented by Fleischmann, Goodridge, Plimley and Backhurst and patented[156] in 1970, has received considerable attention from academic research workers (see Chapter 3), and has frequently been hailed as one of the most important reactors ever conceived.

Until quite recently, however, these expectations were not realised by the commercial marketing of a F.B.E.R. Commercial development work may be said to have originated at Warren Spring Laboratory[164] and CJB Developments Ltd.[165]. The latter work, supported by N.R.D.C., led to the development of a commercial scale pilot plant design. This was tested for a period at South-African hydrometallurgical concerns, but further development ceased rather abruptly and it is understood that operational problems arose. Fig. 5.20 shows a sketch of the planar, side by side arrangement of the CJB cell, where the platinised titanium anode and 1 M sulphuric acid anolyte are separated from the metal containing catholyte by an ion exchange membrane. Both cationic and anionic types were used. The cathode bed consisted of fluidised atomised metal (copper) particles with current applied via copper or titanium feeders in the form of rod or mesh.

A laboratory 30 x 40 cm. cell of this type (100A) was successfully scaled up to a 100 x 100 cm. cell (1000A) before a commercial cell was built.

The ion exchange membrane serves to achieve a low resistance division between the electrodes, to prevent conducting fluidised particles from bridging the electrodes, resulting in cell shorting.

Wilkinson and Haines[165] mention that a possible alternative arrangement is a concentric geometry, and AKZO (see later) have used a modification of this.

It is interesting at this point to consider electrochemical engineering studies of the F.B.E.R. by Backhurst[149]. This author studied both plane-parallel and concentric configurations, and concluded that regarding scale-up, increasing the reactor dimension perpendicular to current flow permits a linear increase in cell capacity. Such an increase in the dimension parallel to current flow, however, is not advisable past a certain length, 0.25 dm. in the above studies. Thus scale-up might be best accomplished via multiple cells rather than a single one. This is in possible conflict with the AKZO developments where single scaled up reactors are being employed.

The AKZO F.B.E.R.[167] has been developed over the past seven years at AKZO Zout Chemie, Hengelo, the Netherlands, and following pilot plant trials since 1975 within and outside the AKZO Group, is now being marketed for the removal of toxic metals from effluent and the electrowinning of metal in hydrometallurgical processing. Two commercial installations were set up in 1978 inside the AKZO Group, each for recovery of ca. 1 Kg/hr copper from 50-100 g.p.l. sulphuric acid.

The AKZO F.B.E.R. (Fig. 5.21) appears to be a well engineered reactor, having the following improvements over past designs:

1. rounded corner and smooth surface design details, together with uniform fluidisation tend to prevent particle agglommeration,

2. the potential and current density distribution over the cathode bed is substantially uniform due to the design,

3. problems with membrane erosion have been 'designed out' by the use of an AKZO developed smooth, cylindrical, porous, ceramic diaphragm which has substantial chemical resistance.

Bed expansions of 10-30% are used to fluidise purposely produced seed particles of the metal to be recovered. The bed particles grow from 0.5 mm. to ca. 1 mm., become heavier and sink gradually to the bottom of the cathode compartment. The process can be operated continuously by addition of fresh feed particles and withdrawal of grown particles. The subsequent short particle residence time in the bed helps prevent agglommeration.

A further feature of the AKZO reactor is sealing of the system, to facilitate overpressuring of the anode compartment, or to prevent atmospheric contamination by e.g. Cl_2 in the case of electrolysis of Cl^- solutions.

A main feature of design is the cylindrical diaphragm construction with an inner rod anode, several anode/diaphragm assemblies being positioned inside the single cathode compartment. This arrangement facilitates simple enlargement and avoids the need for extensive manifolding as with filter press F.B.E.R. designs.

Compared to packed bed reactors, F.B.E.R.'s display less tendency to blocking, but operate at high power consumptions. As demonstrated by the above AKZO design, the possibility of continuous product removal is also an attraction.

In complete contrast to the rather sophisticated and costly engineering design of the AKZO reactor is the 'Chemelec Cell' partly developed by Lopez-Caciçedo et al. at the Central Electricity Research Council, Capenhurst, Cheshire[166,234], and marketed by BEWT[235] (Water Engineers) Ltd., Alcester, Warwicks.

The Chemelec Cell is a modular design (Fig. 5.22) comprising a side by side arrangement of alternating flat meshes, anodes and cathodes. The electrodes are in the form of meshes to encourage turbulence promotion. Unlike the CJB and AKZO F.B.E.R.'s, fluidisation is carried out via non-conducting glass beads, ca. 1 mm diam., rather than metal particles, and metal is deposited on the cathode mesh rather than onto the bed medium, and in the form of hard plate, rather than dendritic powder. Even flow distribution is encouraged by a porous distributor in the cell bottom. 100% bed expansion was used.

A particular advantage of this system is that, in electroplating installations, the deposited metal on the titanium cathode may be removed and used directly in the plating bath as an auxilliary anode. Great care must be taken, however, to avoid bath contamination.

Unlike the AKZO F.B.E.R., the Chemelec Cell is unsealed, overflow taking place by gravity to separate the outlet solution from the glass beads.

The cell has been designed in perspex, for use near room temperature, and to be installed near electroplating drag out and rinse tanks, etc.

Power costs for the cell are stated as lying in the range 6-10 KWhr/Kg electrolysis plus 1.5-10 KWhr/Kg pumping power, i.e. 7.5-20 KWhr/Kg total, depending on the metal and its concentration, and on the conductivity of electrolyte.

The standard module accommodates a maximum of 12 double sided expanded mesh cathodes and 12 anodes, giving a total cathode (and anode) area of 3.3 m^2, the overall cell dimensions being 0.5 x 0.6 x 0.75 m. Half and quarto size units are also available.

The Chemelec Cell is an interesting design in that the simple geometry of parallel plate cells is retained, while the use of fluidisation and mesh electrodes results in a cell capable of respectable mass transfer and electroactive surface area per unit volume.

The cell has been employed to recover many electroplated metals[234] including:

1. copper and zinc from sulphate and pyrophosphate solutions,
2. copper and zinc from cyanide solutions,
3. zinc from zincate solutions,
4. nickel from 'Watts' solutions, and
5. silver and gold from cyanide solutions,

with varying efficiencies.

The absence of a diaphragm raises the objection of hydrogen and oxygen gas in close proximity, but results in a lower cell voltage, simpler engineering and the possibility of simultaneous CN^- oxidation when treating cyanide solutions.

6% Sb/Pb anodes, or 1% Ag/Pb anodes have been used, in addition to more expensive platinised titanium.

The CJB, AKZO and Chemelec F.B.E.R.'s are compared in Table 5.5.

6. THE ROTATING CYLINDER ELECTRODE REACTOR (R.C.E.R.)

The concentric, rotating cylinder electrode (R.C.E.) is an interesting uniform geometry which has been utilised in academic and investigative studies due to its special characteristics regarding uniformity of electrode potential and current density, high mass transport and turbulent hydrodynamics.

These characteristics have resulted in diverse laboratory applications for the geometry, including controlled potential, electrogravimetry, fundamental and applied mass transport studies, corrosion measurements in dynamic environments, strip electroplating simulation and metallographic examination of electrodeposits.

The R.C.E. has also provided a suitable geometry for an increasing number of commercial applications (particularly in the fields of electrowinning and electroforming of metals) including recovery of silver from photographic fixer, hydrometallurgical recovery and refining, electroforming, rapid electroplating and metal powder deposition, effluent treatment of dilute metal-containing solutions and electro-organic and electro-inorganic synthesis.

This Chapter attempts to present and characterise the R.C.E.R. as a special, high performance device having interesting technical possibilities.

6.1 General

Some of the characteristics of the R.C.E. have already been examined in earlier parts of this Thesis. Thus the hydrodynamics of the system was extensively reviewed in Section 2.4, while known mass transport relationships were covered in Section 4.6. The duty of R.C.E.R.'s has been referred to in Section 5.3.

In the majority of practical cases, the R.C.E. is in turbulent flow, and the electrode surface is the smooth exterior of an inner rotating electrode.

The generalised characteristics of the R.C.E.R. are as follows:

1. the electrode surface is substantially equipotential due to the uniform geometry (see Section 5.3.2),
2. the current density experienced is also substantially uniform (Section 5.3.2.),
3. the turbulent, three dimensional flow in a R.C.E.R. provides a good approximation to the C.S.T.R. model (Section 5.1),
4. the mass transport is uniform and relatively high, being readily controlled by the rotation of the cylinder rather than the axial flow through the reactor,

5. rough rotating cylinders display markedly higher mass transport than their smooth counterparts, and the mass transport also shows a stronger dependence on peripheral velocity, (Section 4.6).

These characteristics may be examined in more detail. The uniform electrode potential property facilitates potentiostatic control (Section 5.3.2) of the R.C.E., which may be utilised for the mass transport controlled deposition of a single metal, or the selective deposition of the more noble metal from a mixture of one or more metals. This aspect will be examined in detail later in this Chapter and in the experimental part of this Thesis. Controlled potential deposition may also be utilised to deliberately produce metal alloys of known composition.

The uniform current density at the R.C.E. enables the system to be utilised for the electrodeposition of compact deposits of guaranteed thickness at sub-limiting currents (as in electroforming) or of reproducible metal powders, under mass transport control. The spacially invariant current density and mass transport render the R.C.E. an ideal tool for the microscopic or profilometric study of the surfaces of metal deposits.

The approximation to C.S.T.R. behaviour leads to a reactor whose mass transport capabilities are not significantly affected by the volumetric throughput. The mass transport (and hence the rate of metal recovery) is, however, strongly dependent on the rotational velocity. In addition, the turbulent hydrodynamics in the R.C.E.

enables reactants to be mixed at the reactor inlet, without the need for an external agitator vessel, or an in-line mixer; gas evolution from the electrode is also promoted. The practical result of the C.S.T.R. approximation is that the inlet concentration reduces to the reactor concentration (which is identical to that of the outlet) over the inlet manifold. In large reactors, employing low rotational speeds, small annular gaps and low volume hold up, it is considered a wise precaution to manifold the fluid nozzles to aid dispersion and preserve the C.S.T.R. approximation.

The enhancement of mass transport at rough rotating cylinders is an essential theme of this Thesis, and is examined in detail in the experimental Chapters.

In the case of the electrodeposition of metal powders (Chapter 7), the geometry of the R.C.E.R. allows a stationary or near stationary scraper to be used to facilitate continuous metal product removal.

6.2 Basic Design Considerations

This section considers only single unit R.C.E.R.'s, multiple (cascade) reactors are discussed later, in Section 6.6. The majority of the text refers to monopolar electrodes and to the (mass transport controlled) deposition of metals at an inner R.C.E.

6.2.1 Design Equations

The fundamental design equations for a R.C.E.R. may be arrived at by considering the reactor to be a special case of a general C.S.T.R. which has been described earlier (Section 5.2.2).

Consider Fig. 6.1 where a R.C.E.R. operates under mass transport control in the simple batch mode. The concentration at time t, C_t, may be related to the initial value, C_o by

$$C_t = C_o \exp\left[-kt\right] \qquad \text{Equation 6.1}$$

where the apparent first order rate constant, k, may be expressed in terms of the electroactive area, the effective reactor volume, $V_{reactor}$, and the mass transport coefficient, K_L :

$$C_t = C_o \exp\left[-K_L \frac{A}{V_{reactor}} . t\right] \qquad \text{Equation 6.1a}$$

The resulting fractional conversion is

$$1 - \frac{C_t}{C_o} = 1 - \exp\left[\frac{-K_L A.t}{V}\right] \qquad \text{Equation 6.2}$$

Thus the conversion at any time t may be increased by increasing K_L or A, or by decreasing V.

Fig. 6.2 illustrates this by considering a hypothetical example where $A = 100\ \text{cm}^2$, $V = 1000\ \text{cm}^3$ and $K_L = 0.1\ \text{cm s}^{-1}$. This yields

$$1 - \frac{C_t}{C_o} = 1 - \exp - \left[10^{-2} t \right] \qquad \text{Equation 6.3}$$

which is displayed as curve a) in Fig. 6.2. Curve b) shows the increased conversion obtained by doubling k. This may be accomplished for a given volume by doubling A, or K_L or by increasing both.

The area of the cylinder in the above example may be readily doubled by doubling its length for a given diameter. (The mass transport coefficient is largely insensitive to the length to diameter aspect ratio). The expensive alternative is to employ two identical R.C.E.'s.

The mass transport coefficient may be enhanced by increasing the peripheral velocity. In the case of a smooth cylinder

$$K_L = 0.079\ d^{-0.3}\ \nu^{-0.344}\ D^{-0.644}\ U^{0.7} \qquad \text{Equation 6.4}$$

$$\text{i.e. } K_L \propto U^{0.7} \qquad \text{Equation 6.5}$$

while for a rough (e.g. knurled) cylinder

$$K_L = \left[1.25 + 5.76 \log_{10} \frac{d}{e} \right]^{-2} Sc.^{-0.644} U \qquad \text{Equation 6.6}$$

$$\text{i.e. } K_L \propto U^{1} \qquad \text{Equation 6.7}$$

For example, if the diameter of the cylinder is maintained, K_L may be doubled by doubling the rotational velocity in the case of a rough cylinder, and increasing it by a factor of 2.69 for a smooth one.

In the above cases, the increase in performance was gained by increasing the size (length) of the electrode with the attendant increase in materials and fabrication, or by increasing the rotational speed and hence the rotational power consumption (see later). While power costs and mechanical limitations impose a constraint upon K_L for a given electrode size, the area is constrained by the ratio $\frac{A}{V}$. It has already been noted in Section 5.3.2 that this ratio approaches $1 cm^{-1}$ for a concentric R.C.E.R. with negligibly small volume ($r_o \simeq r_I$) and an annular gap $(r_o - r_I)$ of 1 cm.

The limiting current-time expression corresponding to Equation 6.1 is

$$I_{L,t} = I_{L,o} \exp \left[-kt \right] \qquad \text{Equation 6.8}$$

For sub-limiting current operation, Equations 6.1 and 6.8 become

$$C_t = C_o \exp \left[\frac{-KA}{V} \right] \qquad \text{Equation 6.9}$$

$$\text{where} \quad k = \frac{\gamma K_L A}{V} \qquad \text{Equation 6.10}$$

γ is a dimensionless parameter $= i/i_L$

This may be rewritten

$$C_t = C_o \exp\left[- \frac{I}{zFCV} .t\right] \qquad \text{Equation 6.11}$$

The corresponding current history is

$$I_t . = I_o \exp\left[\frac{-I}{zFCV}.t\right] \qquad \text{Equation 6.12}$$

The behaviour described by Equations 6.1 and 6.8 assumes that the exponential factor k is constant, that is, for a given reactor volume, K_L and A are time invariant. As will be seen in the experimental section, K_L and A increase during the deposition of metal powders under near-limiting current conditions.

The simple batch reactor is of only limited use industrially, as noted in Section 5.1, and a continuous flow through,single-pass R.C.E.R. may now be considered. Fig. 6.3 illustrates this mode with a steady volumetric flow rate of L $cm^3 s^{-1}$, and inlet and outlet concentrations C_{IN} and C_{OUT}. Under limiting current conditions, a steady state mass balance across the reactor yields

MASS INPUT - MASS OUTPUT = MASS ELECTROLYSED

$$N (C_{IN} - C_{OUT}) = K_L A C_{REACTOR} \qquad \text{Equation 6.13}$$

according to the C.S.T.R. approximation, $C_{REACTOR} = C_{OUT}$, and

$$N (C_{IN} - C_{OUT}) = K_L A C_{OUT} \qquad \text{Equation 6.14}$$

The terminal concentrations are related by

$$\frac{C_{OUT}}{C_{IN}} = \frac{1}{1 + K_L A/N} \qquad \text{Equation 6.15}$$

with a fractional conversion

$$f_R = \frac{C_{IN} - C_{OUT}}{C_{IN}} = 1 - \frac{C_{OUT}}{C_{IN}} \qquad \text{Equation 6.16}$$

$$f_R = \frac{K_L A/N}{1 + K_L A/N} \qquad \text{Equation 6.17}$$

The factor $K_L A/N$ may be regarded as a performance factor (c.f. $K_L A/V$ for the previous, simple batch case). For a given volumetric throughput N, the reactor conversion may be enhanced by increasing K_L, A or both. It has been noted previously that increasing K_L by use of a higher rotational velocity has mechanical and power requirement restraints, while any increase in area must be carried out judiciously with due regard for materials and fabrication costs. In practice, scale-up normally involves an increase in both K_L and A.

The limiting current for the single pass reactor, in terms of the inlet concentration, may be obtained by considering the definition of $K_L = \frac{I_L}{AzFC_{OUT}}$, and manipulation of Equation 6.15

$$I_L = AzFC_{IN} \; K_L \left\{1+\frac{KA}{N}\right\} \qquad \text{Equation 6.18}$$

For a steady state, single pass reactor, with constant R.C.E. characteristics (K_L and A) and a constant throughput (N), Equations 6.15 and 6.18 indicate that both the conversion and the limiting current are time invariant.

In practice, however, the deposition of metal as a powder under mass transport control takes place with a concomitant increase in both K_L and A. This aspect, examined in the experimental section, results in an enhanced conversion and limiting current.

Table 6.1 illustrates Equation 6.14 by considering the conversion of a hypothetical R.C.E.R. with $K_L.A = 1000 \text{ cm}^3 \text{ s}^{-1}$, corresponding to various flow rates in the range $0\text{-}10^4 \text{ cm}^3 \text{ s}^{-1}$. As expected, the conversion is very sensitive to flow rate. In practice, the conversion over a single pass R.C.E.R. for metal powder production is normally in the range 0.1 to 0.9. This value may be considered as rather high for a single compartment reactor, but substantial improvement is achieved by operating a number of compartments in hydraulic series in a 'cascade' R.C.E.R. (see Section 6.6).

It is an interesting thought that the conversion of a R.C.E.R. might be enhanced by recycling, as in Fig. 6.4a. The general case of a C.S.T.R. with recycle has been considered by Pickett[120]. It becomes obvious, however, that for a good C.S.T.R., no amount of recycled flow can increase the mixing inside the reactor, or the apparent residence time (V/N). Recycle is only effective on a poor C.S.T.R. which suffers bypassing from inlet to outlet. The conversion is then invariant with recycle ratio.

It might appear that there is no advantage in including a recycle loop on a R.C.E.R. Consider, however, the case shown in Fig. 6.4b where an inlet concentration from a process stream is time dependent, but a constant recovery rate of metal, i.e. a constant current must be passed through the reactor. The R.C.E.R. must function at a fixed concentration, C_{OUT} and hence a fixed inlet C_{IN}. This may be accomplished, over a restricted range, by diluting $C_{process}$ with treated outlet liquor from the reactor to lower its value to C_{IN}. The control operation may be automated by sensing C_{OUT} and taking appropriate control loop action to open or close valves in the process lines.

Batch Recycle Mode

The general case has been considered in Section 5.2.3, and it has been noted that this mode of operation is useful in the laboratory and in industrial processing. The system approximates to C.S.T.R. behaviour if the reservoir volume is much larger than that of the reactor, and the residence time in the reservoir is high.

This mode is very useful in the laboratory for the following reasons:

1) the well mixed reservoir provides a large buffer capacity to smooth out any concentration fluctuations,

2) additions of replenishment chemicals may be added directly to the reservoir, for rapid and convenient mixing, e.g. metal concentrate solution,

3) the reservoir may be readily diluted in metal either by immersing a secondary electrolytic cell in it, or by addition of background electrolyte,

4) if the reservoir is dosed with metal concentrate (or metal dissolved anodically), the system may be used as a single pass R.C.E.R. with a large inlet concentration buffer capacity.

6.2.2. Power Requirements

The power consumed by a R.C.E.R. may be divided into electrolytic (Faradaic) and rotational power.

Faradaic

The electrolytic power consumption P_E may be obtained as the product of reactor voltage and reactor current

$$P_E = V_{CELL} \cdot I$$

The reactor voltage includes components due to potential drops in the busbars, electrical brushes and electrode feeders, the electrolyte, and the algebraic electrode potentials

$$V_{CELL} = IR_{electrolyte} + IR_{busbars} + E_{anode} + E_{cathode} \qquad \text{Equation 6.19}$$

In the case of a divided cell reactor, the contributions of anolyte and catholyte potential drops may be separated, and the membrane potential drop must be taken into account

$$V_{CELL} = IR_{anolyte} + IR_{catholyte} + IR_{busbars} + E_{anode} + E_{cathode} + IR_{membrane} \qquad \text{Equation 6.20}$$

Recent increases in energy costs have encouraged process technologists to critically examine each of the above components, and power consumption has become a major criterion in reactor performance.

In the case of the R.C.E.R., the electrolyte resistances may be minimised by restricting the annular interelectrode gap. The anode potential contribution in the case of an insoluble anode may be minimised by use of an open mesh design to allow free gas evolution. In the case of divided cells, a thin conductive ion exchange membrane may be employed. Voltage drops in the anode feeders may be minimised by thick cross-sections, while for the rotating cathode correctly machined, large surface area, metal filled graphite brushes running on a conductive slip ring may be employed.

Typically, for deposition of copper powder in an industrial divided R.C.E.R.

$R_{membrane}$ = 3.5 ohm cm^{-2}
$R_{anolyte}$ = 2.5 ohm cm^{-2}
$R_{catholyte}$ = 7.5 ohm cm^{-2}
$R_{busbars}$ = 0.1 mohm
E_{anode} = 1.5 V
$E_{cathode}$ = 1.2 V

At a reactor current of 1 KA ≡ 0.2 Acm^{-2}, Equation 6.20 gives

$$V_{CELL} = V_{anolyte} + V_{catholyte} + V_{busbars}$$
$$+ E_{anode} + E_{cathode} + V_{membrane}$$
$$= (0.2 \, . \, 2.5) + (0.2 \, . \, 7.5) + (1000 \, . \, 0.1 \times 10^{-3})$$
$$+ (1.5) + (1.2) + (0.2 \, . \, 3.5) \text{ V}$$
$$= 0.5 + 1.5 + 0.1 + 1.5 + 1.2 + 0.7 \text{ V}$$

$$\underline{V_{CELL} = 5.2 \text{ V}}$$

It may be noted that the catholyte potential drop results in a heating effect. This may be utilised, however, in order to increase the mass transport of the reactor. The increase in temperature may be estimated as follows

$$\Delta T = \frac{P_{catholyte}}{4.19 \times N} \qquad \text{Equation 6.21}$$

where ΔT is the increase in °C, and

$$P_{catholyte} = I \, V_{catholyte} \qquad \text{Equation 6.22}$$

In the above example,

$$P_{catholyte} = 1.5 \, . \, 1000 \text{ W}$$
$$P_{catholyte} = 1500 \text{ W}$$

and the temperature rise given by Equation 6.21 at a flow rate of 100 $cm^3 \, s^{-1}$ is

$$\Delta T = \frac{1500}{4.19 \times 100} \; ^{o}C$$

$$\underline{\Delta T = 3.6 \; ^{o}C}$$

If the current efficiency is 85% for copper deposition, the 1000A will deposit 1005 g Cu in 1 hour. This is equivalent to a Faradaic yield of 5.2 KW hr/Kg. To this figure must be added the rotational power requirements.

Rotational Power Requirements

There appears to have been very little work reported concerning turbulent flow in fluids of low Schmidt No. with regard to the power required to rotate an inner cylinder within a coaxial stationary outer cylinder. While detailed theoretical and experimental studies have been carried out in the laminar regime, the approach to turbulent flow must be via experimental studies which give rise to empirical relationships.

As reported in Chapter 2, the most comprehensive examination of turbulent flow power requirements has been by Donnelly and Simon[17-20]. Unfortunately, this work was mainly concerned with Reynolds numbers near the critical value (ca. 200), and with small cylinders (d ~ 1 cm). With regard to practical R.C.E.R.'s, the work of Wendt[288] is more relevant as it involved smooth cylinders of radius 13.75, 12.5 and 10.0 cm rotating within a fixed 14.7 cm radius outer cylinder.

For $\left[\frac{U\,(r_o - r_I)}{\nu}\right] > 10^4$, the following empirical expression was derived for the torque transmitted to the outer cylinder

$$G = 0.073\,\pi\, r_I^{\,4}\, \rho\, l\, w^2 \left\{\frac{Sr_o}{r_I^{\,2}}\right\}^{0.25} \left\{\frac{Wr_I S}{\nu}\right\}^{-0.3} \qquad \text{Equation 6.23}$$

The power consumed in rotation may be obtained by multiplying by the angular velocity, w

$$P_{rot} = 0.073 \pi r_I^4 \rho l w^3 \left\{\frac{Sr_o}{r_I}\right\}^{0.25} \left\{\frac{wr_I S}{\nu}\right\}^{-0.3} \qquad \text{Equation 6.24}$$

writing $w = U/r_I$,

$$P_{rot} = 0.073 \pi r_I \rho l U^3 \left\{\frac{Sr_o}{r_I}\right\}^{0.25} \left\{\frac{US}{\nu}\right\}^{-0.3} \qquad \text{Equation 6.25}$$

It may be noted that the equation denotes a small dependence of the power on the (interelectrode) gap $S = r_0 - r_I$ and the radius ratio r_o/r_I. For a given geometry (known r_o, r_I, l) and fluid, (known ρ and ν), the equation may be simplified to

$$P_{rot} = \text{constant } U^{2.7} \qquad \text{Equation 6.26}$$

showing a rapid increase in P with increasing peripheral velocity U.

In Chapter 2, an expression for rotational power derived from fluid mechanic considerations was stated as

$$P_{rot} = \frac{f}{2} \cdot \pi \rho r_I l U^3 \cdot 10^{-7} \qquad \text{Equation 6.27}$$

for a smooth cylinder,

$$\frac{f}{2} = 0.079 (Re)^{-0.30} \qquad \text{Equation 6.28}$$

Combining Equations 6.27 and 6.28

$$P_{rot} = 0.079 \; . \; \pi \rho r_I \cdot l \, U^3 \left\{\frac{Ud}{\nu}\right\}^{-0.30} . \; 10^{-7} \qquad \text{Equation 6.29}$$

It is interesting to compare this with Equation 6.25. While both equations indicate a $U^{2.7}$ dependence, Equation 6.29 shows no dependence on $r_o - r_I$ or $\frac{r_o}{r_I}$ due to the absence of these factors in Equation 6.28.

Considering typical values for the parameters, the respective P_{rot} may be calculated.

$\rho = 1 \text{ g cm}^{-3}$

$r_I = 11.75 \text{ cm}$

$l = 23 \text{ cm}$

$U = 1000 \text{ cm s}^{-1}$

$d = 23.5 \text{ cm}$

$r_o = 12.75 \text{ cm}$

$\nu = 0.00591 \text{ cm}^2 \text{ s}^{-1}$

Equation 6.29 yields 69 W while Equation 6.25 gives 171 W.

For rough cylinders in a saturated roughness condition,

$$\frac{f}{2} = \left(1.25 + 5.76 \log_{10} \frac{d}{e}\right)^{-2} \qquad \text{Equation 6.30}$$

Combining Equations 6.30 and 6.27,

$$P_{rot} = (1.25 + 5.76 \log_{10} \frac{d}{e})^{-2} . \pi \rho \, r_I \, l \, U^3 . 10^{-7} \quad \text{Equation 6.31}$$

Using similar figures to the above example, and assuming the surface roughness e = 0.1 cm, the new rotational power may be evaluated from Equation 6.31 as 385 W, a considerable increase over the case for the smooth cylinder. If e is increased to 0.2 cm, the power figure reaches 483 W.

It should be remembered that the above rotational power figures relate only to the shear force required to turn the cylinder. In practice this is supplemented by motor and drive losses.

6.2.3 Scale-up

As has been noted, the process of scale-up involves increasing the size and duty of the R.C.E.R. by increasing either K_L and/or A. This may now be considered in more detail, with the aid of mass transport correlations.

A generalised mass transport for the R.C.E.R. may be written

$$(St) = a \, (Re)^b \, (Sc)^c \quad \text{Equation 6.32}$$

It has already been seen that for a smooth cylinder, $b = -0.30$, Equation 6.33, while for powder forming conditions in the Eco-Cell, Holland[308] has suggested the useful empirical formula where $b = -0.08$ for copper deposition from acid sulphate solutions, Equation 6.34. In both cases, $a = 0.079$ and $c = -0.644$.

$$St = 0.079 \, (Re)^{-0.30} \, (Sc)^{-0.644} \qquad \text{Equation 6.33}$$

$$St = 0.079 \, (Re)^{-0.08} \, (Sc)^{-0.644} \qquad \text{Equation 6.34}$$

Rewriting Equations 6.33 and 6.34 as an expression of the mass transport coefficient:

$$K_L = 0.079 \, U^{1+b} \left\{\frac{d}{\nu}\right\}^{b} \left\{\frac{\nu}{D}\right\}^{0.644} \qquad \text{Equation 6.35}$$

One obvious concept of scale-up is such as to maintain the value of K_L. For a given metal and ion change, this amounts to maintaining the current density at a fixed metal concentration in the reactor. The increase in A with scale-up will then result in a larger duty, by virtue of the heavier currents involved. For a given solution at constant temperature, ν and D are fixed, and Equation 6.35 simplifies to

$$K_L = \text{constant } U^{1+b} \, d^{b} \qquad \text{Equation 6.36}$$

Equation 6.36 indicates that in order to maintain K_L, $(U^{1+b} \cdot d^{b})$ must itself be held constant during scale-up.

For a hydrodynamically smooth R.C.E.R., this factor is ($U^{0.7}$ $d^{-0.3}$) while for a powdered metal rough R.C.E.R., it becomes ($U^{0.92}$ $d^{-0.08}$). This results in markedly different scale-up requirements. Consider a cylinder where l = d = 20 cm (A = 1257 cm^2) and U = 1000 cm s^{-1} (corresponding to 955 revolutions per minute). For scale-up in the smooth cylinder case, increasing the area of the cylinder by a factor of 2 results in a diameter of 28.3 cm. To maintain the factor $U^{0.7}$ $d^{-0.3}$, U must be 1160 cm s^{-1} (equivalent to 783 revolutions per minute).

For a powdered R.C.E.R. however, maintaining $U^{0.92}$ $d^{-0.08}$ results in U = 1031 cm s^{-1} (equivalent to 696 revolutions per minute). The difference in r.p.m. is more marked with increasing scale-up as will be seen later.

Table 6.2 shows scale-up of 'Eco-Cells' according to Equation 6.34, showing the r.p.m. necessary to maintain K_L at 0.526 cm s^{-1}. In this table, d/l has been varied from 0.67 to 1.5 to allow a smaller number of diameters to be incorporated as a standard range.

For engineering convenience, the peripheral velocity might be maintained during scale-up at say 1145 cm s^{-1}, but according to Equation 6.34, this would result in a fall off in K_L with scale-up (Table 6.3).

It should be noted that as a consequence of scale-up, larger cylinders revolve at a decreasing speed, which facilitates engineering design.

If U is maintained during scale-up, the rotational power density, in W cm^{-2} will be similar for each size of R.C.E.R. .

During a linear scale-up in terms of area, the conversion over the reactor will increase in accordance with an earlier equation:

$$f_R = \frac{K_L A/N}{1 + K_L A/N} \qquad \text{Equation 6.17}$$

If, for example, the area is doubled and the flow rate N and mass transport K_L remain the same,

$$\frac{f_{R'2}}{f_{R'1}} = \frac{2(1+K_L A/N)}{(1+2K_L A/N)}$$

$$= \frac{2 + 2K_L A/N}{1 + 2K_L A/N}$$

If A/N is maintained, the conversion will remain constant.

The increased performance on scale-up may also be regarded as a chance to accept a higher volumetric throughput (i.e. increase N) while maintaining the same conversion.

Mass transfer to the R.C.E.R. is high, and a constraint on the performance of R.C.E.R.'s for a given size is the anode current density, which must not exceed that for known anode materials.

If a perfectly uniform concentric geometry can be assumed, neglecting any volume at the top and bottom of the cylinder, the volume hold up in the cell is that of an annular space defined by

$$V_{reactor} = \pi l \left(r_o^2 - r_I^2\right) \qquad \text{Equation 6.37}$$

The electroactive area is defined by

$$A = 2\pi l \, r_I \qquad \text{Equation 6.38}$$

The area/volume ratio is then

$$\frac{A}{V} = \frac{2\pi l \, r_I}{\pi l \left(r_o^2 - r_I^2\right)} \qquad \text{Equation 6.39}$$

If $d = 2r_I = l$,

$$\frac{A}{V} = \frac{2r_I}{r_o^2 - r_I^2}$$

If $r_o - r_I = 1$ cm

$$\frac{A}{V} = \frac{2r_I}{(r_o + r_I)}$$

Further, if $r_o \longrightarrow r_I$ which is true for larger cells,

$$\frac{A}{V} \longrightarrow 1 \text{ cm}^{-1}$$

Table 6.4 examines the cell volume as a function of reactor size during scale-up. It can be seen that the volume increases with the area as required by Equation 6.37. Further, A/V $\longrightarrow$ 1 cm^{-1} as discussed above.

It can also be seen that for a given flow rate, the nominal residence time V/N increases with reactor size (Table 6.5).

6.3 Design and Construction

6.3.1 General

The design and construction of both laboratory and industrial R.C.E.R.'s may now be discussed. There are many features which have influenced the overall design, but the following points are worthy of special consideration.

1. Is it desirable to seal the reactor?

2. Is division of the reactor necessary?

3. Is the R.C.E. wiped or scraped?

4. Does the reactor incorporate a reference electrode probe to measure the R.C.E. potential, or facilitate potentiostatic control?

Regarding sealing, very few reported reactors have been sealed, presumably due to the additional engineering complexities this introduces such as a rotary shaft seal. There are, however, several practical reasons for sealing the reactor:

1. gases evolved at the electrodes and entrained in the electrolyte may be safely vented,

2. the reactor is more likely to fill, and vortex formation is discouraged,

3. fluidisation and removal of metal powder from the catholyte is encouraged,

4. the reactor flow system may form a closed circuit to prevent air oxidation or atmospheric corrosion of nearby plant.

In laboratory cells, the design is often that of an overhung stirrer in a beaker with clear access at the cell top for introduction of the R.C.E. Vortex formation in such systems may be discouraged by either a baffle plate surrounding the shaft and near the solution level, or by a close fitting lid around the shaft. Air oxidation of the electrolyte may be discouraged by a conventional inert gas (e.g. nitrogen) blanket over the electrolyte.

In the case of continuous metal powder production in the Eco-Cell, (one of the few examples of a sealed cell), consideration must be given to the protection of the shaft seal against the abrasive action of fluidised metal particles.

There are several reasons for dividing a reactor into separate anolyte and catholyte compartments:

1. the use of a separate anolyte facilitates choice of an anode; the provision of a noble anode in aggressive process solutions is often a difficulty,

2. in the case of soluble anodes, such as in a refining cell, the membrane may prevent anode slime from spoiling the cathode deposit,

3. if the membrane has ion exchange properties, the selective directional transport of a given species of ion may be practised, i.e. electrodialysis,

4. a reactor may be utilised for a variety of metal containing catholytes, while retaining the same anode/anolyte (as in the experimental part of this Thesis),

5. if oxygen evolution is the primary anode reaction, and hydrogen evolution occurs as a secondary reaction at the cathode, the membrane serves to separate a potentially hazardous combination of gases in a solution.

Depending upon the application, and the mechanical characteristics required, the reactor may be divided by a porous ceramic cylinder, porous plastics, or ion exchange membranes. The last mentioned dividers have the advantage of being light, thin, of excellent chemical stability, low resistance, and of having a specific mode of ion conduction, but are relatively expensive and need careful support over their area, which tends to increase the complexity of design. The support fabrication necessary may decrease the available membrane surface area, resulting in an increase in membrane (and anode) current density.

The possibility of scraping or wiping the electroactive surface of the R.C.E. has been considered in the literature. Such contact of the cylinder may be continuous or periodic and may serve to clean and activate the electrode, remove the product of reaction, enhance rates of mass transfer or even subdivide the R.C.E. compartment. According to the duty required, the wiper/scraper may be a relatively soft material such as rubber, or a hard machining tool material such as 'Stellite' alloys. Nadebaum and Fahidy[289] have provided a brief tabular review of wiped electrodes.

Strafelda and Singer[294] have reported the use of a small laboratory bismuth R.C.E. which formed a predictable, well characterised, near-ideal pH electrode when wiped continuously with a soft rubber blade. In a second paper, Strafelda and Kozak[293] employed a wiped graphite R.C.E. as a continuous amperometric analyser for the determination of phenol in water via anodic oxidation.

Spencer et al.[296,297] have described[296] and patented[297] a wiped rotating cylinder for an electroorganic reaction; the cathodic reduction of bisulphite to dithionate. This reactor is described in detail later in this Chapter.

Chin et al.[72] have described mass transport studies to a rotating cylinder wiped by a 'skimmer plate' of PTFE. These studies, described later, were undertaken in order to model mass transport to a moving sheet.

The novel 'rotating multipolar electrode' reactor of Nadebaum and Fahidy[289-292], utilises PTFE wiper blades to divide the reactor into several compartments, with an improvement in mass transport[290] and continuous activation of the surface[295]. This reactor, which has also been scaled to pilot plant size[298], is considered in detail later.

Considering reactors for the electrodeposition of metals, the rotating cylinder provides a useful geometry which may be readily scraped by either static or dynamic, partial or full, continuous or periodic, single or multiple devices. The patent literature contains several references to the use of such reactors in the production of metal flakes and powders. The scraper may dislodge powder to the bottom of the reactor, where it may be periodically withdrawn, or it may allow the powder to fluidise out of the reactor, or act as a chute to carry the powder away from the cylinder.

These scraped reactors[299-307], including the recently developed Eco-Cell[306-309] R.C.E.R., will be reviewed in detail later in this Chapter.

Controlled potential electrolysis of a R.C.E.R. by means of a potentiostat has been referred to in Section 5.3.1. In order to exert potentiostatic control the R.C.E. potential must be measured with respect to a standard reference electrode. This necessitates the introduction of a probe into the reactor which must be tough, resistant to chemical and abrasive action, and which must pass through the reactor body such that its tip lies near the active surface of a central portion of the R.C.E. The probe connects via a salt bridge to a reservoir containing the reference element. In practice, it may be necessary to seal or pressurise the reservoir to prevent bulk diffusion of liquid from the cell. In addition, the R.C.E. shaft must be fitted with an auxiliary potential sensing or 'zero line' brush (Fig. 6.6b). This brush connection carries only the minute (pA) measurement current in a high impedance circuit, and in this way voltage drops across the power brushes are not included. In the absence of this brush (Fig. 6.6a) the reactor effectively operates in a partially galvonostatic mode.

6.3.2 Laboratory Reactors

It is now interesting to compare the construction of laboratory cells which have been described in the literature. The majority of these studies involve mass transport measurements, and have been described in an earlier part of this Thesis (Section 4.6). Table 6.7 attempts a broad comparison of laboratory R.C.E. cells and reactors with regard to design, materials of construction, and mode of control. The complexity of these cells ranges from a rudimentary, unsealed, undivided 'pole in beaker' design[73], to an engineered divided and sealed cell[94] (present work).

Cell Body

Swalheim's early cell employed a bakelite material, but the majority of later ones have utilised acrylic plastics ('Lucite', 'Perspex', 'Plexiglas') as an insulating, transparent casing. Acrylics have several advantages; from the constructional point of view they are readily available in standard forms including tube, bar and sheet, may be bonded by welding, or use of a solvent or solvent cement, and are readily machined and polished. From an operational point of view, the material aids visibility (although this advantage is of course largely lost if the counter electrode is a continuous cylinder).

Glass (including simple beakers) has also been employed[73], as a vessel. An alternative to an insulating cell body is to fabricate it in the anode material. This feature was incorporated into Robinson's[68,84] cell (Fig. 6.12), where a cylindrical copper vessel was employed as a soluble anode, the cup shaped body being directly clamped to an 'O' ring in a phenol-formaldehyde resin top plate. The bottom of the vessel was treated with an insulating layer of polystyrene to limit anodic dissolution to the cylinder sides. A similar approach could undoubtedly be adopted for nickel counter electrodes for the ferro/ferricyanide redox reaction. The use of discrete foil or mesh counter electrodes in an insulating vessel minimises investment, especially in the case of more exotic anode materials such as platinised titanium[89], and results in a more versatile cell where a soluble or insoluble anode may be utilised. Certain materials (e.g. lead) are either too heavy or soft to be utilised as a vessel.

For particularly aggressive solutions containing organics or operating at high temperatures, acrylic plastics have a limited lifetime and more suitable materials include polypropylene, PTFE[289] or ceramics. Polypropylene, used for certain Eco-Cell designs (see later) must be welded (suitable adhesives are not available) and the cell designed for strength, as the material is less rigid than acrylics. PTFE is rather expensive, is not readily available in some standard forms, and may not be easily bonded by either welding or adhesives.

Sealing and Covering

The majority of cells have been covered by a top plate to prevent splashing and vortexing, and discourage heat loss. This top plate may conveniently incorporate a steady gland[68,84,284] for the shaft (which may tend to act as a seal if close fitting) or a pukka seal.

Care must be taken to ensure that electrodeposition or dissolution does not occur in the seal area, and the cell may be only partially filled[284] for this reason.

The cell body, if cylindrical, may be conveniently sealed to one[68,84] or both[94,82] of the end plates by an 'O' ring seal compressed into a groove with appropriate tie bars[68,84,94,82,58].

This arrangement has the advantages that disassembly is relatively easy, and different sizes of cell body tubes may be accommodated by a series of concentric 'O' ring grooves in the end plates[58]. This design would also accommodate a diaphragm cell divider in the form of a ceramic tube. Such an arrangement has been constructed by Sudall[201], but for an agitated vessel rather than a R.C.E.R., and by Postlethwaite et al. for a R.C.E.R.[94] (Fig.6.13).

It has already been noted that, with the exception of Eco-Cells and the reactor described in the experimental section of this Thesis, there are very few examples of fully sealed cells in the literature. Moreover, almost all of the laboratory cells have been used in the batch mode, with no provision for flow through the reactor.

Rotor and Drive

The design of the R.C.E. depends very much on the study in hand. In the simplest case, the R.C.E. and the drive shaft may be continuous, having been machined from a solid bar of material; the electroactive area of the cylinder may be delineated by insulating laquer, tape or sleeves and discs. In practice, a much more versatile cell results if the cylindrical electrode is demountable from the shaft, when different sizes and types of electrode may be used, and electrode preparation and cleaning are facilitated. Such preparation may include abrasion, chemical or electropolishing, pickling or chemical cleaning, or electroplating to yield a fresh, reproducible metal surface.

In the particular case of surface studies by, for example, microscopy, a metal foil may be employed, wrapped around the rotor, (Robinson[68,84], Beard et al.[312] and the present work). This is facilitated by the fitting of machined end caps.

Swalheim[310] and Beard et al.[312], utilised the R.C.E. to simulate high speed plating of steel strip, and the plated foil could be removed for further treatment or examination.

Eisenberg et al.[57] and Sherwood and Ryan[313] have studied chemical dissolution by casting organic acids directly as a solid rotor, and machining the surface.

It is interesting to compare the shape of R.C.E.'s in laboratory cells, by means of the ratio d/1. Normally, this ratio is approximately unity, although it has been systematically varied from 0.33 to 3.3 by Eisenberg et al.[58,112]. The majority of investigators have used a fixed geometry, and a d/l ratio of $\leqslant 1$, i.e. long cylinders. Aside from the convenience of simply extending the drive shaft to form the rotor, long cylinders have the advantage of minimising the contribution of any edge effects near the end caps due to a change in hydrodynamics or current density distribution. Squat cylinders of high d/l ratio have, however, been reported by von Hahn and Ingraham[314], and the study of Pini and DeAnna[316] used a R.C.E. with d = 5 cm, l = 0.25 cm. Robinson and Gabe[68] have pointed out the advantages of using a low ratio d/l, but using only a portion of the active area.

All of the cells in Table 6.7 have utilised a vertical R.C.E., and this no doubt reflects the ease and convenience of such a system, where a cell seal may be avoided, and the cell may be separated either by raising the electrode and drive, or lowering the cell. In common with the rotating disc electrode, the R.C.E. requires a variable speed, controlled drive. Eccentricity and vibration, although deleterious from the mechanical point of view, have far less effect on the already turbulent R.C.E. than on a normally laminar R.D.E. The drive to the shaft may be either direct or via a pulley and belt arrangement, and this is largely a matter of mechanical convenience. One point which should be borne in mind, however, is that it may be desirable to electrically insulate the shaft from the drive motor. The use of different ratio pulleys generally enables a wide range of rotational speeds to be realised. If a high r.p.m. drive motor is directly coupled to the shaft, without an intermediate gearbox or pulley system, it may be difficult to realise low rotational speed due to commutating from the motor, or mechanical resistance in the bearings.

Normally an electric motor is used but hydraulic and pneumatic drives are possible, and an air motor has been used[310].

Rotational speed may be measured with a mechanical tachometer or stroboscope, but a more accurate and suitable device is an electronic tachometer which may be used to automatically control the speed.

A whole variety of bearing arrangements have been utilised in the literature. The simplest designs have utilised a stirrer motor with no additional bearings, or with merely a guiding gland near the cell top. Other designs have utilised one or more bearings between the motor and the cell to produce a rigid assembly[58,68,84,282,190,94]. A bearing may be mounted on the cell top[315]. In the absence of bearings between the cell and the drive motor, or for additional support, the top plate of the cell[68,84],(present work) the bottom plate[94,310] or both[284,58,82] may be fitted with steady bearings, typically fabricated as a PTFE sleeve in the top plate or a cup in the bottom.

Power Supply and Control

Conventionally, power may be supplied to the rotating cylinder electrode via brushes, or liquid metal contact. The latter is suitable for laboratory cells involving small currents, as the mercury may be held in a cup with a platinum wire or rod making electrical contact. For higher current, however, a larger surface area inverted cup design (see Fig. 6.11) is normally used and this may suffer from hazardous splashing, with poor contact at higher rotational speeds[68]. The use of a conducting mercury well[190,73,58,284,311,74,82,94,282] conveniently avoids the need for a separate potential measurement contact.

Metal brushes have been employed for higher currents, but graphite brushes, especially when metal filled and running on a well-machined matching slip ring, are preferred and have been used by several groups of workers[68,84,315,310,89], as well as in the present study.

It has been noted that a second brush is necessary for potential measurement, and this has been incorporated by several research workers[190,89] as well as by the present author.

Unusual Features

Certain specific features of R.C.E. cells have already been mentioned, including the design of rotors to hold foil electrodes[68,84,312,310].

In contrast to the R.D.E., which is normally restricted to an active surface area appreciably below 1 cm^2, the majority of laboratory R.C.E.'s are 'macro' electrodes, having typical surface areas in the range 10-200 cm^2. In view of this, it is interesting to note that a study has been reported[316] on a 'micro' cylinder of apparent surface area 3.93 cm^2, being a platinum plated, nickel plated brass cylinder of diameter 5 cm and length 0.25 cm. Current densities of approx. 2-12 mA cm^{-2} were obtained by rotating this electrode at 480-1980 r.p.m., corresponding to currents of approximately 8-48 mA only.

A vertically finned R.C.E. has been studied by Sedahmed et al., as described previously in Chapter 4.

Normally, the inner cylinder is rotated in a fixed outer coaxial cylinder, but Ramaraju et al[114] have reported work on a cylindrical anode vessel rotated about a fixed cylindrical cathode. This cell employed a horizontal ring plate baffle near the solution level, presumably to avoid vortexing.

Several workers have included vertical baffles inside the R.C.E.R., sometimes in order to aid mass transfer by encouraging random turbulent flow. Thus Swalheim[310] (Fig. 6.6) included baffles "... for the purpose of acting as plates in breaking or retarding the excessive rotation of the plating solution". This author also considered that baffles were necessary "to confine the current largely to one half of the total cathode area", in order to facilitate accuracy in calculating anode efficiencies. Krishna and Jagannadharaju[74] included vertical baffles fixed to the outer cylindrical container walls (Fig. 6.9) to impede rotational flow. These authors state that narrow vertical baffles considerably influence flow, but studies to this effect have concerned impeller stirrers[318] which would be expected to give rise to strong rotational flow. The authors also sought to improve mass transfer by including an impeller at the bottom of the R.C.E., but there was no marked enhancement.

Recently[319], a pump impeller has been included on the bottom of a R.C.E. to render the reactor self pumping and increase fluidisation of metal powder scraped from the cathode. It will be seen later that several reactors in the patent literature have included R.C.E. fitted with impellers.

The use of a rotating coaxial outer cylinder for corrosion studies in a dynamic fluid has been discussed by Heitz[320] et al.

The judicious use of expensive platinum foil on a fixed titanium anode[311] or a PTFE R.C.E. cathode[289] has been described in the literature.

A case of severely impeded flow around a R.C.E. is, perhaps inadvertently, provided by Chin et al.[315]. These authors used a R.C.E. to simulate mass transfer to a continuous moving strip, and provided a single, full length, close fitting baffle in the form of a PTFE 'skimmer' plate (Fig. 6.19). The mass transport results were markedly different to those known for the R.C.E.

The R.C.E.R. invented by Nadebaum and Fahidy[292] and studied by Fahidy et al[289-292] is worthy of special consideration due to its novelty and sophistication. This device, referred to as a rotating bipolar electrode (R.B.E.) cell is depicted in Fig. 6.15, and has several distinguishing features:

1. the R.C.E. is wiped continuously by close fitting PTFE blades which subdivide the reactor,

2. the R.C.E. is bipolar, as the anodes in the subdivided compartments are held at different potentials, and as a consequence the R.C.E. is voltage pulsed.

   Indeed, the R.C.E. may be cathodic in one compartment, and anodic in the other,

3. the device normally operates at rather low rotational velocities, but the mass transfer is enhanced by the wiper blades.

The earlier design of a bipolar electrode, used for an examination of the mass transfer characteristics, was superceded by an improved tripolar design using three carefully machined wiper blades to yield a low intercompartmental leakage current. This design employed a platinum surface R.C.E., 12.50 cm long and 3.176 cm diameter, giving an electroactive area of 145.8 cm^2. The R.C.E. was installed inside a PTFE cylinder supported by a steel sheath. The R.C.E. was driven from below with a PTFE-PTFE bottom bearing and a close fitting top bearing. Inert gas was passed through the bottom bearing obviating a continuous electrolyte film under the electrode and reducing current leakage. The specially designed wiper blades maintained an average gap size of $<$ 0.0015 cm.

Mass transport in this reactor[289,290] has been described in Chapter 4. The reactor has normally been potentiostatically controlled.

It is understood that the development of a pilot plant version of the above reactor is proceeding (Fig. 6.16), but full details are as yet unavailable.

The applications of the R.B.E. reactor will be reviewed in a following section. An industrial scale version has been envisaged for the purpose of a recent economic analysis[258].

A comparison between the above reactor and the multicompartment Cascade R.C.E.R. is made in a later part of this Chapter (Section 6.6 and Table 6.6).

Several other laboratory reactors are of interest. Fig. 6.17 shows an undivided R.C.E.R. with a hexagonal arrangement of graphite plate anodes, and a stainless steel/polypropylene rotor. This reactor, suitably engineered, has been employed in the recovery of precious metals including silver from photographic fixer solutions, and gold from an alkaline cyanide solution[321].

In laboratory cells, it is often convenient to employ plate anodes and flat membranes, and Fig. 6.18 shows a suitable arrangement for this. Fig. 6.18 a) shows an open catholyte, where the cell body may be formed by a large tank, while 6.18 b) depicts a closed catholyte arrangement for handling smaller volumes.

6.4 Laboratory Applications

6.4.1 Mass Transport Studies

It has been seen in Chapter 2 that a wide range of flow patterns is possible in a R.C.E. geometry merely by changing the rotational speed, and this has encouraged hydrodynamic and mass transfer studies involving the R.C.E. geometry (see Chapters 3 and 4), with and without axial flow. The electrochemical study of mass transfer is a particularly elegant means of obtaining mass transfer data, and its use as a routine tool has been encouraged in recent years by the development of mass transfer correlations (see Section 4.6).

The last ten years or so have seen growing interest in voltammetry as a means of obtaining electrokinetic data, and for analytical purposes. Forced convection is often employed to obtain sensitive, steady-state reproducible conditions at an electrode, the technique then being referred to as 'hydrodynamic voltammetry'. Forced convection electrodes have been reviewed by Adams[118], and may be divided into static electrodes with moving electrolyte, or dynamic electrodes. There are many examples of stationary electrodes including conical, spherical, wire, tubular, channel, micromesh screen and wall-jet types. Also included in this class are the numerous porous columnar electrodes. The most studied stationary electrode is the tubular variety which may be utilised for the quantitative analysis of flowing streams.

The most studied dynamic electrode is undoubtedly the rotating disc which along with the ring disc has found extensive use in the elucidation of electrochemical kinetics as noted in Chapter 4. Other rotated electrodes include the wire, hemisphere and sphere.

The majority of the above electrodes are best suited to laminar flow conditions, which restricts studies to low mass transfer rates, below 0.01 cm s^{-1} say. Turbulent flow, characterised by random chaotic eddy motion, is often avoided in academic studies as it is invariably more difficult to treat from a theoretical standpoint. However, turbulent systems are essentially for high mass transport studies, and the rotating cylinder supplements the rotating ring electrode, the turbulent tube electrode and the micro-ring electrode in pipe flow.

The R.C.E. has found surprisingly little use in hydrodynamic voltammetry, despite established mass transport correlations. It possesses several possible advantages, however, including a very high mass transfer (making it suitable for very fast reactions) which is readily varied by changing the rotation rate, and a very uniform electrode potential and current density distribution. In addition, the mass transport rate at the turbulent R.C.E. is substantially independent of velocity, and the device is thus well suited to the analysis of electrolyte streams.

One possible disadvantage of the R.C.E. here is the incidence of turbulent fluctuations of the voltammogram in the limiting current region. This feature, common to other turbulent electrodes, may be attributed to microscopic velocity changes due to eddy penetration into the laminar sub-layer. This effect has been studied at a R.C.E.[282].

6.4.2 Electroanalysis

As mentioned above, hydrodynamic voltammetry may be used as an analytical tool, for gravimetric and coulometric techniques as well as in the separation of metals prior to analysis.

The controlled potential separation of the more noble metal at a R.C.E. has been referred to previously in Section 5.3.2, and the technique is described in detail by lingane[211] in Vogel's text book[210], and by Rechnitz[226]. Vogel's book[210] provides an example.

(p.525) of a rotating platinum gauze anode cell used to selectively deposit metals at a cylindrical platinum gauze cathode whose potential is closely controlled. Depending on the ease of separation, control of cell voltage or potentiostatic control may be required. The rotating cylinder has a substantially uniform electrode potential across its entire surface, facilitating a clean separation, and the high rates of mass transfer ensure a reasonably rapid analysis time. The inert platinum cathode facilitates chemical cleaning and being static is less likely to lose metal than a rotating cylindrical cathode. A great advantage of electrolysis is that it avoids addition of extraneous reagents which may complicate subsequent determinations. In addition, it avoids the loss of constituents via coprecipitation, which is a drawback of chemical precipitation methods of separation.

The industrial separation of metals by the R.C.E.R.[323] is being encouraged by the development of large scale potentiostats and suitable reactors such as the Eco-Cell.

One of the few examples in the literature of a flow through R.C.E. cell is the one due to Johansson, (Fig. 6.20) which has been employed as a controlled potential coulometric device.

6.4.3 Electrodeposition

The R.C.E. has been utilised to examine various aspects of electrodeposition, including electroplating deposit quality, surface morphology of powdered deposits, electrowinning and electrorefining.

The studies of Swalheim[310], Beard et al.[312] and Chin et al.[72] in simulating strip plating have already been noted. The electroforming of metal foils on a horizontal, partially immersed, slowly rotating cylinder cathode is accepted industrial practice, and is routinely used for nickel and copper foil production. Electroforming may be contrasted with the application of the Eco-Cell to metal recovery. The latter is a high peripheral velocity, high mass transfer device well suited to the recovery of metal from relatively dilute solutions ($<$ 2 gpl), whereas electroforming is invariably carried out in high concentration ($\sim$ 60 gpl) solutions with a rotational velocity in the order of several r.p.m. In the case of electroforming, close conforming anodes help to ensure a low IR drop in solution with uniform current density, while pumping the electrolyte through the annular gap provides increased rates of plating and uniform solution composition. It may be noted that the hydrodynamics at the partially immersed cylinder are not well defined.

Metal mesh may also be produced at R.C.E.'s[324,302] and this will be referred to later.

Earlier work on electrodeposition has been reviewed by Narasimham and Udupa[255] and is essentially qualitative making use of the R.C.E. motion to improve the rate of deposition or the deposit quality.

Edwards and Wall[284] have considered experimental power consumption in a copper electrowinning R.C.E. cell.

The presence of uniform potential and current density over a substantial area of the R.C.E. facilitates studies involving microscopic or profilometric examination of deposit morphology[320,68,84], as in the present work.

The uniform deposit morphology extends to the case of metal powder deposition, and forms an important aspect of the experimental work in the present study. Nadebaum and Fahidy[291] have employed the novel 'rotating bipolar electrode cell' to concentrate, refine and purify copper in sulphuric acid solution.

The use of the copper deposition reaction to study mass transfer at a R.C.E. has been discussed in Chapter 3.

6.4.4 Corrosion

The use of the R.C.E. to study corrosion in dynamic environments is a developing field which owes much to the endeavours of Heitz and his colleagues at the Dechema Institut, Frankfurt.

Much of the earlier literature is confused due to a tendency for chemical reactions to be rate controlling at higher rotational speeds rather than mass transfer[270-277] control. At intermediate speeds, the velocity index was found to have values between 0.7-1.0. Gas evolution may also have an important effect, and Roald and Beck[175] found that at low acidities the rate of corrosion of magnesium by hydrochloric acid was proportional to (angular velocity)$^{0.71}$ as expected, but for HCl $>$ 1.4 M, the corrosion rate was apparently independent of rotation.

Heitz[287] has pointed out that the R.C.E. offers a much more convenient laboratory tool than a flow through pipe geometry. There are several reasons for this:

1. a small volume of fluid may be used,

2. flow rigs may be avoided, including rotammeters and pumps,

3. there is greater access to the specimen for pretreatment and examination,

4. the effect of relative flow may be easily studied by altering the rotational speed.

While an inner R.C.E. may be studied for corrosion tests, Heitz et al.[325] have preferred an outer rotating cylinder with a static cylindrical specimen, referring to this as a 'coaxial cylinder'.

With increasing rotational velocity, three separate regions may be discerned. After a region in which the mixed kinetics of mass transfer and phase boundary kinetics predominate (region I), a region virtually independent of flow rate follows (region II) as with earlier studies. Finally, typical erosion corrosion ensues with a further increase in corrosion rate (region III) after an induction time of several hours. The above workers have used the 'coaxial cylinder' for the selection of resistant materials for the casings of seawater pumps[325]. Studies involving a flow through 'coaxial cylinder' (described in detail by Loss and Heitz[326]) involved a rotation speed of up to 7000 r.p.m. about an inner cylinder of 12 m diameter, with an annular gap of 0.4 cm. There are several advantages of the static inner sample electrode:

1. surface corrosion products are not removed by centrifugal force,

2. the flow pattern is considerably more stable; no Taylor vortices occur,

3. difficulties of electrical contacts to a rotating assembly are avoided.

A 'rotating drum' corrosion test, relevant again to erosion corrosion, is described by Syrett[332].

The effect of dissolved oxygen[327] and chloride[328,329] ions on the rate of corrosion has been studied.

The cathodic protection of a Monel R.C.E. in 4% sodium chloride at 23°C has been examined by Cornet and Kappesser[89], while Kar et al.[285,311] have studied the effects of alkyl amine surfactants on cathodic protection.

Sedahmed et al.[90] have described the reduction of the corrosion of copper via use of inhibiting drag reducing agents added to the orthophosphoric acid.

Makrides et al.[191,330,331] have attempted to incorporate a roughness factor into mass transport relationships for corroding specimens.

6.5 Commercial Applications

Despite a host of diverse laboratory studies, there has been relatively few reports of commercial R.C.E.R.'s in the technical literature with the exception of the Eco-Cell. It is necessary instead to explore the patent literature, where a whole variety of R.C.E. assemblies are found, particularly for metal deposition, but also for organic synthesis. Some of these patents date back to the turn of the century, showing that commercial R.C.E. assemblies are by no means a recent introduction.

6.5.1 Organic Synthesis

Udupa et al.[333] have synthesised salicylaldehyde on a pilot plant scale by reduction of salicylic acid. Production was carried out on a semi-continuous basis using a reactor incorporating three amalgamated copper R.C.E. cathodes (Fig. 6.21). The reactor employed 10 cm. diameter seamless copper pipes, cored with wood, and stopped off at the bottom with black pitch, rotating at 1800 r.p.m. The salicylic acid catholyte was separated from the sulphuric acid anolyte and lead anodes by a porous rubber diaphragm. This process was scaled up from a laboratory cell to a 300 A unit capable of producing 1 Kg of the aldehyde in four hours at 18°C and a current density of 12-15 A dm^{-2}.

Spencer et al. , as previously noted, have described[296] and patented[297] a novel wiped R.C.E.R. to synthesise dithionite by cathodic reduction of bisulphite. The authors had employed both R.D.E. and R.C.E. cells in early studies,but decided to concentrate their efforts on the latter for process development, due to higher mass transfer and more uniform current density and wiper pressure. The reactor (Fig. 6.22) was used in a continuous mode, with bismuth, nickel or stainless steel rotating cylinders, 3 in. diameter and 3 in. high, rotated at 10-100 rpm. A perspex cone was glued to the cathode base to minimise cell volume, and the reactor was divided by a cylindrical cation exchange membrane from a quartered cylindrical carbon anode in a brine anolyte. The unit was capable of 30 A current. Four vertical wiper blades pressed against the cylinder to increase mass transport and activate the electrode surface. The efficiency of wiping was demonstrated by the current efficiency of the process at 20-30 Adm^{-2} which increased from 26% with a cathode-wiper clearance of 0.062 cm, to 96% with a zero nominal clearance.

6.5.2 Electrodeposition

Of the many references to electrodeposition at a rotating cylinder geometry in the patent literature, it is difficult to know which designs have eventually been incorporated into industrial practice. The review of the patent literature which follows is not exhaustive, but nevertheless serves to illustrate interesting features and applications of the R.C.E.R. An overall comparison is offered in Table 6.8.

The device described by Benner[334] is the only known example of a bipolar R.C.E.R., apart from the previously described reactor of Nadebaum and Fahidy[292]. The main aim of the invention is the removal of ions from a liquid by segregation into anionic and cationic streams. Fig. 6.23 shows one version of the reactor, employing two horizontal R.C.E.'s, although a greater number may be used, as may a vertical rotating assembly. Separate power supplies and a resistor network are used to control the potentials of each R.C.E. relative to counter electrodes. The resulting polarities are such that the facing sides of the cylinders are of opposite sign, as are the opposite sides of each cylinder. Liquid enters the reactor in the space between the contrarotating cylinders, and is pumped through narrow conforming gaps between the R.C.E.'s and the reactor body. Cations are induced to preferentially pass towards one outlet, and anions to the other. This is facilitated by coating the R.C.E. surfaces with the appropriate ion exchange material.

It is interesting to compare this reactor with the rotating multipolar electrode reactor (Fig. 6.15). The latter is undoubtedly a more versatile reactor and necessitates the use of closely fitting wiper blades to maintain a low intercompartment leakage; Benner's device, however, utilises no such wiper and compartment division.

It should be noted that no details of dimensions, materials or performance are divulged in Benner's patent; the device seems little known and might be expected to be very inefficient.

A further point of interest is that the above author has suggested the use of a number of such units connected in hydraulic series, i.e. a cascade arrangement of separate R.C.E. reactors.

Two of the earliest patents on the R.C.E.R. are those assigned to Lacroix[335] and Cowper-Cowles[336]. Lacroix[335] has described a R.C.E. for the extraction of metals from hydrometallurgical solutions, such as copper from sulphuric acid, (Fig. 6.24). An insoluble anode is employed, electrolyte passing from the catholyte, through the anode, to overflow through the cell body. It is suggested that a cylinder of diameter 1 metre, with a similar circumference (area = 10^4 cm^2) may be rotated at 40 r.p.m., to obtain regular non-spongy deposits, even at current densities of 200-400 A m^{-2} and copper concentrations $\leqslant$1%. The author commented on the uniformity of the deposits, attributing this to the symmetry, and on the current efficiency. Normally current efficiencies were low in the presence of ferric ions due to redissolution, but the 'rotary electrolyser' was stated to overcome this problem.

One of the simplest (and shortest) patents is due to Cowper-Coles[336] who has described the deposition of smooth iron as tube or sheet. These deposits were adherent and non-brittle even at relatively high current densities of 40 $A(ft)^{-2}$. The cell was specifically designed to provide good mixing for the 'in situ' dissolution of iron sponge in hydrochloric or sulphuric acid, or ferrous sulphate and could be operated just below the boiling point of saturated ferrous sulphate solution. It is interesting that the author included an additional impeller attached to the underside of the R.C.E. (Fig. 6.25).

The increased rate of deposition of silver was the motive for a patent by Schaefer[337]. The device described is a cell in which a cyanidic silver electrolyte recirculates, and which is equipped with soluble silver rod anodes and a R.C.E. cathode (Fig. 6.26). Cathode current densities of 75-200 A ft^{-2} are claimed at silver cyanide concentrations of 40-50 g l^{-1}, but no details of cathode rotational speed are given.

British Patent 1,349,672 describes the electrowinning of metals at a rotating horizontal hollow drum[338] (Fig. 6.27). This invention is an unusual device in that both the anode and cathode rotate (in the same direction), and the containing vessel also serves as a cathode at its inner surface. The vessel is charged with crushed ore in a batchwise fashion via an insulating bush around the anode rod, and the inlet/outlet pipe may act as a gas vent. No further details of the device or examples of its performance are disclosed in the patent. The possibility is mentioned of inclining the rotating drum to facilitate the continuous charging of fresh ore and discharging of spent ore.

One of the main practical applications of the R.C.E. geometry has been the removal and recovery of silver from photographic fixing solutions, and several R.C.E.R.'s appear in the technical and patent literature, in cells of varying complexity. The removal of silver is practised for several reasons:

1. the inventory of a precious metal is kept low,

2. the fixing rate increases with silver build up in solution,

3. silver may be removed from unused or waste film by fixing out, followed by electrolysis.

Fulweiler[339] has described a cell with an hexagonal arrangement of graphite plate anodes surrounding a central hollow stainless steel rotating cylinder, equipped with an impeller on its top surface, (Fig. 6.28). This unit claimed to have a current efficiency of about 88-92%, appreciably greater than existing units which operated at 75 percent under similar conditions. The R.C.E. was reported to be capable of operation at silver concentrations as low as 0.2 g l^{-1}, but preferably between 0.3-0.5 g l^{-1}. At the 0.5 g l^{-1} level, an optimum design of cylinder, with a diameter of 12 in. and a length of 6 in., rotated at 317 cm s^{-1} and was capable of current densities of 8-10 A ft^{-2}. It was stated that the diameter/length ratio of about 2 to 1 was a preferred characteristic. The hollow cylinder fabricated from '16 gauge', stainless steel was equipped with a bottom support bearing and a top-mounted impeller to promote fluid circulation, and vertical baffles were provided in the tank to impede rotational flow. The essential features of this invention are incorporated in a commercial cell marketed in the U.S.A.[340].

The cell described by Fischer[341] for photographic-silver recovery is rather more sophisticated. This device comprises a cylindrical cathode surrounded by four carbon rods as anodes (Fig. 6.29). To improve circumferential fluid movement, the cylinder is provided with a number of full length, vertical, helical fins. The possibility of using a rotating polygon with, for example, 8 sides is also discussed. The hollow rotating cylinder is equipped with an impeller at its upper surface to encourage downward axial motion of fluid, speeds of 50-200 r.p.m. are mentioned which enable silver to be recovered at 57 grams per hour (equivalent to 14.3 A at 100% current efficiency). To the author's knowledge there are no commercially marketed units incorporating the features of the above invention.

Another polygonal rotating electrode is described in an Australian patent[342] (Fig. 6.30), and was devised to electrowin metals. Advantages claimed were depolarisation of the electrodes, and the maintenance of current densities of approximately 50 $A(ft)^{-2}$. A novel feature is that the polygonal cathode was made to oscillate, i.e. to revolve in one direction, then the other. As with a previous reactor[358] (Fig. 6.27), the crushed ore was introduced directly into the well-agitated electrolyte in the cell, thus conveniently combining leaching and electrowinning in the same reactor. The oscillating rotary motion was claimed to avoid vortexing. Another interesting claim is that the polygonal cathode was directly compared with a cylindrical one, when the former demonstrated a superior current efficiency of 80% rather than 50%. This was conjectured to be due to the voltage pulsing arising as a consequence of the changing distance between the electrodes. The deposit was hard and crystalline, and uniform in thickness.

Examples indicate that the reactor typically operated at concentrations in the order of $\geqslant 1\ g\ l^{-1}$.

Julien[343] has described the electrowinning of copper in sheet form at a R.C.E. (Fig. 6.31). The main purpose of this invention was to adequately support an anode basket containing soluble copper by suitably positioned braces, the anode arrangement being devised to yield a uniform cathode current density.

A patent dated in 1968[344] involves the use of a rotating cylinder for the electroplating of metals, with special reference to the recovery of silver from photographic solutions. The apparatus (Fig. 6.32) involves a closely conforming thin sheet counter electrode which is free to adjust itself to a relatively constant spacing (ca. 0.003-0.020 in.) from the R.C.E., which may serve as either anode or cathode. The patent claims that the device is capable of treating quite viscous solutions, yielding silver as a thin plate which may be stripped from the R.C.E. Electrolyte is removed from the rotating drum via a rubber wiper blade exerting a "squeegee" action. This geometry, while ingenious, would appear to present difficulties in engineering and maintenance and, to the author's knowledge, is not commercially marketed. The device appears to have been effective, though, and at a silver concentration of 2.5 to 10 $g\ l^{-1}$, a voltage of 1.5 to 2 volts, anode rotational speeds of 5 to 115 r.p.m., and an interelectrode spacing of 0.005 in., current densities of up to 3 $A\ ft^{-2}$ were realised.

The action of scraping or wiping a R.C.E. may accomplish one or more of a variety of purposes. In a patent by Arrigo Pini[305], 'doctor blades' are employed to remove metal from a R.C.E. which then settles in the electrolyte, to be removed from the bottom of the cell (Fig. 6.33). The doctor blades are mounted in an annular cavity formed between coaxial surfaces of the rotating cathode and scraped opposing faces of the cathode. The static anodes which were dissolved and replaced, were interspersed between doctor blades in the annular cavity. Metal was recovered from the cell via settlement as tiny crystallites, and apart from periodically replacing the consumable anodes, and the metal product, the reactor was continuous. No process details or examples are given in the patent.

While the general aim of the above patent is the production of pure (silver) metal, a British Patent[300] describes the production of a cupro-lead alloy powder from a cyanide/EDTA complexed bath containing both metals. The alloy powder was deposited (Fig. 6.34) on the outer surface of a partially immersed horizontal R.C.E., and scraped from its exposed surface, either continuously or discontinuously, then transferred via the scraper trough from the electrolysis cell. The anode was typically a bed of mixed copper and lead turnings, and the geometry was rather irregular (Fig. 6.34). Typically the cell operated at a current density of 50 A dm^{-2}, a cell voltage of 8 V and a temperature of 80°C to produce fine homogeneous metal powder.

The recovery of zinc from an alkaline solution has been reported in a French patent[299]. The invention (Fig. 6.35), typically operated at zinc concentrations of 30-40 g l^{-1}, a current density of 10-15 A dm^{-2}, with an electrolyte temperature of 25-30°C and a current efficiency of 90-93%. Zinc was deposited in a spongy form with a typical specific surface area of 4000 cm^2 g^{-1} employing a R.C.E. travelling at 5-10 r.p.m. As shown in Fig. 6.35, the apparatus utilised either a horizontal or a vertical R.C.E. In the former case, the R.C.E. was less than half immersed, with a scraper-trough conveying the powder away from the exposed surface, as in a previous example[300], (Fig. 6.34). In the vertical design (Fig. 6.35), insulating plastic scrapers are incorporated on the R.C.E. anode, and the metal powder formed on the cell body/cathode is allowed to settle to a conical section in the lower part of the cell (c.f. Fig. 6.33)[305].

Alternatively, the roles of the R.C.E. and stationary electrodes may be reversed. In the case of the horizontal design, the cell body conveniently doubled as an anode and the scraper trough, whose tension against the cylinder was regulated, acted as an electrical contact taking the place of a conventional power brush/slip ring arrangement. The R.C.E. drive shaft and end cap are fabricated from an insulating material, to prevent electrical shorting to the anode.

A recent patent due to Gordy[303] describes a R.C.E. which, in common with one version of the above patent[299], has the feature that the partially immersed horizontal R.C.E. is scraped by a tensioned trough, which doubles as a power feeder, (Fig. 6.36). The main aim of this invention is the anodic dissolution of metal e.g. copper ores in acidic cuprous halide solution, the resultant copper cations being electrodialysed through a porous dividing pot around the anode. Deposition of recovered copper then takes place on a R.C.E. cathode. The cell operated at a typical cell voltage in the range 6-12 V, and an anode current density of 8-10 A $(ft)^{-2}$, and produced copper either as a shiny plate or a powder.

British patent 506,590[304] to Johnson (communicated by I.G.Farbenindustrie Aktiengesellschaft) concerns the recovery of zinc 'dust' from zincate solutions on a R.C.E. cathode. A novel feature of this reactor (Fig. 6.37) is the provision of a hollow drive shaft and cylinder, to facilitate cooling by a recycled fluid. Zinc dust is deposited on the vertical cylinder, and its lateral growth is controlled by static rubber scrapers attached to the anodes. In use the device was typically used to electrolyse zincate solutions containing 50-120 g l^{-1} ZnO, with a cell voltage of 3-4 V, and current densities of 15-25 A dm^{-2}. Zinc of 90-99% purity was obtained at 90-98% current efficiency. The cathode was typically rotated at 1 r.p.m.

Cleave[301] has patented a rather complicated reactor involving a R.C.E. cathode for electrodeposition of metals (Fig. 6.38), with special reference to the refining of silver. The device utilises static anodes incorporated into an insulating, inverted (earthenware) vessel. The segmented plate, rotating cylindrical cathode is scraped by a resilient rubber strip set at an angle to the vertical surface of the cylinder, and the product collects in a jar to be removed at intervals. The patent incorrectly refers to current pulsing as a major cause of the production of loose deposits. Advantages of the device were stated to include a small volume, the minimal attention required, automatic scraping, reduced inventory of silver and low cell resistance.

In contrast to all of the above patents which concern metal plate or powder production, Nordblom[302] has described the electroforming of nickel flake at a partially submerged R.C.E. (Fig. 6.39). The metal flakes, utilised as the positive plate of nickel alkaline batteries, were typically 0.1 in. square & about 0.000040 in. thick. This flake was produced continuously, by contacting the surface of the cylinder with a special non-conducting matrix (e.g. a phenolic resin). The nickel was removed from the cathode by electrolyte jets. Typically, a nickel sulphamate bath was used containing 150 g l^{-1} nickel carbonate at 48°C, with current densities of up to 200 A ft^{-2}.

The most recent patent literature concerning rotating cylinders is due to F.S.Holland and Ecological Engineering Ltd.[306,307] While being superficially similar to some previous R.C.E.R. designs, the Eco-Cell is an engineered, scaleable reactor capable of continuous production of metal powder with continuous electrolyte flow[306-309] (Fig. 6.40). The current density on the R.C.E. is chosen in accordance with the formula

$$i = KCV^{x} \qquad \text{Equation 6.40}$$

where $x = 0.7$ to 1.0 , such that powder production ensues. A divided cell is preferably used, and the reactor is capable of treating relatively dilute (2 ppm - 10,000 ppm) metal containing liquors. Fig. 6.40 shows a flow schematic of a typical Eco-Cell process. The catholyte comprising the metal containing process solution is circulated through the Eco-Cell where metal powder is deposited on the R.C.E. cathode. The metal product is continuously dislodged and is fluidised out of the reactor in the metal depleted liquor. This three phase (gas, metal, and electrolyte) may be separated by conventional means, for example, following gas separation the metal may be recovered by gravity settlement, filtration, cycloning or centrifuge. The Eco-Cell is designed to sustain reproducible turbulent hydrodynamics around the inner rotating cylinder, and this gives rise to very high mass transfer, enabling the device to achieve realistic metal recovery rates even from dilute solutions. The substantially uniform electrode potential experienced at the R.C.E. facilitates the controlled potential separation of metals (see the experimental section) and the reproducible deposition of characterised metal powder deposits. The design of a scraper in the Eco-Cell is of paramount importance. Ideally, the scraping operation is required to remove metal product continuously while not affecting the roughness of the growing deposit. Thus mass transfer may be maintained at a high value by virtue of the high surface area and hydrodynamic shear at the R.C.E. In practice, there are several ways of accomplishing this, including a rotating helical blade scraper, or a reciprocating 'point' blade scraper.

The Eco-Cell and its multicompartment modification, the Cascade Eco-Cell (Section 6.6) form a large part of the experimental works for this Thesis, and will be described in further detail.

It is interesting to compare the R.C.E.R.'s described in the literature (Table 6.9). Firstly, the diverse applications of the geometry include academic laboratory studies of mass transfer, industrial production of organics, electrophoresis[354] and a host of electrodeposition applications. The last mentioned include reactors for producing compact electroplate or foil[343] for decorative or engineering use[335-337], metal powders[299-309], or flake[302].

The symmetry of the described R.C.E.R.'s varies tremendously from coaxial arrangements utilising a full anode[299b,335,338,304,361] via partial but concentric anodes[299a,364,302,306-309] to offset irregular geometries[300,303]. Certain of the reactors employ a series of plates[342] or a polygonal arrangement[341] rather than a true cylinder. A distinct advantage of a large anode is the permissible anode current density; irregular geometries may give rise to current pulsing but this has been claimed to be advantageous in at least one example.[342]

Baffles have been introduced into the 'annular' gap in certain designs[339] either to reduce free rotational fluid flow or increase turbulence. While baffles may be effective in laminar flow or free rotational flow around a conventional impeller, it is doubtful if they serve any useful purpose in a turbulent R.C.E.R. In one design, the baffles also deliberately act as scrapers[299b].

The use of a metallic vessel lining as an insoluble anode must be approached with caution and correct design, as any localised corrosion is a threat to integrity. Nevertheless, it represents an engineering convenience and has been utilised[299]. Certain devices also utilise the internal sides of the vessel as a cathode for electroreduction of ores[338] or a direct cathode[344].

Horizontally rotating, partially immersed R.C.E.R.'s are often employed for electroforming[324], when the foil or flake[302] may be conveniently stripped from the exposed surface of the cylinder. This has been extended to scraping powder from the R.C.E. by means of a trough[299a,300,303]. It is interesting to note that a scraper has also been utilised to remove electrolyte from a R.C.E.[364]. In addition to mechanical scrapers[299-301,303-306], electrolyte jets[302] may also be employed to remove loose metal product from the R.C.E. Depending upon the application, mechanical scrapers may be fixed[299-301,303-305] or moving[306-309], and may be incorporated into the reactor body[299b], the anodes[304], or a rotating electrode[299]. They may also convey electrical power to the R.C.E.[299a,303].

Several reactors have been fitted with additional impellers attached to the R.C.E.[339,336,341]. This is largely unnecessary in fully turbulent reactors, but is nevertheless a safeguard against poor mixing. In addition, the impeller may promote fluidisation of the scraped product to facilitate removal by outlet liquor. Conversely, the reactor may be designed with a quiet lower cone to promote settling of the product, pending withdrawal as a sludge[304,299b], or with recesses in the reactor body[305] to perform a similar task.

There appear to be very few diaphragm R.C.E.R.'s described for electrowinning and electrorefining, although the inclusion of a membrane may greatly improve current efficiency, minimise anode corrosion and prevent undue reactions such as chlorine evolution in chloride solution hydrometallurgy. At least one patent has employed a porous pot cell divider, however[303], and the Eco-Cell[306-309] is normally constructed with an integral ion exchange membrane diaphragm.

Apart from the Eco-Cell, there appear to be few examples of a sealed reactor; several reactors employ gravity overflow outlets instead[304,305,335,342]. In the case of electrorefining, the use of an open topped anolyte compartment or cell greatly facilitates the periodic replacement of soluble anodes.

It should be noted that the majority of R.C.E.R.'s described above were operated with rather high metal concentrations and only moderate current densities with relatively low peripheral velocities i.e. they were low mass transfer devices. They may thus be contrasted with reactors such as the Eco-Cell, where the high peripheral velocity, turbulent flow, and the rough powdered deposit combine to give a very high mass transfer, facilitating the treatment of dilute metal containing solutions.

6.6 Multiple (Cascade) Rotating Cylinder Electrode Reactors

It has already been noted (in Section 6.2.1) that the conversion in a single element R.C.E.R. may be enhanced by increasing the mass transport coefficient (by raising the peripheral velocity), or by an increase in surface area. There are obvious limitations however, on cost, space, and engineering feasibility here, especially in view of the fact that the rotational power requirement increases approximately as the cube of the rotational velocity (see Section 6.2.2).

The Concept of a Cascade Eco-Cell

An alternative approach to the realisation of a high overall conversion is to employ an array of reactors in hydraulic series (Fig. 6.41). Such a cascade allows stepwise reduction of the metal concentration over each reactor element. If the n elements in the cascade are identical (which could tend to minimise investment costs), and each operates under mass transport control (which results in maximum duty for given conditions), the terminal concentrations are related by the overall fractional conversion $(f_R)_n$

$$(f_R)_n = \frac{C_{IN} - C_{OUT}}{C_{IN}} = 1 - \frac{1}{(1 + K_L A/N)^n} \qquad \text{Equation 6.38}$$

Furthermore, in the case of rotating electrode reactors, the possibility occurs of assembling all the reactor elements on a common shaft for engineering convenience, minimisation of space, and to lower investment and maintenance costs. Such an arrangement has been considered for the rotor electrodes of the 'electrochemical pump cell' developed at Southampton University[215], and a multiplicity of disc electrodes on a common rotating shaft is commonly employed in the photographic industry for cathodic silver recovery from fixing solutions[394,395], although it must be noted that these assemblies do not function as cascades. A further possibility, in the case of rotating cylinder reactors, is to employ a single extended cylindrical cathode, inside one reactor body, and to subdivide this into identical elements by means of regularly spaced internal baffles, (Fig. 6.42).

Division of the cascade reactor by means of internal baffles results in a versatile fabrication offering considerable scope for alteration of the number of compartments and the extent of each one. This construction will approximate to a series of C.S.T.R.'s as long as the cylinder rotational velocity is sufficiently high (maintaining effective stirring in each element), the axial flow rate is not excessive, and the baffle aperture is sufficiently small (which discourages bypassing).

The concept of idealised Eco-Cascade-Cell operation is illustrated in Table 6.10, where an inlet metal (copper) concentration of 100 mg dm^{-3} is reduced stepwise to an outlet of 1.6 mg dm^{-3}. Here, a conversion, f_R of 0.5 is assumed, the concentration thus halving over each element. If the electrolyte flow rate is 1000 cm^3 s^{-1}, the individual compartment currents may be calculated by means of the following analysis.

A mass balance over each element yields the removal rate of copper,

$$R = 10^{-6}.N\,(C_{IN} - C_{OUT}) \qquad \text{Equation 6.39}$$

R will have units g s^{-1} if N is expressed as $cm^3\ s^{-1}$ and C as mg dm^{-3}. The rate of copper removal may be related to the current, I, by application of Faraday's law and assumption of 100% current efficiency:

$$R = \frac{I.M}{zF} \qquad \text{Equation 6.40}$$

where I is in amps, F is the Faraday (= 96498 Coulombs), z is the electron change and M the molecular weight of the metal. For copper, z = 2 and M = 63.54 giving

$$R = 3.292 \times 10^{-4}.I \qquad \text{Equation 6.41}$$

Coupling Equations ~~4~~ 6.39 and ~~6~~ 6.41,

$$I = \frac{N(C_{IN} - C_{OUT})}{329.2} \qquad \text{Equation 6.42}$$

Equation 6.38 shows that to attain a fractional conversion of 0.5 with a flow rate of $\underline{1000\ cm^3\ s^{-1}}$ (as in Table 6.10) the factor K.A must equal $\underline{1000\ cm^3\ s^{-1}}$, and this must be achieved by suitable choice of electrode size and rotational velocity.

It has already been noted that for maximum duty, each individual compartment of the Eco-Cascade-Cell should function under limiting current conditions. An additional consideration is that electrodeposition must be maintained at or near the limiting current in order to produce metal in powder form, rather than as a hard, adherent electroplate. The latter might present removal problems and a lowering of mass transport due to the less favourable hydrodynamics and lower electrochemically active surface area.

The most satisfactory method of supplying electrical power would undoubtedly be achieved through a potentiostatic approach, where the electrode potential in each compartment could be automatically controlled at a preselected value, regardless of metal concentration. This is rather impractical, however, as a separate control circuit would be necessary for each compartment. Moreover, each compartment would require its own independent, electrically insulated cathode and power feed brush, or separate anodes would be required in each compartment.

To overcome these problems, alternative approaches have been adopted, utilising simple, moderately priced, constant current transformer/rectifier power supplies. In the case of divided cell reactors (Fig. 6.42), it has been found possible to tailor the anode size, position and effective surface area to achieve substantially uniform electrode potential in each compartment, with a suitable current profile over the reactor length. This has been achieved by modifying the position of the anode along the reactor length, the length of anode, and strategic masking of the anode. The number and the nature of the variables involved in the resultant current density profile here, e.g. anode geometry, membrane resistance, inter-compartmental current leakage via baffles, anolyte and catholyte resistance, and effect of gas evolution, is such that a wholly empirical approach has been adopted, guided by experience. For undivided cell reactors (Fig. 6.43), individual anodes have been provided in each compartment, and a suitable resistor network has been employed to achieve desired current density profile over the reactor. This second approach, while more costly in terms of power, anode material, additional electronic components and wiring results in a versatile reactor, capable of being easily modified to suit different needs.

The development of practical pilot plant/commercial cascade R.C.E.R.'s is described in Chapter 11.

It is interesting to make a general comparison between the 'Cascade Eco-Cell' and the 'Rotating Multipolar Electrode' (R.B.E.) reactor (Table 6.6). The two reactor types both employ the outer surface of an inner rotating cylinder as the working electrode. The reactors may, however, be strongly contrasted with respect to design and application. The 'Cascade Eco-Cell' is subdivided axially and employs a high peripheral velocity, while the R.B.E. rotates only slowly. The R.B.E. requires a smooth regular surface finish electrode, to facilitate reactor division by means of the wiper blades. The 'Cascade Eco-Cell' utilises a rough, metal powder electrode; this electrode is scraped rather than wiped.

The scraping action in the Cascade reactor does not markedly affect the mass transport, while a severe enhancement is provided by the closely conforming PTFE wiper blades in the R.B.E.R.

Normally, all individual working electrode compartments in the 'Cascade Eco-Cell' are cathodic, and of a similar potential, whereas in the R.B.E.R., the potential of the working electrode may be varied and even reversed in the various compartments.

The 'Cascade Eco-Cell' has been employed for cathodic metal removal and recovery from dilute process streams. The R.B.E.R. has been mainly investigated for inorganic and organic synthesis, although metal refining has been considered.[291]

7. ELECTRODEPOSITION OF METAL POWDERS

The fundamentals of the electrodeposition of metal powders are presented, followed by a review of the present theories of powder formation. The recent literature is then reviewed, with special reference to the application of novel electrochemical reactors, and the possibility of controlled potential 'tailoring' of the powder deposits.

7.1 Introduction

The production and working of metal powders dates back some five thousand years. Since the early 1930's,however, the realisation of powder metallurgical pressing of metals and alloys has greatly encouraged interest and provided the driving force for the development of new production methods, including electrolysis. A large range of metal components, some of complex shape, can be cheaply and readily manufactured by compression and sintering of powders; mass production is also facilitated.

Traditionally, atomised metals have been preferred for powder metallurgy, but there is evidence of a growing interest in the electrolytic method, due to the high purity of the product and the low cost.

As early as 1803, Priestly had discovered that a black, finely divided metallic sediment could be produced at a cathode by electrolysis of silver nitrate solution, but the first serious studies on powder electrodeposition may be said to have been instigated by Smee [345].

There have been several reviews of aspects of the electrodeposition of metal powders (Table 7.1), the most notable being due to Ibl [193] in 1962. The remainder of this chapter will attempt to update and build upon the information contained in Ibl's work [193]. The most recent and most extensive review is due to Calusaru [357].

Before a fuller consideration of electrodeposition of powders, alternative methods of powder production will be briefly reviewed.

While the sintered products, powder metallurgy industry is undoubtedly the greatest user of metal powders, particularly iron, other eixsting markets may be identified according to products as follows:

1. batteries
2. bearings
3. printed circuits
4. brake and clutch linings
5. metallic pigment paints
6. catalysts, and
7. chemicals, including photographic film

In general metal powders may be used wherever it is impractical to use prefabricated forms (e.g. sheet or rod) or to melt the massive metal to obtain the desired shape.

The diverse use of various individual metals is illustrated in Table 7.2, while Table 7.3 provides greater detail for the case of copper powder.

7.2 Methods of Metal Powder Production

7.2.1 General

The main industrial techniques used to produce metal powders are:

1. chemical reaction
2. mechanical comminution
3. atomisation
4. electrodeposition.

The choice of technique is important not only from an economic and convenience point of view, but because the properties of the resultant powder vary with the production method. Chemical reactions generally yield cheap, porous, readily-compressible powders, but alloy production is not possible. Mechanical comminution is a convenient technique for brittle metals, and results in powders of irregular shape. The most prolific technique, atomisation, gives a spherical particle shape. In theory, electrodeposition is one of the most convenient and versatile techniques; not only can a wide variety of metals be produced, but codeposition of metals as an alloy powder is possible. Both aqueous solutions and fused salts[352] may be employed, but the former are always preferred from the standpoints of energy use, safety and operating convenience.

2.2 Chemical Reaction

This method may be subdivided into reduction, displacement, decomposition from the vapour phase, and oxidation followed by decarburisation and intergranular corrosion.

Reduction involves the chemical production of metal by reaction between a reducing agent and a compound of the metal. Examples of reducing agents include carbon, hydrogen and sodium. Carbon is much preferred on a cost basis, but provides insufficient driving force in some cases, and tends to cause product contamination. An example of reduction by hydrogen is provided by the Peace River Process where ferrous chloride is reduced to iron, and by the Sherritt Gordon Process.

Displacement reactions involve precipitation of metal from solution by addition of a less noble metal. A well-known example is the cementation of copper from hydrometallurgical leach liquors using steel scrap or zinc dust.

Production of metal from the gaseous phase may occur via reduction or by decomposition of a volatile metallic compound. An example of the latter is the production of nickel from the carbonyl $Ni(CO)_4$ by heating to 200° C at 1 atm. pressure. The Mannesmann process for the production of pure iron involves the oxidation of the metal carbide

$$MO + MC \longrightarrow 2M + CO$$

.2.3 Mechanical Comminution

The term 'comminution' includes machining, crushing and milling. This method is expensive and tedious, and restricted to brittle metals such as iron, manganese, cobalt and beryllium. Metal flake or powder produced by the technique is often used as a pigment for paints. Wet milling may be used to realise low particle sizes, down to 1 micron. An example of a product normally obtained by the method is dental alloy powder which is a tin-silver alloy manufactured by lathe cutting and milling of the bulk material.

.2.4 Atomisation

This normally involves the spraying of the molten metal through a small orifice whereupon mechanical disintegration occurs to produce droplets or small solid particles, depending on the cooling rate by a fluid jet (air, water or inert gas). It is the most common technique employed to produce metal powders, especially for the powder metallurgy industry, and is capable of producing a wide variety of metals and alloys.

.2.5 Electrodeposition

Metal powders may be prepared electrolytically by either a direct or indirect route. In the indirect method, the metal may be electrodeposited in a coherent but brittle form, which may be rendered powdery by mechanical comminution. This chapter, however, concerns the direct electrodeposition of metal powder, which is more important for low overvoltage metals. As will be seen, a wide variety of cell geometries and electrolytes are possible, and powder production may be continuous (see also Section 6.5).

The electrolytic deposition technique may be considered to offer the following potential advantages:

1. a high purity product,
2. a favourable scaleup cost,
3. a considerable range of powder qualities are possible by varying either the electrolysis conditions or the electrolyte composition,

4. The dendritic nature of the powder may serve to confer good compacting properties,
5. the product has a very high specific surface area,
6. production may be automated by the use of, for example, soluble anodes, or a flow-through reactor.

Disadvantages of the technique for certain applications include the irregular, non-spheroidal particle shape, and the ease with which untreated powder may corrode, due to its high activity.

.3 Fundamental Aspects

.1 Conditions Favouring Powder Deposition

Depending upon the electrolysis conditions, many metals may be obtained either in a compact, adherent form or as a loose deposit capable of being easily stripped from the cathode. Empirically, it is known that powder formation is usually encouraged by:

1. a decrease in the concentration of metal ion
2. an increase in concentration of indifferent electrolyte
3. a decrease in the rate of stirring
4. an increase in current density
5. a decrease in temperature
6. an increase in viscosity

The above factors are all consistent with the theory that powder deposition is a mass transport controlled phenomenon [193]. The structure of the deposit also depends on the individual metal and solution composition. For example, copper, nickel and iron readily yield dense deposits at low current densities, whereas a silver, lead and cadmium tend to form flakes or needles from simple solutions, and smooth deposits from complexed solutions, e.g. cyanides. Deposit quality and adhesion may be severely altered by surfactants [358], electroactive substances such as thiourea [359], passivation of the cathode or incorporation of codeposited species. Passivation tends to give rise to a multiplicity of nucleation sites for electrocrystallisation, and spongy growth.

3.2 Properties of Metal Powders

There is a multitude of interrelated chemical and physical properties of powders used to characterise a particular product[360]. Of these, the most important are:

1. apparent density
2. particle size and distribution
3. flow rate
4. chemical and thermal stability
5. particle shape.

For powder metallurgical applications the property of a pressed and sintered compact is of paramount importance, and for catalytic applications, the specific surface area is important.

For most commercially available powders, the product specification provided by the manufacturer normally includes, as a minimum, a statement of the following properties:

1. purity
2. apparent density
3. tapped density (when the powder has been settled)
4. average particle size
5. sieve analysis.

Problems exist in the standardisation of methods for the measurement of the properties of interest, and the British Metal Sinterings Association has attempted to provide a guide[361], for iron powders. The most important general property of a metal powder is its consistency, in order to facilitate the reproducible preparation of good quality compacts.

7.4 Theories of Powder Formation

Any theory of powder formation would perhaps be expected to start from a knowledge of electrocrystallisation. Unfortunately, despite great progress in recent years, a relatively large volume of work by, for example, Ibl, Pomosov, Calusaru, Despic and their collaborators has resulted in no precise relationship between powder formation and electrocrystallisation. The approach to the problem has been largely qualitative and phenomenological, although Calusaru[357] has attempted a quantum mechanical treatment. Ibl[193], considering that powder production is largely a convective diffusion problem (concerning concentration polarisation), has proposed a widely accepted mass transport theory.

.1 Hydrogen Evolution

Early workers attributed powder formation to hydrogen evolution, the intergrowth of crystals being prevented by gas bubbles or by adsorbed hydrogen. While many cases of simultaneous hydrogen evolution and metal powder deposition are known, it has been demonstrated many times that powdery deposits may be produced without any hydrogen evolution, so disproving this theory. The evolution of hydrogen may, however, serve to loosen powdery deposits from the substrate or encourage hydroxide/oxide formation due to localised pH changes in the cathode layer. It may also locally increase mass transport rates (Chapter 3).

.2 Oxide Formation

Substantial amounts of oxide are sometimes found in electrolytic powders, particularly from near neutral or alkaline solutions, and this led Kudra and others to postulate that powder formation was due to such codeposition. It should be noted, however, that powder is often obtained under conditions where the deposit is essentially free of oxides.

.3 Discharge of Complex Ions

Kudra has postulated that disperse metallic powder deposits are formed by the incorporation into the metal lattice of cations originating from the discharge of complex ions of the type $(Cd_2SO_4)^{2+}$. The theory was largely and erroneously based on the apparent experimental evidence for two discharge potentials on polarisation curves. The first potential corresponded to the reduction of simple metal cations, while the second was attributed to the discharge of the complex ion. The deposit was invariably compact at the first potential, and powdery at the second. However, no limiting current corresponding to the complex ion dissociation has been observed. This theory is in contradiction of the known theory concerning the direct hydrogen discharge from water molecules at the secondary discharge potential.

4 Colloidal Substances

The presence of colloidal substances, either added directly or codeposited, has often been suggested as a cause of sponge or powder formation. Certainly, colloids are known to inhibit crystal growth and lower grain size, but this does not necessarily lead to formation of a loose powder. Indeed, colloids form one type of addition agent used to promote fine-grained, smooth deposits in electroplating. It is probable that such colloids enhance the rate of nucleation, thereby providing greater tendency for powder formation.

.5 Ion Depletion in the Cathode Layer

Loshkarev et al.[362] and Ibl[193] have promoted this theory which postulates that due to metal ion depletion near the cathode, powdery deposits develop at (or near) the limiting current. Ibl[193] has extensively discussed mass transport considerations regarding the theory, and Chapters 3 and 4 have discussed mass transport and its implications for metal recovery.

Calusaru[352] has accepted that the above theory satisfactorily explains the transition from compact to powdery deposits, but considers that the theory does not explain the intrinsic dispersion or the absence of interparticle binding. This author argues that a dendrite would be expected to adhere to the cathode.

.6 Quantum Mechanical Electron Tunnelling

Calusaru[357] further considers that the above mass transport theory concerns only transport phenomena, and ignores the most important phenomenon of electrocrystallisation i.e. the overpotential at which powder formation takes place (equivalent to supersaturation in ordinary crystallisation).

dSeveral works have indeed studied the transition from compact to powdery deposits as a function of potential[363, 364], rather than current density. In the case of copper and gold, Calusaru[357] claimed that the potentials of powder formation were larger than those corresponding to the beginning of the limiting current plateau region, and that this finding could not be interpreted in terms of previous theories. Rather, a new theory based on quantum mechanics was constructed[365, 366].

7.5 Apparatus

Traditionally, metal powders have been produced on static flat plate electrodes, with electrolyte agitation, the product being removed periodically and scraped from the cathode. This is not only a labour intensive, messy and costly operation, but the product is time dependent, as growth of the metal powder takes place on the cathode. These facts have encouraged the development of continuous cells and reactors such as the rotating cylinder versions discussed in Chapter 6.

Removal of the metal powder product is a problem which has received considerable attention in the literature, and methods include:

1. periodic current reversal[367]
2. vibrating the cathode[350, 368]
3. amalgamating[369]
4. a moving band cathode with product removal outside of the cell
5. a two-layer bath, with a horizontal rotating cathode. This cathode moves through and is passivated by an organic solvent containing a surfactant; it then travels into the aqueous electrolyte. A fine powder is deposited at unpassivated sites, and the particles, being lyophobic, disperse in the organic solvent[351]
6. mechanical scraping which may be divided into static scraping of a moving electrode, or a static electrode with moving scrapers
7. use of solution additives (although this may have a deleterious effect on the powder).

Cells for metal powder production may utilise soluble replaceable anodes[368], as in electrorefining, and the anode may be installed inside a porous container to prevent anode sludge contaminating the catholyte or the powder deposit. In the case of cells utilising very insoluble anodes, the metal concentration in the cell may be maintained by solution flow.

7.6 Operating Variables and the Transition from Compact to Powdery Deposits

The properties of metal powders and the effect of operating variables have been especially well studied in the case of copper deposition from acid sulphate solutions. In an early study, Tyrrell[370] found that the apparent density increased with increasing metal concentration, increasing temperature, decreasing current density and increasing rate of stirring, and similar results have been obtained by other workers. This change of apparent density may be roughly linked to a variation in particle size, although it should be noted that the apparent density is a function of particle size and shape.

It has generally been found that particle size decreases with increasing current density (or increasing overpotential)[193]. The particle size appears to increase with increasing temperature, increasing metal concentration and increasing rates of stirring. Thus the changes in particle size roughly parallel those in apparent density, according to the mass transport control. The wide particle size distribution, together with an irregular shape, helps explain why electrolytic metal powders are well suited to powder metallurgical processing.

The transition from smooth, compact to dendritic, rough deposits has been studied by a number of authors[68, 83, 194, 193, 371-376], under galvanostatic[68, 83, 194, 371, 374], potentiostatic[68, 83, 194, 371, 374-377], and pulsating potentiostatic[372, 373] control of the cathode.

The transition to powder growth, as has been noted elsewhere, is accompanied by an increase in both surface area and roughness of the deposit. It follows from this that experimental measurements of the powder transition might be made by sensing of an area-dependent parameter such as electrode capacitance[378] or reactance[194, 379, 193], or of the roughness by microscopy (optical or electron)[68, 83, 357], surface profilometry[380] or increased shear stress (or torque). In addition, electrochemical study of the transition may be accomplished by polarisation curves, potentiostatic current-time curves, galvanostatic potential-time curves, or current efficiency[374]. The measurement of surface changes represents a more direct approach in practice. The direct measurement of potentiostatic increase of current with time is a powerful method as it may be utilised on both laboratory and industrial scales; and shows the current corresponding to both a smooth and a rough deposit, as well as the transition zone.

The electrocrysallisation of metallic powders takes place under highly irreversible conditions, and Gorbachev and his collaborators[381] have studied the thermal effect involved in the separation of metal powders. This requires very careful experimental conditions, and the transition is marked by a small but measurable temperature 'jump'. This effect may be attributed[357] to an appreciable increase in ohmic resistance of the cathode layer following ion discharge.

A distinction may be made between the smooth-rough transition under free and forced convection conditions. In the former case[193], a definite initiation time is felt, equivalent to the time taken for the interfacial concentration to fall to zero. This time t_p, follows the law $i\sqrt{t_p}$ = constant. The case of free convection, although important from an academic viewpoint, will not be further considered here.

As has been seen, there are relatively few studies stressing the importance of electrode potential. In this context, the work of Popov et al.[372-375] merits attention. These authors studied the electrodeposition of copper from acid sulphate solutions on to copper and aluminium wires under controlled potential. Apart from constant potential, triangular, sinusoidal and square wave pulsating potential control were employed. The conclusions of these studies may be summarised as follows:

1. a lowering of energy consumption is possible by means of pulsating potential[382]
2. for sinusoidal, pulsating overpotential deposition, increasing frequency leads to an increase in particle size, as well as a decrease of amplitude in the value of pulsating overpotential for the same frequency of pulsation[372]

3. smooth copper deposits may be obtained in the limiting current density range by pulsating overpotential of frequency 10^4-10^5 Hz. At lower frequencies, the deposits are rough and dendritic, but more compact compared to those obtained by constant potential deposition [382]
4. in the case of constant potential electrolysis, morphology and particle size are functions of overpotential[372, 373], particle size decreasing with an increase in overpotential, and a narrow distribution ensuing with an increase in potential[373]
5. a narrow size distribution results in the case of pulsating potential compared with constant potential[403]
6. for square wave pulsating overpotential, an increase in mark to space ratio results in a larger particle size, and a sharper particle size distribution [373]
7. energy consumption is smaller for deposition on aluminium electrodes than for platinum electrodes[374]
8. galvanostatic operation requires a smaller energy consumption than does potentiostatic deposition
9. the critical cathodic overpotential for copper dendrite growth is ~550 mV.

7.7 Closure

This chapter has indicated that electrodeposition of metal powders is a versatile technique, capable of yielding a product of deliberate characteristics by altering the electrolysis conditions. The economic and technological viability and increased adoption of the technique depend upon several factors including the cost of electricity, the cost of electrolyte and the existence of an efficient, versatile and continuous reactor.

Considering cheap electrolytes, a very attractive idea is to recycle industrial process solutions through a reactor and remove metal as powder in the process. Ideally, the reactor, may be controlled to produce a continuous, premium product which is directly saleable, perhaps to the powder metallurgy market. To minimise energy and investment costs, such a reactor must have a low interelectrode gap, and be capable of high rate production of metal powder, often from rather dilute solutions (≤ 1 gl^{-1} metal). In addition, the electrode potential of the reactor cathode should be uniform and capable of being controlled to alter the powder characteristics, either to produce a premium product, or to facilitate removal of a loose product.

Apart from the scavenging of metal from dilute solutions, using an insoluble anode, scrap metal may be used as a soluble anode in metal powder production.

In both cases, the need often arises for a divided cell, to prevent anode corrosion and fouling in the case of insoluble anodes, or to prevent anode slime reaching the cathode in the case of soluble anodes.

The above requirements are well met by rotating cylinder electrode reactors such as the Eco-Cell.

The potentiostatic control of a reactor not only facilitates the separation of a valuable, pure, noble metal powder from a mixed metal solution, but may also be used to deliberately produce an alloy whose composition can be selected to a degree. The possibility of direct alloy powder production has not been extensively examined, but recent literature (mostly Russian) shows a developing interest in this aspect. Table 7.4 indicates known work on metal alloy powders. Alloys for the powder metallurgy industry may be formed by combination of separate powders or the plating of one metal on another, although the results are generally not as satisfactory as when a directly deposited alloy is used.

Sintered compacts prepared from a mixture of metals can have properties which are radically different from the components, and this shows promise for the production of exciting compacts.

SOURCE	METAL	TOTAL PRODUCTION
Free World	Copper	6,200
"	Zinc	4,500
"	Lead	2,500
"	Nickel	540
"	Tin	183
Total World	Molybdenum	72
"	Cadmium	11
"	Mercury	9.1
Free World	Silver	7.4

TABLE 1.1[1] MINE PRODUCTION OF METALS (1974)

figures are in.kilo tonnes

Geometry	$(Re)_{crit.}$ *	x based on
Rotating Cylinder	200	diameter
Rotating Disc	$2 - 3 \times 10^5$	radius
Pipe Flow	2100	diameter

* $(Re)_{crit} = \frac{U x}{\nu}$

TABLE 2.1 CRITICAL REYNOLDS NUMBER FOR THE LAMINAR TO TURBULENT FLOW TRANSITION FOR VARIOUS CASES, showing the importance of geometry.

Function	Mode	ROTATING CYLINDER	ROTATING DISC	PIPE FLOW
$f/2$	Laminar Flow	$\frac{2}{(Re)}$	$\frac{0.62}{(Re)^{\frac{1}{2}}}$	$\frac{8}{(Re)}$
$(f/2)^{-\frac{1}{2}}$	Turbulent Flow Smooth Surface	-17.5+ $5.75 \log_{10}(Re)\ F/2$	$-3.05 + 5.75$ $\log_{10}(Re)\sqrt{F/2}$	0.30+ $5.75 \log_{10}(Re)\ F/2$
$\frac{F}{2}$	"	$0.0791(Re)^{-0-30}$	$0.0265(Re)^{-0.2}$	$0.0396(Re)^{-0.25}$
$(F/2)^{-\frac{1}{2}}$	Turbulent Flow Rough Surface	1.25+ $5.76 \log_{10}\frac{d}{e}$		$3.2 - 5.76$ $\log_{10}(Re)\ F/2$

TABLE 2.2 FRICTION FACTOR EXPRESSIONS FOR VARIOUS GEOMETRIES

CASE	ROTATION OF INNER CYLINDER	ROTATION OF OUTER CYLINDER	AXIAL FLOW
1	Zero	Zero	Zero
+2	Zero	Zero	Positive
+3	Clockwise	Zero	Zero
+4	Clockwise	Zero	Positive
5	Clockwise	Clockwise	Zero
6	Zero	Clockwise	Zero
7	Zero	Clockwise	Positive
8	Clockwise	Clockwise	Positive
9	Clockwise	Counterclockwise	Zero
10	Counterclockwise	Clockwise	Positive

TABLE 2.3 POSSIBLE FLOW COMBINATIONS FOR A CONCENTRIC CYLINDRICAL GEOMETRY

+ Cases of practical importance in electrochemical engineering.

PROPERTY	ROTATING	
	DISC	CYLINDER
radius/cm.	10	10
area/cm^2	314	3948
RPM	95.5	95.5
peripheral velocity/cm s^{-1}	100	100
flow regime	LAMINAR	TURBULENT
expression for friction factor f/2 =	$0.62(Re)^{-0.5}$	$0.0791(Re)^{-0.3}$
*(Re)	10^5	2×10^5
f/2	1.96×10^{-3}	2.03×10^{-3}
rotational power/W	0.062	0.26

TABLE 2.4 COMPARISON OF ROTATING DISC AND ROTATING CYLINDER

* (Re) based on r for disc, d for cylinder

HYDRODYNAMIC SYSTEM	i_L /mA cm^{-2}	δ_N /mm
natural convection at vertical electrode (height :10 cm)	14.4	0.2
natural convection at horizontal electrode	36.5	0.08
laminar flow along plate electrode (v = 25 cm/s, length 10 cm)	30	0.1
turbulent channel flow (v = 25 m/s)	3650	0.0008
rotating cylinder (180 rpm peripheral velocity 94 cm/s)	81	0.036
cathode with H_2 -evolution (13 cm^3 gas cm^{-2} min^{-1})	194	0.015
cathode with H_2 -evolution (1 cm^3 gas cm^{-2} min^{-1})	27.6	0.1
bubbling of gas through fritte (17 lt/min)	132	0.02
wiping of electrode with net moving along interface	228	0.013
ultra sound (7 W/cm^2)	500	0.006

The figures given for the limiting current refer to a 0.3 M solution with a diffusion coefficient of 10^{-5} cm^2/s and a kinematic viscosity of 10^{-2} cm^2/s.

TABLE 3.1 LIMITING CURRENT DENSITY (i_L) AND EQUIVALENT THICKNESS OF DIFFUSION LAYER (δ_N) FOR VARIOUS HYDRODYNAMIC SYSTEMS [46]

SYMBOL	NAME	DEFINITION	DESCRIPTION
(Sc)	Schmidt No.	$\frac{\nu}{D}$	transport properties
(Re)	Reynolds No.	$\frac{Ux}{\nu}$	fluid flow
(St)	Stanton No.	$\frac{i_L}{zFCU} = \frac{K_L}{U}$	concentration dependent mass transport
(Sh)	Sherwood No.	$\frac{i_L x}{zFCD} = \frac{K_L x}{D}$	mass transport
(Gr)	Grashof No.	$\frac{g\Delta\rho}{\rho\nu^2} L^3$	free convective mass transport
(Ra)	Rayleigh No.	(Gr)(Sc)	"
(Pe)	Peclet No.	$(Re)(Sc) = \frac{UL}{D}$	"

Note:

1. (Sh) is sometimes replaced by (Nu), the Nusselt No.
2. (Pr), the Prandtl number, is sometimes written in place of the equivalent (Sc), especially in Russian literature.
3. $(Sh) = \frac{(St)(Re)}{(Sc)}$

TABLE 3.2 DIMENSIONLESS GROUPS COMMONLY USED IN ELECTROCHEMICAL MASS TRANSFER STUDIES.

AUTHORS	REFERENCE	EXPRESSION
CHILTON AND COLBURN	61	$(St) = \frac{f}{2} (Sc)^{-\frac{2}{3}}$
DEISSLER	63	$(St) = \frac{0.248}{\pi} \sqrt{f} \; (Sc)^{-\frac{3}{4}}$
LEVICH	59	$(St) \propto \sqrt{f} \; (Sc)^{-\frac{3}{4}}$ $(St) \propto \sqrt{f} \; (Sc)^{-\frac{2}{3}}$
LIN et al.	64	$(St) = \frac{9}{(14.5)(2 \quad 3)} \sqrt{f} \; (Sc)^{-\frac{2}{3}}$
VIETH et al.	65	$(St) = \frac{3\sqrt{3}}{2\pi} (1.77)^3 \; \frac{f}{2} \; (Sc)^{-\frac{2}{3}}$ $\times \; \frac{Umax}{Uave}$

TABLE 3.3 ASYMPTOTIC FORMS OF SOME COMMONLY USED HEAT AND MASS TRANSFER CORRELATIONS.

TEMP. /°C.	ANODIC OR CATHODIC	CONCENTRATION / M		(Sc) RANGE	SYSTEM STUDIED	REF.
		REDOX SPECIES	KOH/ NaOH			
25	A/C	0.009- 0.204	2.0	2230- 3650	RCE	58 57
25	C	0.025	1.0	1923- 2127	RCE	73
25?	A/C	0.01	0.5	?	RCE	74
1-25	C	0.005	1.0- 4.0	1700 30,000	FT PP	62
24-40	A/C	0.0004- 0.1	0.5	?	RDE	75
25	C	0.0128	0.1	?	TPPP	76
25	A/C	0.0128	2.0	2698	RCE	77
10-29	A/C	0.005- 0.01	0.5.	?	ANNULUS FT	78
ROOM	C	0.025	0.5	700, 1800	moving wire	79
ROOM	A/C	0.0002- 0.02	0.02	?	FBE PBE	87
22	C	0.0005 0.05	1 KCl	?	FT mesh	80
22	C	0.01	0.01 + $0.5Na_2SO_4$	1800- 29,000	RCE	72
20-40	C	0.001- 0.005	0.5 + 0.1KCl	?	HDE	97
?	A/C?	0.05	1.0	?	RPPE	61

Key:

RCE	Rotating Cylinder Electrode
FTPP	Flow Through Parallel Plate
RDE	Rotating Disc Electrode
PBE	Packed Bed Electrode
HDE	Hanging Hg Drop Electrode
RPPE	Rotating Parallel Plate Electrode

TABLE 3.4 MASS TRANSPORT STUDIES INVOLVING THE FERROCYANIDE/FERRICYANIDE REDOX REACTION.

TEMP. /°C.	CONCENTRATION/M		(Sc) RANGE	SYSTEM STUDIED	REF.
	$CuSO_4$	H_2SO_4			
16-40	0.0059- 0.050	1.5	3300- 28000 *	RCE	77
15-40	0.055 - 0.025	1.5	2450	RCE	82
22-45	0.014	1.5	790 2240	RCE	68, 83, 84
22-40	0.005- 0.57	0.05	750- 1780	FBE	85, 86
20	0.010- 0.013	1.0	2830- 3040	PBE single layer	93
19-26	0.01- 0.74	1.38- 1.57	1750- 3400	vertical plate natural conv.	91
				moving wire	92
25	0.08- 0.54	1.6	2700 3880	gassed electrode	96
20	0.05- 0.460	1.5	2340 2690	horizontal screen	95
20-22	0.05- 0.1	1.5	2470 2860	vertical array horizontal cyl.	98
18	0.01 or 0.05	1.5	2380- 3080	annulus	100
22	0.01- 0.7	1.5	2100- 52000 *	horizontal plate, FC	101
35-125	0.005- 0.15	1.5	1120-	Free conv. + heat transfer	102
22?	0.03 0.47	1.5	600- 12000 *	hor. plate Free + forced	104
17-45	0.067 or 0.015	1.5	960 3300	FTPP	105

TABLE 3.5 MASS TRANSPORT STUDIES INVOLVING THE CATHODIC DEPOSITION OF COPPER.

* glycerol additions used to increase (Sc)

FLOW REGIME	ELECTRODES	CORRELATION
LAMINAR	(INFINITE WIDTH)	$(Sh) = 1.85(Re)^{\frac{1}{3}}(Sc)^{\frac{1}{3}} \left[\frac{d_e}{L}\right]^{\frac{1}{3}}$
LAMINAR	(FINITE WIDTH)	$(Sh) = 1.467(Re)^{\frac{1}{3}}(Sc)^{\frac{1}{3}} \frac{d_e}{L}^{\frac{1}{3}} \left[\frac{2}{1+\gamma}\right]^{1/3}$
LAMINAR	LONG	$(Sh) = 2.692 \frac{d_e}{S}$
TURBULENT	LONG	$(Sh) = 0.023 (Re)^{0.8} (Sc)^{\frac{1}{3}}$
* TURBULENT	SHORT	$(Sh) = 0.145(Re)^{\frac{2}{3}}(Sc)^{\frac{1}{3}} \left[\frac{d_e}{L}\right]^{\frac{1}{4}}$

* $L/d_e < 12.5$

d_e = equivalent diameter = $\frac{2BS}{B+S}$

B = width

L = length

S = Separation

$(Re) = U d_e / \nu$

(Sh) = average Sherwood No. = $\frac{K_L d_e}{D}$

γ = aspect ratio = S/B

TABLE 4.1 MASS TRANSFER CORRELATIONS FOR THE PARALLEL PLATE GEOMETRY.
(Compiled from reference 120.)

AUTHORS	a	b	z
Lin et al.	1.62	0.33	0.33
Friend and Metzner	1.94	0.33	0.33
Ross and Wraag	1.76 - 2.03	0.33	0.33
Coeuret et al.	0.45	0.53	-
Bazan and Arvia	0.525	0.50	+ 0.25
Carbin and Gabe	3.93	0.32	0.35

$$(Sh) = a(Sc)^{0.33} (Re)^{b} \left[\frac{d_e}{L}\right]^{z}$$

TABLE 4.2 MASS TRANSFER CORRELATIONS FOR LAMINAR FLOW IN AN ANNULAR GEOMETRY.
After Carbin and Gabe [195]

AUTHORS	REF.	PROPOSED CORRELATION
Wilson & Geankoplis shallow packed beds	145	$\frac{ed_pk}{D} = 1.09 \left[\frac{\nu d}{D}\right]^{\frac{1}{3}}$ $,(Re) = \frac{v}{a\nu} = 5 \times 10^{-4}$ to 15
Colquhoun-Lee & Stepanek	146	$\frac{k}{aD} = 0.62 \left[\frac{\nu}{D}\right]^{\frac{1}{3}} \left[\frac{v}{a\nu}\right]^{0.61}$ $(Re) = \frac{v}{a\nu} = 14 - 1400$

TABLE 4.3 MASS TRANSFER CORRELATIONS FOR POROUS AND PACKED BED ELECTRODES.

AUTHOR(S)	REF.	CONSTANTS IN EQUATION $J_D = a\left[\frac{Re_{dp}}{1-e}\right]^x$		d_e/d_p	SYSTEM	$\frac{(Re)_{dp}}{(1-e)}$	(Sc)
		a	x				
Smith & King	163	0.32 0.54	0.38 0.44	41-105 17-27	Cylindrical wall mass transfer	7-1067 34-2334	580-2100
Jottrand and Grunchard	161	0.45	0.375	93-360	Plannar test electrode in cylindrical bed	6-200	1250
Jagannadharaju and Venkata Rao	162	0.43	0.38	8-27	Inner anode of annular bed	200-23800	1300
Coeuret et al.	160	1.2	0.52	93-290	Various cylindrical probes	6-200	1250
Carbin and Gabe	85, 86	1.24	0.57	80-150	Cylindrical test electrode in cylindrical bed	0.1-70	787-1777
Walker & Wragg	157, 158	0.6	0.39	43	Rectangular channel wall mass transfer	936-67	2675

TABLE 4.4 COMPARISON OF MASS TRANSFER STUDIES FOR THE FLUIDISED BED ELECTRODE.

After Walker and Wragg [157, 158]

SYSTEM	FLOW	CORRELATION	REF.
Disc	Laminar	$Sh = 0.62\ Re^{\frac{1}{2}}Sc^{\frac{1}{3}}$	59
Disc	Turbulent	$Sh = 0.02\ Re^{0.8}Sc^{\frac{1}{3}}$	59
Cylinder	Critical	$Sh = 0.97\ Re^{0.64}$	89
Cylinder	Turbulent	$Sh = 0.079\ Re^{0.30}Sc^{0.644}$	91
Wire	Laminar	——	257
Cone	Laminar	——	259
Sphere	Laminar	——	258

TABLE 4.5 MASS TRANSFER CORRELATIONS FOR (SMOOTH) ROTATING ELECTRODES

SYSTEM	average limiting current density ~
natural convection at vertical electrodes (laminar)	$h^{-\frac{1}{4}}$
natural convection at horizontal electrodes (turbulent)	l^{0}
laminar flow along plate	$l^{-\frac{1}{2}}$
channel flow (laminar)	$(D_h l)^{-\frac{1}{3}}$
channel flow (turbulent)	$D_h^{-0.09} l^{-\frac{1}{3}}$
rotating disk (Laminar)	r^{0}
rotating disk (turbulent)	$r^{0.8}$
rotating cylinder (laminar)	$r^{0.4}$
rotating cylinder (turbulent)	$r^{0.2}$

TABLE 5.1 INFLUENCE OF ELECTRODE SIZE ON LIMITING CURRENT DENSITY

after Ibl[209]

h = height of electrode

l = length of electrode

r = radius

D_h = equivalent diameter

ELECTRODE SYSTEM		MASS TRANSFER COEFFICIENT VARIES AS U^n WHERE n =
smooth RDE	laminar flow	0.5
smooth RDE	turbulent flow	0.9
smooth RCE	laminar flow	0.33
smooth RCE	turbulent flow	0.70
rough RCE	turbulent flow	1.0

TABLE 5.2 INFLUENCE OF PERIPHERAL VELOCITY ON MASS TRANSFER TO ROTATING ELECTRODES.

TYPE OF REACTOR	A_s/cm^{-1}	Y_{ST}/(hr)$^{-1}$
Filterpress	0.3-1.7	0.12-0.68
capillary gap	1.0-5.0	0.4-2.0
rotating disc	1	4
rotating cylinder	0.1-1	0.4-4
packed bed	10-50	4 - 20
fluidised bed	20-100	8 - 40
Swiss roll	20-50	–

TABLE 5.3 COMPARISON OF REACTOR DESIGN IN TERMS OF SPACE TIME YIELD AND ELECTRODE AREA PER UNIT CELL VOLUME.
(After Goodridge + additions [213])

DESIRABLE PROPERTIES	CRITERIA AFFECTED
high area/unit cell volume	Y_{ST}
uniform electrode potential	Y_C Y_{ST} Y_E ease of control
low internal ohmic drop	Y_E
good heat and mass transfer	Y_C Y_{ST}
ability to act in flow through mode	Y_C Y_{ST} control
simplicity of construction) electrode renewal) product recovery)	cheapness, reliability ease of automation and maintenance
ability to deal with gases	Y_E
ability to operate at pressure	Y_{ST}

TABLE 5.4 IMPORTANCE OF SPACE-TIME YIELD, CHEMICAL YIELD AND EASE OF CONTROL ON REACTOR PERFORMANCE.

(After Goodridge[213])

PROPERTY	AKZO	CJB	CHEMELEC
Divided	Yes	Yes	No
Fluidised by	metal particles	metal particles	glass beads
geometry cathode feeder	? cylindrical	planar or cylindrical	planar mesh
cathode	metal parts/ + feeder	metal parts/ feeder	metal mesh (expanded)
geometry anode	cylindrical rods around cathode	planar	planar
FIG.	5.42	5.41	5.43
REFS.	167	165	166, 234, 235
overall geometry concept	concentric cylinder	planar side by side	planar side by side (multiple plate)
metal recovery	continuous via gravity separation as metal powder	discontinuous as metal powder	discontinuous as hard plate

TABLE 5.5 COMMERCIALLY DEVELOPED, FLUIDISED BED ELECTRODE REACTORS

$N/cm^3\ s^{-1}$	f_R
1	0.9990
10	0.9901
100	0.9091
1000	0.5
10000	0.09091

$$f_R = \frac{KA/N}{1 + KA/N} = \frac{1000}{N(1+100/N)}$$

$$KA = 1000\ cm^3\ s^{-1}$$

TABLE 6.1 EFFECT OF FLOW RATE, N ON THE FRACTIONAL CONVERSION, f_R for a R.C.E.R.

CYLINDER AREA A/m^2	DIAMETER d /cm	LENGTH l /cm	PERIPHERAL VELOCITY U/cms^{-1}	R.P.M.	d/l
0.05	12.6	12.6	1145	1735	1
0.1	20.6	15.45	1195	1108	1.33
0.2	20.6	30.9	1195	1108	0.67
0.4	40	31.8	1265	604	1.26
0.625	40	49.7	1265	604	0.80
1.25	72.7	54.7	1333	350	1.33
2.5	72.7	109.5	1333	350	0.67
5.0	154.5	103.0	1423.5	176	1.5
7.5	154.5	154.5	1423.5	176	1
10.0	154.5	206.0	1423.5	176	0.75

TABLE 6.2 POSSIBLE SCALE-UP OF ECO-CELLS

(maintaining the mass transfer coefficient, K_L, according to equation 6.34)

CYLINDER AREA A/m^2	DIAMETER d /cm	LENGTH l /cm	R.P.M.	MASS TRANSFER COEFFICIENT K_L/cms^{-1}	% REDUCTION in K
0.05	12.6	12.6	1735	0.526	0
0.1	20.6	15.45	1062	0.506	3.8
0.2	20.6	30.9	1062	0.506	3.8
0.4	40	31.8	547	0.476	9.5
0.625	40	49.7	547	0.476	9.5
1.25	72.7	54.7	301	0.457	13.1
2.5	72.7	109.5	301	0.457	13.1
5.0	154.5	103.0	142	0.431	18.1
7.5	154.5	154.5	142	0.431	18.1
10.0	154.5	206.0	142	0.431	18.1

TABLE 6.3 POSSIBLE SCALE-UP OF ECO-CELLS

(maintaining the peripheral velocity, U, according to equation 6.34)

r_I /cm	A /cm^2	V /cm^3	A/V /cm^{-1}
1	4π	6π	0.67
10	400π	420π	0.95
100	40000π	40200π	1

$$A = 2\pi r_I l$$

$$V = \pi l \left(r_o^2 - r_I^2\right)$$

$$r_o - r_I = 1 \text{ cm}$$

TABLE 6.4 IDEALISED 'ECO-CELL' VOLUME AS A FUNCTION OF REACTOR SIZE according to equation 6.37

CURRENT LOADING I /KA	CELL VOLUME V /dm^3	NOMINAL RESIDENCE TIME τ /s
0.5	0.852	0.852
1	1.692	1.692
2.5	4.207	4.207
5	8.391	8.391
7.5	12.573	12.573
10	16.750	16.750
20	33.449	33.449
40	66.830	66.830
50	83.518	83.518

Assumptions:

$V = \pi l (r_o^2 - r_I^2)$ (annular volume)

$r_o - r_I = 1$ cm

$\tau = \frac{V}{L}$

$L = 1000 \text{ cm}^3 \text{ s}^{-1}$

TABLE 6.5 NOMINAL RESIDENCE TIME AS A FUNCTION OF FLOW-RATE for idealised Eco-Cells

PARAMETER	R.B.E.R.	CASCADE ECO-CELL
subdivision of reactor	radially	axially
working electrodes	anode or cathode depending on compartment	normally all cathode
number of elements	2 (or 3)	6 - 12
typical r.p.m.	20	100 - 1000
Flow	nominally laminar	highly turbulent
division into anolyte + catholyte	undivided	may be divided by IX membrane
roughness of R.C.E.	exceptionally smooth	rough and powdery deposits
Wiping/ scraping	PTFE blade, continuous, full length wiper	metal or ceramic blade discontinuous traversing point scraper
intercompartment leakage of current	very low	appreciable
subdivision accomplished by	PTFE blades, touching R.C.E.	internal baffle rings with clearance
effect of wiper/ scraper	increases mass transfer divides the reactor	removes powder product from the cathode
electrode potential profile	varies with compartment	normally same for each compartment
mass transfer	low	very high
approx. to CSTR	poor	good

TABLE 6.6 COMPARISON OF ROTATING BIPOLAR ELECTRODE AND CASCADE ECO-CELL REACTORS.

d/l	BODY MATERIAL	CYLINDER DETAILS					BEARING FITTED	POWER VIA	ELECTRODE	CELL	OR G/STAT	REF.	FIG.	R.P.M.
		MATERIAL	DIAM. /cm.	HT./ cm.	ACTIVE AREA/ cm^2									
0.64	BAKELITE /PYREX	STRIP STEEL	9.7	15.2	464	C	NO	Cu- CARBON BRUSHES	STEEL	NO	G	310	6.6	50 - 1250
0.08- 0.40	LUCITE	CHEMICAL OR NICKEL	1.27 TO 5.98	15	60 TO 284	A C	YES	MERCURY WELL	NICKEL	NO	G	58	6.7	30 - 1650
1.09 0.61 0.90	LUCITE	COPPER	2.17 3.75 6.60	2.0 6.1 7.3	14 TO 275	A	YES	MERCURY WELL	COPPER	NO	P	82	6.8	0 - 350
0.60	COPPER/ PERSPEX	COPPER	1.52	2.53	12.1	C	NO	MERCURY WELL	COPPER	NO	P	74	6.9	60 - 1800
0.17		MONEL	6.35	38	304	C	NO	Cu CARBON BRUSH	PLATINISED TITANIUM	NO	P G	89	6.10	0 - 201
0.33	PERSPEX	COPPER	2.5	7.6	5.0	C	YES	MERCURY WELL	COPPER	NO	G	284	6.11	470- 3860
0.99	COPPER	STAINLESS STEEL + COPPER	5.9	6.0	22.4	A C	NO	Ag- CARBON BRUSHES	COPPER	NO	P G	84, 68	6.12	180- 1500
1·91	PERSPEX	COPPER	2.47	1·3	10	C	YES	MERCURY WELL	LEAD	YES	TRANSIENT G	94	6.13	0 - 2500
?	GLASS	NICKEL PLATED Cu COPPER	2.0	?	?	C	NO	MERCURY WELL	NICKEL COPPER	NO	G	73	6.14	200- 2000
0.92	PERSPEX	VARIOUS	5.5	6.0	100	A C	NO	Ag- CARBON BRUSH	LEAD	YES	P	present work		200- 2500

TABLE 6.7 COMPARISON OF LABORATORY R.C.E. CELLS REGARDING DESIGN OR CONSTRUCTION

REF.	ASSIGNEE	DATE	METAL	APPLICATION	ANODES	R.C.E. DETAILS						SPECIAL FEATURES
						MATERIAL	d	L	A	RPM	U	
301	CLEAVE	1925	SILVER	REFINING	SOLUBLE		—	—	—	—	—	SCRAPED R.C.E. POWDER PRODUCT
302	NORDBLOM	1968	NICKEL	PRODUCTION OF NICKEL FLAKE	?	STAINLESS STEEL	—	—	—	—	—	GRIDDED BELT ON R.C.E.
306-309	HOLLAND	1977	VARIOUS	ELECTROWINNING, ELECTROREFINING EFFLUENT TREATMENT	VARIOUS, NORMALLY INSOLUBLE	STAINLESS STEEL TITANIUM	← Various →				$1-10^4$	SCRAPED R.C.E. CONTINUOUS POWDER PRODUCTION

TABLE 6.8 PATENTED R.C.E. CELLS

REF.	ASSIGNEE	DATE	METAL	APPLICATION	ANODES	R.C.E. DETAILS						SPECIAL FEATURES
						MATERIAL	d	ℓ	A	rpm	U	
305	ARRIGO PINI SpA	1963	SILVER	REFINING OF SILVER FROM NITRATE SOLUTIONS	SOLUBLE SILVER	METAL	—	—	—	—	—	SCRAPED R.C.E. POWDER PRODUCT
300	SOCIETE INDUSTRIELLE DES COUSSINETS	1961	COPPER-LEAD ALLOY	ALLOY POWDER PRODUCTION	SOLUBLE LEAD/ COPPER	STEEL	—	—	—	—	—	SCRAPED R.C.E. POWDER PRODUCT
299	PRUNET AND GUILLEN	1961	ZINC	RECOVERY FROM ZINCATE	INSOLUBLE	METAL	—	—	—	5 - 10	—	SCRAPED R.C.E. POWDER PRODUCT
303	GORDY	1973	COPPER	ELECTROWINNING OF ORES	ORE	COPPER	—	—	—	—	—	SCRAPED R.C.E. POSSIBLY POWDER PRODUCT
304	JOHNSON	1939	ZINC	ELECTRO-DEPOSITION OF ZINC DUST	?	IRON OR NICKEL	—	—	—	1	—	SCRAPED R.C.E. POWDER PRODUCT COOLED R.C.E.
334	BENNER	1969	(DESALINATION)	REMOVAL OF IONS FROM A LIQUID	?	ION XS MATERIAL MAY BE USED	—	—	—	—	—	2 RCE's CONTRA-ROTATING BIPOLAR PARTIALLY IMMERSED FLOW THROUGH

						MATERIAL	d/ cm	l/ cm	A/ cm^2	RPM	U/ cms	FEATURES
335	LACROIX	1912	VARIOUS COPPER	ELECTROWINNING	INSOLUBLE	METAL	31.8	100	10^4	40	67	BOTTOM BEARING
336	COWPER-COLES	1915	IRON	ELECTROWINNING & ELECTRO-REFINING	INSOLUBLE /SOLUBLE	METAL	—	—	—	—	—	PROPELLER
337	SCHAEFER	1945	SILVER	ELECTROPLATING	SILVER RODS	METAL (WORK-PIECE)	—	—	—	—	—	RECYCLING
338	I.C.I.	1974	VARIOUS	ELECTROWINNING	INSOLUBLE	METAL	—	—	—	—	—	ROTATING ANODE + VESSEL (R.C.E.)
339	BERKEY PHOTO INC. (FULWEILER)	1971	SILVER	RECOVERY OF SILVER FROM PHOTOGRAPHIC FIXER	GRAPHITE PLATES (6)	STAINLESS STEEL	30	15	1460	230	367	IMPELLER AT TOP OF R.C.E.
341	FISCHER	1972	SILVER	"	GRAPHITE POLES (4)	"	—	—	—	50-200	—	VANED R.C.E. OR POLYGON
342	GOOLD et al.	1975	COPPER + OTHERS	ELECTROWINNING	INSOLUBLE e.g. LEAD	METAL (STAINLESS STEEL)	—	—	—	—	—	POLYGONAL ROTATING ELECTRODE
343	JULIEN	1925	COPPER	ELECTROPLATING OF FOIL	SOLUBLE COPPER	METAL	—	—	—	—	—	ANODE BASKET
344	COOLEY	1968	SILVER	RECOVERY OF METALS	GRAPHITE	STAINLESS	13	25	323	150 max.	100	CLOSELY CONFORMING COUNTER ELECTRODE

REF.	ANODES		DIVIDED	SEALED	SCRAPED	R.C.E.		PLATE	POWDER	IMMERSION		DRIVE		BAFFLES	FLOW THRO'	R.C.E. IMPELLER	FIG.
	SOL.	INSOL.				A⊕	C⊖			PART	TOTAL	↑	→				
299b		√			√	√			√		√	√					6.35b
299a		√			√		√		√	√			√		√		6.35a
300	√				√		√		√	√			√		√		6.34
301	√				√		√		√		√	√					6.38
302					√		√	* √		√			√				6.39
303	√		√		√		√		√	√	√		√				6.36
304					√				√		√	√			√		6.37
305	√				√		√		√	√		√					6.33
† 306		√	√	√	√		√		√		√	√			√		6.40
339		√					√				√	√		√		√	6.28
341		√					√	√			√	√			√	√	6.29
342		√					√	√		√		√			√		6.30
343	√						√	√					√				6.31
344		√			√	√	√	√		√			√		√		6.32
338		√				√	√		x √	√			√				6.27
337	√						√	√			√	√			√		6.26
336	√	√					√	√		√		√				√	6.25
335		√					√	√		√		√			√		6.24

* FLAKE † ECO-CELL x 'finely divided form'

TABLE 6.9 COMPARISON OF PATENTED R.C.E.R.'s FOR ELECTRODEPOSITION

Compartment No.	C_{IN} /mg dm^{-3}	C_{OUT} /mg dm^{-3}	C /mg dm^{-3}	R /g(hr)$^{-1}$	$(f_R)_n$	I /A
1	100	50	50	180	0.500	151.88
2	50	25	25	90	0.750	75.94
3	25	12.5	12.5	45	0.875	37.97
4	12.5	6.25	6.25	22.5	0.938	18.99
5	6.25	3.125	3.125	11.25	0.969	9.49
6	3.125	1.5625	1.5625	5.625	0.984	4.75
Overall	100	1.56	98.44	354.375	0.984	300

TABLE 6.10 PERFORMANCE OF HYPOTHETICAL ECO-CASCADE-CELL

Copper deposition under limiting current conditions, with a fractional conversion of 0.5 in each compartment.

100% cathode current efficiency.

(some figures have been rounded off for convenience)

AUTHOR(S)	REF.	SCOPE	YEAR
ROSSMAN	347	U.S. Patents 1894 - 1931	1932
ROSSMAN	348	U.S. Patents 1932 - 1943	1944
IBL	193	Patents 1894 - 1959	1962
MANTELL	349 350	Metals for Powder Metallurgy (examples listed by the metal)	1959
WRANGLEN	370	Metal Powders in General (deposit properties)	1950
IBL	193	Metal Powders in General (mass transport)	1962
IBL	193	Metal Powders in General (Mass transport)	1964
WALKER & SANDFORD	351	Production of Metal Powders	1979
WALKER	351A	Alloy Powders	1979
KROLL	352	Fused Salt Electrolysis	1945
SHAFER & HARR	353	Iron Powders - Production & Properties	1958
MEHL	354	Copper Powder	1958
KUMAR & GAUR	355	Copper Powder	1973
MITAL	356	Metal and Alloy Powders	1973
CALUSARU	357	Metal Powders in General	1979

TABLE 7.1 REVIEWS OF ELECTROLYTIC METAL POWDER DEPOSITION

METAL	USES
i) Cadmium	speciality batteries, phosphorus for TV tubes, low melting alloys.
ii) Cobalt	specialised magnetic and high temperature alloys preparation of X-ray sources
iii) Silver	printed circuits (by powdered inks) dental fillings decorative trades speciality batteries spark plugs electrical contacts conductive resins and chemicals industrial chemicals
iv) Manganese	chemicals, electrical dry cells alloy production (especially non-ferrous alloys)
v) Lead	lead-bronze metal oil-less bearings special purpose paints sprayed protective coatings preparation of battery plates special lubricating greases (for oil exploration gasket materials and gland packing (as filler for asbestos and rubber) brake linings metallic threads thin rolled and cast sheets with plastic mouldings, PVC sheets as radiation guards, and sound insulant tyre balancing superconductors between deposited metal films and external electric circuits
vi) Tin	as a sintering medium in bronze sintered parts laboratory applications additives protective coatings solder component
vii) Nickel	fuel cells electrodes plates for speciality batteries porous metal filters welding electrodes binding agent for metal carbides chemicals (especially catalysts) sintered products (e.g. magnets) coating of steel strips (e.g. for strip wound covers, transformer laminations and magnetic shields) coinage

TABLE 7.2 USE OF INDIVIDUAL METAL POWDERS

METAL	USES
viii) Zinc	surface coating for steel (paints, etc.) reducing agents (especially for paper industry) dye production welding primers pyrotechnics (smoke producing compositions) gold extraction from cyanide solutions electrolyte purification in zinc production
ix) Copper	unalloyed - decorative trade - filter applications - sintered component parts - chemical catalysts - bonding adhesives - friction materials
	bronze - decorative trades (spherical) - filter components (spherical) - sinter components (spherical) - coating applications (spherical) - metal filled plastics (irregular) - diamond tool and wheel trade (irregular) - alloy powders and premixed powders (irregular)
	brass - decorative trades brake linings

TABLE 7.2 USE OF INDIVIDUAL METAL POWDERS (Cont'd.)

Uses	Grade/Type	Powder
1. Aerospace Brake lining counter weights, filters, bearings	Atomised powders (Pre-alloyed) and others	Atomised Cu 90/Pb 10
2. Agricultural Farm machinery parts, Garden equipment parts, Food enrichment, fungicides, soil conditioning	Atomised powders Hydro refined, Electrolytic	Cu and Cu base
3. Automotive Brake lining Brake bands Bushes Clutch facings Engine parts Transmission parts Dynamo parts	Atomised powders Hydro refined, Electrolytic	Cu and Cu base
4. Building/construction Conductive concrete flooring (non-spark, fungus proof, structurally stronger for hospitals, theatres, shower baths, dairies, locker rooms etc).	Atomised powders, Hydro-refined Electrolytic	Cu and Cu base
Decorative plastics Linoleum Pipe jointing	Extrafine grades preferred	Cu and Cu base
Magnesium Oxychloride cements (shrinkage promotion, increased moisture resistance.	Atomised can also be used	
5. Chemical Catalysts Reactants	Ultra fine grades preferred Atomised can also be used	55 Cu/45 Al 50 Cu/45 Al/5 Zn
6. Domestic Cordless Electric Tooth Brushes, Razors, Finger nail laquer, etc.	Atomised, hydrorefined milled and other types	Cu and Cu base

TABLE 7.3 USE OF COPPER AND COPPER BASED POWDERS

Uses	Grade/Type	Powder
7. Electronics/Electrical		
Contacts Crystal Supports Printed Circuits (ink)	Low density gas reduced powders	Cu and Cu based Cu-W Cu-Ag-Cd
Electrodes		
Permanent magnets commutators	High density/low porosity with 3.2 to 3.3 gm/cc density irregular preferred	Cu and Cu-Ag
Semi conducting polymers	Ultrafine powders	
Motor brushes	Various grades, including Dispersion hardened copper and atomised powders	Cu-graphite
8. Lubricants		
Anti-galling-jointing Copper bearing-lubricants plastic filled metals	Various finer grades	Cu and Cu base powders
9. Medical		
Dressing superficial wounds	Various finer grades	Cu
10. Nuclear Engineering		
Gamma ray shielding (attenuation)	Various grades	Cu-W-Ni
11. Ordnance		
Armour piercing cores, Incendiary Bombs, Flares, Torpedo parts, Tracers, Projectile rotating bands	Electrolytic and other grades (explosive compacting also used)	Cu and Cu base powders
12. Powder Metallurgy (P/M) and other mechanical applications		
Abrasive wheels, Metal bonded diamond tools, Bearings/Bushes Low porosity	Atomised and others (hot or cold pressed sintered to make grit matrix) Atomised, irregular and gas reduced high density grades	Cu, bronze, brass or/Cu-Ni alloys Leaded Brass (77 Cu/2 Pb Zn) Nickel Brass (69 Cu/9 Ni/Zn)

TABLE 7.3 USE OF COPPER AND COPPER BASED POWDERS (CONT'D)

Uses	Grade/Type	Powder
12. (Cont'd)		
Porous	Atomised, irregular and gas reduced low density grades	Copper/Tin 88 Cu/10 Sn 1 Fe/1C
Steel backed Al backed	Atomised pre-alloyed	20 to 30% Pb/Cu 20 Pb/5Sn/Cu 89 Cu/11 Zn
Plastic field	Atomised	Tin-bronze - 20% Wt. PTFE
Oil impregnated	Pre-mixed grades	Up to 10% Pb 1-5% graphite
Filters	Atomised (spherical high density grades with narrow sieve cuts)	5 - 20 Sn/0.7-1.0 P/Cu
13. Friction material		
	Hydro-refined atomised, ementation, coated	Cu-Sn mixes 2 to 10 Cu/Fe
		Copper coated 78 Fe/20 Cu/2Sn
		20 Cu/0.8 C/Fe
		Cu-Sn-Fe-Pb-C-Si Mixes for heavy duty use.
Infiltrants	Various grades for compact-densification	5 Fe/5 Mn/Cu
Iron-copper compacts	Atomised irregular	Various grades by Powder Metallurgy Ltd., (UK[15]), MSP (India)6
Mechanical components	Atomised, electrolytic or hydrorefined	3 to 14 Cu/Fe
	Leaded brass	77 to 90 Cu/1 to 1 Pb/Zn
	Nickel silver	62 to 66 Cu/16 to 19 Ni/Zn
(mechanical components)		
	Leaded nickel Silver	62 to 66 Cu/16 to 19 Ni/1 to 1.8 Pb/Zn
	Infiltrated iron	7.0 to 85 Fe/1.5 to 25 Cu/0 to 1 C
	Copper steel	86 to 98 Fe/15 to 11 Cu/0.6 to 1 C

TABLE 7.3 USE OF COPPER AND COPPER BASED POWDERS (CONT'D.)

Uses	Grade/Type	Powder
13. (Cont'd)		
	Aluminium bronzes (irregular)	13 Al/4 Fe/83 Cu
	Atomised Copper/Lead/Tin	69 to 89 Cu 3 to 7 Pb 3 to 11 Sn 1 Zn (max)
	Atomised copper-lead	49 to 77 Cu/23 to 51 Pb
	Atomised brasses	55 Cu/44.75 Zn/0.2 Mg 90 Cu/10 Zn 90 Cu/9.5 Zn/P 90 Cu/9.5 Zn/1.5 P 78.5 Cu/20 Zn/1.5 Pb/P 89 Cu/10 Zn/0.8 Fe 70 to 85 Cu/15 to 30 Zn 73 to 85 Cu/14 to 28 Zn/0.25 to 0.5 Al
Resistance welding electrodes	Suitable grades	Cu/W/Ag
Rolled strip, Extruded tube preforms	Electrolytic (dendritic reduced) (spongy) DHC	Cu and Cu base sintered slugs/ forged preforms
Self brazing	Atomised, others	Cu/Fe
Slip castings	Ultra fine electrolytic	Cu/Fe
Miscellaneous heavy alloys	Atomised (spherical)	Cu (high density) Cu/W/Ni
Others	Atomised	Al base containing up to 2.5% Cu
14. Rail roads		
Brake lining Pantographs Friction strips	Electrolytic and other grades	Cu and Cu base
15. Surface coatings		
Anti-fouling marine paints Conductive paints Corrosion resistance paints Decorative paints	Atomised/Milled Cu grades are usually used	Cu and Cu base
Special varnished Protection of Silvering on mirrors Dye preparations Coloured plastics	Ultra-fine Electrolytic, atomised, milled	100% Cu (red) to 70% Cu/30% Zn (green gold)

TABLE 7.3 USE OF COPPER AND COPPER BASED POWDERS (CONT'D)

Uses	Grade/Type	Powder
15. Cont'd. Spray coating Vacuum metallizing		
16. Gold Bronze		
Paints Inks	Atomised/Milled/Polished	Cu base alloys (brasses)
Decorative applications. Labels Calendars Cigar bands etc. Brush or spray Coated paper	Dusting Bronzing (30% + 325 mesh) (30% - 325 mesh)	Pale golds: Brasses 85 to 95 Cu/4 to 15 Zn
Decals Roller coating Embossing Transfer foils	General/Decorative (85% - 325 mesh) (15% + 325 mesh)	Rich golds: Brasses 70 Cu to 30 Zn 50 micron size average 60 to 100 million particles/gm
Intaglio Surface printing, Stencils	100% - 325 mesh	25 micron size average up to 500 million particles/gm.
Inks Linings Striping	100% - 400	

TABLE 7.3 USE OF COPPER AND COPPER BASED POWDERS (CONT'D)

AUTHOR(S)	REF.	ALLOY	POSSIBLE APPLICATION
PRITHVIRAJ et al.	383	Cu - Ni	Electrical Resistance Alloy
YUREV et al.	384	Co - Ni	Magnetic Material
BONDARENKO et al.	385	Fe - Co - Ni	Magnetic Materials
NAGANATHAN et al.	386	Cu - Zn	Brass products
SEDZIMIR et al.	371	Cu - Sn	Bronze products
ASHWORTH et al.	216, 223	Cu - Sn	" "
FEDYUSHKINA et al.	387	Cu - Sn	Bronze Bearings
NATANSON et al.	388	Fe - Co - Ni	Magnetic Material
POMOSOV et al.	389	Ni - Fe	" "
YUREV et al.	390	Fe - Co	" "
YUREV et al.	391	Cu - Zn	Brass products
YUREV et al.	392	Co - Ni	Magnetic material
DUBE et al.	393	Cu - Zn	Brass products

TABLE 7.4 ELECTRODEPOSITION OF ALLOY POWDERS

FIG. 1.1 PATHWAYS OF TOXIC METALS FROM THE ENVIRONMENT TO MAN

(adapted from reference 2)

Key:

━━━━ food chains

════ respiration

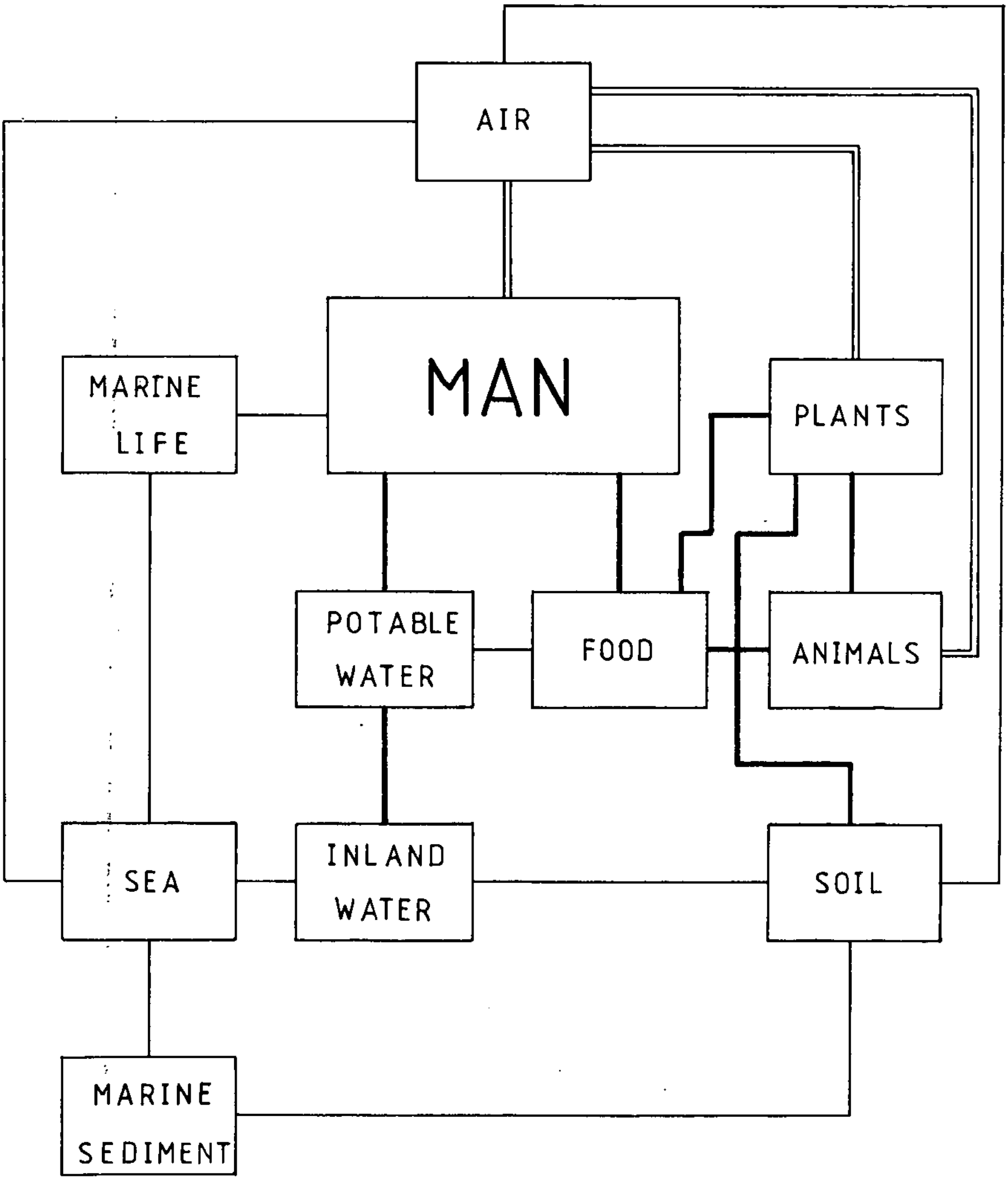
AIR
MARINE LIFE
MAN
PLANTS
POTABLE WATER
FOOD
ANIMALS
SEA
INLAND WATER
SOIL
MARINE SEDIMENT

FIG. 2.1 PRESSURE GRADIENT AS A FUNCTION OF REYNOLDS NUMBER FOR PIPE FLOW

showing the laminar and turbulent zones

FIG. 2.2 FRICTION FACTOR AS A FUNCTION OF REYNOLDS NUMBER FOR PIPE FLOW

showing the laminar and turbulent zones

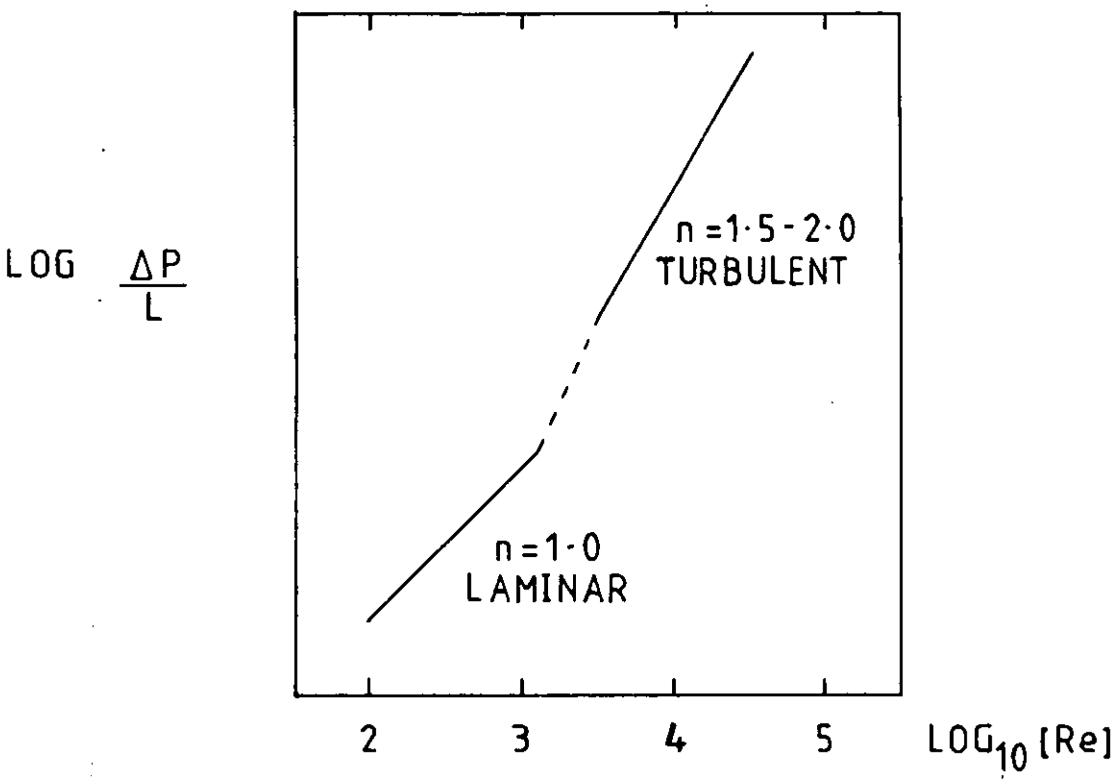
LOG $\frac{\Delta P}{L}$
n = 1·5 - 2·0
TURBULENT
n = 1·0
LAMINAR
2
3
4
5
LOG_{10} [Re]

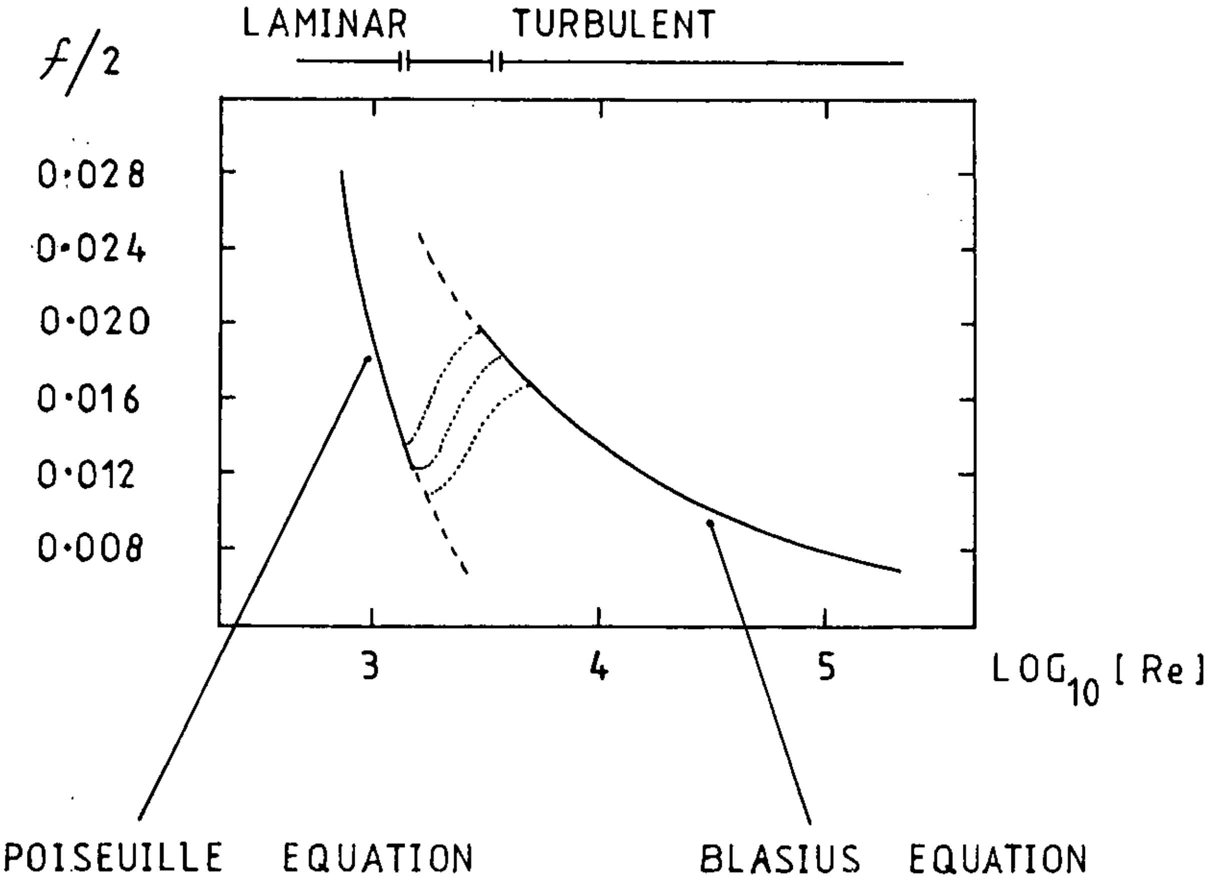
LAMINAR
TURBULENT
$f/2$
0·028
0·024
0·020
0·016
0·012
0·008
3
4
5
LOG_{10} [Re]
POISEUILLE EQUATION
BLASIUS EQUATION

FIG..2.3 FRICTION FACTOR AS A FUNCTION OF
REYNOLDS NUMBER FOR PIPE FLOW
showing the effect of roughness.
After Moody[7]

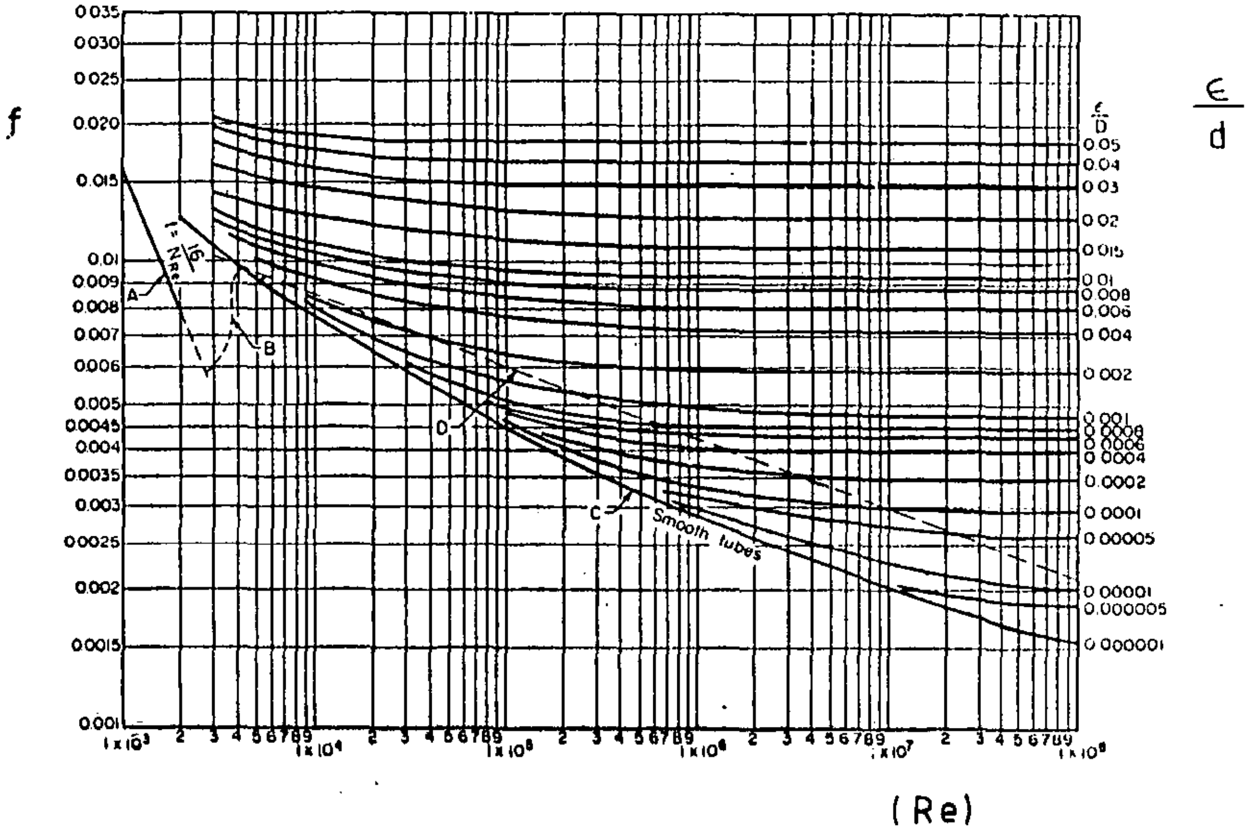
f
0.035
0.030
0.025
0.020
0.015
0.01
0.009
0.008
0.007
0.006
0.005
0.0045
0.004
0.0035
0.003
0.0025
0.002
0.0015
0.001
1×10³ 2 3 4 5 6 7 8 9 1×10⁴ 2 3 4 5 6 7 8 9 1×10⁵ 2 3 4 5 6 7 8 9 1×10⁶ 2 3 4 5 6 7 8 9 1×10⁷ 2 3 4 5 6 7 8 9 1×10⁸
(Re)
ε/D
0.05
0.04
0.03
0.02
0.015
0.01
0.008
0.006
0.004
0.002
0.001
0.0008
0.0006
0.0004
0.0002
0.0001
0.00005
0.00001
0.000005
0.000001
ε/d
f = 16/N_Re
A
B
C
D
Smooth tubes

FIG. 2.4 VELOCITY PROFILES FOR PIPE FLOW

for various Reynolds Numbers

FIG. 2.5 MODEL OF TURBULENT DAMPING NEAR A SOLID WALL

showing a three zone distribution of concentration

After Gabe and Robinson [113]

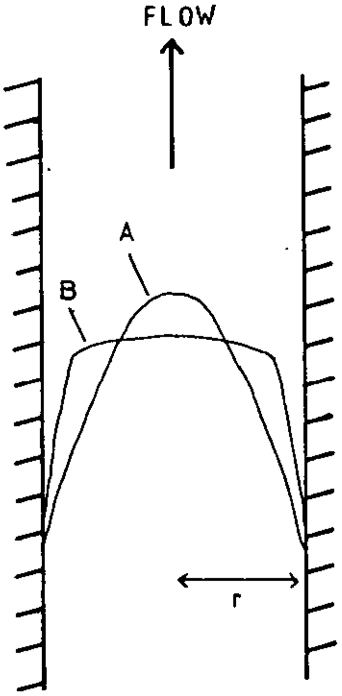
FLOW
A
B
r

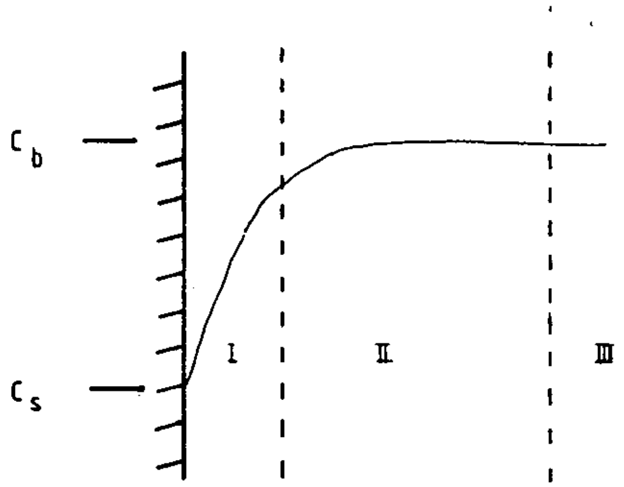
C b
C s
I
II
III

FIG. 2.6 TANTENTIAL FLUID MOTION FOR THE LAMINAR REGIME AROUND A ROTATING CYLINDER

After Newman [10]

FIG. 2.7 TAYLOR VORTICES AROUND A ROTATING CYLINDER in transitional region flow.

After Schlichting [14]

Outer cylinder stationary

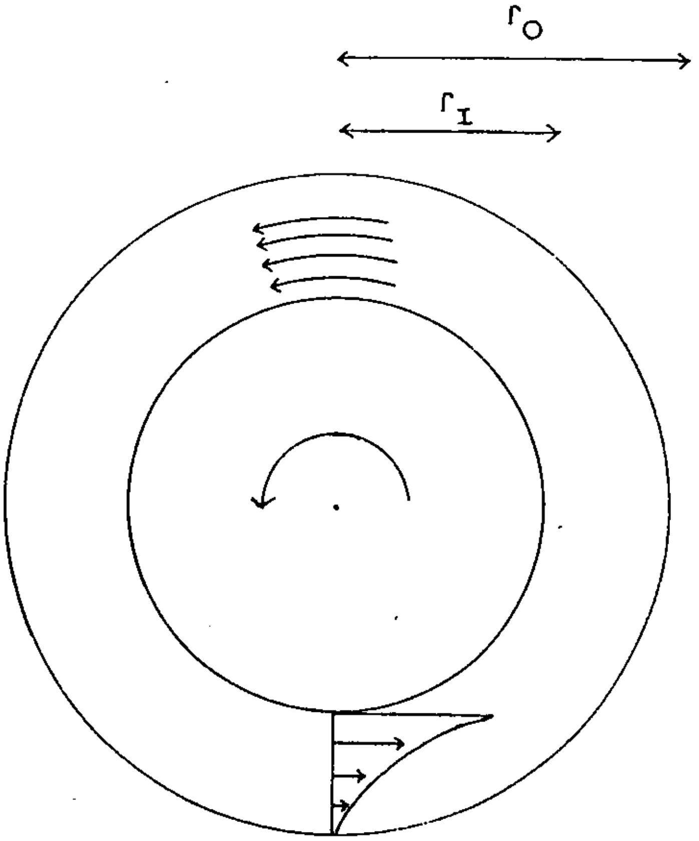
r_O
r_I

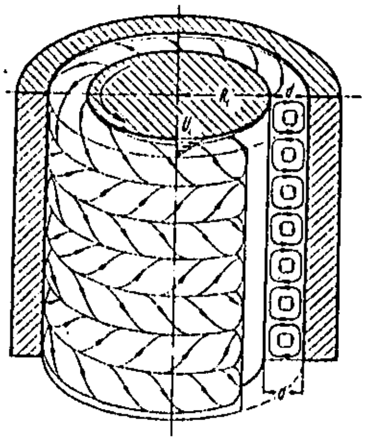
R_1
d
U_1
d

FIG. 2.8 FRICTION FACTOR AS A FUNCTION OF REYNOLDS NUMBER FOR A ROTATING CYLINDER

showing the limits of stability for laminar flow.

After Gabe [25]

FIG. 2.9 TORQUE AS A FUNCTION OF REYNOLDS NUMBER FOR A ROTATING CYLINDER

showing the transition to turbulent flow

Relative gap size

$$\frac{r_I - r_o}{r_I} = 0.028$$

Key:

o	experimental measurements by Taylor [13]
———	non-linear theory, Stuart
- - - - -	linear theory, Schlichting [14]

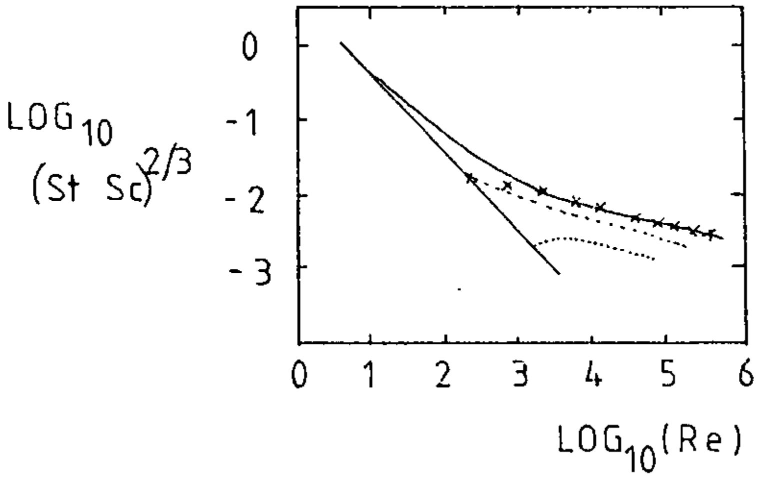
0
-1
-2
-3
LOG10 (St Sc)2/3
0
1
2
3
4
5
6
LOG10(Re)

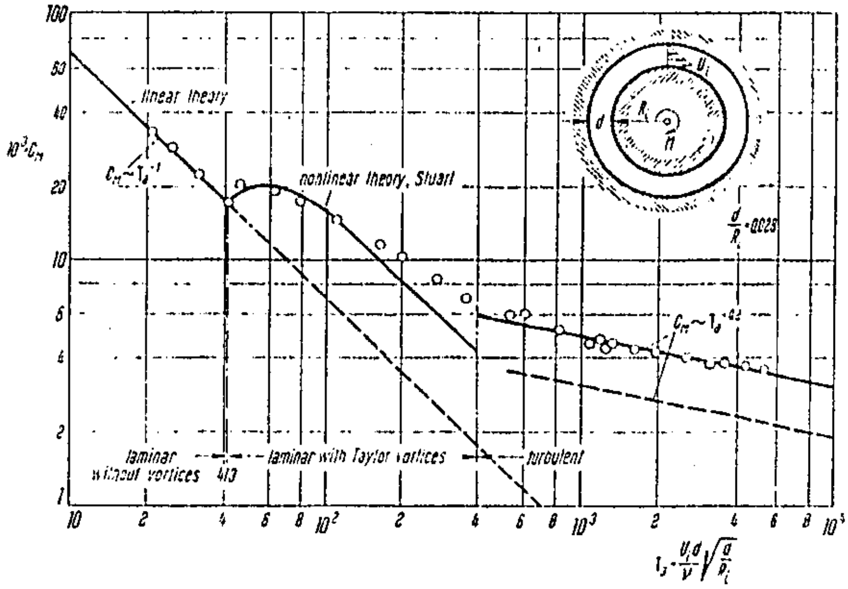
100
60
40
20
10
6
4
2
1
$10^3 c_M$
linear theory
$c_M \sim T_a^{-1}$
nonlinear theory, Stuart
U_i
R_i
d
Ω
$\frac{d}{R_i} = 0.028$
$c_M \sim T_a^{-0.2}$
laminar without vortices
413
laminar with Taylor vortices
turbulent
10
2
4
6
8
10^2
2
4
6
8
10^3
2
4
6
8
10^4
$T_a = \frac{U_i d}{\nu}\sqrt{\frac{d}{R_i}}$

FIG. 2.10 SECONDARY FLOWS AROUND A ROTATING CYLINDER IN THE TURBULENT REGIME

a) observed by Taylor [11]

b) observed by Pai [22]

FIG. 2.11 VELOCITY PROFILES IN THE ANNULAR GAP BETWEEN A ROTATING INNER CYLINDER AND A STATIONARY CONCENTRIC OUTER CYLINDER

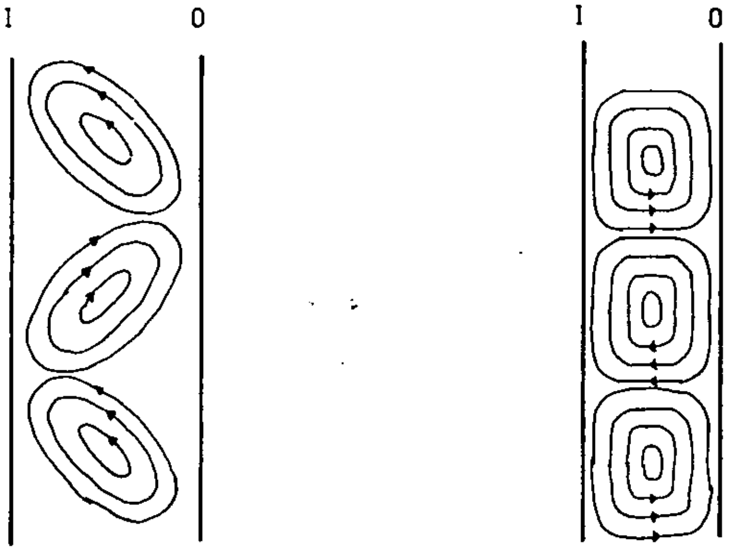

b) a)

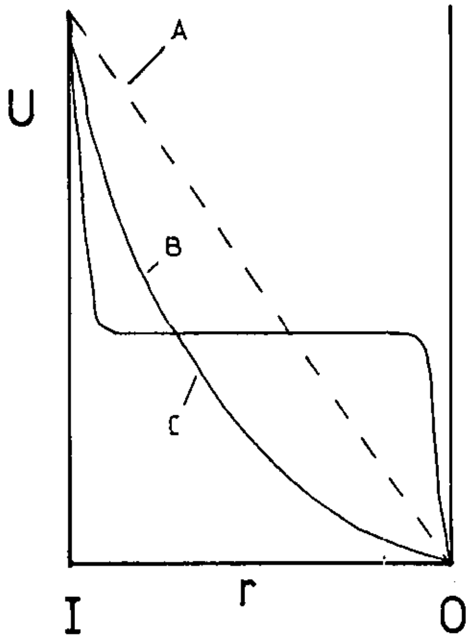

FIG. 2.12 FRICTION FACTOR AS A FUNCTION OF REYNOLDS NUMBER FOR A ROTATING CYLINDER

showing the limits of stability.

After Theodorsen and Regier [9]

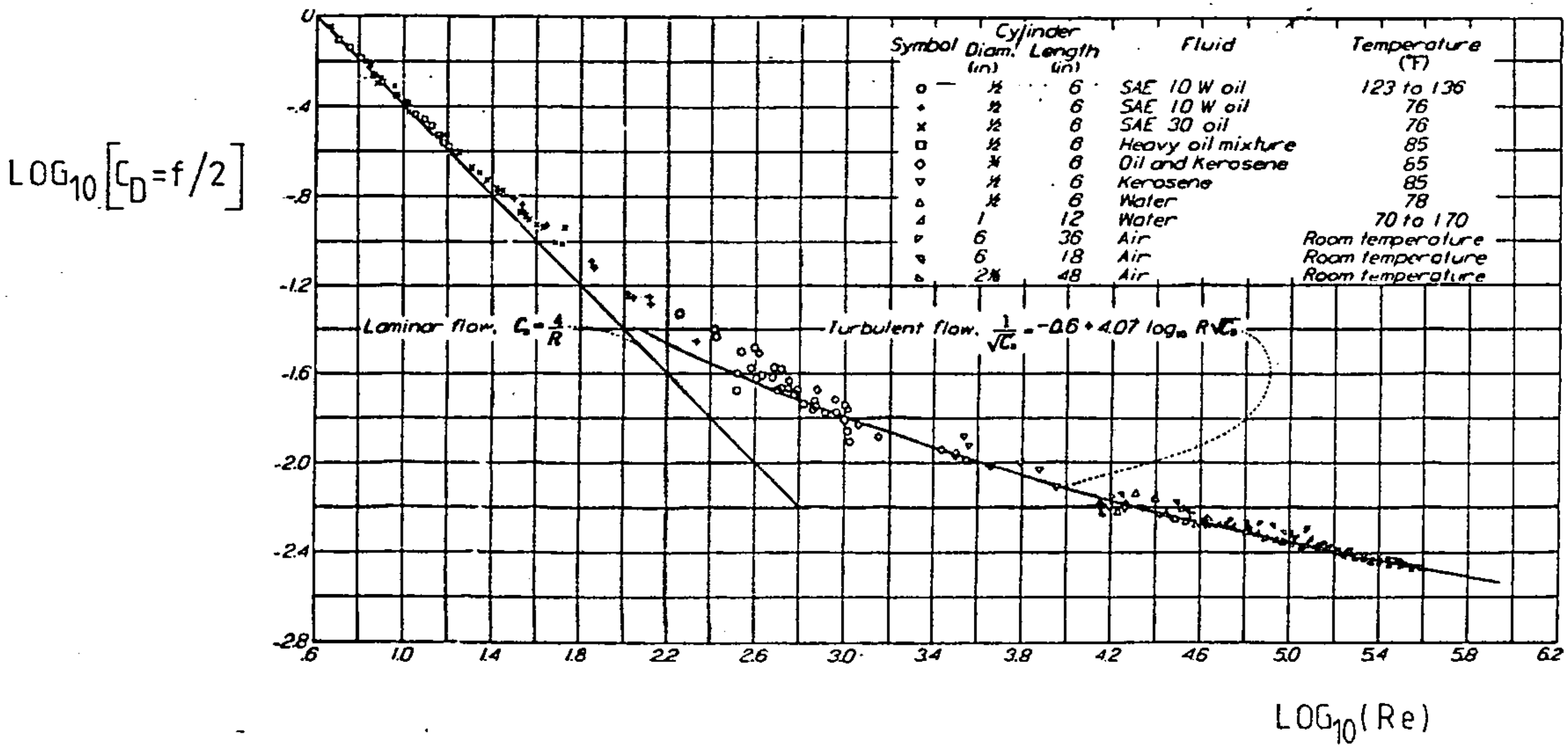LOG10[CD=f/2]
LOG10(Re)
0
-.4
-.8
-1.2
-1.6
-2.0
-2.4
-2.8
.6
1.0
1.4
1.8
2.2
2.6
3.0
3.4
3.8
4.2
4.6
5.0
5.4
5.8
6.2
Laminar flow. $C_0 = \frac{4}{R}$
Turbulent flow. $\frac{1}{\sqrt{C_0}} = -0.6 + 4.07 \log_{10} R\sqrt{C_0}$
Symbol | Cylinder Diam. (in) | Cylinder Length (in) | Fluid | Temperature (°F)
○ ½ 6 SAE 10 W oil 123 to 136
• ½ 6 SAE 10 W oil 76
× ½ 6 SAE 30 oil 76
□ ½ 6 Heavy oil mixture 85
◇ ¾ 6 Oil and Kerosene 65
▽ ¼ 6 Kerosene 85
△ ¼ 6 Water 78
◿ 1 12 Water 70 to 170
▾ 6 36 Air Room temperature
◥ 6 18 Air Room temperature
▴ 2⅜ 48 Air Room temperature

FIG. 2.13 a FRICTION FACTOR AS A FUNCTION OF REYNOLDS NUMBER FOR A ROTATING CYLINDER

showing the effect of saturated roughness.

After Theodorsen and Regier [9]

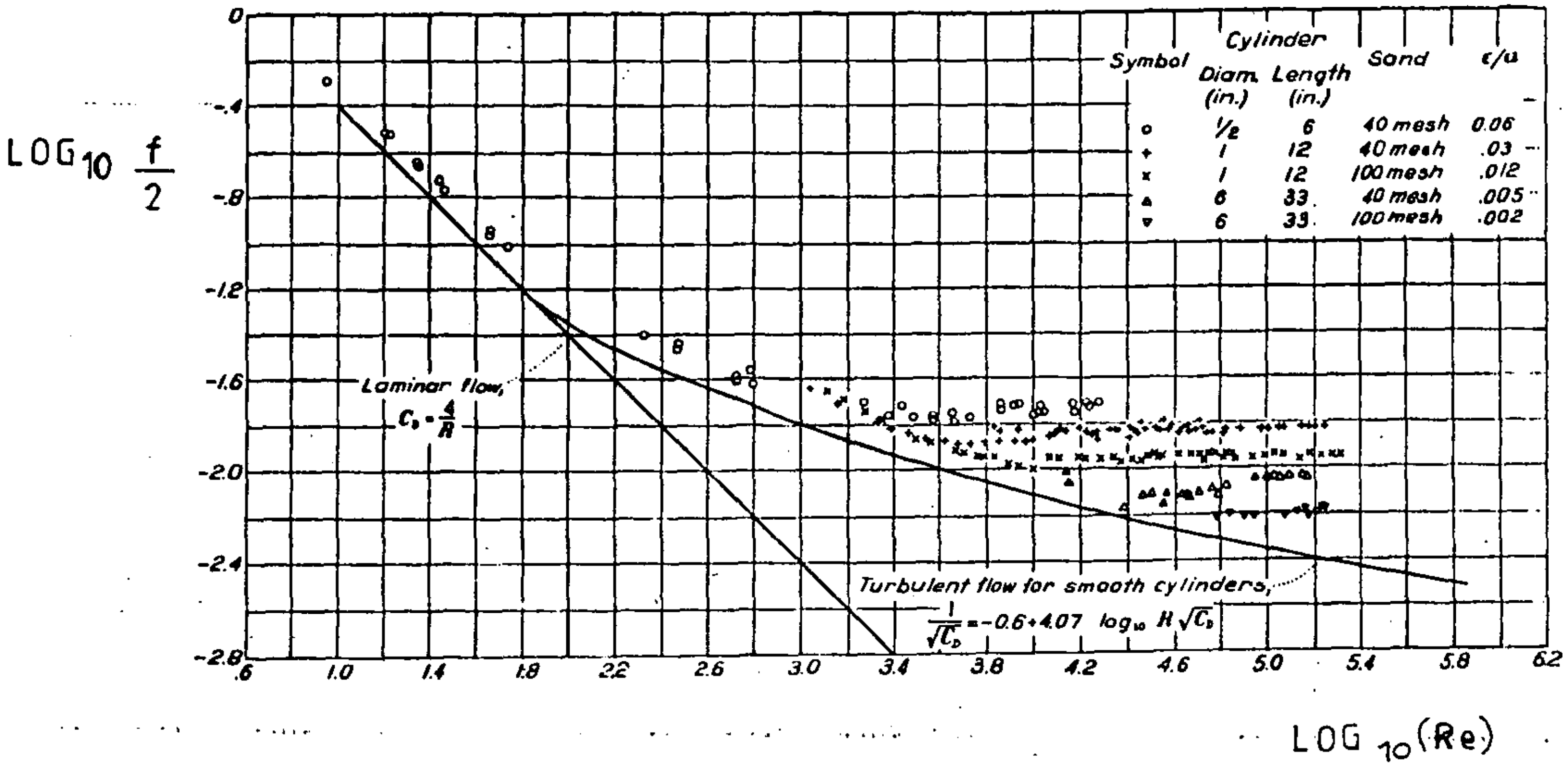
LOG10 f/2
0
-.4
-.8
-1.2
-1.6
-2.0
-2.4
-2.8
.6
1.0
1.4
1.8
2.2
2.6
3.0
3.4
3.8
4.2
4.6
5.0
5.4
5.8
6.2
LOG 10 (Re)
Symbol
Cylinder
Diam. (in.)
Length (in.)
Sand
ε/u
○ ½ 6 40 mesh 0.06
+ 1 12 40 mesh .03
× 1 12 100 mesh .012
▲ 6 33 40 mesh .005
▼ 6 33 100 mesh .002
Laminar flow, $C_D = \frac{4}{R}$
Turbulent flow for smooth cylinders, $\frac{1}{\sqrt{C_D}} = -0.6 + 4.07 \log_{10} R\sqrt{C_D}$

FIG. 2.13 b FRICTION FACTOR AS A FUNCTION OF REYNOLDS NUMBER FOR A ROTATING CYLINDER

showing the effect of unsaturated roughness.

After Theodorsen and Regier [9]

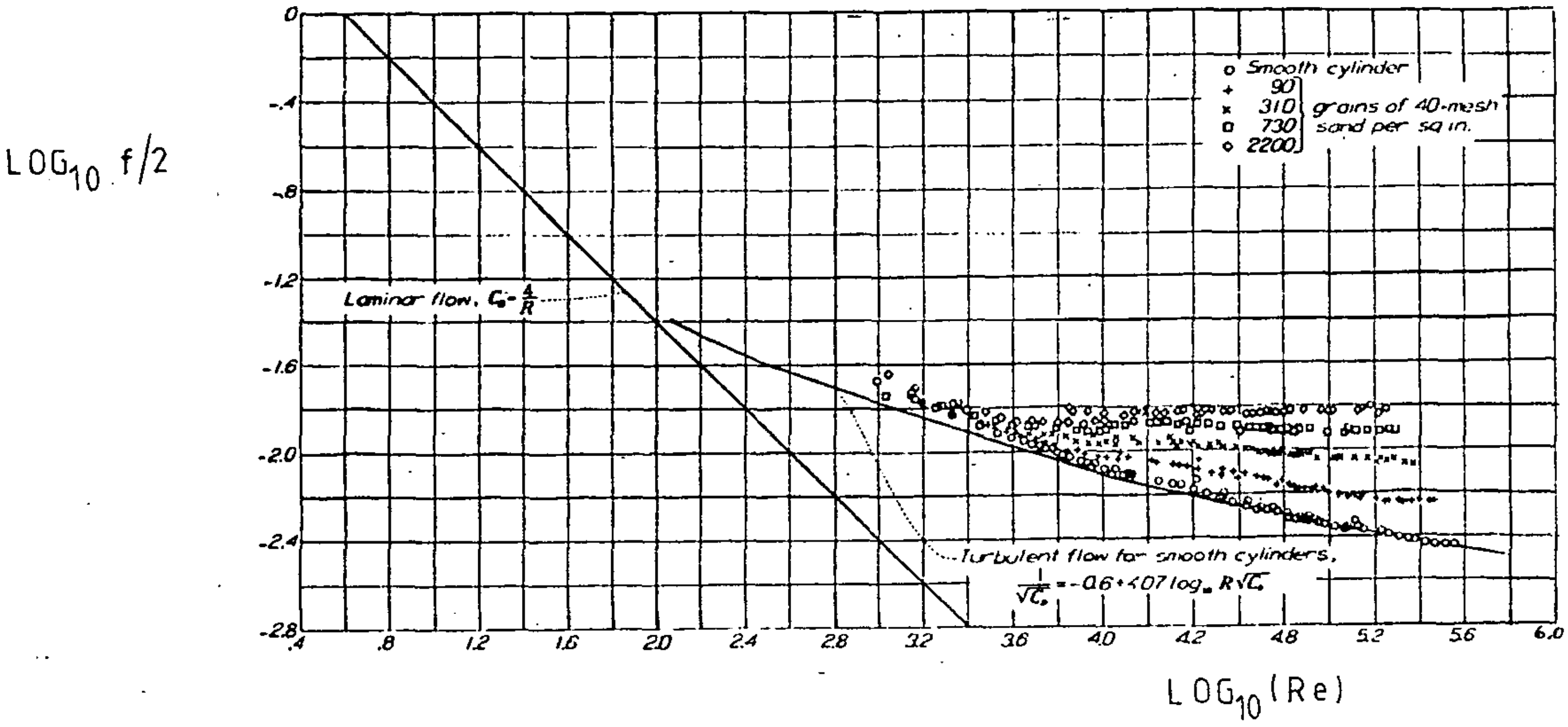
LOG10 f/2
0
-.4
-.8
-1.2
-1.6
-2.0
-2.4
-2.8
.4
.8
1.2
1.6
2.0
2.4
2.8
3.2
3.6
4.0
4.2
4.8
5.2
5.6
6.0
LOG10 (Re)
o Smooth cylinder
+ 90
x 310
□ 730
◇ 2200
grains of 40-mesh sand per sq in.
Laminar flow, $C_f = \frac{4}{R}$
Turbulent flow for smooth cylinders,
$\frac{1}{\sqrt{C_f}} = -0.6 + 4.07 \log_e R\sqrt{C_f}$

FIG. 2.14 DEVELOPMENT OF A TANGENTIAL VELOCITY PROFILE AROUND A ROTATING CYLINDER

showing an axial flow entrance length.

After Martin and Payne [29]

FIG. 2.15 SCHEMATIC REPRESENTATION OF DOMAINS OF FLOW REGIMES AROUND A ROTATING CYLINDER.

After Kaye and Elgar [34]

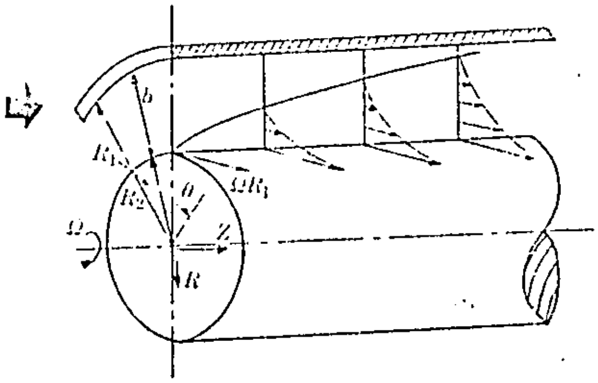
b
R1
R2
ΩR1
θ
Ω
Z
R

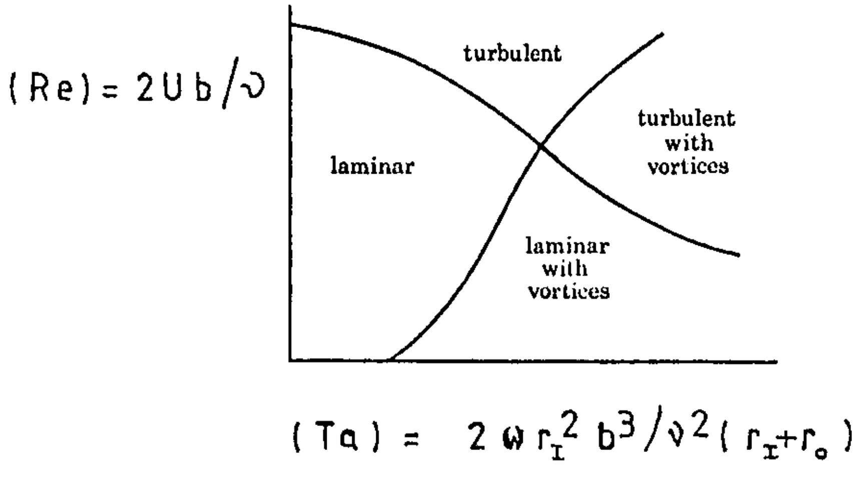
(Re) = 2Ub/ν
turbulent
laminar
turbulent with vortices
laminar with vortices
(Ta) = 2ω r_I^2 b^3/ν^2 (r_I+r_o)

FIG. 2.16 AXIAL REYNOLDS NUMBER AS A FUNCTION OF TAYLOR NUMBER FOR A ROTATING CYLINDER

showing the transition zone between turbulent and turbulent + vortices regimes for axial flow through a rotating cylinder.

After Kosterin, Koshmarov and Finatov[40]

A. laminar flow

B. laminar + vortices

C. true turbulent flow

D. turbulent flow + vortices

FIG. 2.17 TANGENTIAL STRESS AS A FUNCTION OF AXIAL REYNOLDS NUMBER FOR A ROTATING CYLINDER

After Kosterin, Koshmarov and Finatov[40]

C. true turbulent flow

D. turbulent flow + vortices

rotational speed : 4 3 2 1

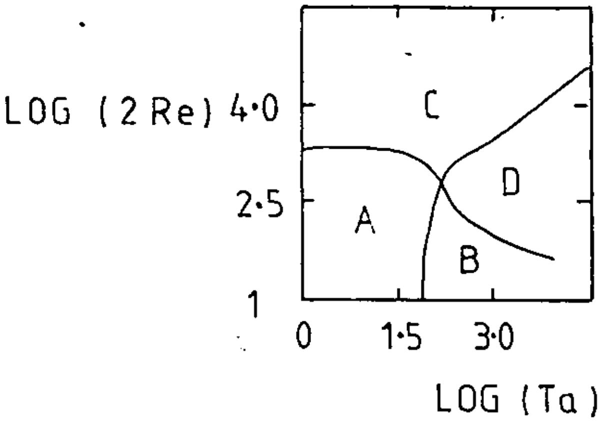
LOG (2Re)
4·0
2·5
1
0
1·5
3·0
LOG (Ta)
A
B
C
D

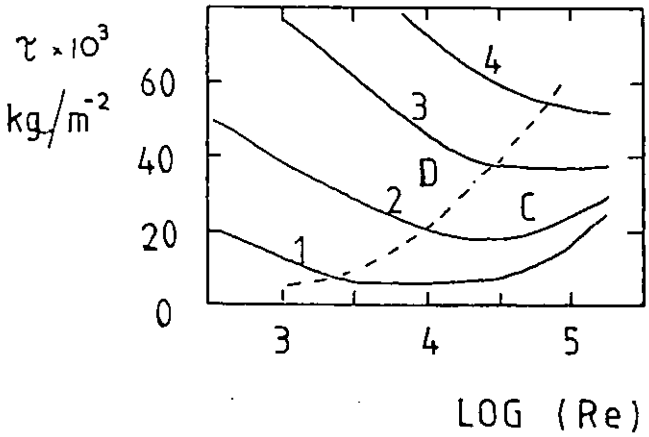
τ × 10³
kg/m⁻²
60
40
20
0
3
4
5
LOG (Re)
1
2
3
4
C
D

FIG. 3.1 SCHEMATIC POLARISATION CURVE FOR COPPER DEPOSITION FROM ACID SULPHATE SOLUTIONS showing the well-defined limiting current plateau, and the onset of hydrogen evolution.

A : $Cu^{2+} + 2e^- = Cu$

B : A and $H^+ + e^- = \frac{1}{2} H_2$

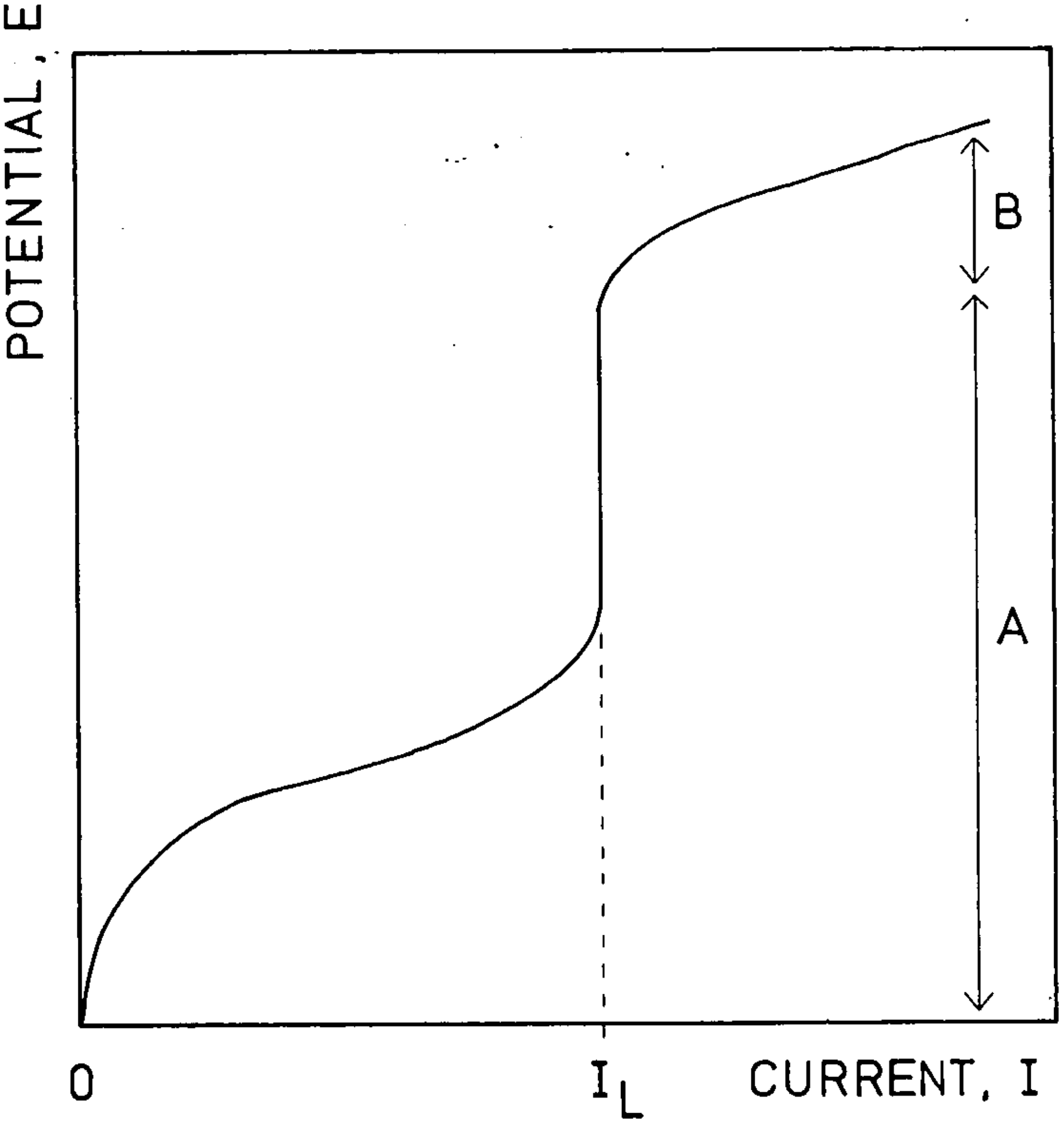
POTENTIAL, E
B
A
0
I_L
CURRENT, I

FIG. 3.2 SCHEMATIC POLARISATION CURVES FOR COPPER DEPOSITION FROM ACID SULPHATE SOLUTIONS showing the effect of agitation

Agitation: 3 > 2 > 1

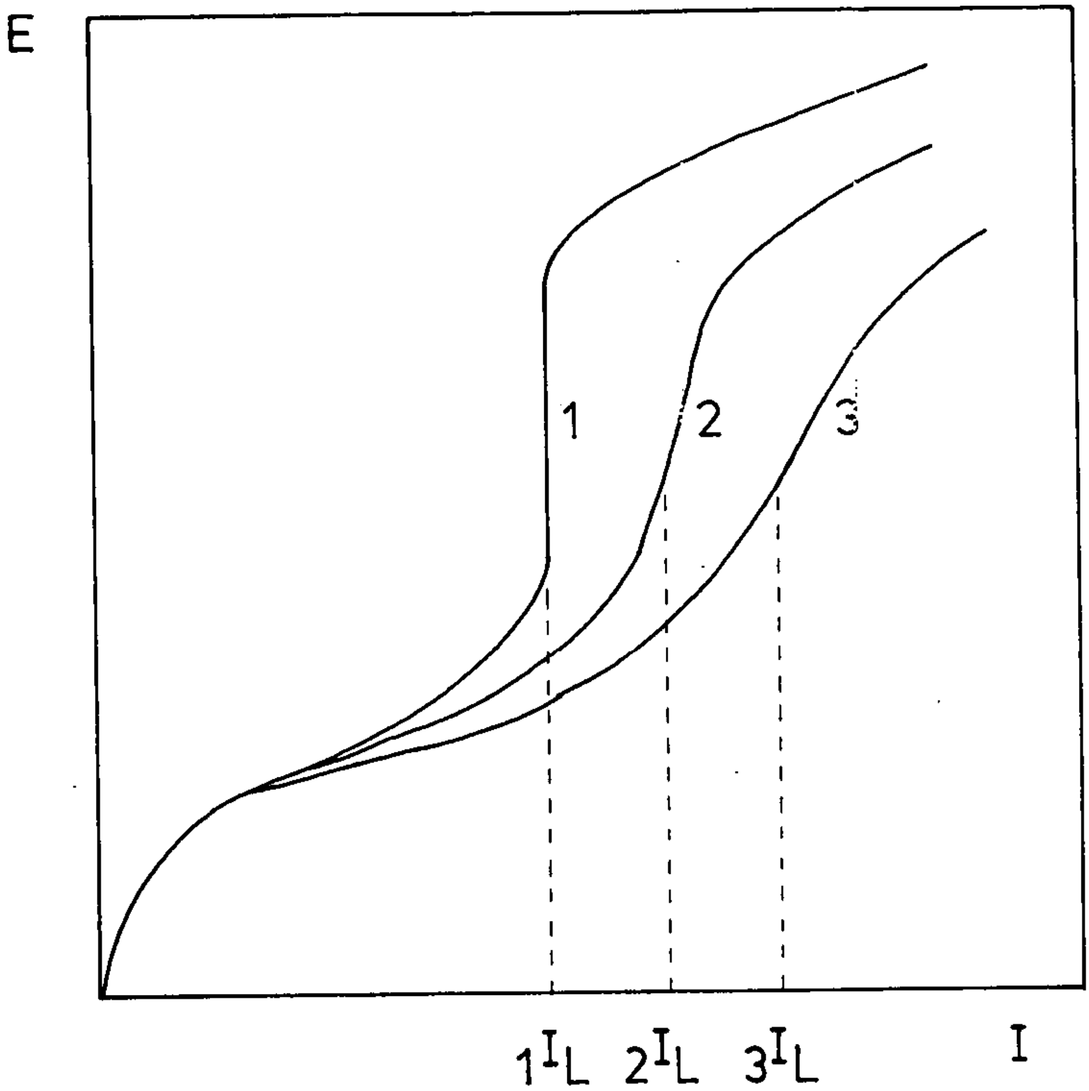
E
1
2
3
1IL
2IL
3IL
I

FIG. 3.3 a

CONCENTRATION PROFILE NEAR AN ELECTRODE defining the Nemst Diffusion layer thickness, δ_N

FIG. 3.3 b

VELOCITY PROFILE NEAR AN ELECTRODE defining the Prandtl Hydrodynamic layer thickness, δ_{pr}

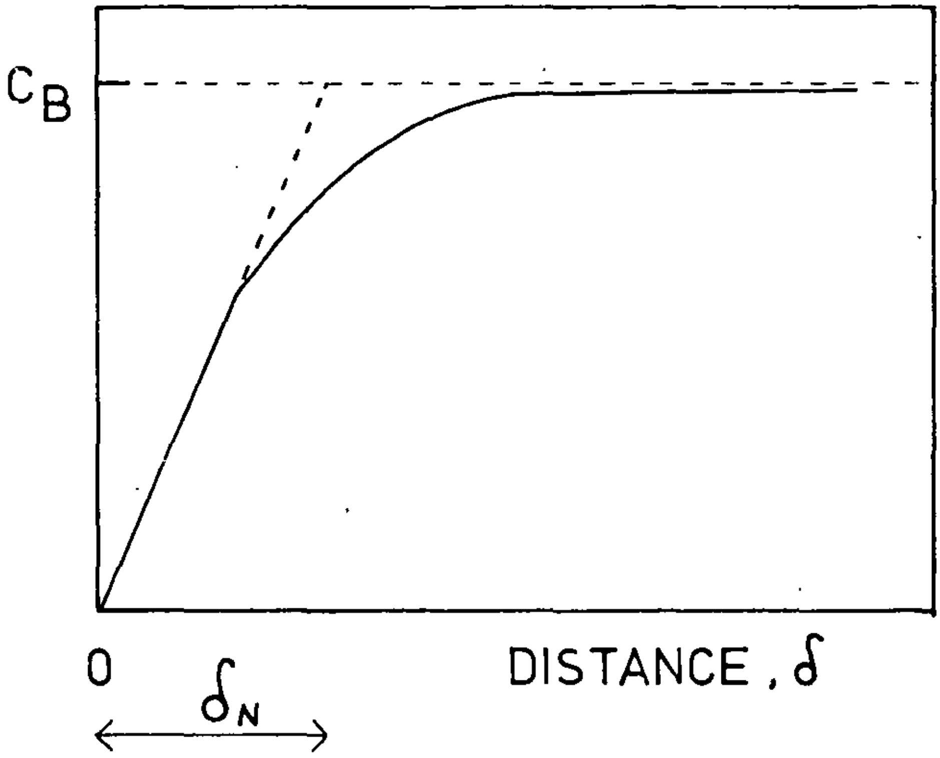

a)

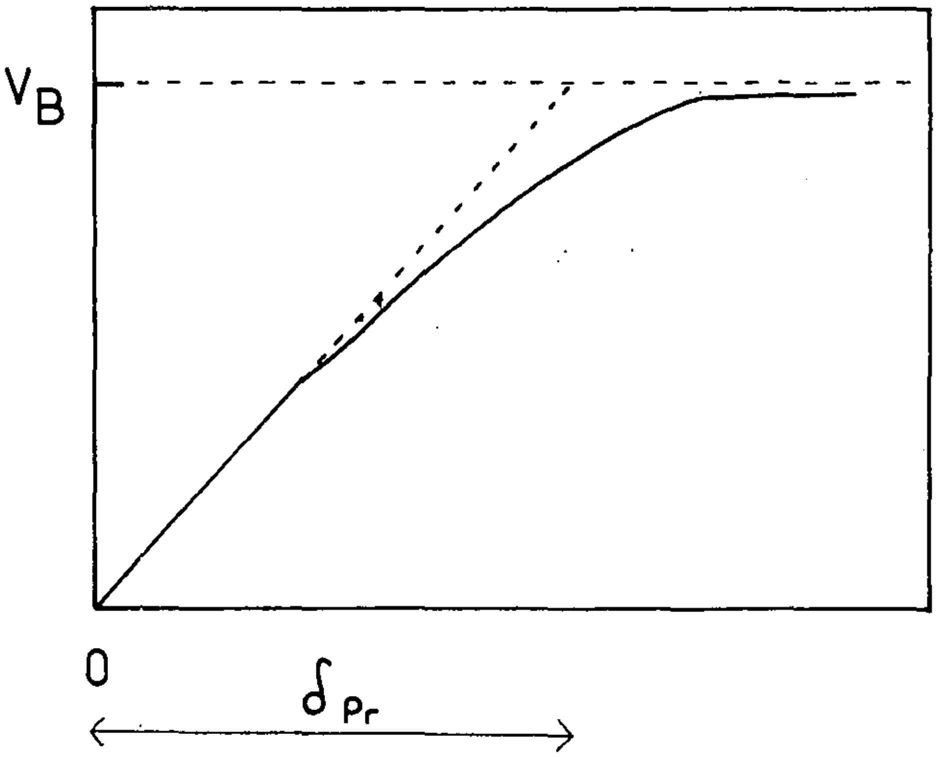

b)

FIG. 3.4 SCHEMATIC POLARISATION CURVES FOR COPPER DEPOSITION showing ill-defined limiting current plateaux, as concentration is decreased

Concentration, C : $C_3 > C_2 > C_1$

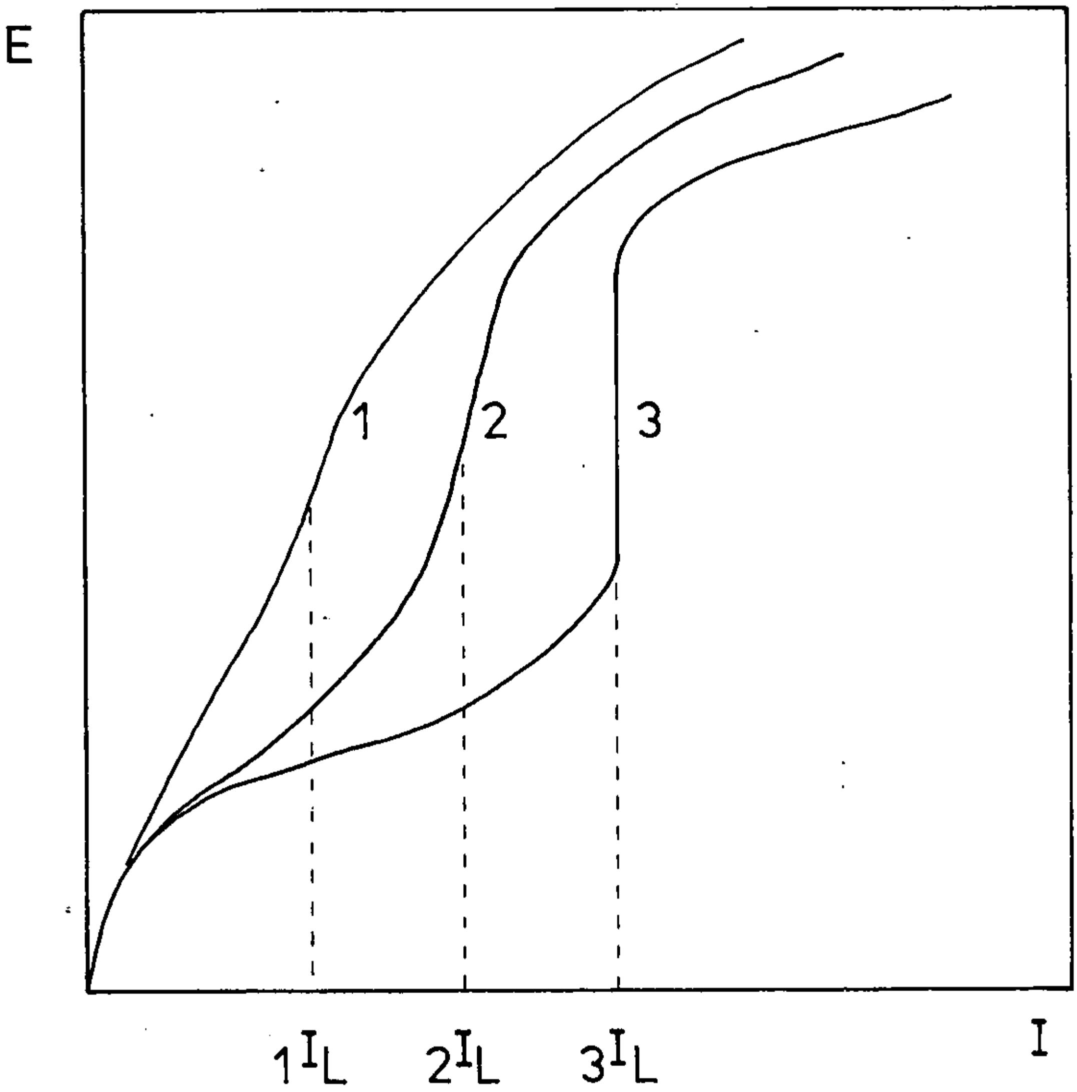
E
1
2
3
$_1I_L$
$_2I_L$
$_3I_L$
I

FIG. 4.1 CONFIGURATIONS FOR FLOW-THROUGH, POROUS ELECTRODES relative to the direction of fluid flow

a) common feed for electrolyte; solution flow from front fact (combines favourable electrode potential and mass transfer conditions to produce maximum rate at the front with minimum overall potential drop in solution)

b) solution flow from back to front (ohmic potential drop works against the favourable mass transfer conditions near the inlet, hopefully resulting in a more uniform reaction distribution)

c) perpendicular (permits a higher flow rate while maintaining a large electrical driving force over the reactor length, but this case is more difficult to analyse)

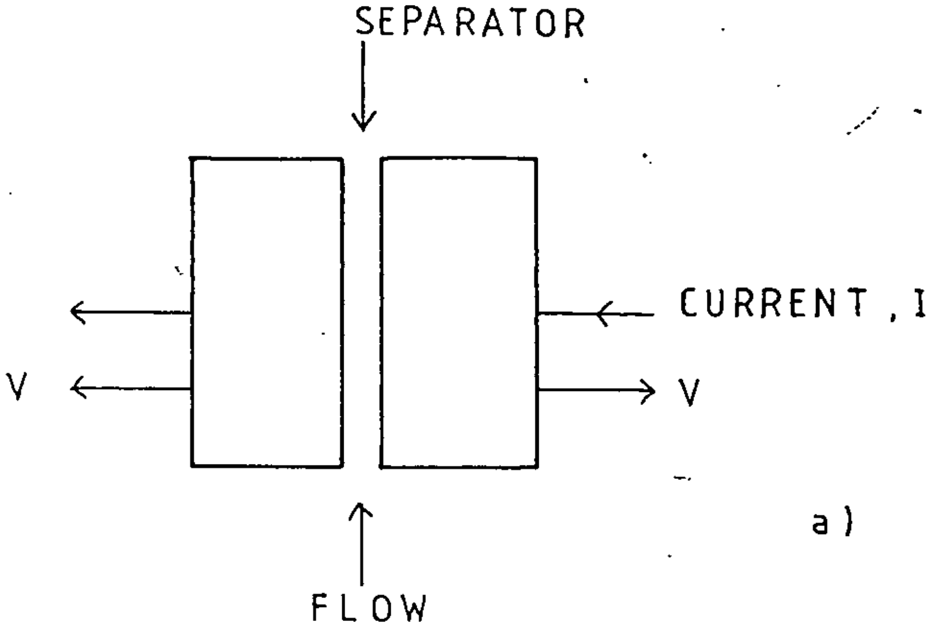
SEPARATOR
CURRENT , I
V
V
FLOW

a)

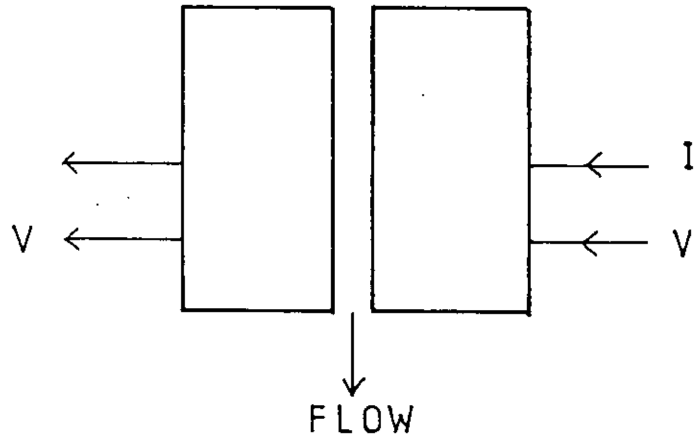

b)

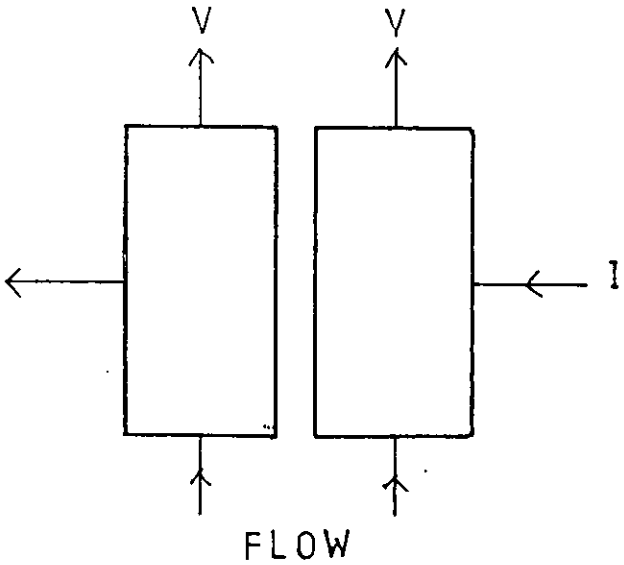

c)

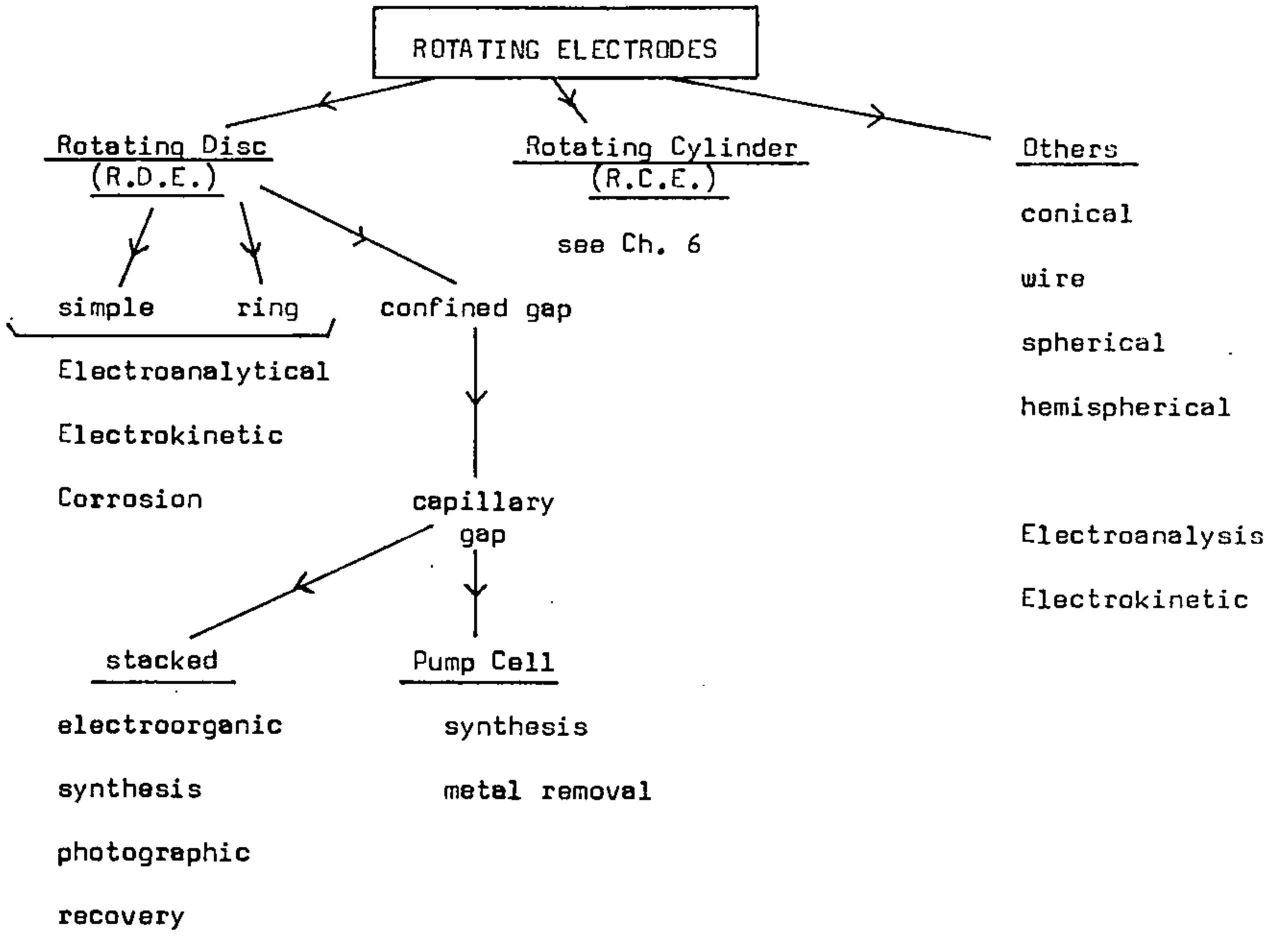
ROTATING ELECTRODES
Rotating Disc (R.D.E.)
Rotating Cylinder (R.C.E.)
Others
see Ch. 6
conical
wire
spherical
hemispherical
Electroanalysis
Electrokinetic
simple
ring
confined gap
Electroanalytical
Electrokinetic
Corrosion
capillary gap
stacked
Pump Cell
electroorganic
synthesis
photographic
recovery
synthesis
metal removal

FIG. 4.2 CLASSIFICATION OF ROTATING ELECTRODES.

FIG. 5.1 MODES OF OPERATION OF ELECTROCHEMICAL REACTORS

a) Simple Batch

b) Single Pass

c) Batch with Recycle

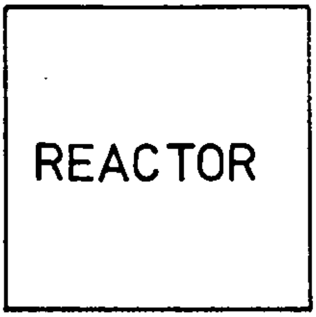

a)

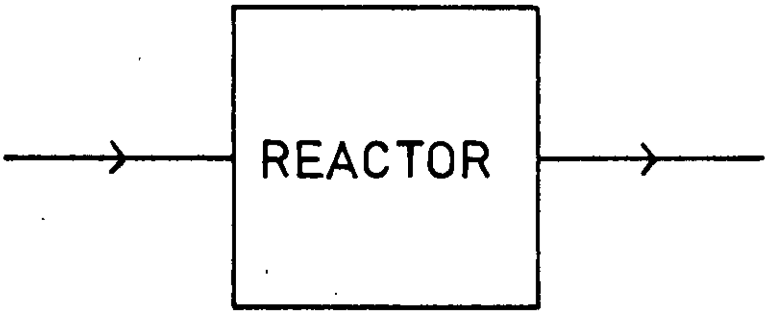

b)

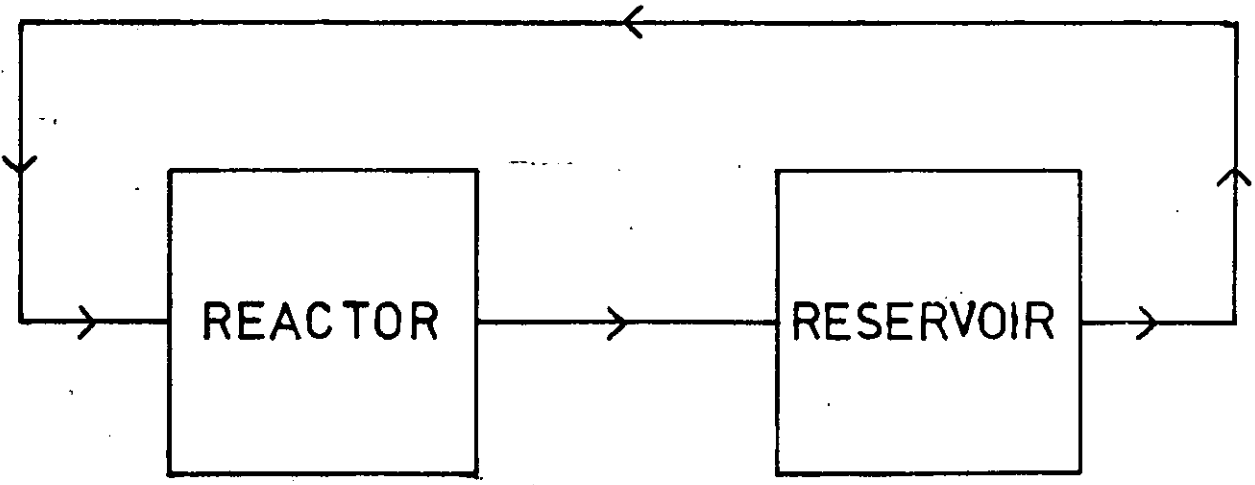
REACTOR
RESERVOIR

c)

FIG. 5.2 OPERATIONAL SKETCH FOR PLUG FLOW REACTORS

a) Single Pass

b) Recycle

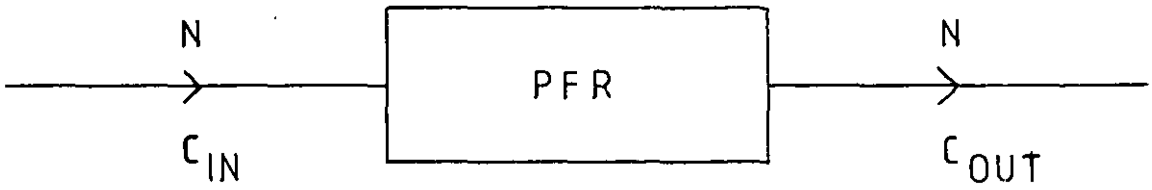
N
PFR
N
c_{IN}
c_{OUT}

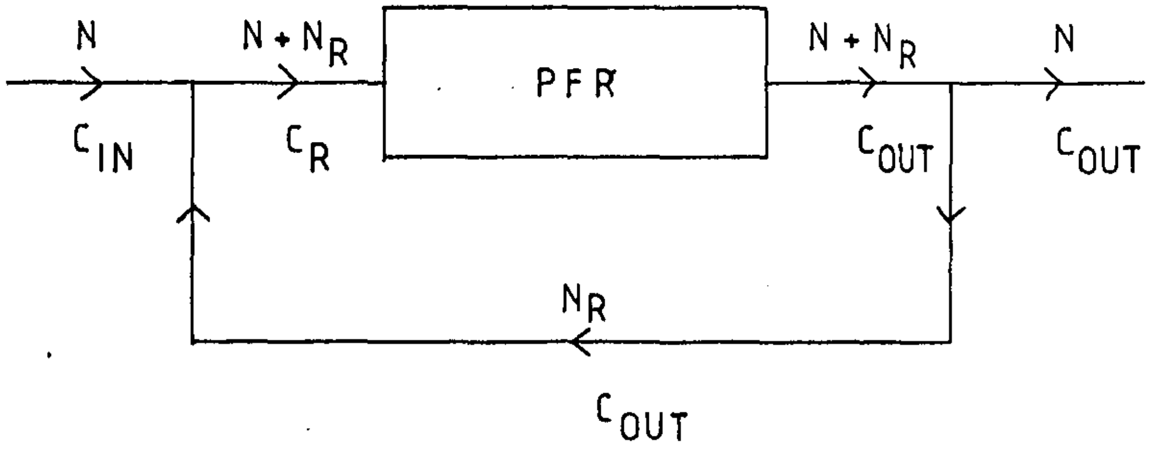
N
$N + N_R$
PFR
$N + N_R$
N
c_{IN}
c_R
c_{OUT}
c_{OUT}
N_R
c_{OUT}

FIG. 5.3 OPERATIONAL SKETCH FOR AN ANNULAR PLUG FLOW REACTOR

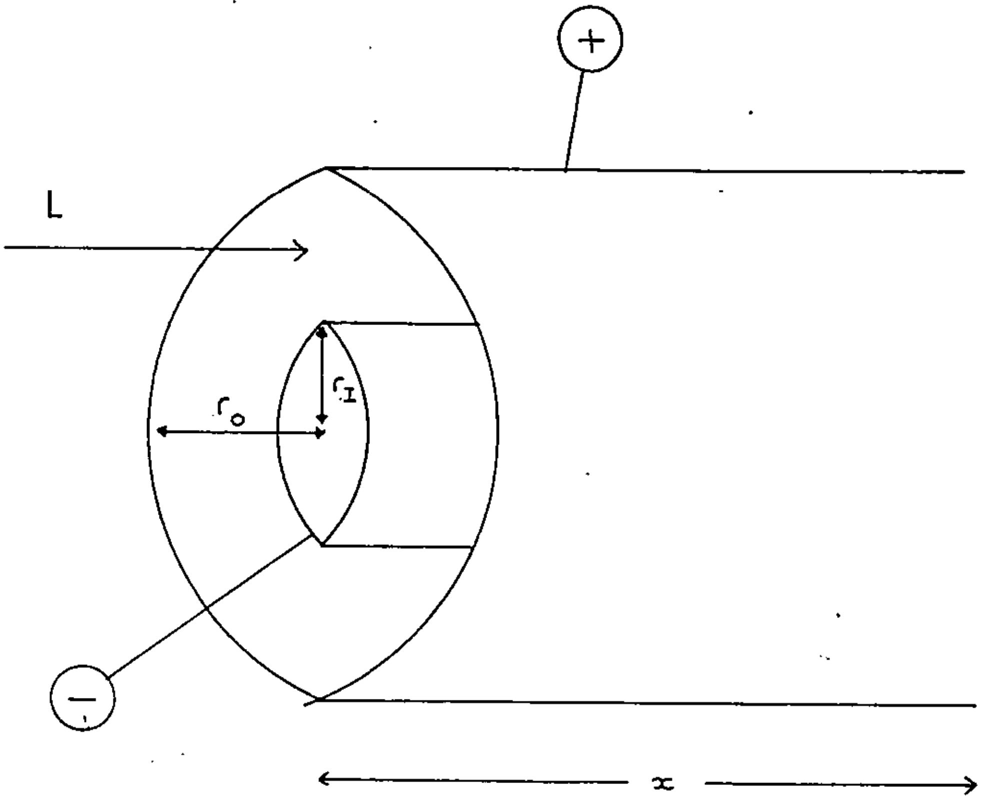
+
L
r_I
r_o
−
x

FIG. 5.4 OPERATIONAL SKETCH FOR A CONTINUOUSLY STIRRED TANK REACTOR

a) Batch

b) Single Pass

c) Recycle

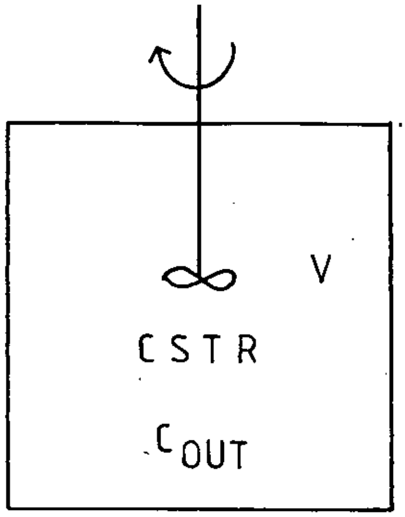
V
CSTR
C_{OUT}

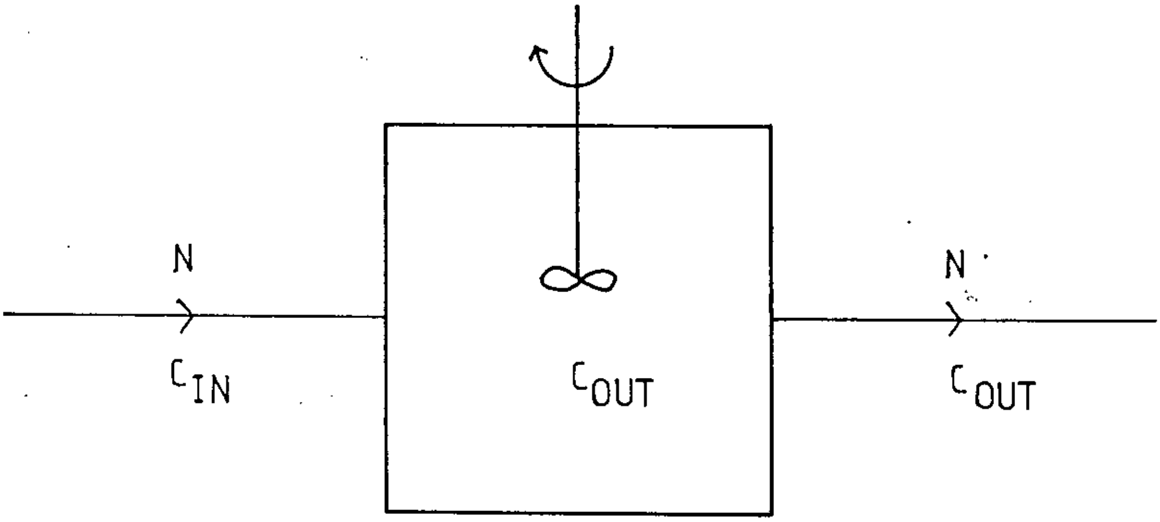
N
C_{IN}
C_{OUT}
N
C_{OUT}

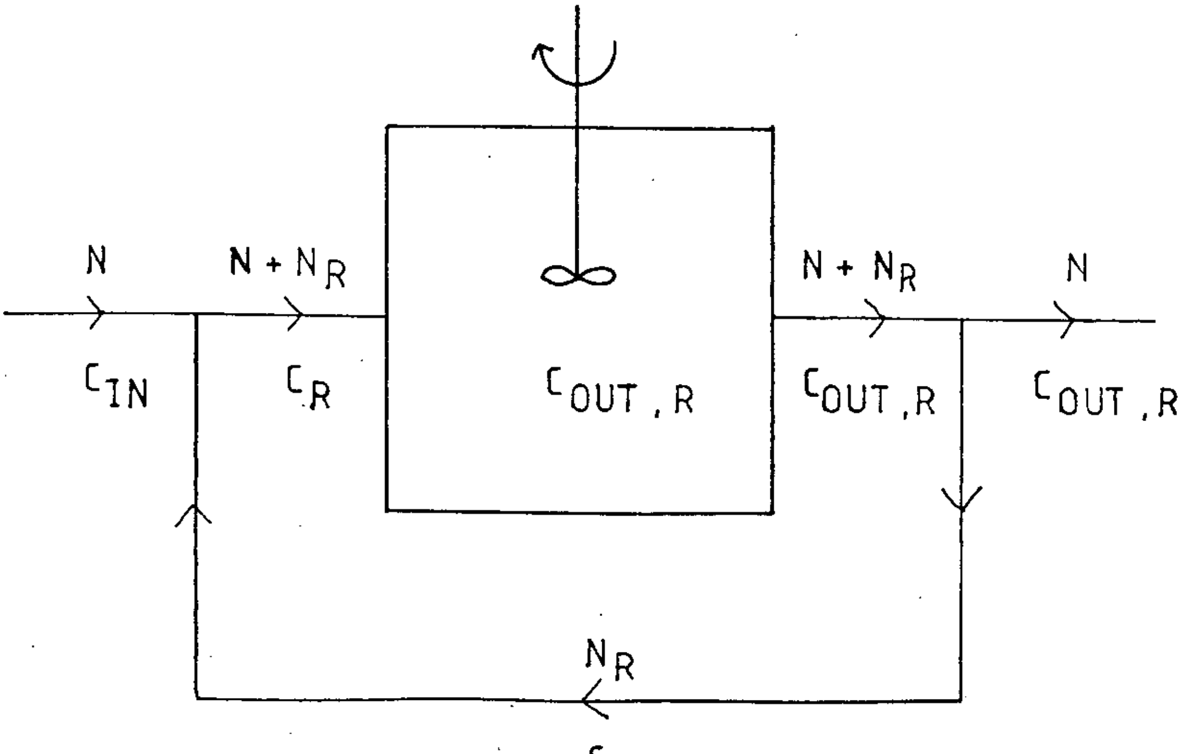
N
C_{IN}
$N + N_R$
C_R
$C_{OUT,R}$
$N + N_R$
$C_{OUT,R}$
N
$C_{OUT,R}$
N_R

FIG. 5.5 SKETCH OF AN EXPERIMENTAL CSTR

After Sudall [200, 201]

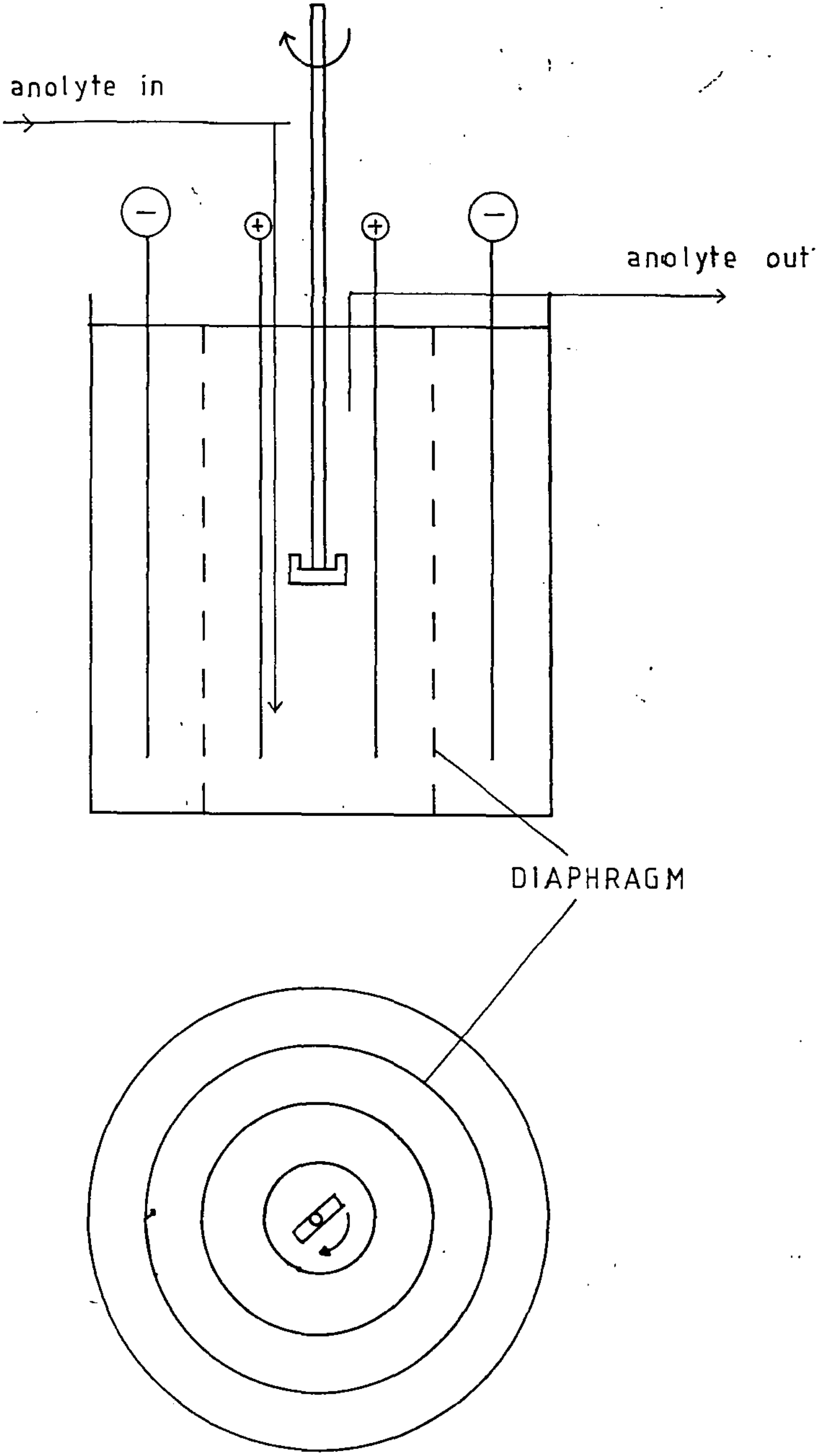
anolyte in
−
+
+
−
anolyte out
DIAPHRAGM

FIG. 5.6 OPERATIONAL SKETCH FOR AN ELECTROCHEMICAL REACTOR IN THE 'BATCH RECYCLE' MODE

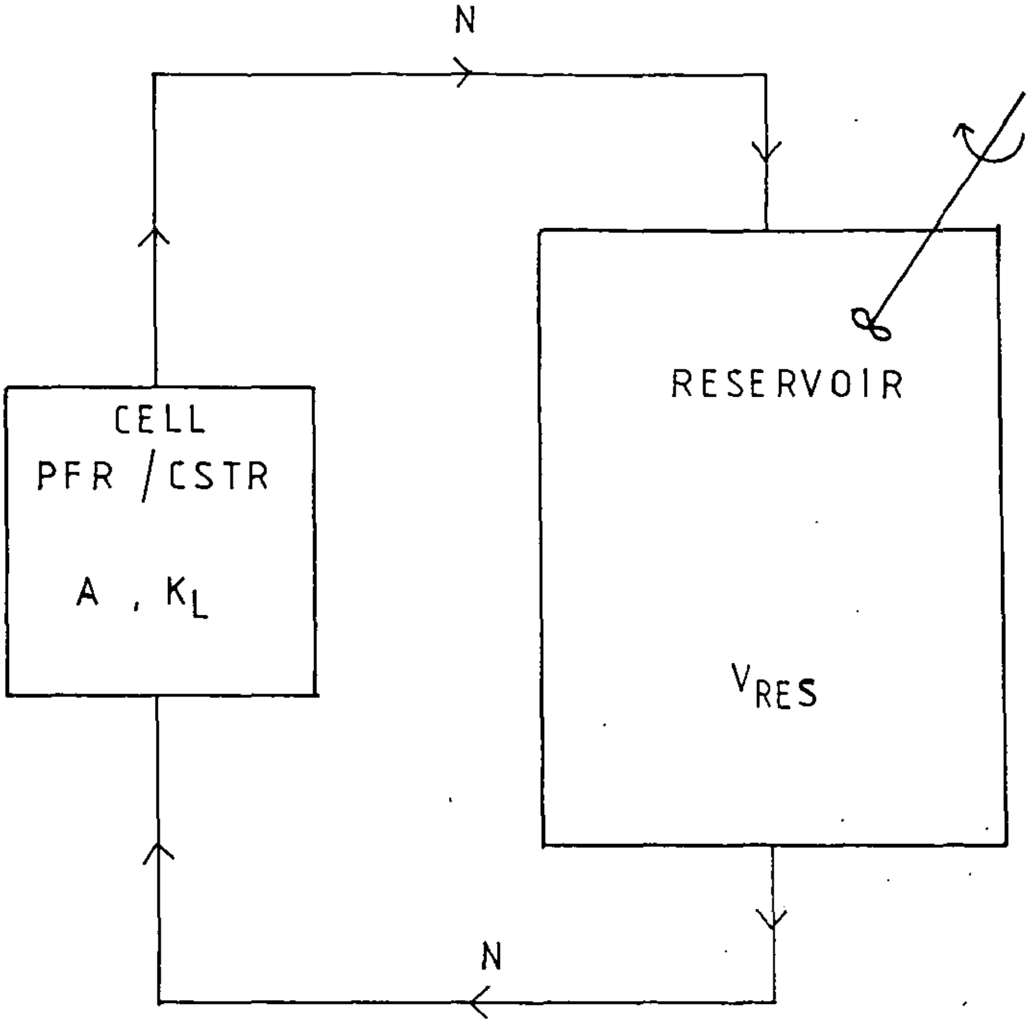
N
CELL
PFR / CSTR
A , K_L
RESERVOIR
V_{RES}
N

FIG. 5.7 AGITATED VESSEL FOR ELECTROCHEMICAL MASS TRANSPORT STUDIES

After Mizushina et al.[205, 206]

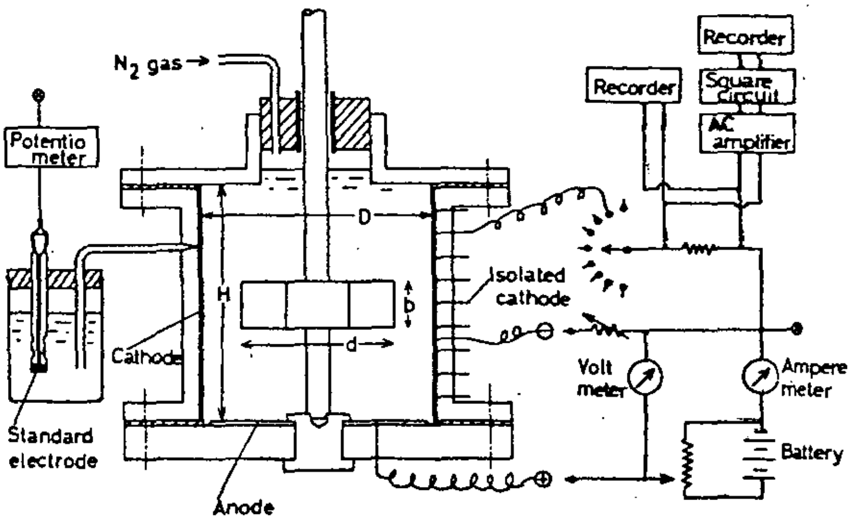
N$_2$ gas
Potentio meter
Standard electrode
Cathode
Anode
H
D
b
d
Isolated cathode
Recorder
Recorder
Square circuit
AC amplifier
Volt meter
Ampere meter
Battery

FIG. 5.8 SCHEMATIC POLARISATION CURVES FOR COPPER DEPOSITION FROM ACID SULPHATE SOLUTIONS indicating the effect under controlled current operation of

a) Concentration $C_3 > C_2 > C_1$

b) Surface Area $A_3 > A_2 > A_1$

c) Relative Motion $V_3 > V_2 > V_1$

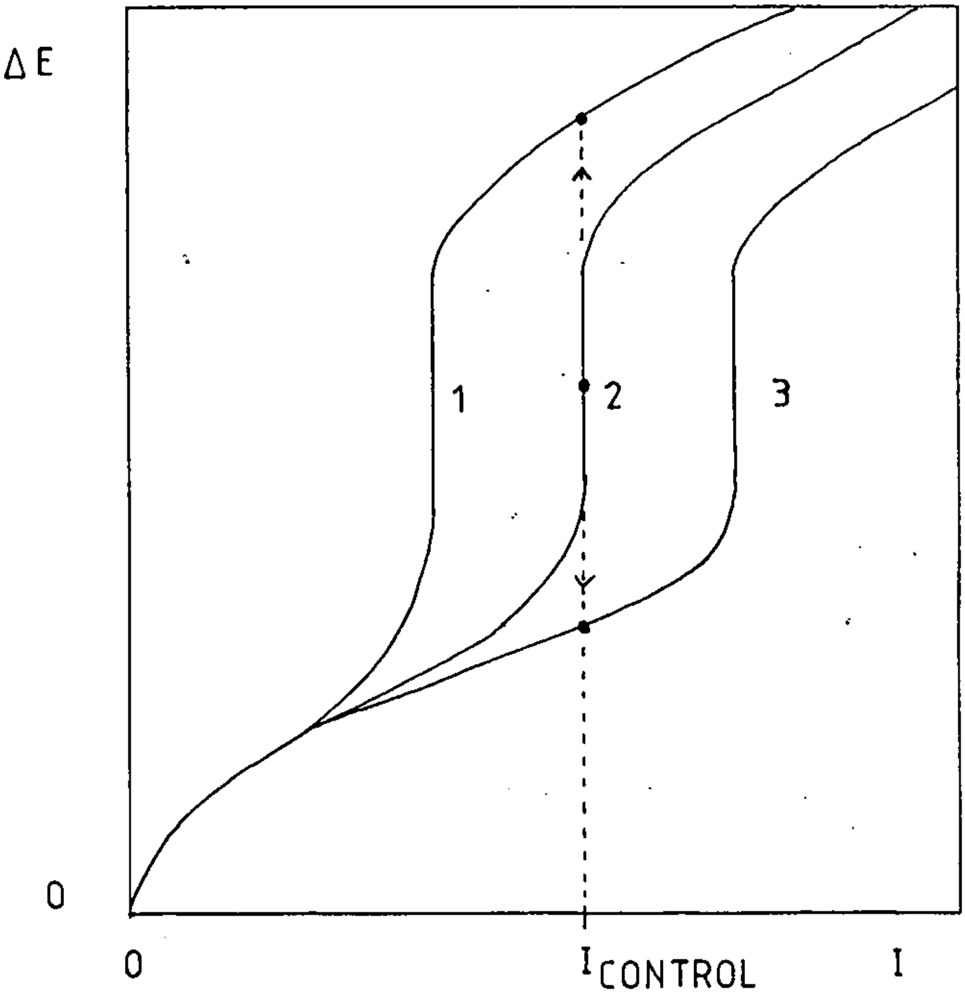
ΔE
0
0
I
CONTROL
I
1
2
3

FIG. 5.9 SCHEMATIC POLARISATION CURVE FOR IDEALISED DEPOSITION OF A SERIES OF METALS

comparable to an idealised polagraphic wave

Control Potentials : E_1, E_2, E_3

Limiting Currents :

${}_1I_L$	Metal 1
${}_2I_L$	Metals 1 + 2
${}_3I_L$	Metals 1, 2 + 3

Nobility : Metal $1 > 2 > 3$

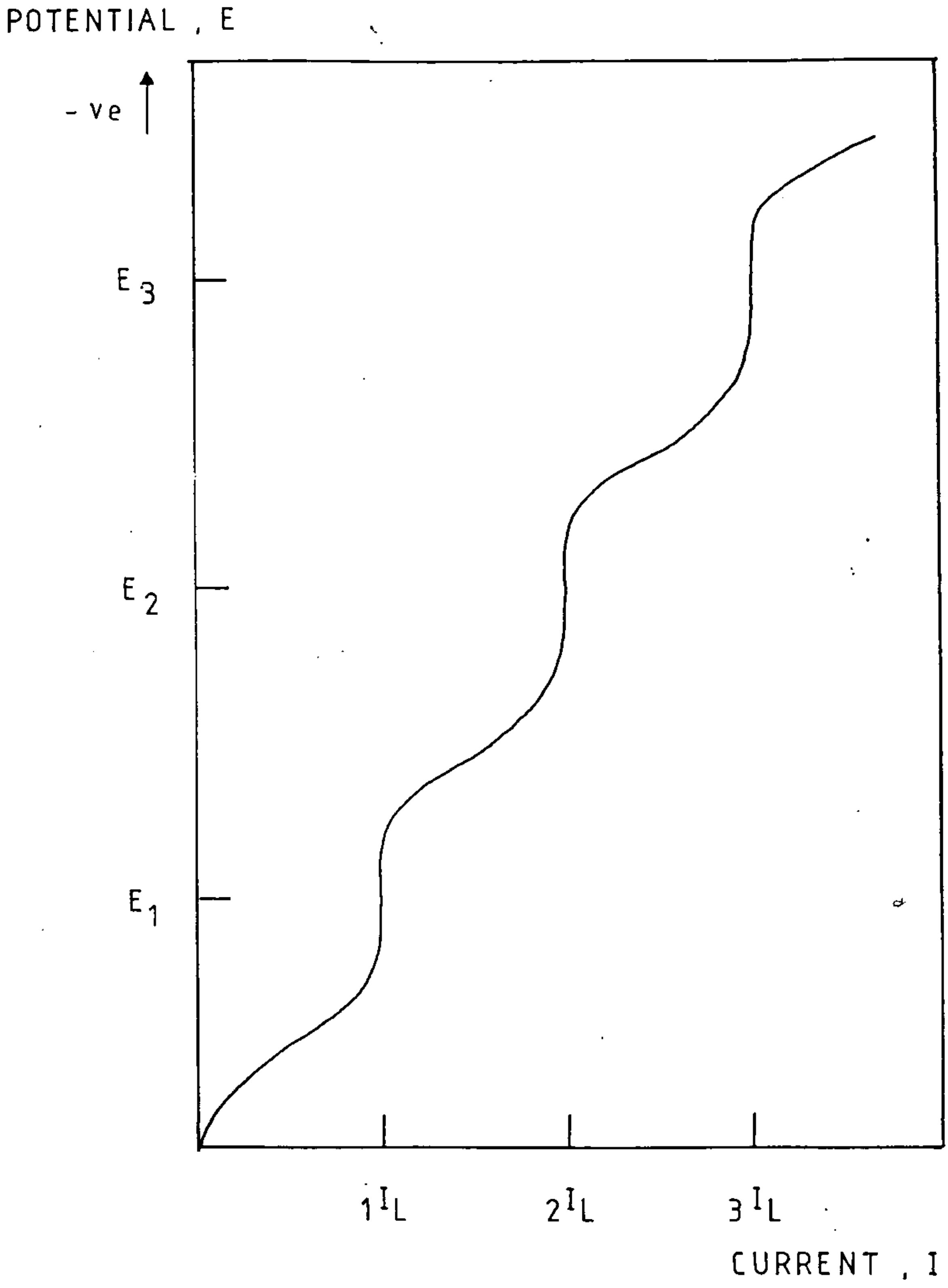
POTENTIAL , E
- ve
E 3
E 2
E 1
1 I L
2 I L
3 I L
CURRENT , I

FIG. 5.10 NERNSTIAN PLOT FOR SELECTED METAL CATIONS, 25° C

representing :

$$E = E^{o} + \frac{RT}{zF} \log a_{M^{z+}}$$

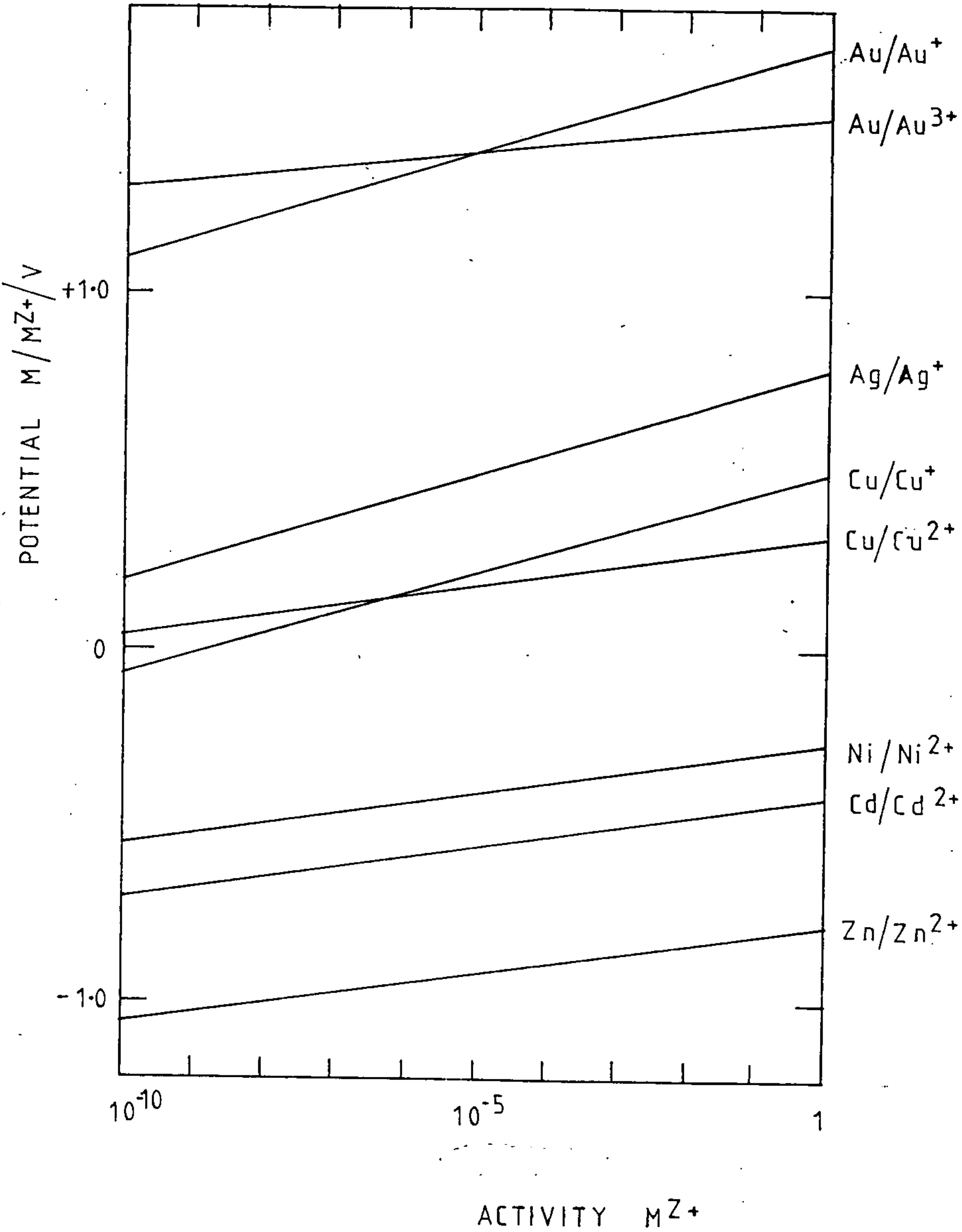

Au/Au$^+$
Au/Au^{3+}
Ag/Ag$^+$
Cu/Cu$^+$
Cu/Cu^{2+}
Ni/Ni^{2+}
Cd/Cd^{2+}
Zn/Zn^{2+}
POTENTIAL M/M^{Z+}/V
+1·0
0
-1·0
10^{-10}
10^{-5}
1
ACTIVITY M^{Z+}

FIG. 5.11 CURRENT DENSITY DISTRIBUTION FOR UNBOUNDED PARALLEL PLATE ELECTRODES

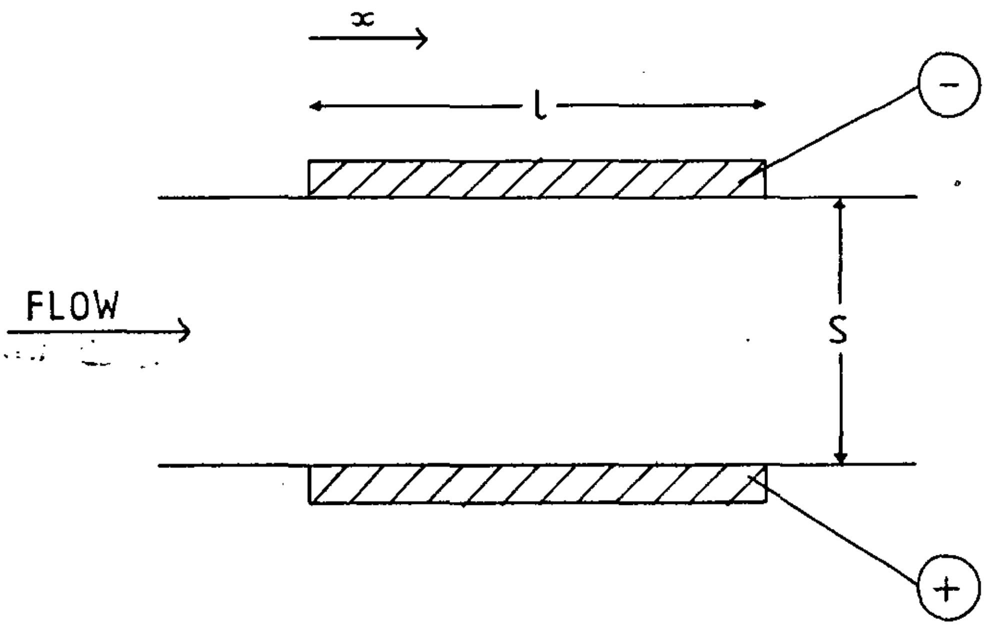
x
l
FLOW
S
−
+

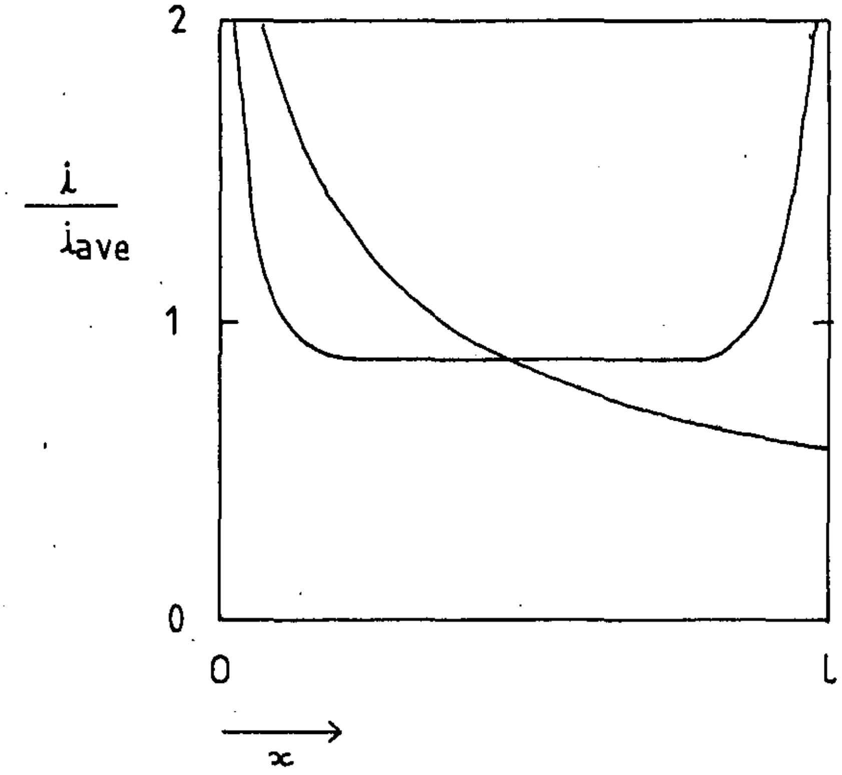
2
1
0
i / iave
0
l
x

FIG. 5.12

CURRENT DENSITY DISTRIBUTION FOR BOUNDED PARALLEL PLATE ELECTRODES

(which comprise the ends of a rectangular cell)

Natural Convection.

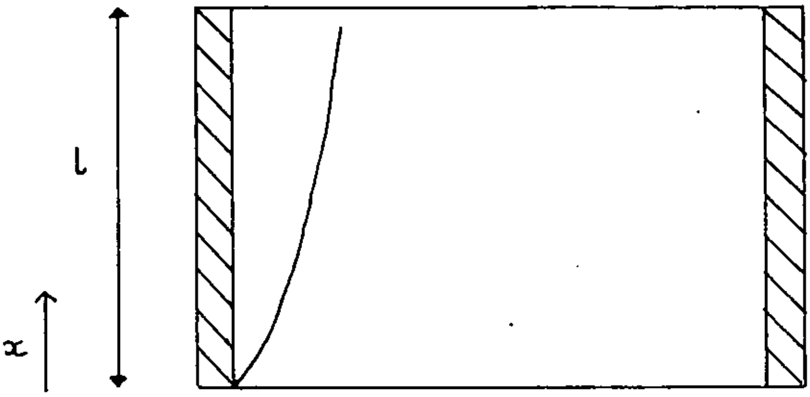
l
x

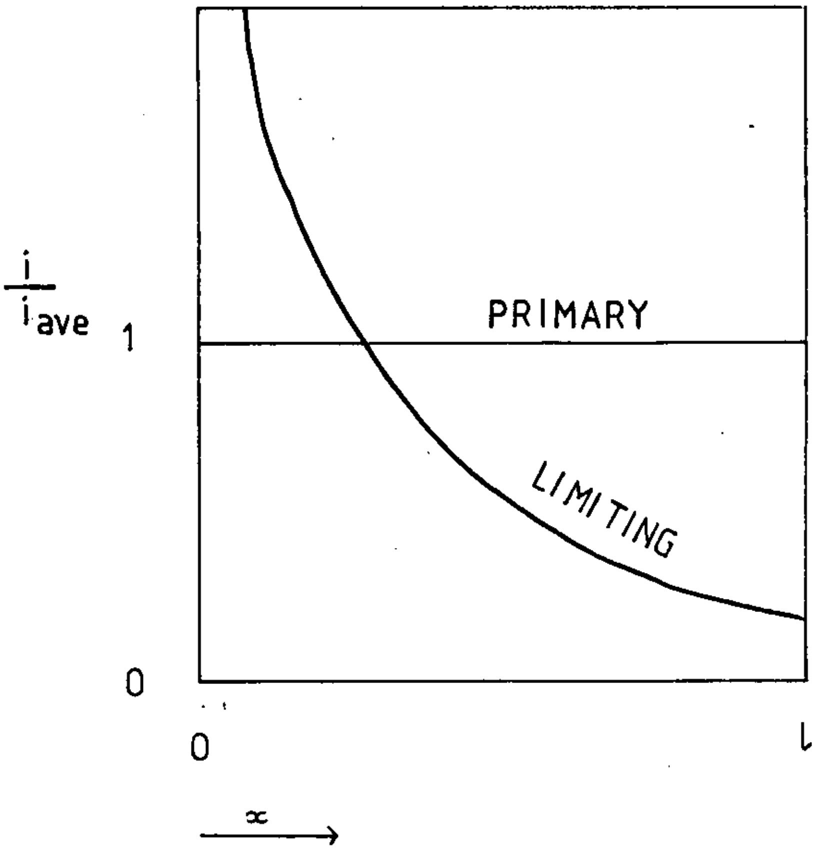
i/i_ave
1
0
PRIMARY
LIMITING
0
l
x

FIG. 5.13 SCHEMATIC REPRESENTATION OF CURRENT (solid) AND EQUIPOTENTIAL (broken) LINES FOR A PARALLEL PLATE ELECTRODE

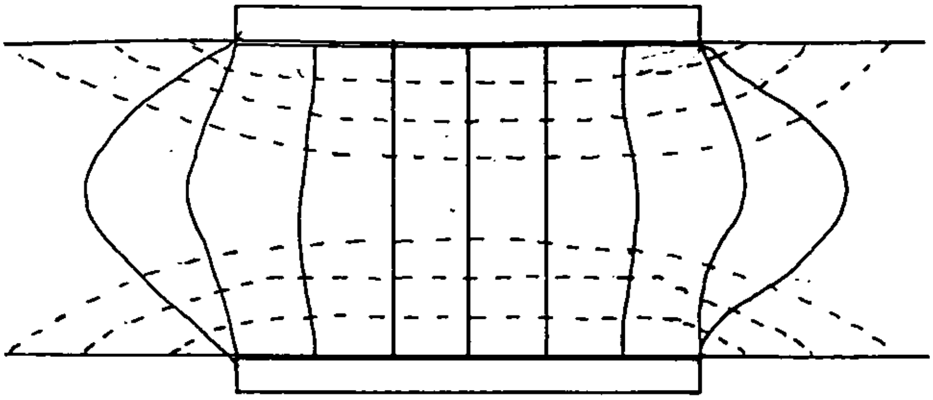

UNBOUNDED

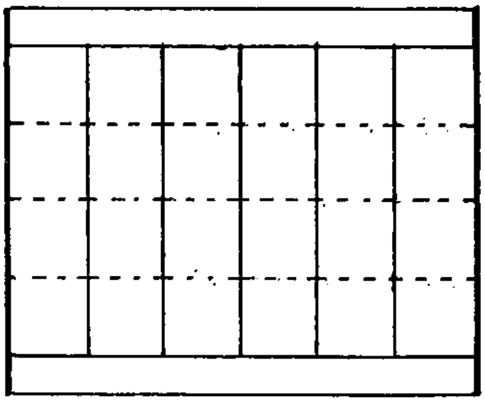

BOUNDED

FIG. 5.14 CURRENT DENSITY DISTRIBUTIONS FOR THE ROTATING DISC ELECTRODE

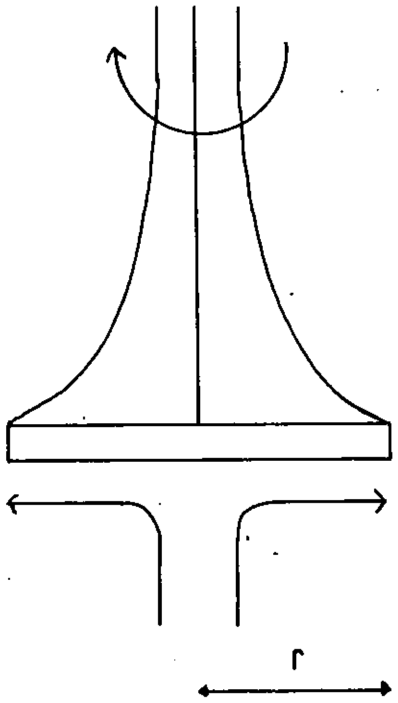
r

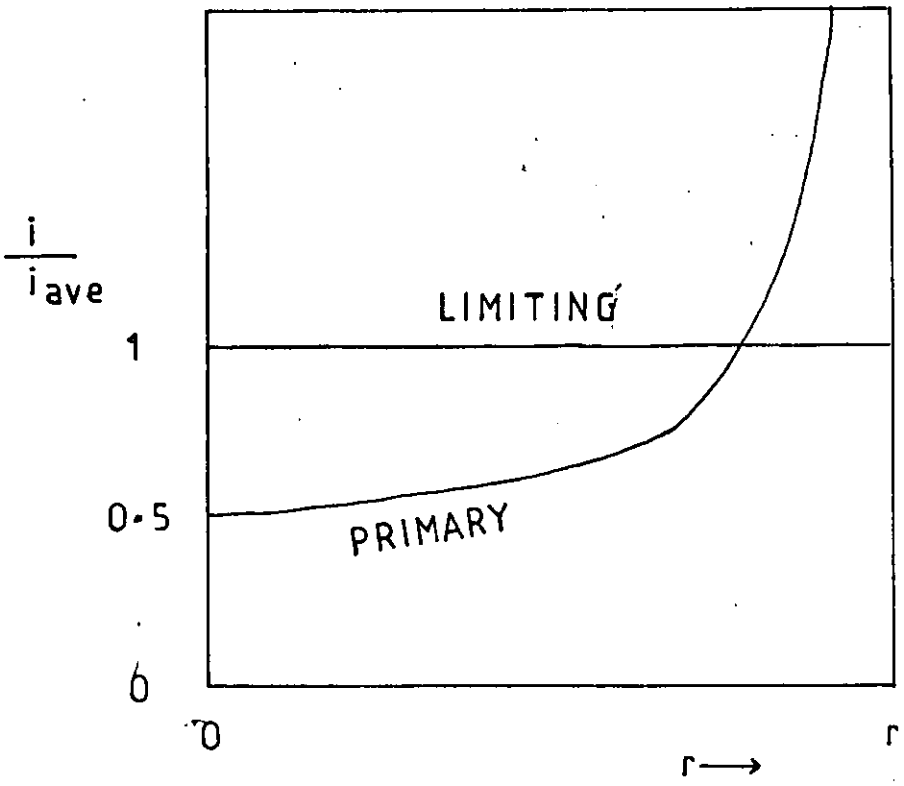
$\frac{i}{i_{ave}}$
1
0·5
0
LIMITING
PRIMARY
0
r
r ⟶

FIG. 5.15

SKETCH OF A ROTATING CYLINDER ELECTRODE REACTOR

showing area, volume and area/volume ratio for various cylinder radiae

FIG. 5.16

SKETCH OF A ROTATING DISC ELECTRODE REACTOR

with an interelectrode gap of 1 cm and a radius r

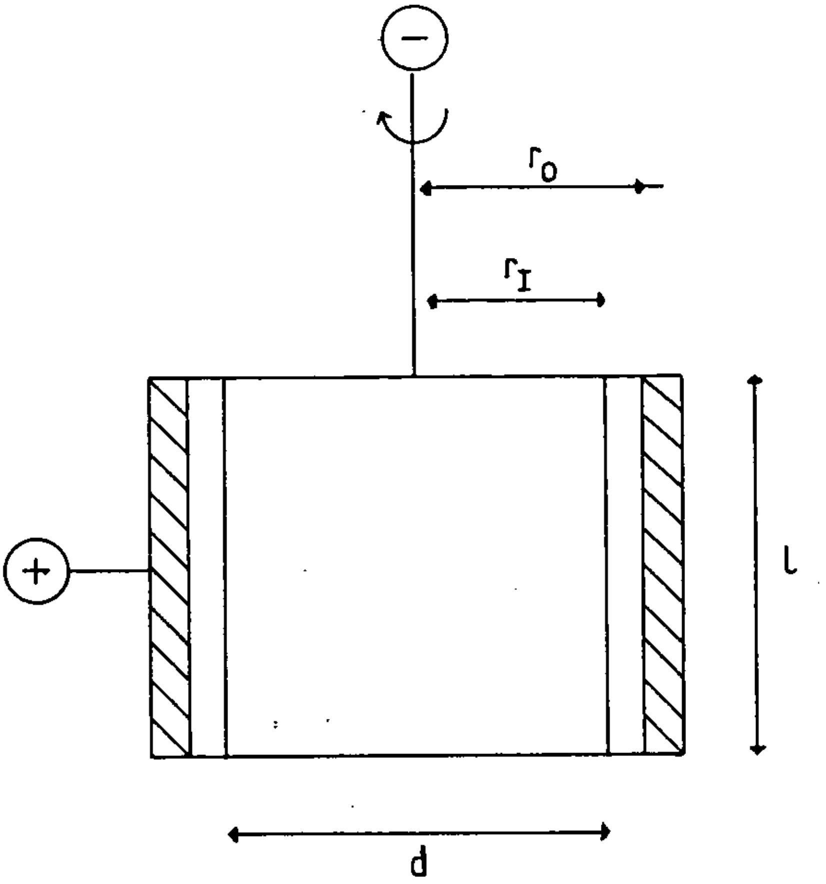
−
r0
rI
+
l
d

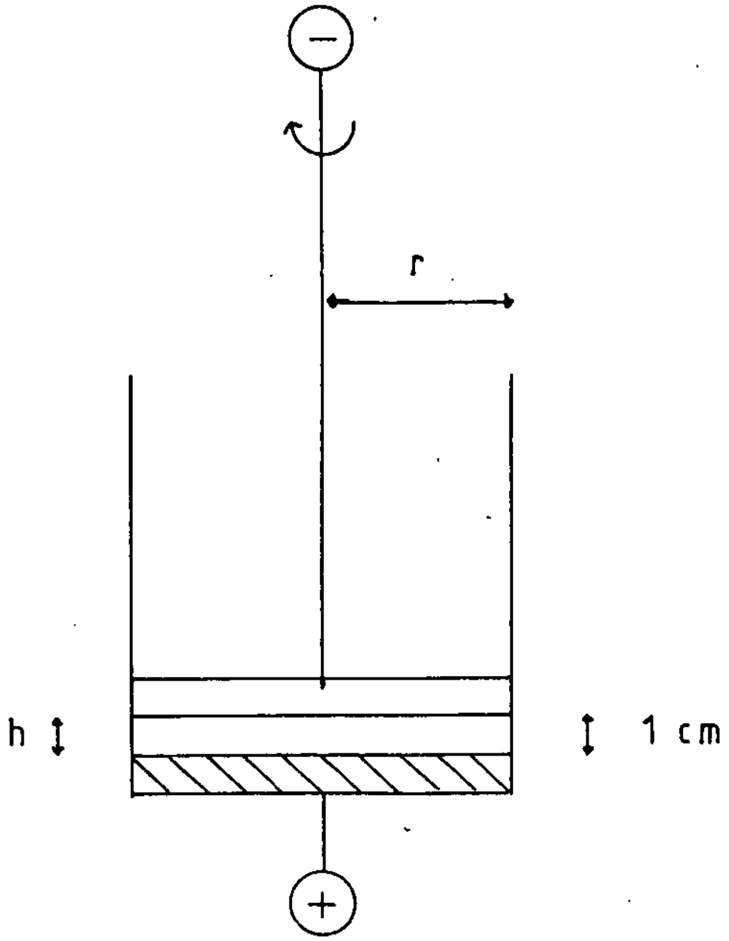
−
r
h
1 cm
+

FIG. 5.17 CLASSIFICATION OF ELECTROCHEMICAL REACTORS

showing interrelationships

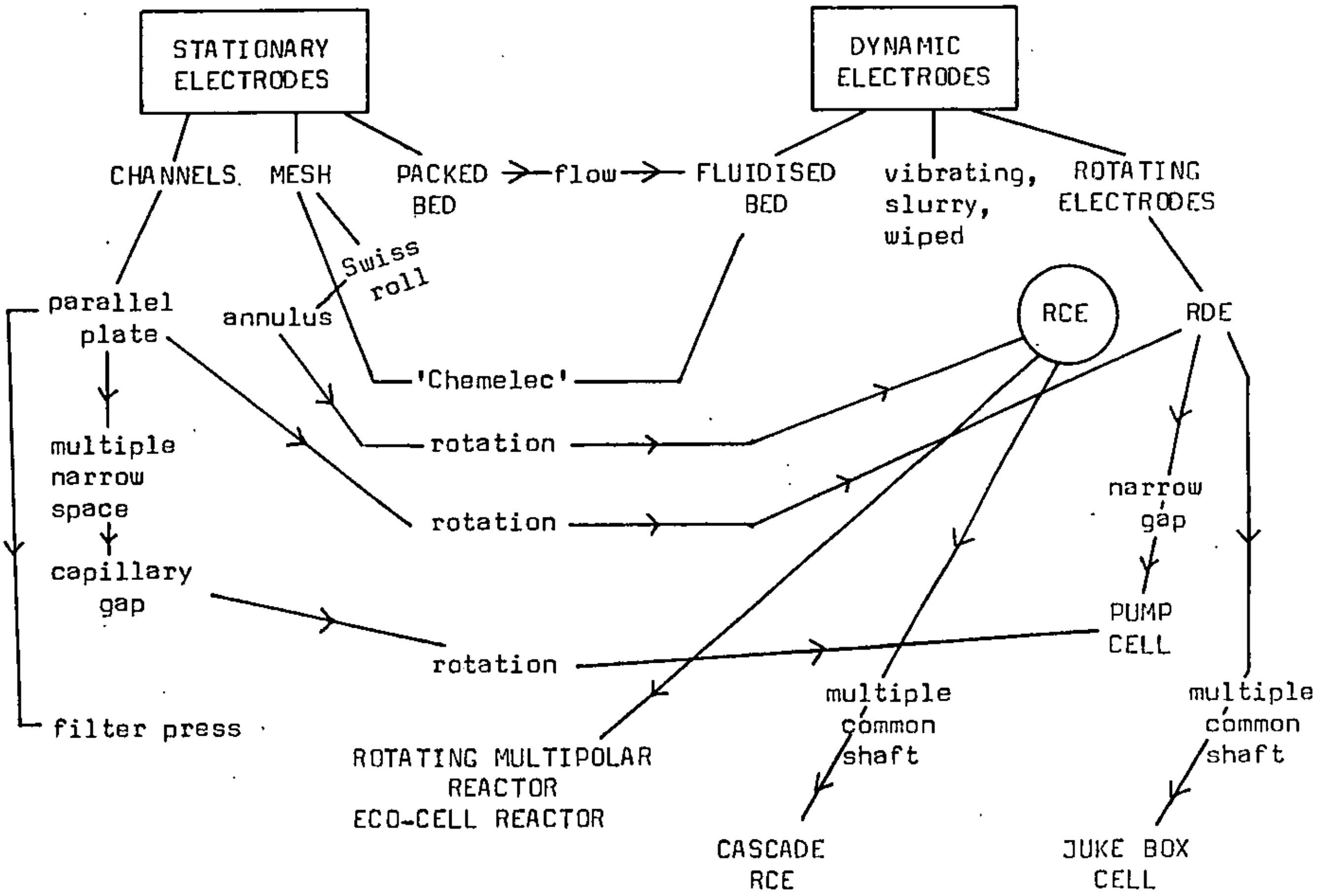
STATIONARY ELECTRODES
DYNAMIC ELECTRODES
CHANNELS
MESH
PACKED BED
flow
FLUIDISED BED
vibrating, slurry, wiped
ROTATING ELECTRODES
Swiss roll
parallel plate
annulus
RCE
RDE
'Chemelec'
multiple narrow space
rotation
rotation
narrow gap
capillary gap
PUMP CELL
rotation
multiple common shaft
multiple common shaft
filter press
ROTATING MULTIPOLAR REACTOR
ECO-CELL REACTOR
CASCADE RCE
JUKE BOX CELL

FIG. 5.18 THE ELECTROCHEMICAL PUMP CELL 215 - 224

(Southampton University)

a) Schematic Bipolar Cell

b) Laboratory Cell for Metal Powder Production

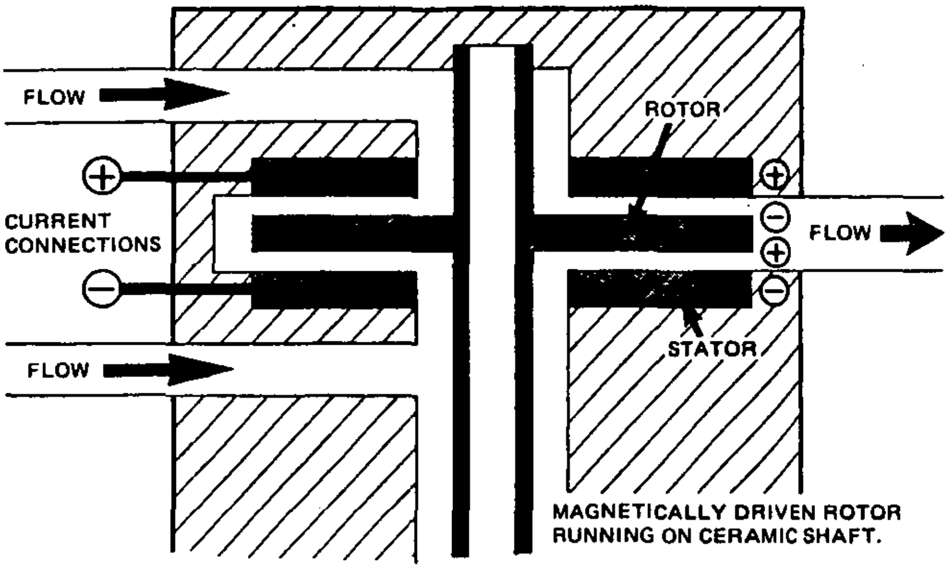
FLOW
ROTOR
CURRENT CONNECTIONS
FLOW
STATOR
FLOW
MAGNETICALLY DRIVEN ROTOR RUNNING ON CERAMIC SHAFT.

a)

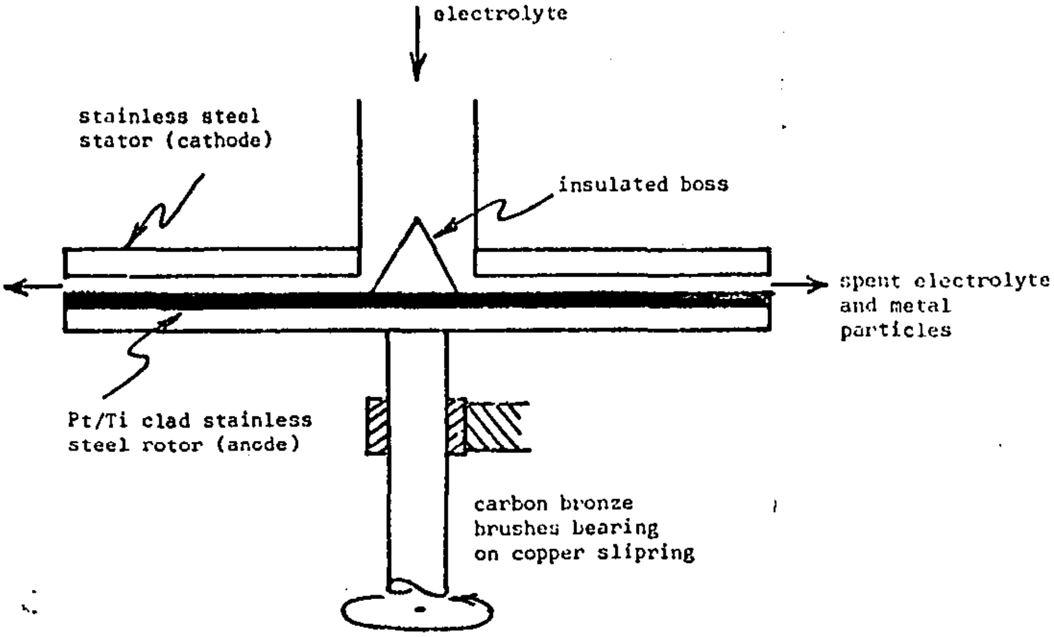
electrolyte
stainless steel stator (cathode)
insulated boss
spent electrolyte and metal particles
Pt/Ti clad stainless steel rotor (anode)
carbon bronze brushes bearing on copper slipring

b)

FIG. 5.19 THE "SWISS-ROLL" CELL [228]

(Z.T.H., Zurich, Switzerland)

a) Sectional view of the Cell and Ancillary equipment

b) The "Swiss-Roll" sandwich used for copper deposition

1. cathode cloth separator
2. cathode
3. ion-exchange membrane
4. anode cloth separator
5. anode

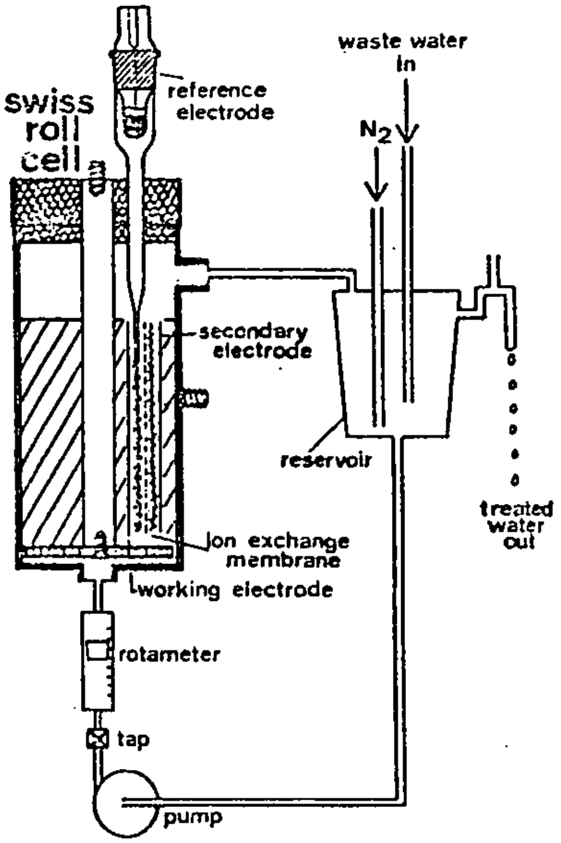
swiss roll cell
reference electrode
waste water in
N_2
secondary electrode
reservoir
treated water out
ion exchange membrane
working electrode
rotameter
tap
pump

a)

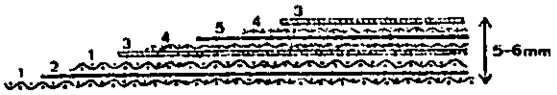
5-6mm

b)

FIG. 5.20 PLANAR, SIDE BY SIDE FLUIDISED BED ELECTRODE REACTOR

(C.J.B, Portsmouth)

After Wilkinson and Haines[165]

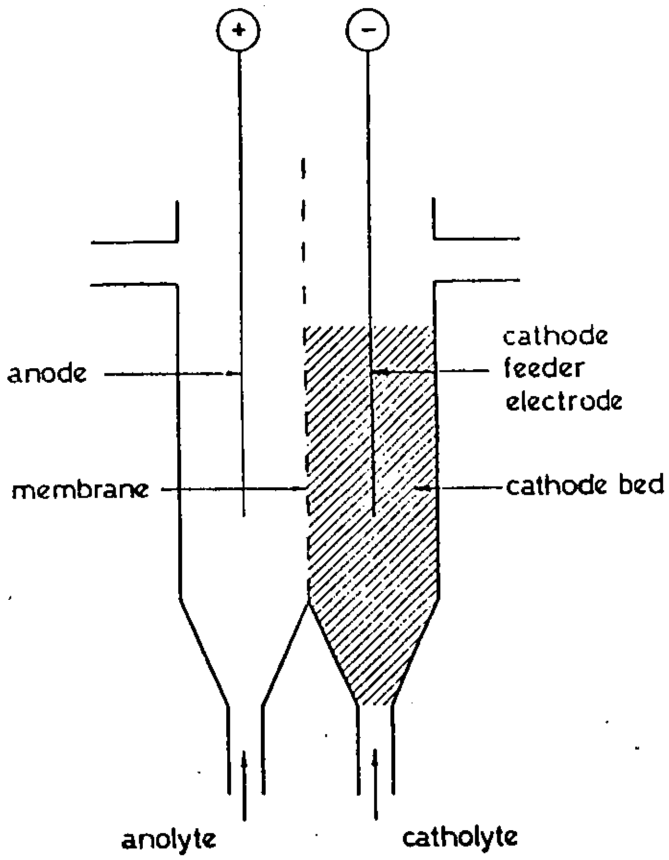
+
−
anode
cathode
feeder
electrode
membrane
cathode bed
anolyte
catholyte

FIG. 5.21 TUBE, FLUIDISED BED ELECTRODE REACTOR

(AKZO, Hengelo, NL)

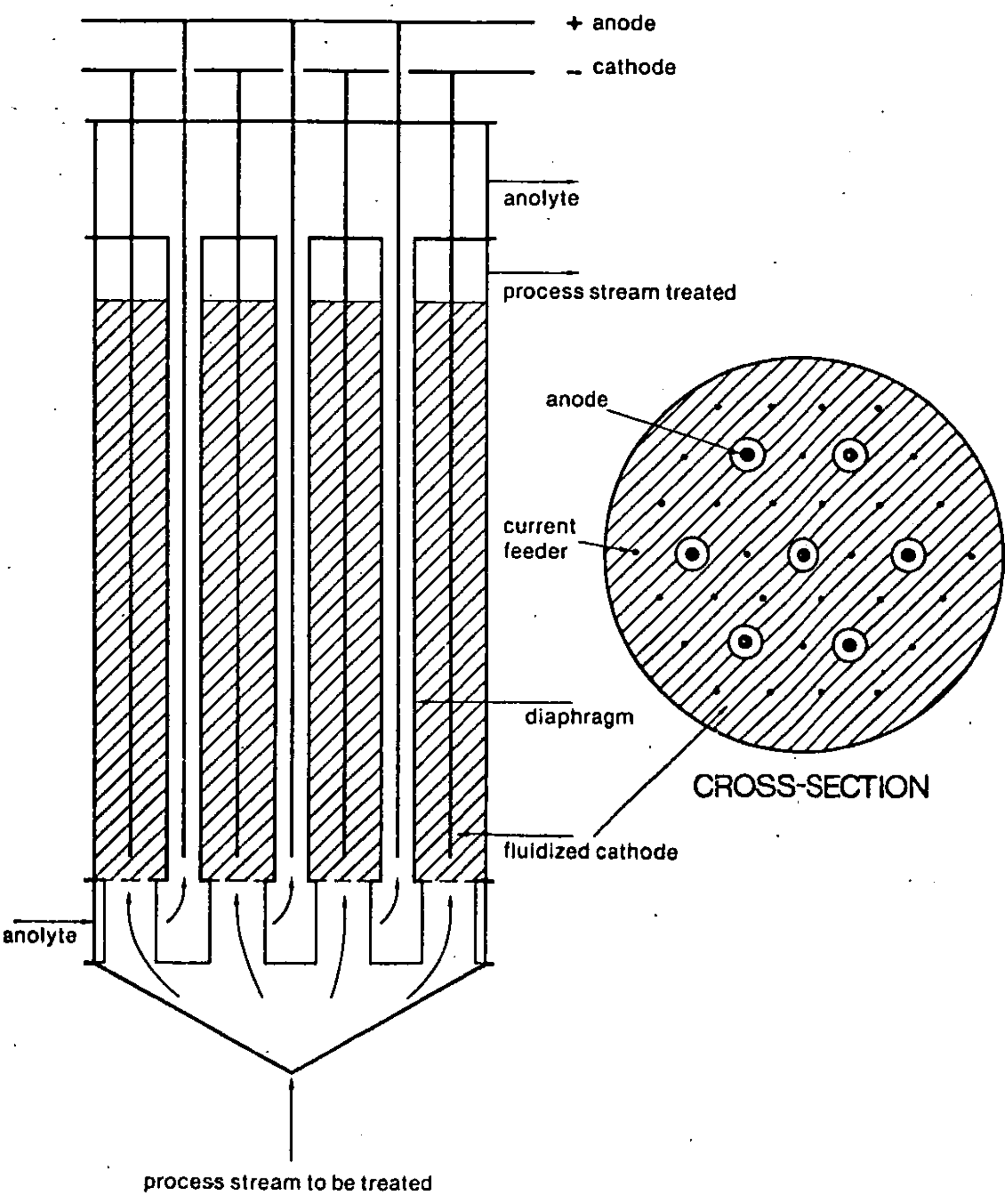
+ anode
– cathode
anolyte
process stream treated
anode
current feeder
diaphragm
CROSS-SECTION
fluidized cathode
anolyte
process stream to be treated

FIG. 5.22 PLANAR FLUIDISED BED ELECTRODE CELL

('CHEMELEC' CELL) [234]

(ECRC, Capenhurst, Cheshire)

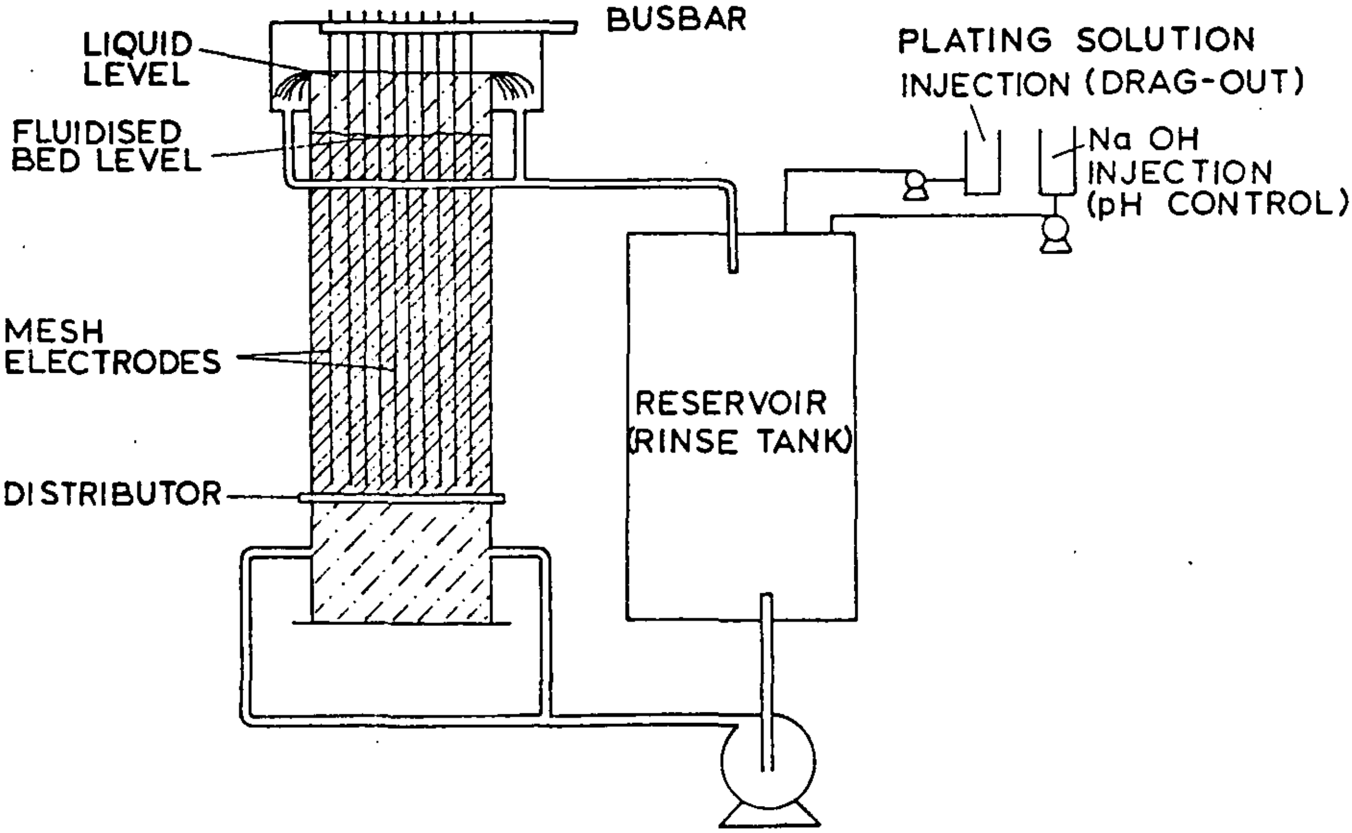
BUSBAR
LIQUID LEVEL
PLATING SOLUTION INJECTION (DRAG-OUT)
FLUIDISED BED LEVEL
Na OH INJECTION (pH CONTROL)
MESH ELECTRODES
RESERVOIR (RINSE TANK)
DISTRIBUTOR

FIG. 6.1 DEFINITION SKETCH FOR A BATCH ROTATING CYLINDER ELECTRODE REACTOR

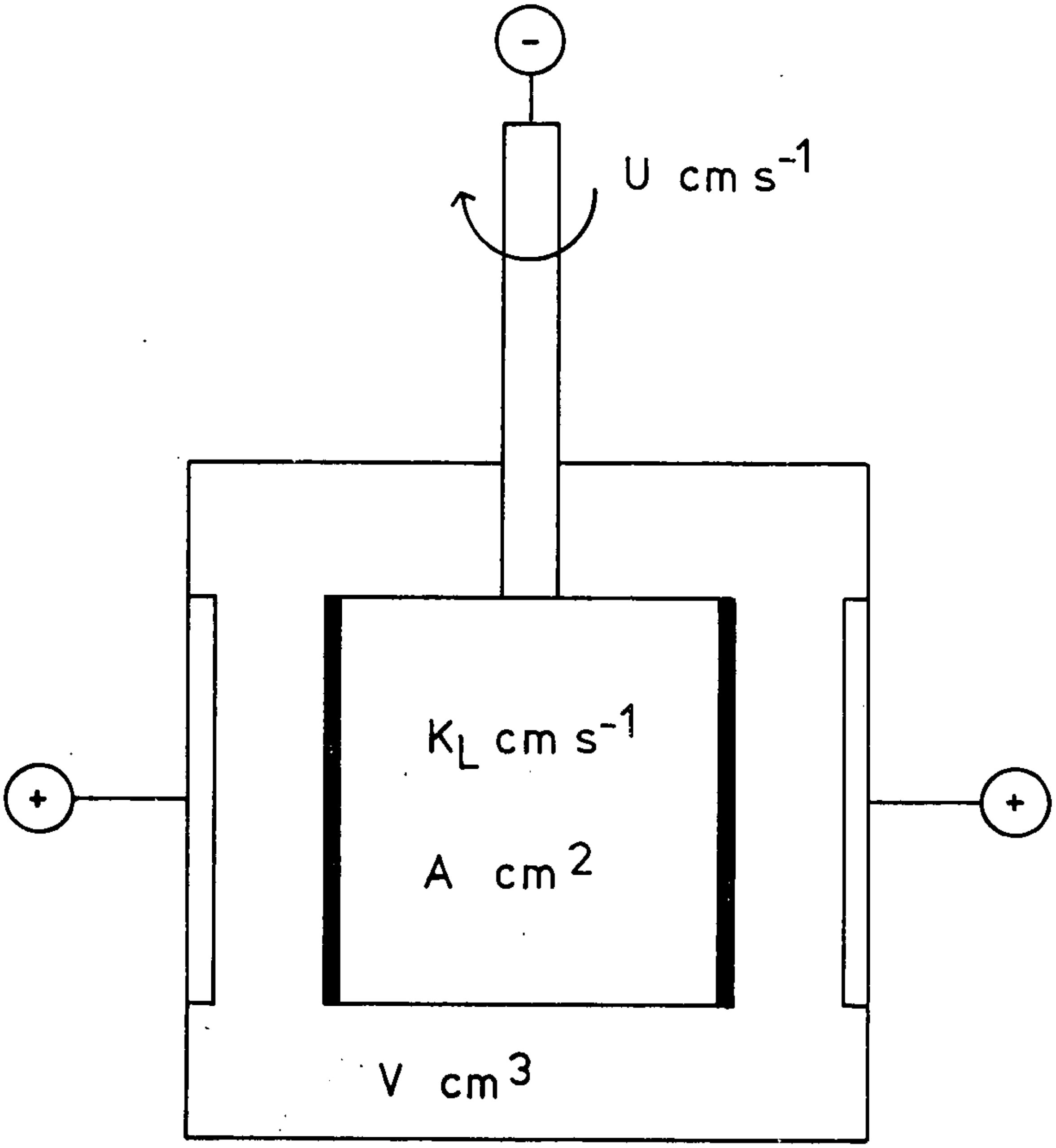
-
U cm s^{-1}
K_L cm s^{-1}
A cm^2
+
+
V cm^3

FIG. 6.2

CONVERSION AS A FUNCTION OF TIME FOR A THEORETICAL BATCH R.C.E.R.

showing the effect of surface area A and mass transport coefficient, K_L for a given peripheral velocity V = 1000 cms^{-1}

CURVE	A/cm^2	K/cms^{-1}
A	100	0.1
B	200	0.1
C	100	0.2

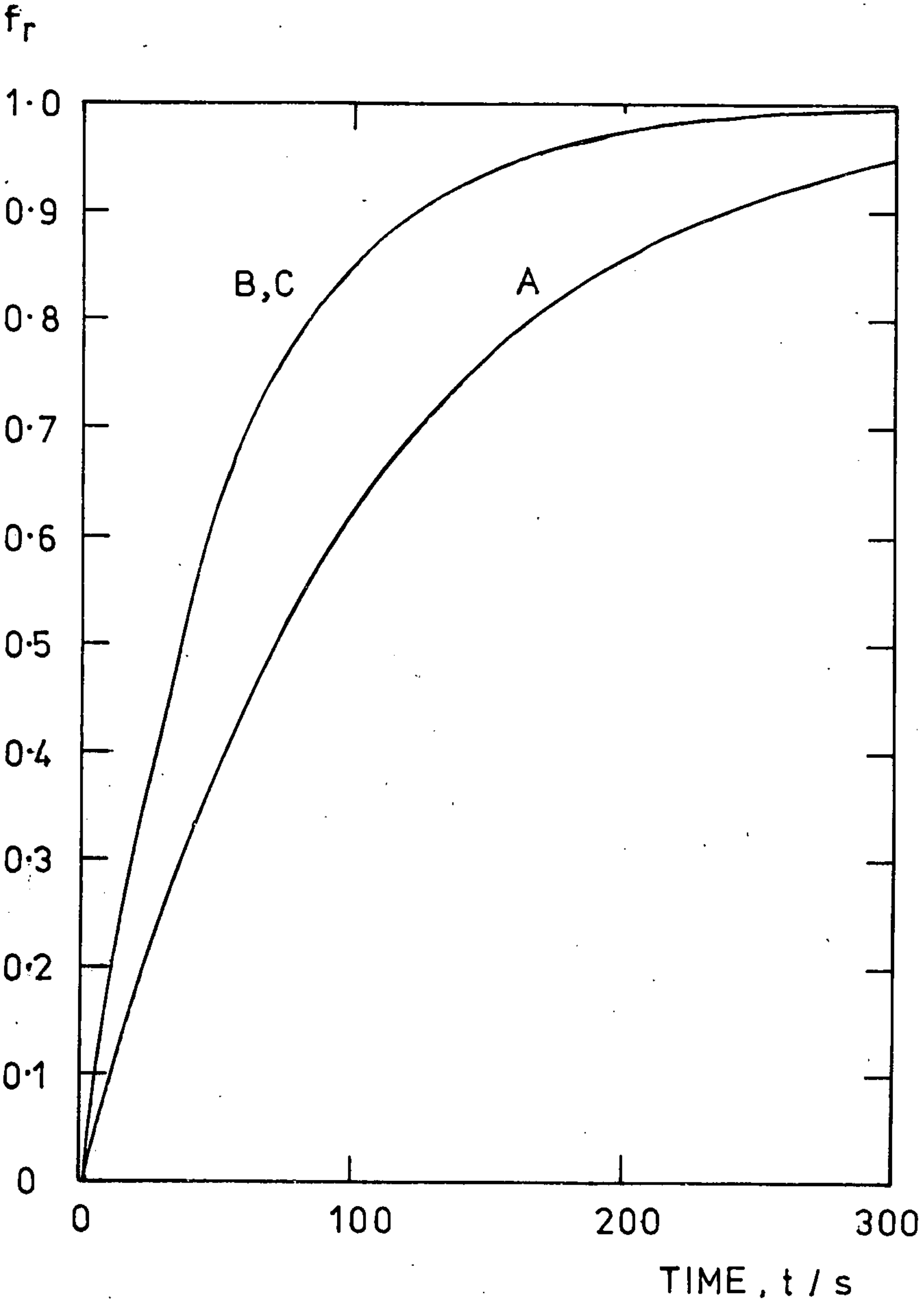

f_r
1·0
0·9
0·8
0·7
0·6
0·5
0·4
0·3
0·2
0·1
0
B, C
A
0
100
200
300
TIME, t / s

FIG. 6.3 DEFINITION SKETCH FOR A SINGLE PASS ROTATING CYLINDER ELECTRODE REACTOR

(electrical connections and anode omitted for clarity)

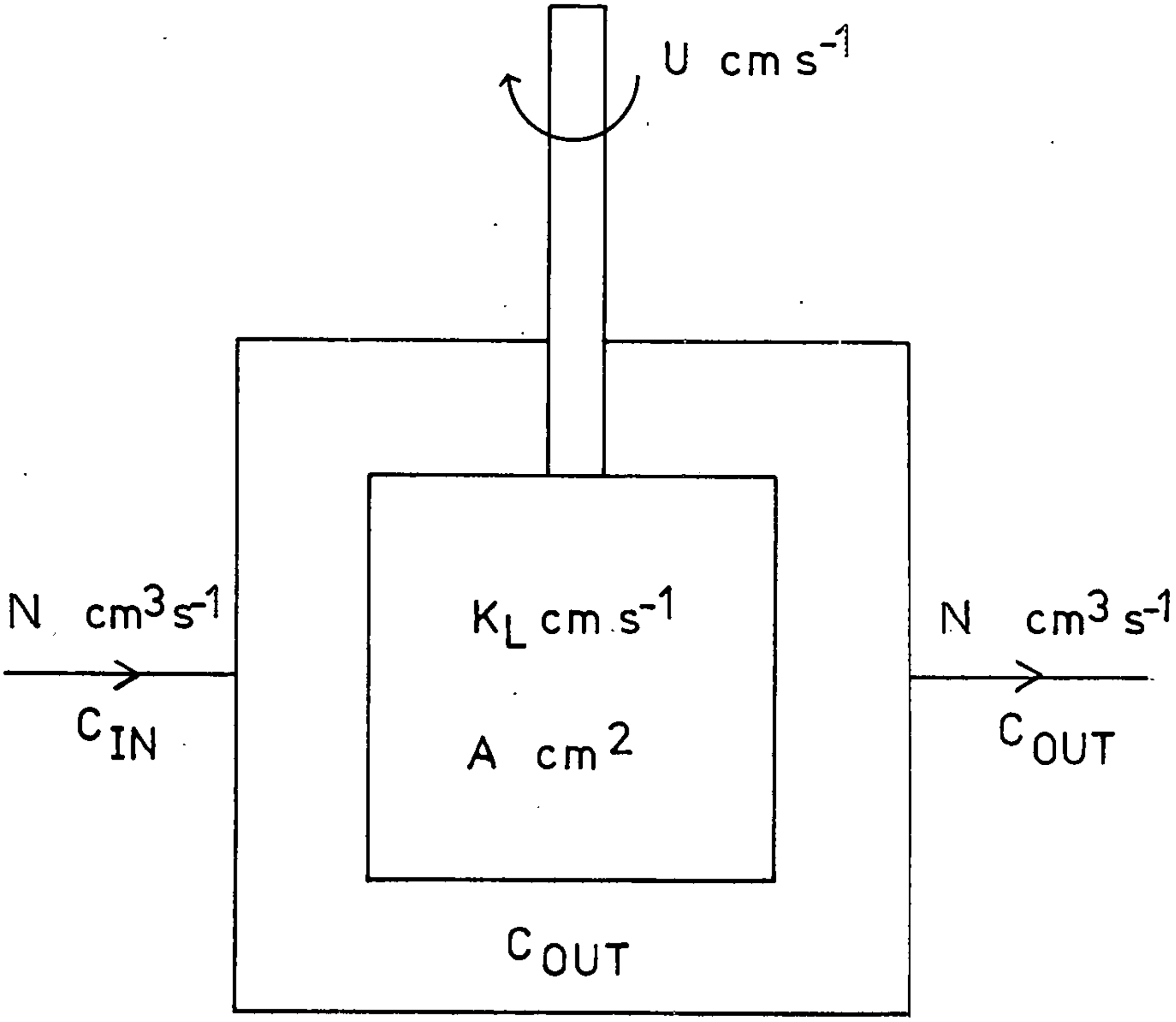
U cm s-1
N cm3 s-1
C_IN
K_L cm s-1
A cm2
N cm3 s-1
C_OUT
C_OUT

FIG. 6.4 a DEFINITION SKETCH FOR A ROTATING CYLINDER ELECTRODE REACTOR WITH RECYCLE

FIG. 6.4 b PROCESS SCHEMATIC OF A R.C.E.R. WITH RECYCLE AND FIXED INLET AND OUTLET CONCENTRATIONS

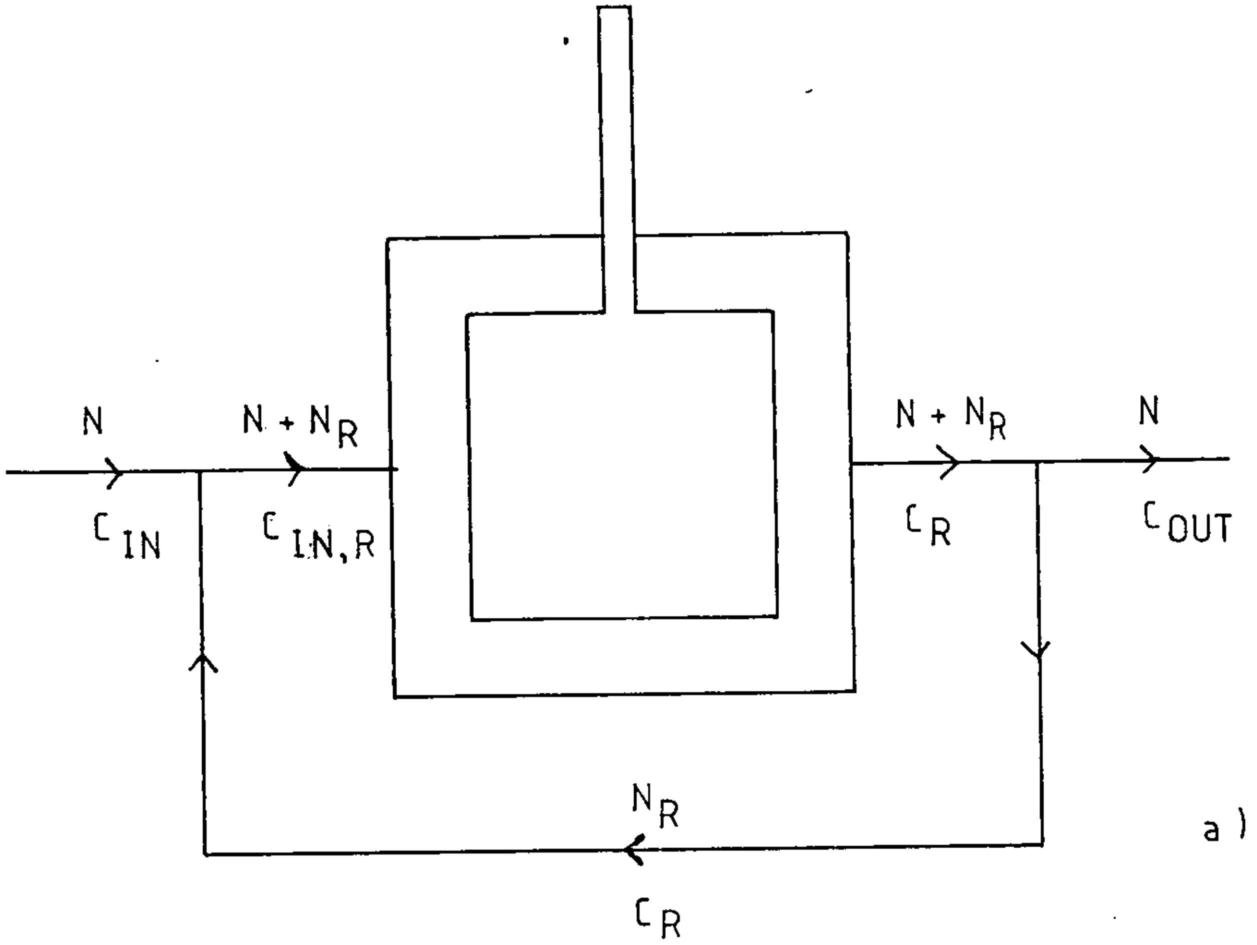
N
N + N_R
N + N_R
N
C_IN
C_IN,R
C_R
C_OUT
N_R
C_R
a)

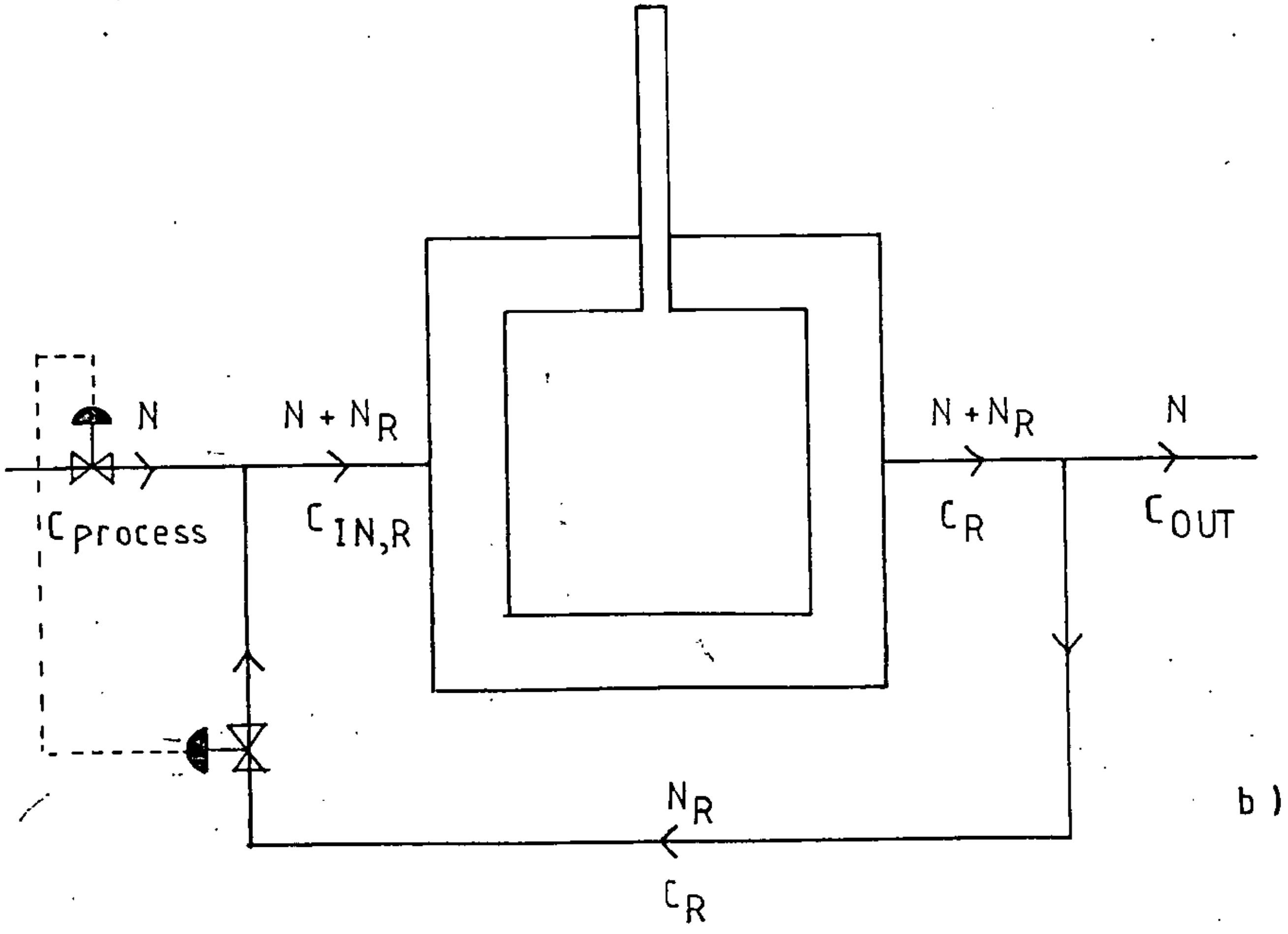
N
N + N_R
N + N_R
N
C_process
C_IN,R
C_R
C_OUT
N_R
C_R
b)

FIG. 6.5 ELECTRODE CONNECTIONS FOR POTENTIOSTATIC CONTROL OF A ROTATING CYLINDER ELECTRODE at a point P.

Z.L.	Zero Line Potential Pick up
R.E.	Reference Electrode
S.E.	Secondary Electrode
W.E.	Working Electrode

a) incorrect 3 terminal connection

b) correct 4 terminal connection

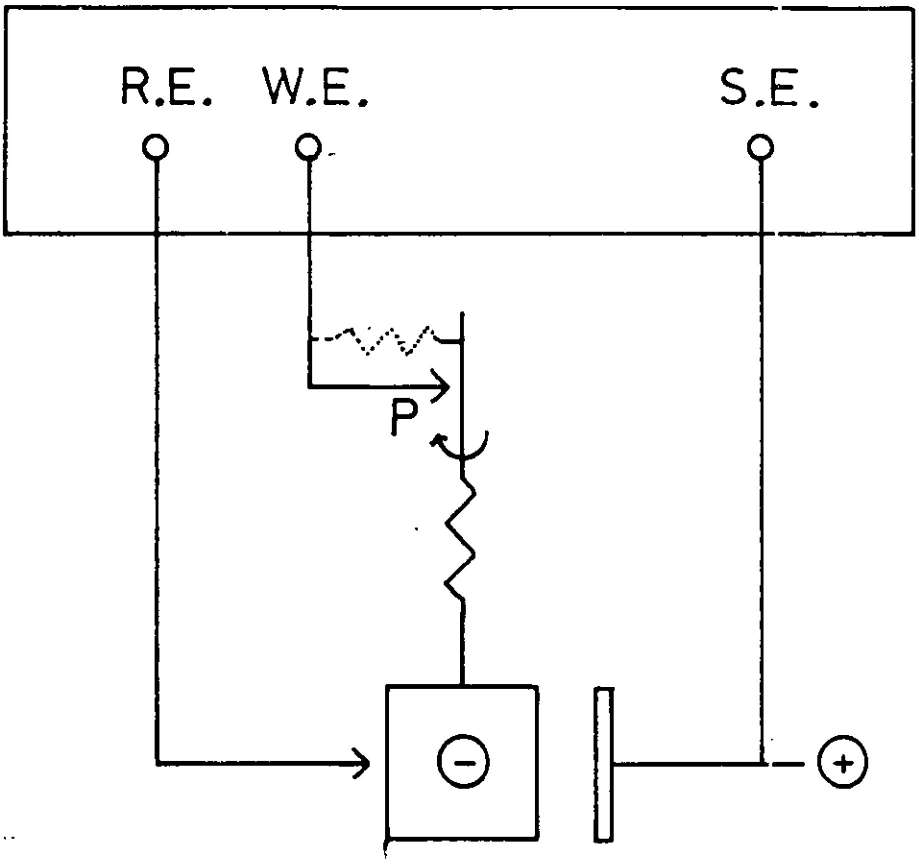

a)

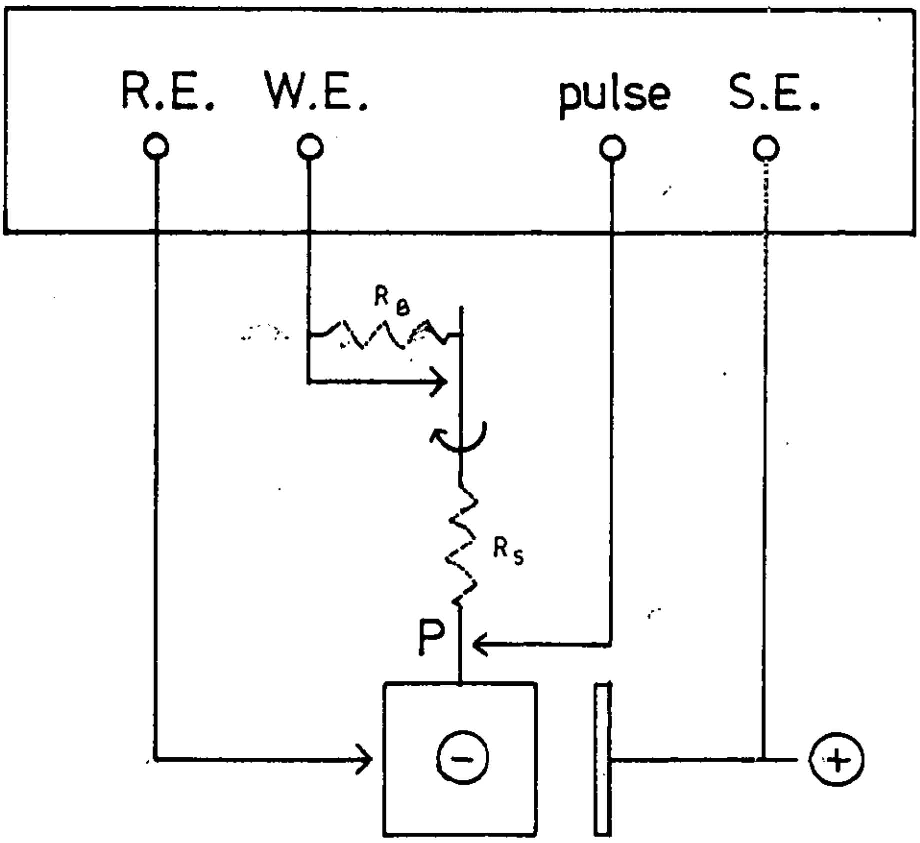
R.E.
W.E.
pulse
S.E.
R_B
R_s
P
−
+

b)

FIG. 6.6 LABORATORY ROTATING CYLINDER ELECTRODE due to Swalheim [310], (1944)

a) Plan view of cell

b) Sectional view of rotating cathode

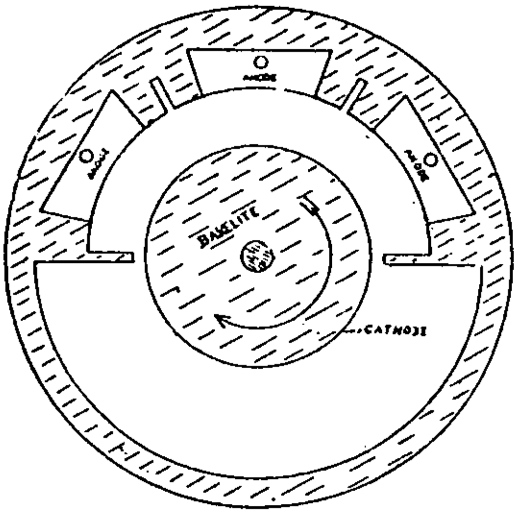
ANODE
ANODE
ANODE
BAKELITE
CATHODE

a)

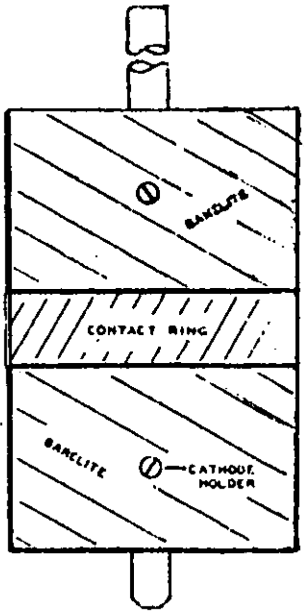
BAKELITE
CONTACT RING
BAKELITE
CATHODE HOLDER

b)

FIG. 6.7 LABORATORY ROTATING CYLINDER ELECTRODE

due to Eisenberg et al. [58], (1954)

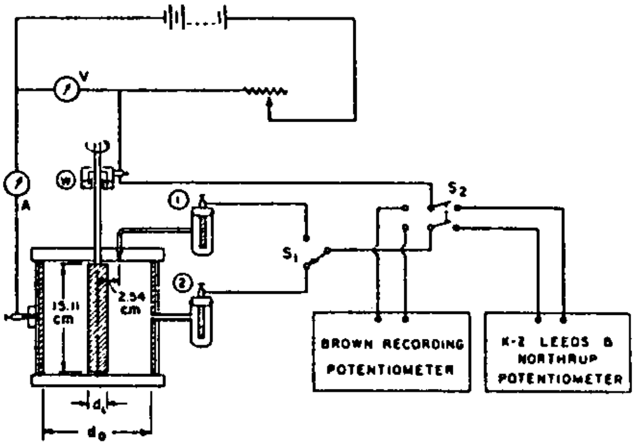
V
W
A
①
②
S₁
S₂
15.11 cm
2.54 cm
d_i
d_o
BROWN RECORDING POTENTIOMETER
K-2 LEEDS & NORTHRUP POTENTIOMETER

FIG. 6.8 LABORATORY ROTATING CYLINDER ELECTRODE
due to Arvia et al.[82], (1962)

A	copper anode
C	copper cathode
S	electrolytic solution
R.E.	reference electrode
E.C.	electrical contacts
H.C.	heating coils
L	'Lucite' boards
St	stirrer shaft
I	insulator material
M.C.	mercury cap. for E.C.

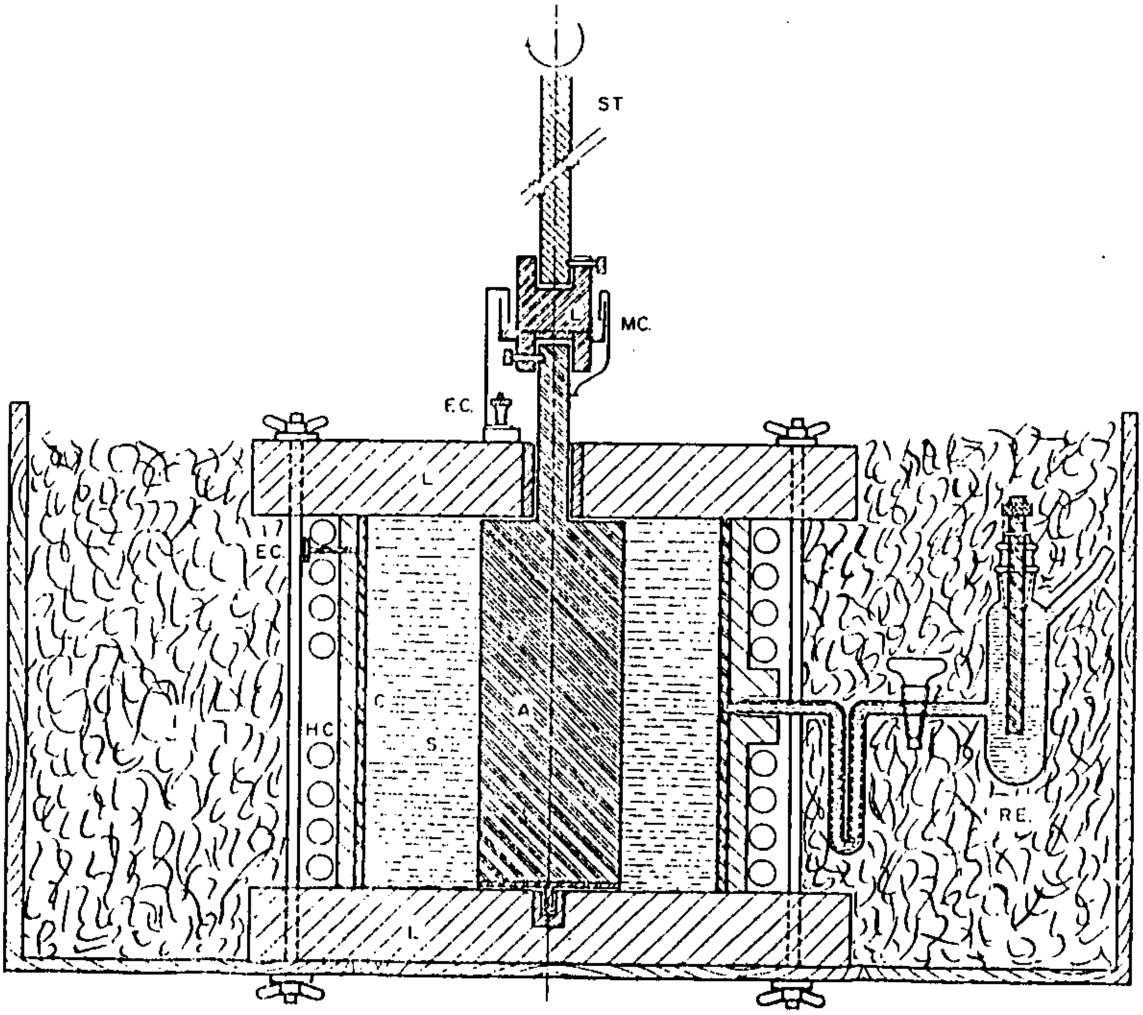
ST
MC.
F.C.
L
E.C.
HC
C
S.
A
L
RE.

FIG. 6.9 LABORATORY ROTATING CYLINDER ELECTRODE

due to Krishna et al. [74], (1965)

a) electrolytic cell, sectional view

b) plan view

c) rotating electrode

1. rotating shaft
2. inverted cup
3. mercury bowl
4. "hylam" cover plate
5. capillary
6. grooved "hylam" plate
7. ring electrodes
8. copper shell
9. electrical connections
10. 'L' - clamps
11. baffles
12. bottom support
13. copper ring electrodes
14. steel rod
15. 'allsathene'insulators
16. "Hylam" rod
17. copper ring
18. "hylam" ring
19. impeller

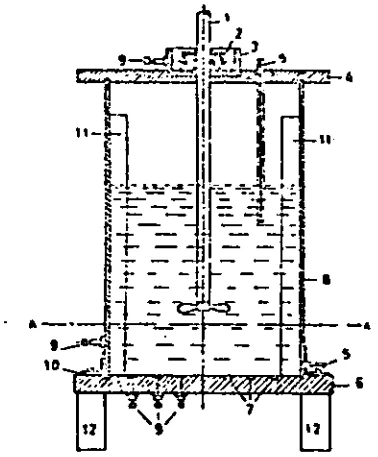
A
A

a)

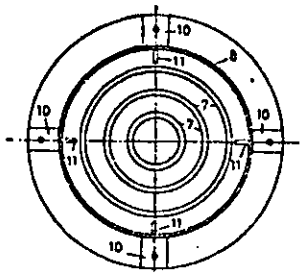

b)

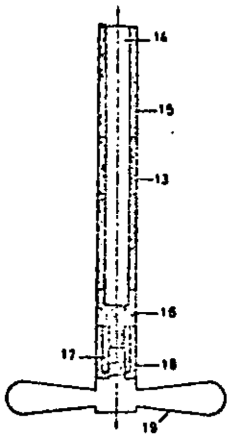

c)

FIG. 6.10 LABORATORY ROTATING CYLINDER ELECTRODE due to Kappesser et al. [89], (1971)

FIG. 6.11 LABORATORY ROTATING CYLINDER ELECTRODE due to Edwards and Wall [284], (1966)

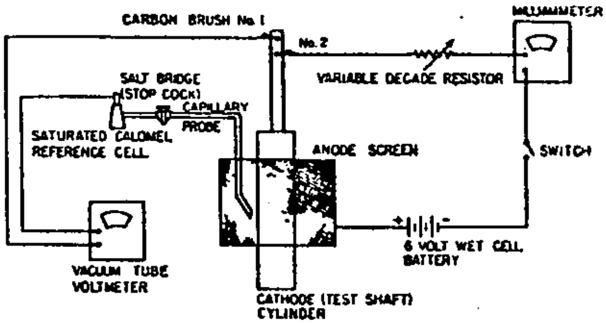
CARBON BRUSH No. 1
No. 2
MILLIAMMETER
SALT BRIDGE
(STOP COCK)
CAPILLARY
PROBE
VARIABLE DECADE RESISTOR
SATURATED CALOMEL
REFERENCE CELL
ANODE SCREEN
SWITCH
6 VOLT WET CELL
BATTERY
VACUUM TUBE
VOLTMETER
CATHODE (TEST SHAFT)
CYLINDER

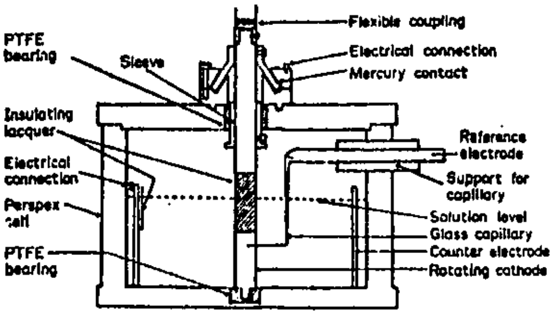
Flexible coupling
PTFE
bearing
Sleeve
Electrical connection
Mercury contact
Insulating
lacquer
Reference
electrode
Electrical
connection
Support for
capillary
Perspex
cell
Solution level
Glass capillary
Counter electrode
PTFE
bearing
Rotating cathode

FIG. 6.12

LABORATORY ROTATING CYLINDER ELECTRODE

due to Robinson and Gabe [68, 84], (1970)

FIG. 6.13

LABORATORY ROTATING CYLINDER ELECTRODE

due to Postlethwaite et al. [94], (1971)

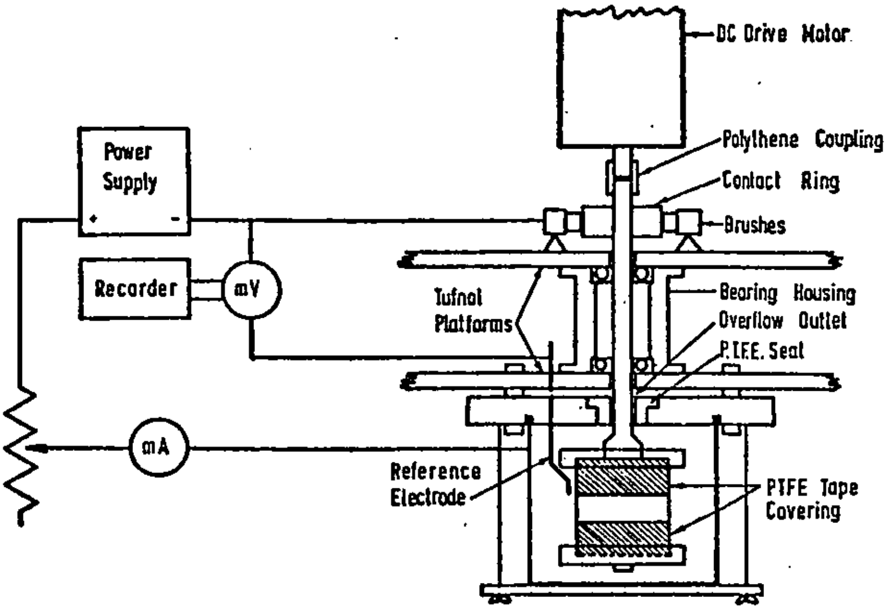
DC Drive Motor
Polythene Coupling
Contact Ring
Brushes
Power Supply
+
-
Recorder
mV
Tufnol Platforms
Bearing Housing
Overflow Outlet
P.T.F.E. Seat
mA
Reference Electrode
PTFE Tape Covering

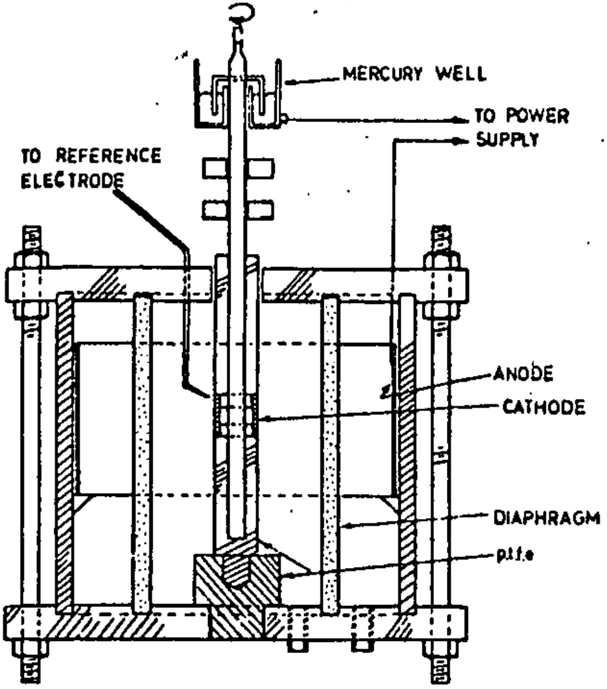
MERCURY WELL
TO POWER SUPPLY
TO REFERENCE ELECTRODE
ANODE
CATHODE
DIAPHRAGM
p.t.f.e

FIG. 6.14 LABORATORY ROTATING CYLINDER ELECTRODE
due to Sedahmed et al.[73], (1977)

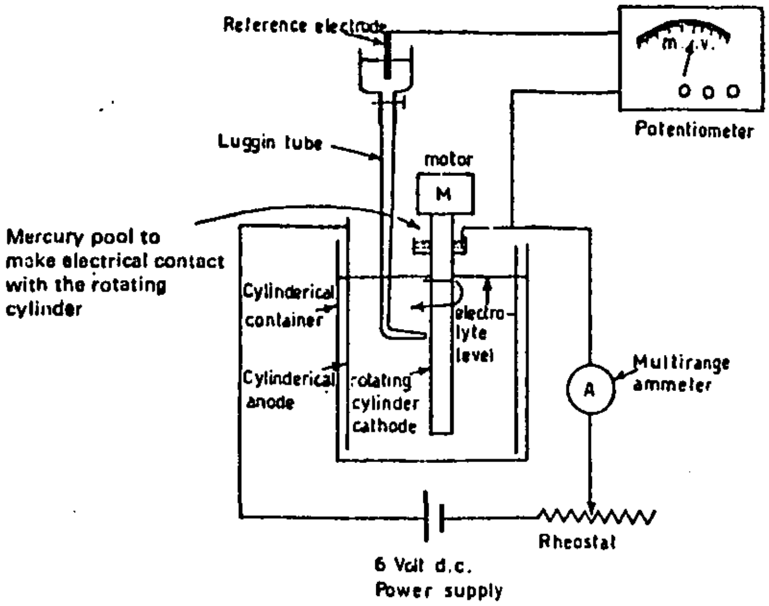
Reference electrode
m.v.
Potentiometer
Luggin tube
motor
M
Mercury pool to make electrical contact with the rotating cylinder
Cylinderical container
electrolyte level
Cylinderical anode
rotating cylinder cathode
Multirange ammeter
A
Rheostat
6 Volt d.c.
Power supply

FIG. 6.15 LABORATORY ROTATING TRIPOLAR ELECTRODE CELL

due to Nadebaum and Fahidy [289 - 292], (1973)

a) plan view of cell

b) sectional views of cell

c) plan view of wiper

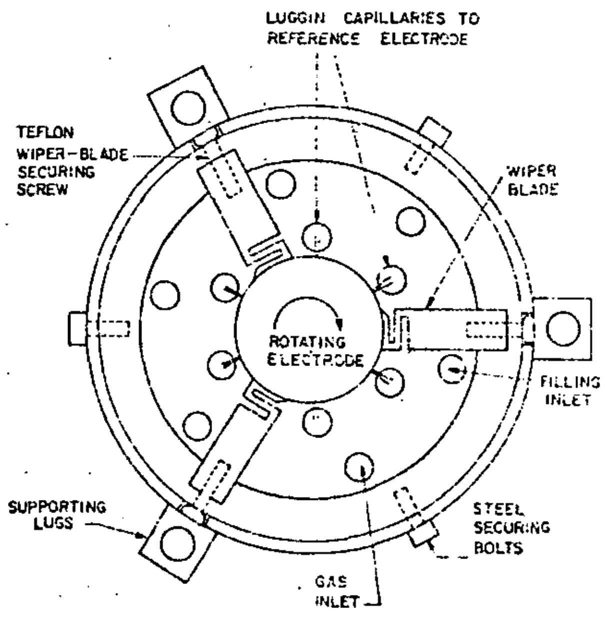
LUGGIN CAPILLARIES TO REFERENCE ELECTRODE
TEFLON WIPER-BLADE SECURING SCREW
WIPER BLADE
ROTATING ELECTRODE
FILLING INLET
SUPPORTING LUGS
STEEL SECURING BOLTS
GAS INLET

a)

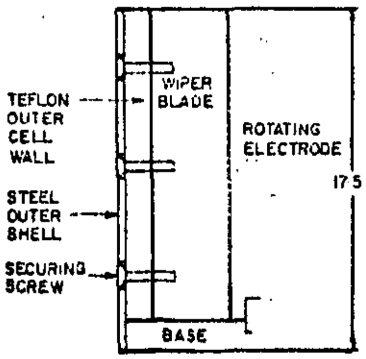
TEFLON OUTER CELL WALL
STEEL OUTER SHELL
SECURING SCREW
WIPER BLADE
ROTATING ELECTRODE
17·5
BASE

b)

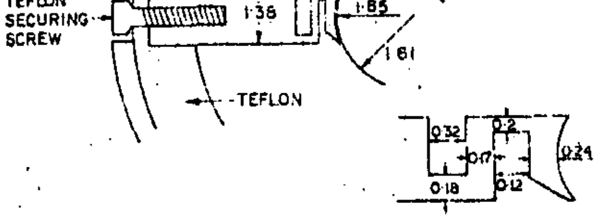
TEFLON SECURING SCREW
3·2
1·36
ROTATING ELECTRODE
1·85
1·61
TEFLON
0·32
0·2
0·17
0·24
0·18
0·12

c)

FIG. 6.16 INDUSTRIAL ROTATING BIPOLAR ELECTRODE REACTOR envisaged for the purpose of economic analysis

After Nadebaum and Fahidy [298]

a) sketch of the principle

b) section of the apparatus

c) & (d) industrial scale reactor

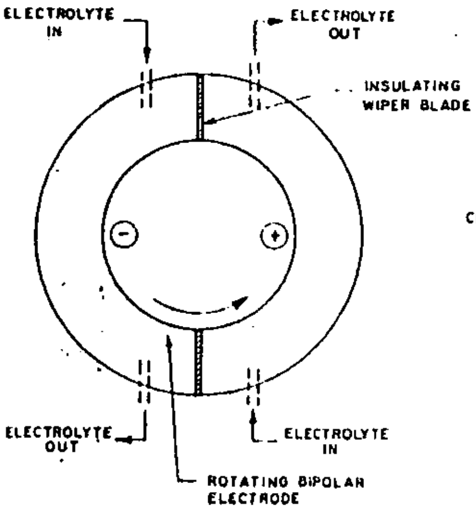
ELECTROLYTE IN
ELECTROLYTE OUT
INSULATING WIPER BLADE
−
+
ELECTROLYTE OUT
ELECTROLYTE IN
ROTATING BIPOLAR ELECTRODE

a)

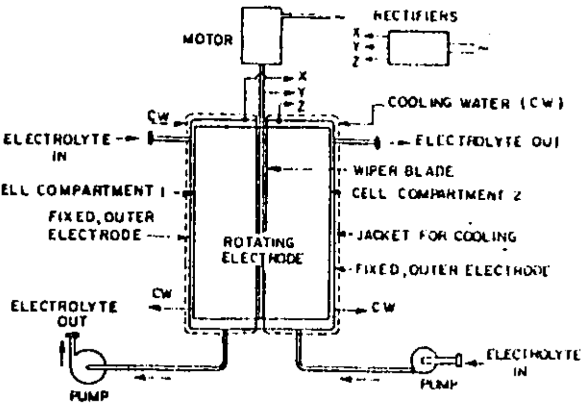
MOTOR
RECTIFIERS
X
Y
Z
COOLING WATER (CW)
CW
ELECTROLYTE IN
ELECTROLYTE OUT
WIPER BLADE
CELL COMPARTMENT 1
CELL COMPARTMENT 2
FIXED, OUTER ELECTRODE
JACKET FOR COOLING
ROTATING ELECTRODE
FIXED, OUTER ELECTRODE
CW
ELECTROLYTE OUT
CW
PUMP
PUMP
ELECTROLYTE IN

b)

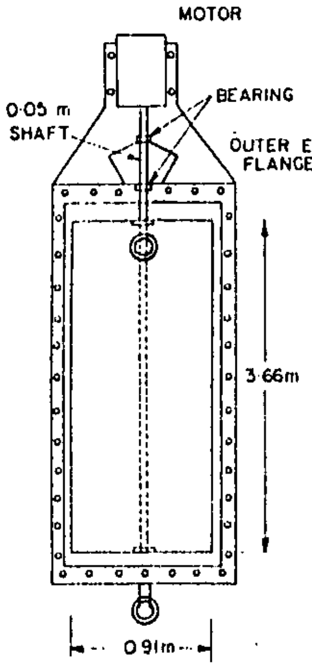
MOTOR
0·05 m SHAFT
BEARING
OUTER ELECTRODE FLANGES
3·66m
0·91m

c)

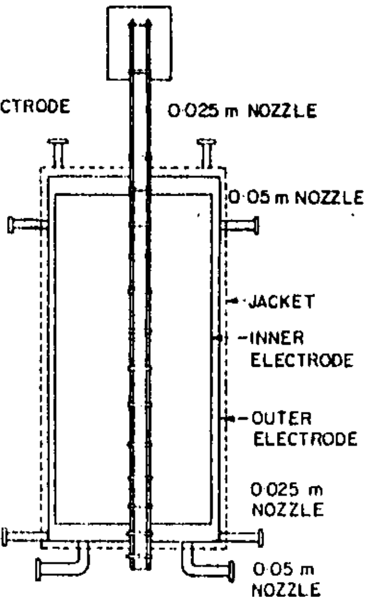
0·025 m NOZZLE
0·05 m NOZZLE
JACKET
INNER ELECTRODE
OUTER ELECTRODE
0·025 m NOZZLE
0·05 m NOZZLE

d)

FIG. 6.17 UNDIVIDED LABORATORY ROTATING CYLINDER ELECTRODE FOR PRECIOUS METAL RECOVERY
(Walsh, Ecological Engineering Ltd.)

a) Section
b) Plan

A. Rotating Cylinder Cathode (Stainless steel)
B. Insulating End Caps (Polypropylene)
C. Graphite Plate anodes
D. Titanium anode feeder/support ring
E. Glass or Plastic Vessel
F. Powdery Metal Deposit

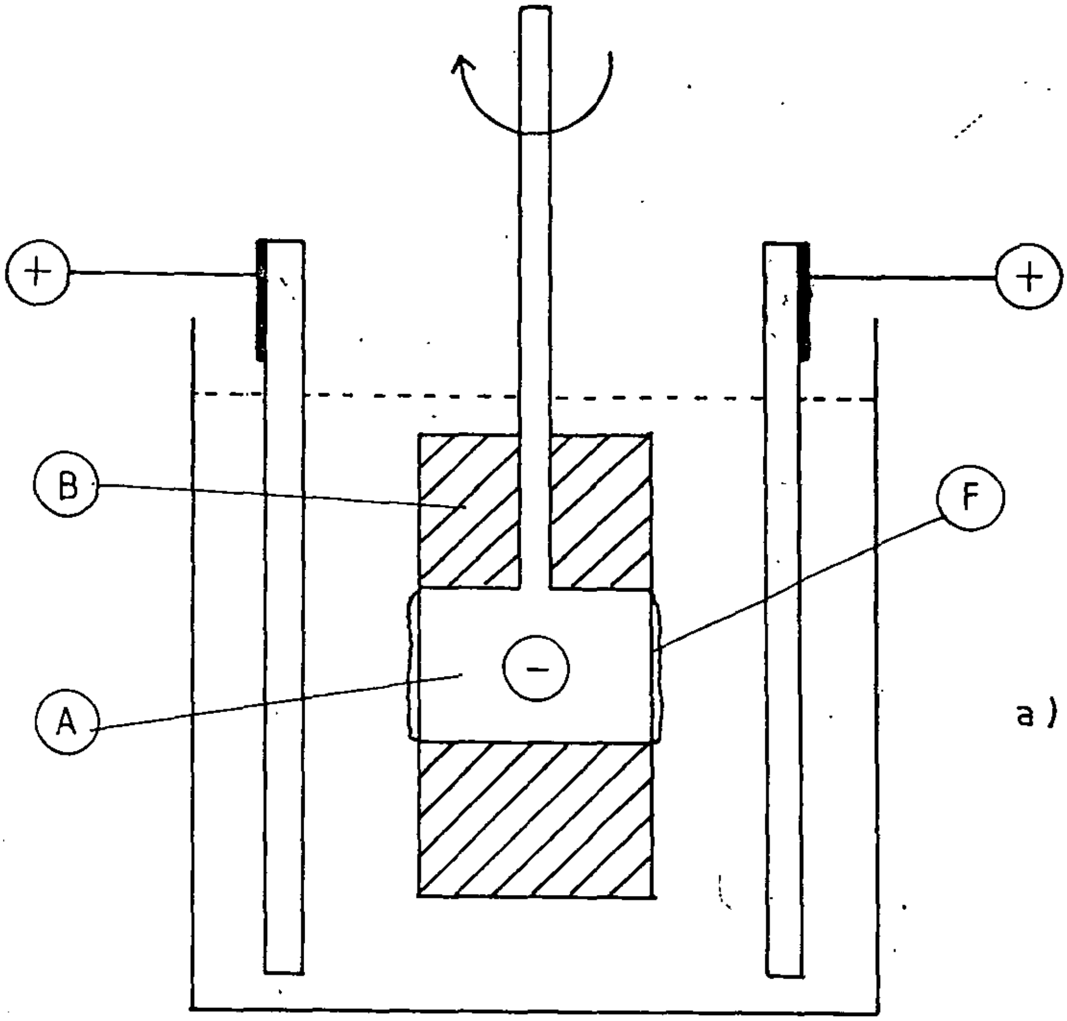

a)

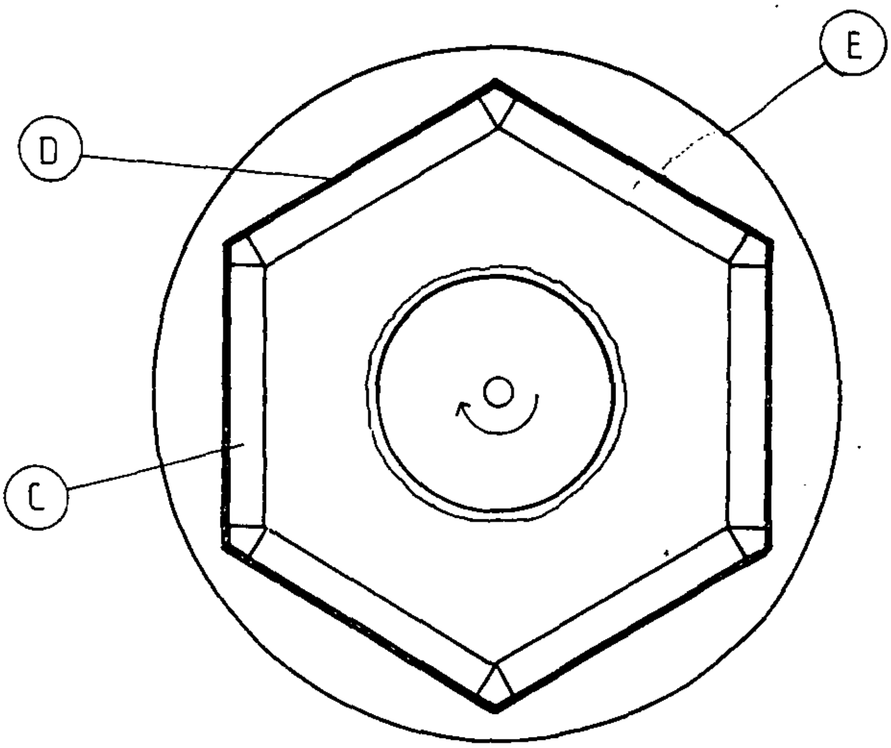

b)

FIG. 6.18 DIVIDED LABORATORY ROTATING CYLINDER ELECTRODE REACTORS

utilising planar anodes

(Ecological Engineering Ltd.)

a) open catholyte compartment

b) closed catholyte compartment

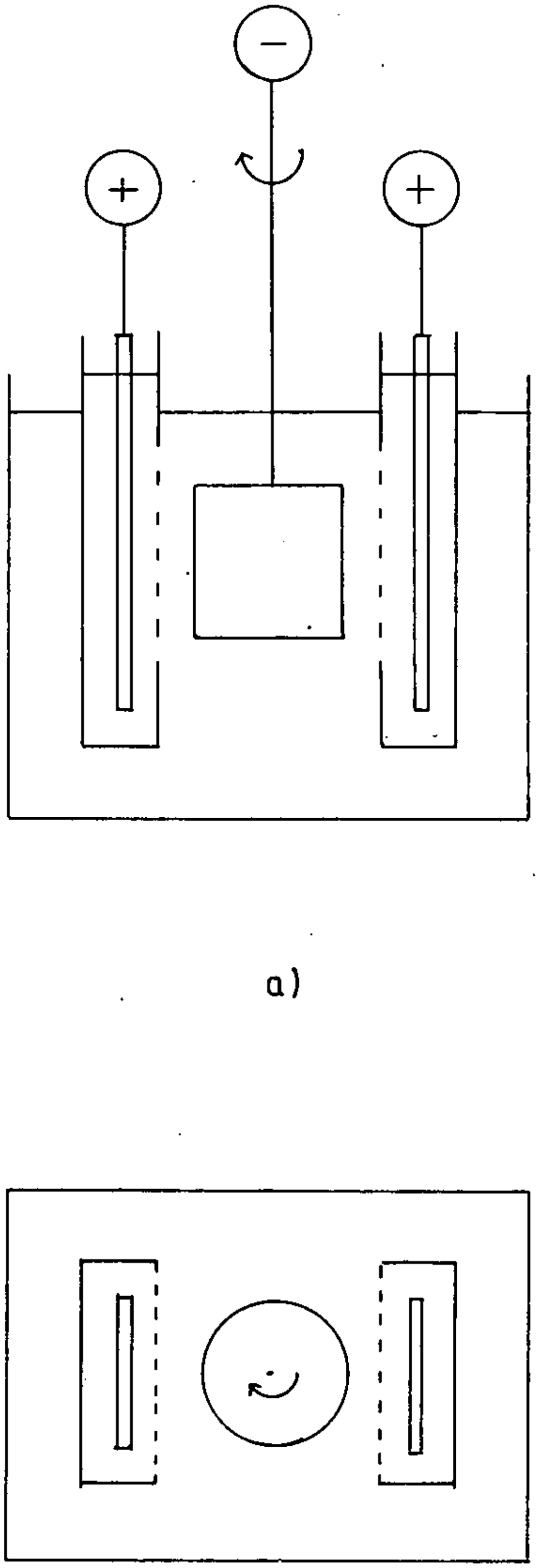

a)

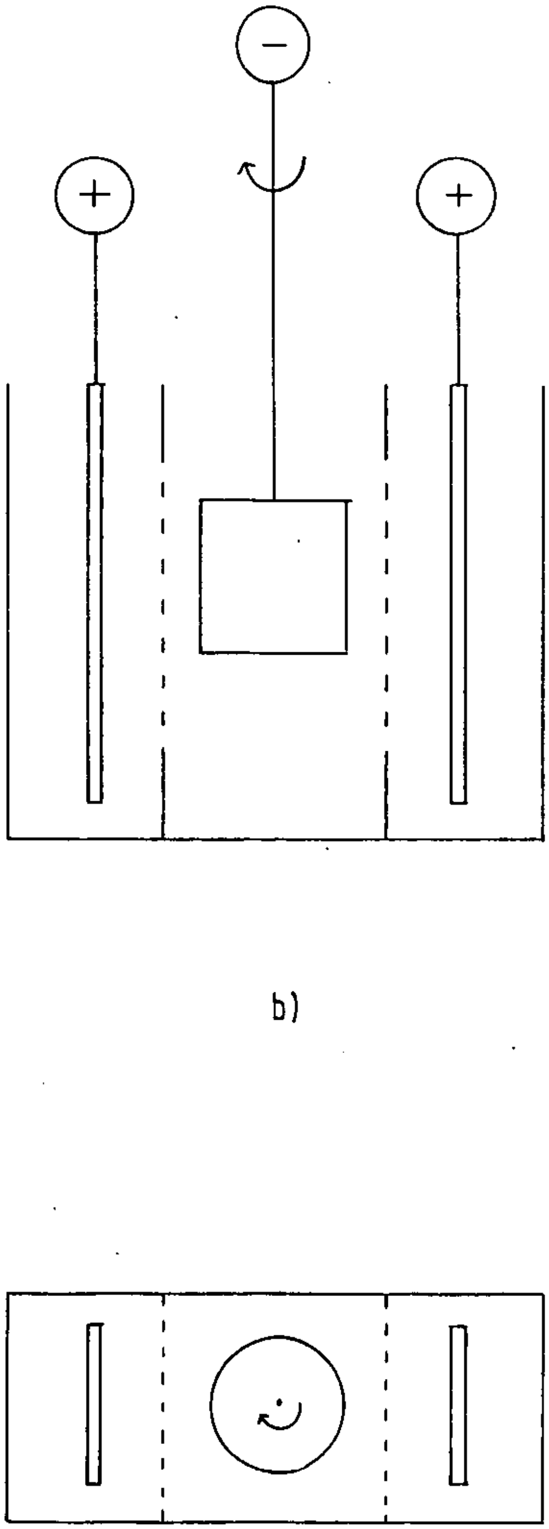

b)

FIG. 6.19 LABORATORY ROTATING CYLINDER ELECTRODE
due to Chin et al. [72], (1977)

a) plan view

b) sectional view

FIG. 6.20 EXPERIMENTAL ROTATING CYLINDER ELECTRODE CELL
For controlled potential coulometric analysis
Due to Johansson [286], (1965)

AUX.	auxiliary electrode
REF.	reference electrode salt bridge
C	platinised rotating cylinder

------	dialysis tubing
□	sintered glass
▨	platinum
▧	perspex

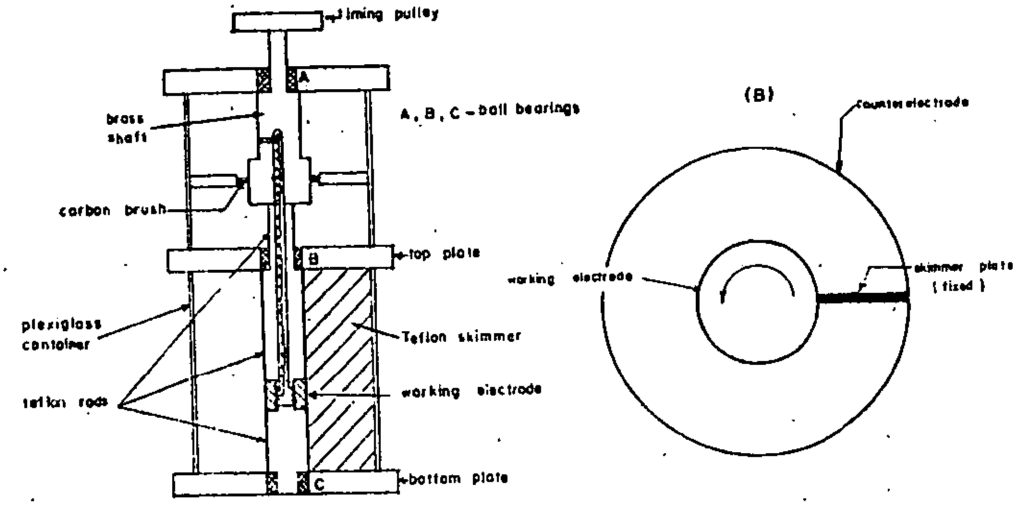
timing pulley
A
A, B, C – ball bearings
brass shaft
carbon brush
B
top plate
plexiglass container
Teflon skimmer
teflon rods
working electrode
C
bottom plate
(B)
counter electrode
working electrode
skimmer plate (fixed)

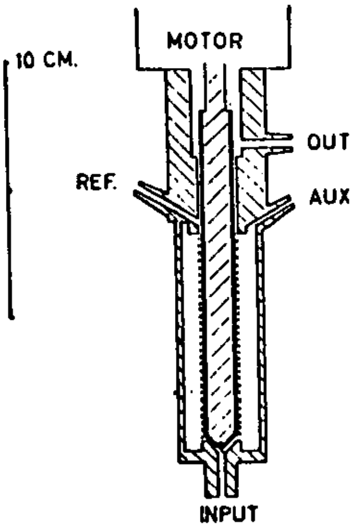
MOTOR
10 CM.
OUT
REF.
AUX
INPUT

FIG. 6.21 AMALGAMATED ROTATING CYLINDER ELECTRODE REACTOR for synthesis of salicylaldehyde. After Udupa et al.[333], (1963)

a) sectional view

b) plan view

1. pitch-lined mild steel tank
2. copper cathode (rotating)
3. micro-porous rubber diaphragm
4. lead anode
5. lead cooling coils

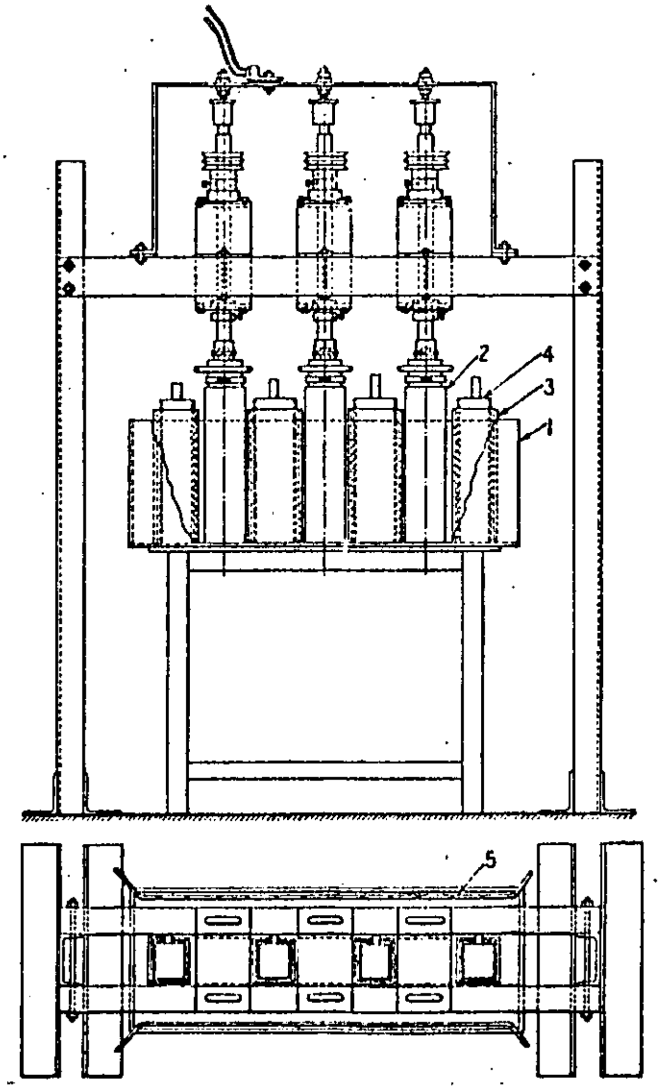

FIG. 6.22 WIPED ROTATING CYLINDER ELECTRODE CELL

for synthesis of sodium dithionite

After Spencer et al.[296, 297], (1969)

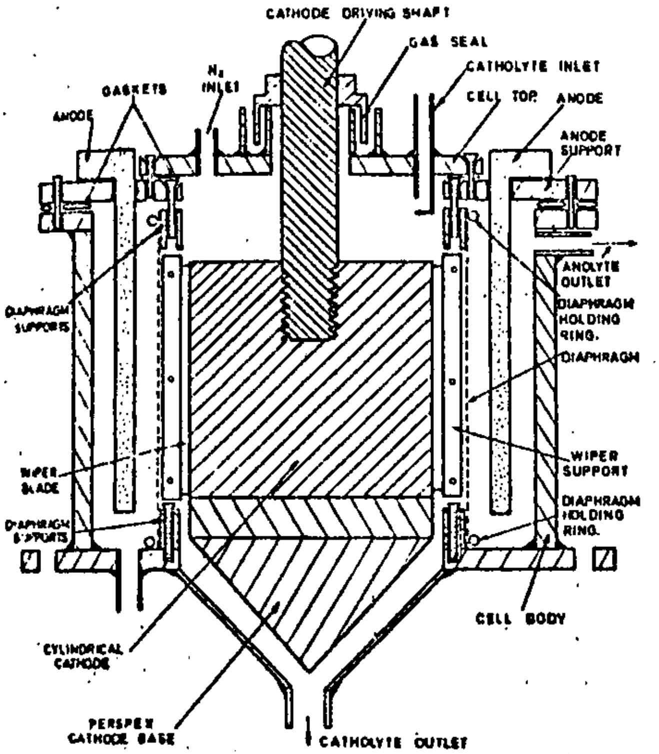
CATHODE DRIVING SHAFT
GAS SEAL
CATHOLYTE INLET
N_2 INLET
GASKETS
CELL TOP
ANODE
ANODE
ANODE SUPPORT
ANOLYTE OUTLET
DIAPHRAGM SUPPORTS
DIAPHRAGM HOLDING RING.
DIAPHRAGM
WIPER BLADE
WIPER SUPPORT
DIAPHRAGM SUPPORTS
DIAPHRAGM HOLDING RING.
CELL BODY
CYLINDRICAL CATHODE
PERSPEX CATHODE BASE
CATHOLYTE OUTLET

FIG. 6.23 PATENTED BIPOLAR ROTATING CYLINDER ELECTRODE
for removal of ions from an ionised liquid
(Benner, 1969)

12, 13.	rotating cylinders
27.	counter electrode
23.	inlet
26.	outlets for segregated ionic streams
20.	overflow
21.	anion rich liquor
22.	cation rich liquor
10.	vessel
15, 16.	power brushes

For other symbols see the cited reference.

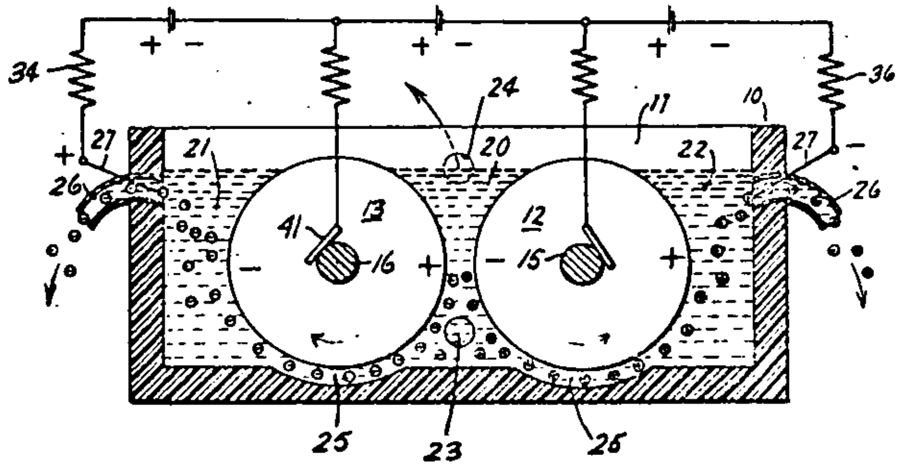
+
-

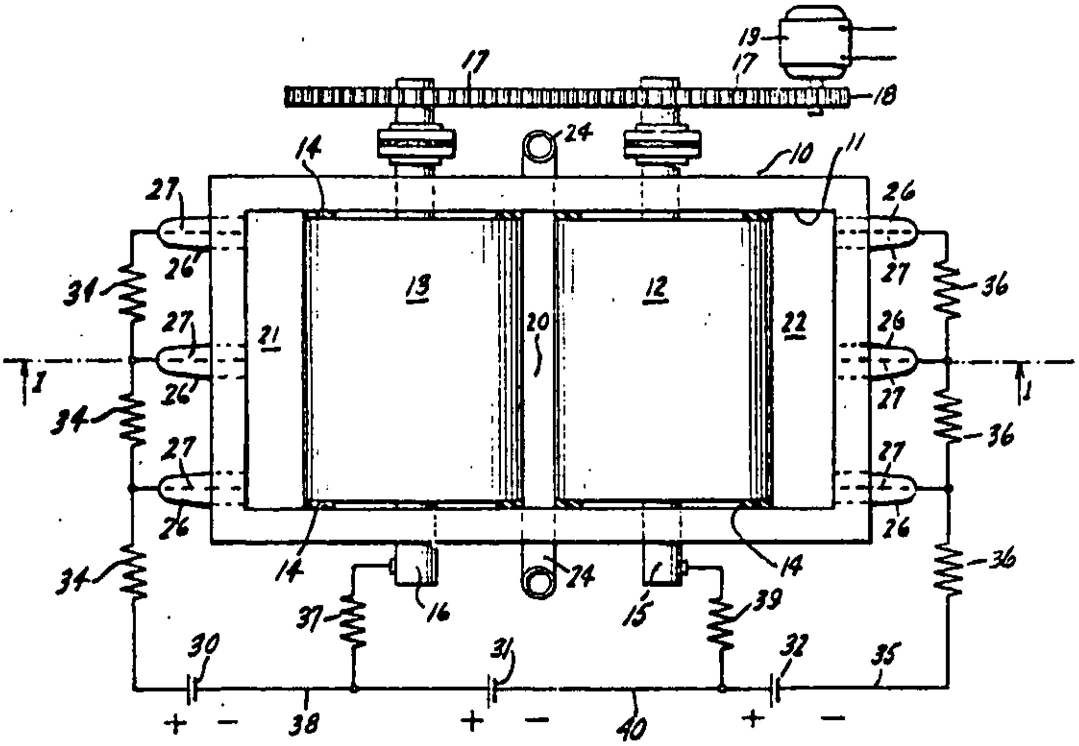
I
+
-

FIG. 6.24 PATENTED ROTATING CYLINDER ELECTRODE
for electrolysis of metallic solutions
(Lacroix, 1912)

a compartment
b rotating cylindrical cathode
c (perforated) insoluble anode
d inlet pipe
e (overflow) outlet pipe

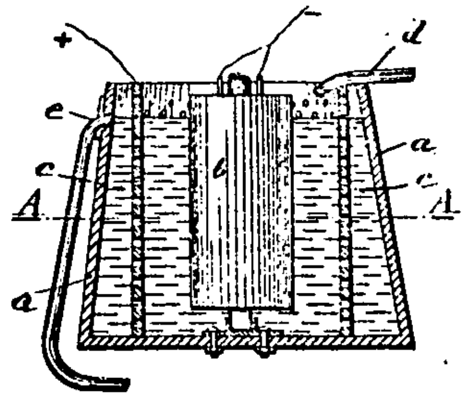
+
−
d
e
c
A
a
b
a
c
A
a

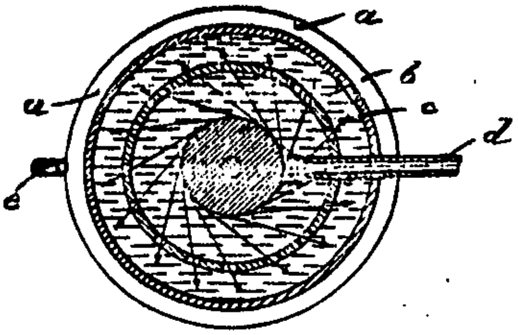
a
b
a
c
d
e

FIG. 6.25 PATENTED ROTATING CYLINDER ELECTRODE
for Electrodeposition of Iron
(Cowper-Coles, 1915)

a containing vessel
b pair of soluble or insoluble anodes
c rotating cylinder cathode
d propeller

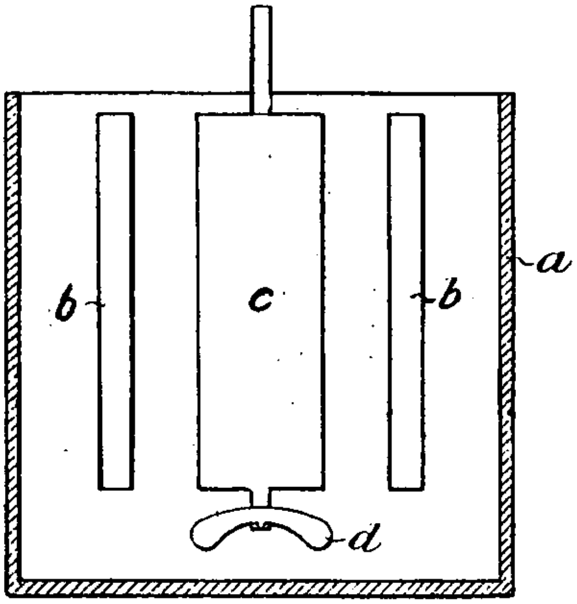
b
c
b
a
d

FIG. 6.26 PATENTED ROTATING CYLINDER ELECTRODE
for coating of metal articles
(Schaefer, 1945)

1. pump
2. inlet
3. rotating cylinder cathode
4. electrolyte chamber
5. silver rode anodes
6. drive motor
7. gear
8. gear
9. slip ring
10. power brush
11. vessel
12. return to pump
13. cell top
14. workpiece rack
15. electrolyte
16. upper portion of tank
17. shaft
18. shaft

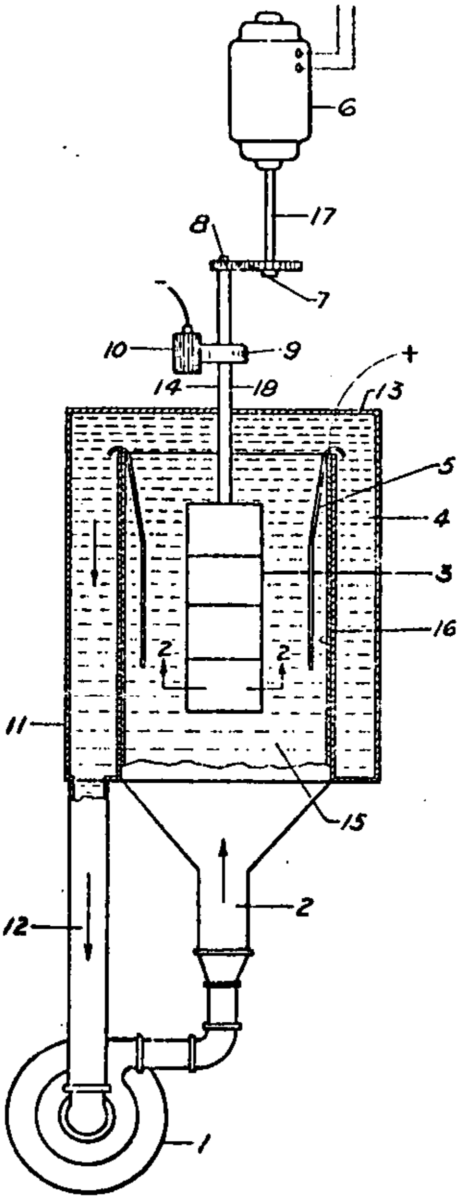
-
+

FIG. 6.27 PATENTED ROTATING CYLINDER ELECTRODE
for metal winning from ores
(Campbell et al., 1974)

16. hollow cylindrical cathode (rotating)
17. crushed ore
18. electrolyte
19. anode rod (rotating)
20. insulating closure (removeable)
21. charging and discharging pipe

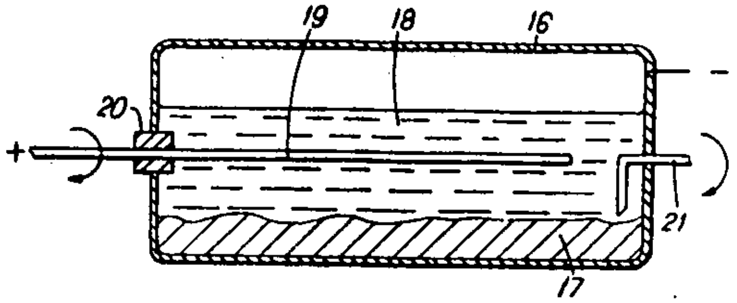
+

FIG. 6.28 PATENTED ROTATING CYLINDER ELECTRODE

for recovering silver from photographic solutions

(Fulweiler, 1971)

10. cell
11. tank
12. bridge
14. rotating cylinder cathode
15. graphite plate anodes (6)
16. shaft
17. nylon bearing
20. impeller
21. impeller carrying plate
22. fasteners
24. vertical baffles

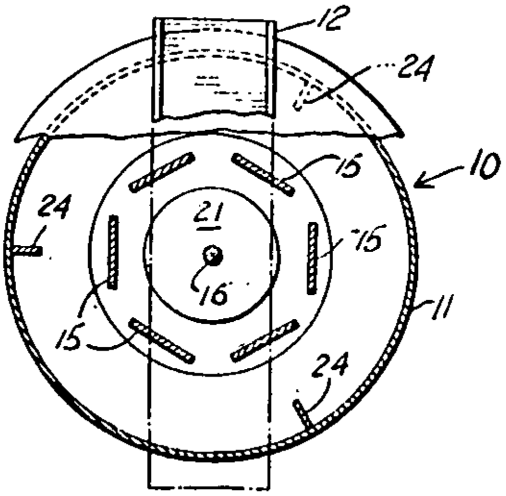

a)

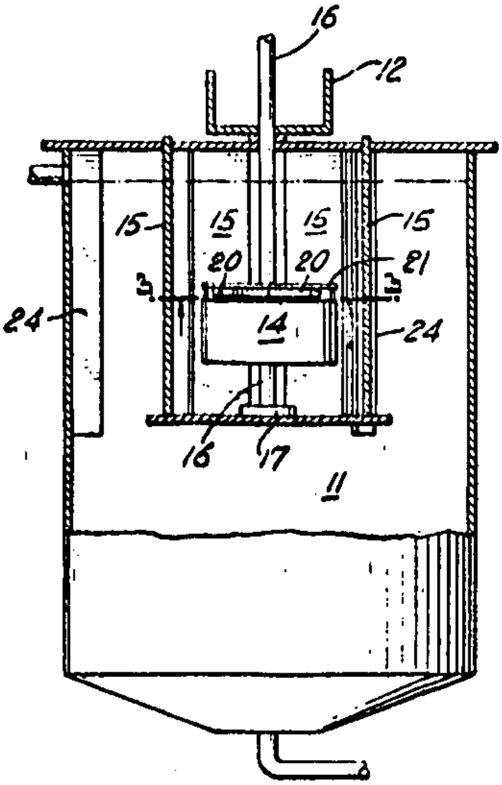

b)

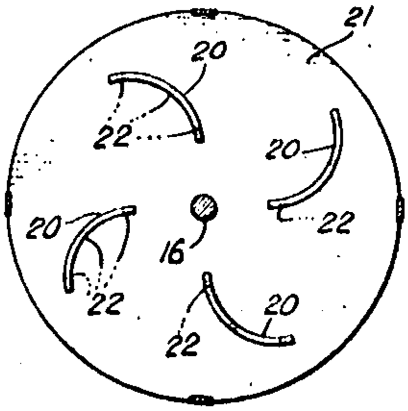

c)

FIG. 6.29 PATENTED ROTATING CYLINDER ELECTRODE
for recovering silver from photographic solutions
(Fisher, 1972)

10. electrical control unit
11. polyethylene drum
12. frame
13. rotating cylindrical cathode
14. carbon rod anodes

20. stainless steel surface (smooth)
21. cross braces
22. bearings
23. impeller
24. leading edge
25. trailing edge
26. downward flow of electrolyte
27. direction of rotation

30-33. impeller fins
34. fluid opening
35. base

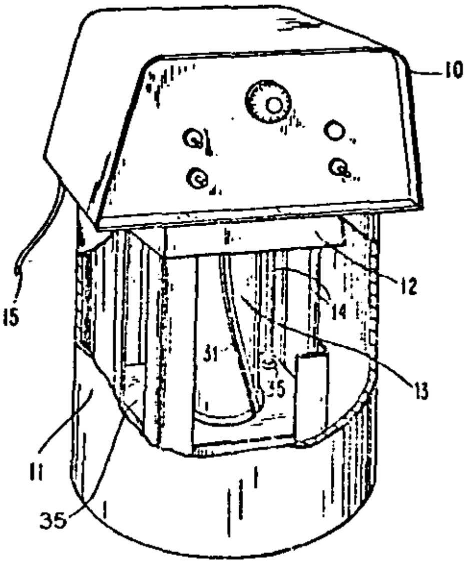

a)

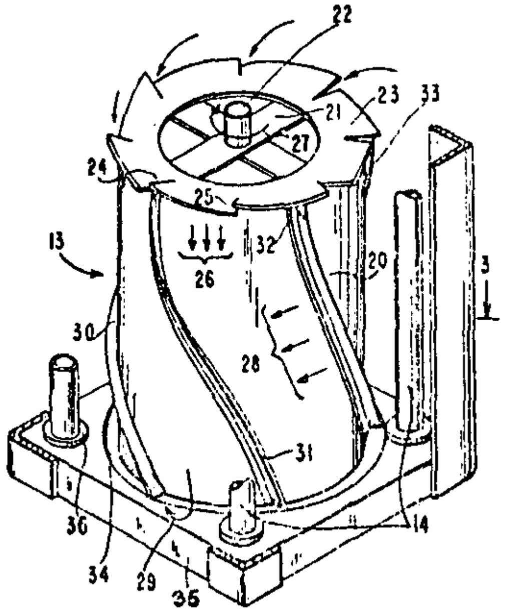

b)

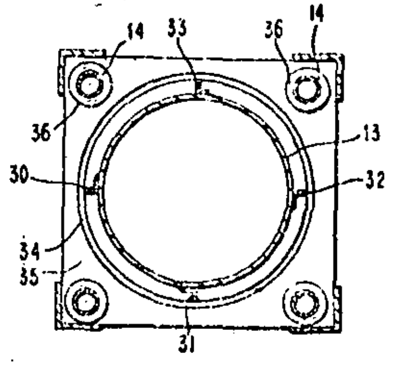

c)

FIG. 6.30 PATENTED ROTATING CYLINDER ELECTRODE

for metal recovery

(Goold et al., 1975)

2.

11. octagonal tank

12. plastic coating

13. insoluble anode

14. conductor

16. insulating lining

17. shaft

18. bearings

19. lever arm

21. lever

22. pitman wheel

23. geared motor

24. oscillating cathode

26. cathode frame members

27. cathode supports

28. metal sheets

29. cathode - shaft conductor

30. slots

31. commutator

32. brush

33. fluid

34. overflow inlet outlet

36. drain valve

37. fins

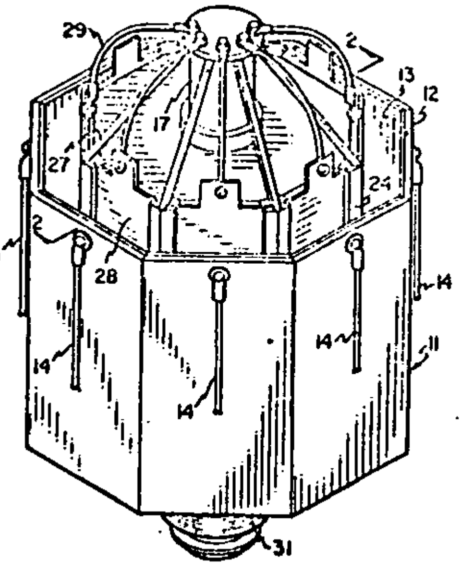

a)

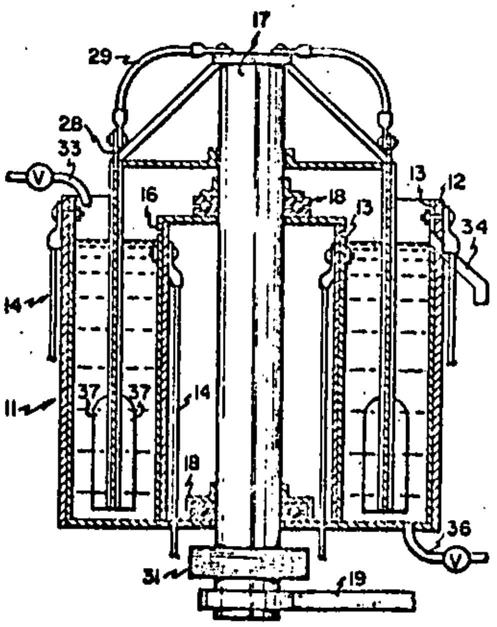
V
V

b)

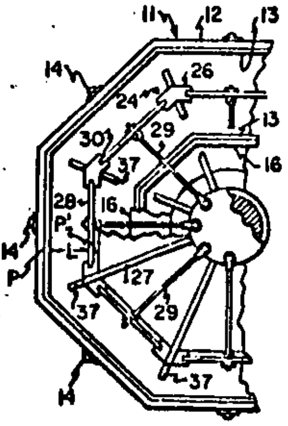
P'
L
P

c)

FIG. 6.31 PATENTED ROTATING CYLINDER ELECTRODE
for copper production
(Julien, 1925)

1. vessel
2. rotating cylindrical cathode
3. anode basket
4. copper particles or pieces
5. anode feeder plates
6. longitudinal braces
7. " "
8. slanting braces
9. upright support

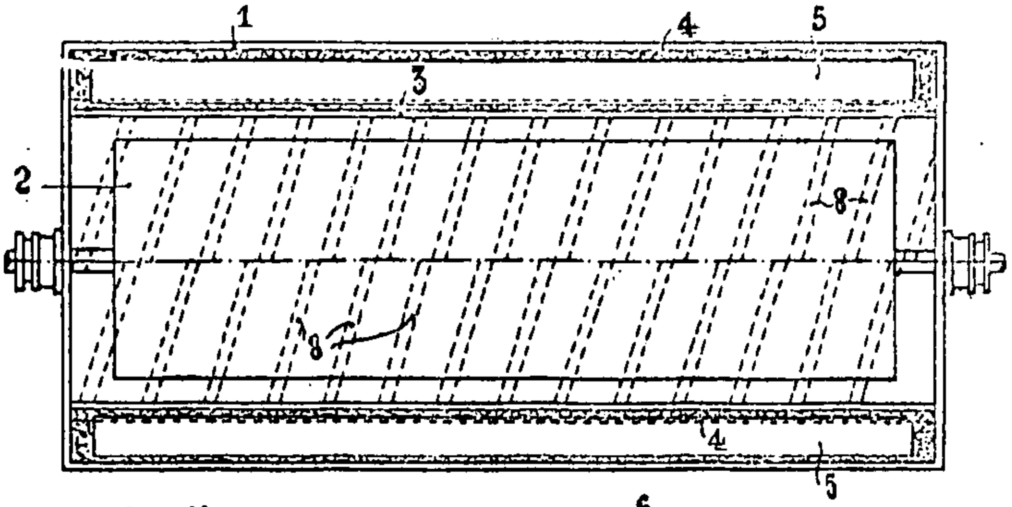

a)

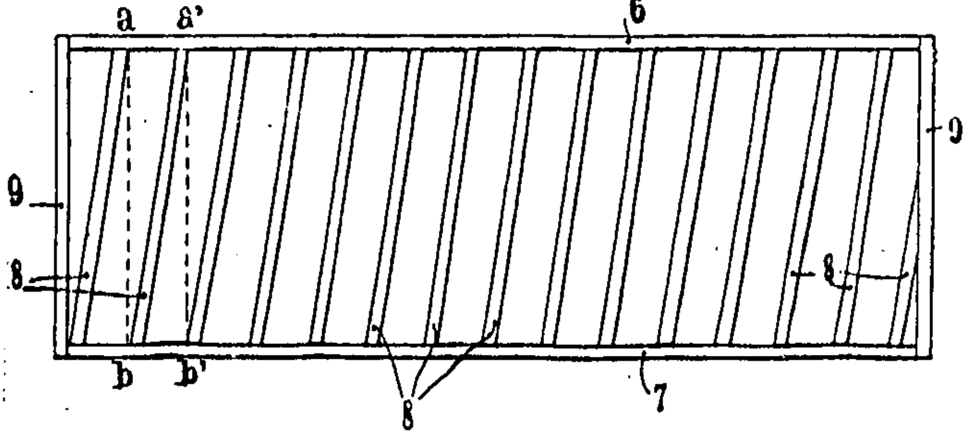
a
a'
6
9
9
8
8
b
b'
8
7

b)

FIG. 6.32 PATENTED ROTATING CYLINDER ELECTRODE
for metal recovery
(Cooley, 1970)

10.	rotating cylindrical anode
12.	shaft
14.	variable speed motor
16.	bench
17.	opening in bench
18.	framework
20.	support for shaft
22.	flexible sheet cathode
24.	rod clamp
30.	anode feeder
32.	cathode feeder
34.	power supply source
36.	tank
38.	solution
40.	pipe
42.	pipe
44.	constant discharge pump
46.	coating hopper
47.	thin layer of plated metal
48.	scraper (rubber)
49.	solution stream

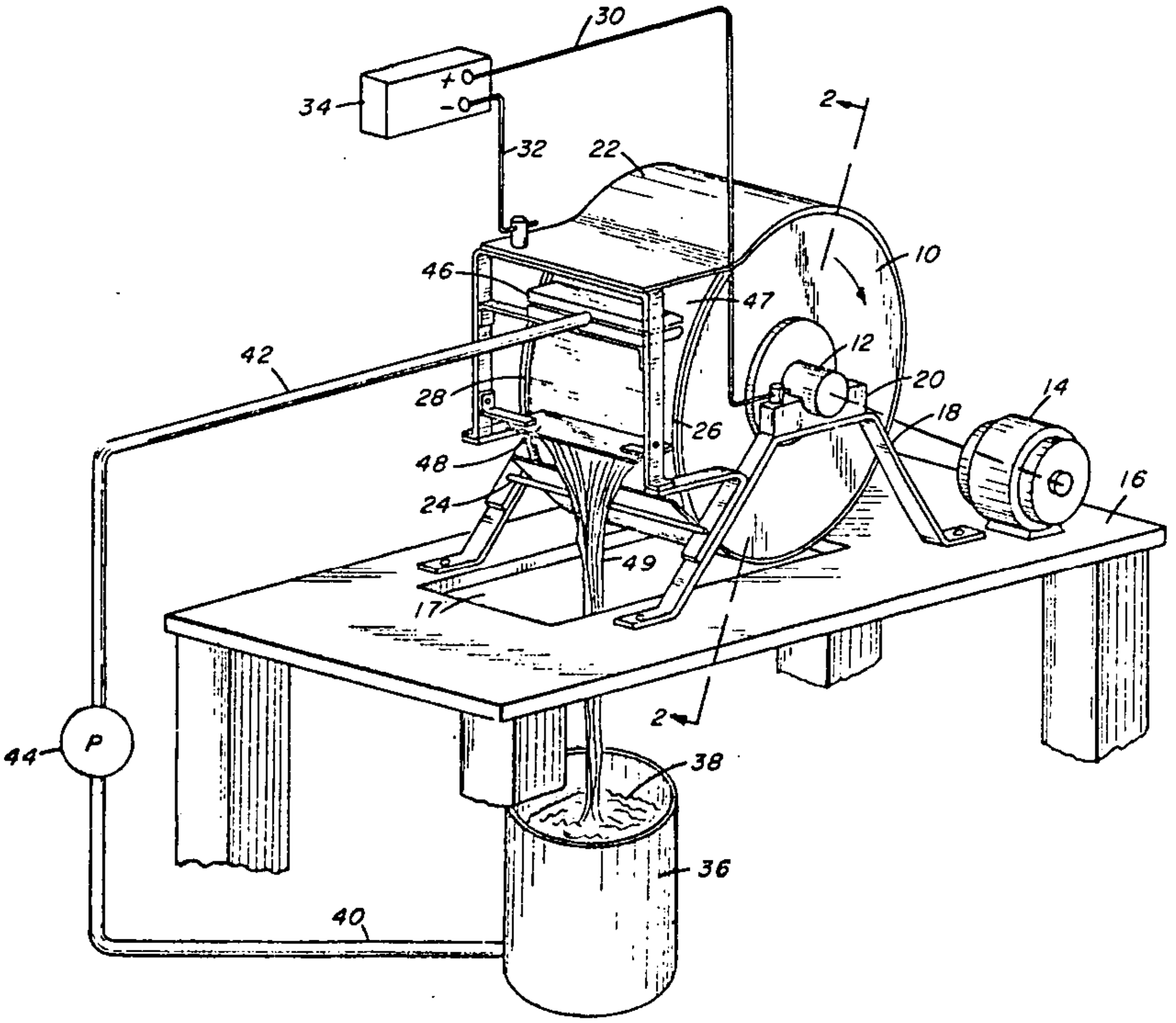
+
−
P

FIG. 6.33 PATENTED ROTATING CYLINDER ELECTRODE

for metal recovery

(Arigo Pini S.p.A., 1966)

1. outer wall of vat
2. inner wall of vat
3. recesses
4. collecting sump
5. sloping floor of vat
6. cylindrical cathode plate
7. " " "
8. cathode bridge connector
9. supporting spider
10. drive shaft
11. electric motor
12. belt drive
13. electrically conducting ring (anode feeder)
14. support for anodes
15. anodes
16. doctor blades

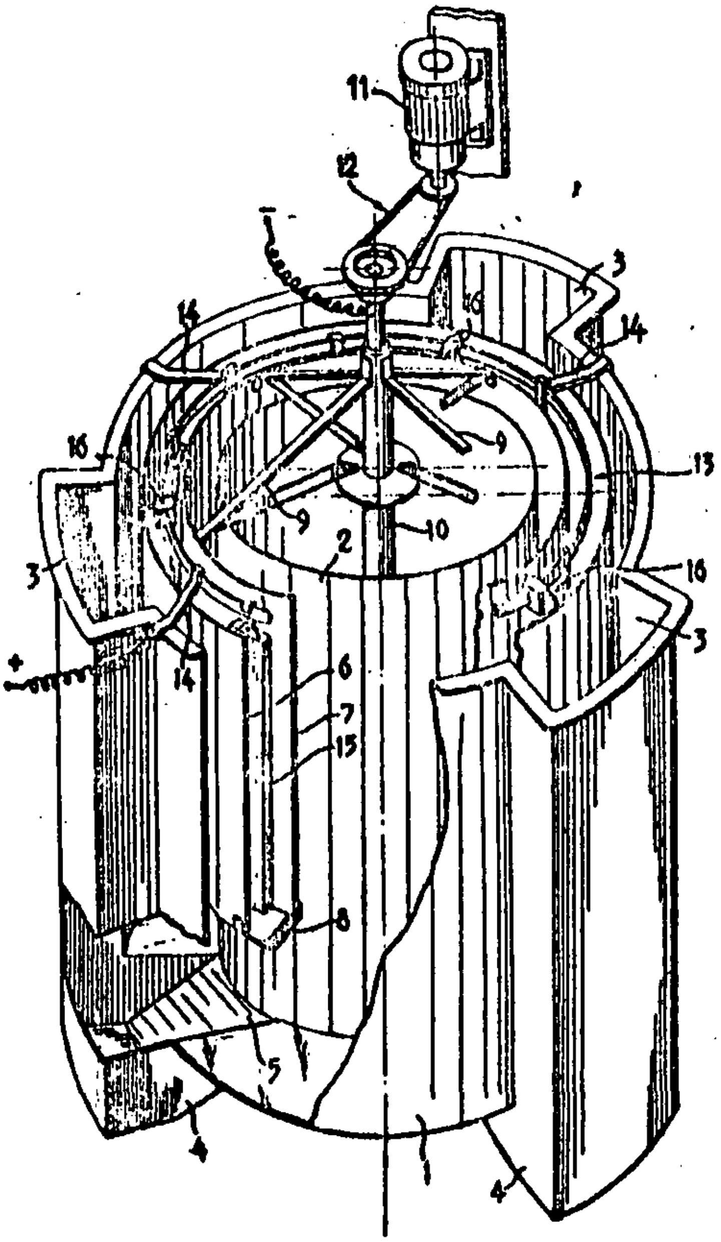
−
+

FIG. 6.34 PATENTED ROTATING CYLINDER ELECTRODE for cupro-lead powder production
(Societe Industrielle des Coussinets, 1961)

a) sectional elevation of the electrolysis tank
b) " " " " whole apparatus

a copper rod anode feeder
b plastic sheath for (a)
d cathode surface

A inner, electrolyte tank
B outer, cooling tank
C anode
R scraper trough
U trough for copper and lead scrap

M disintegrator
E centrifuge
F conduits
D receiver
G valved branch conduit

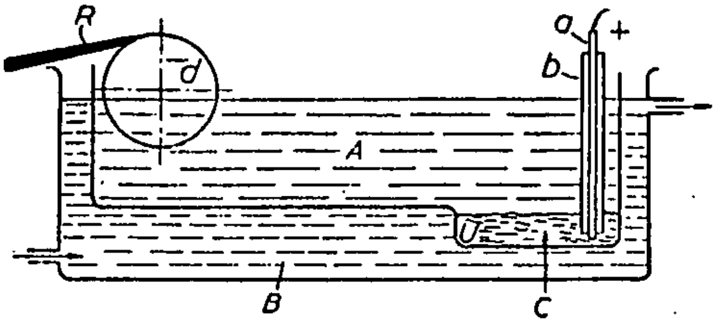

a)

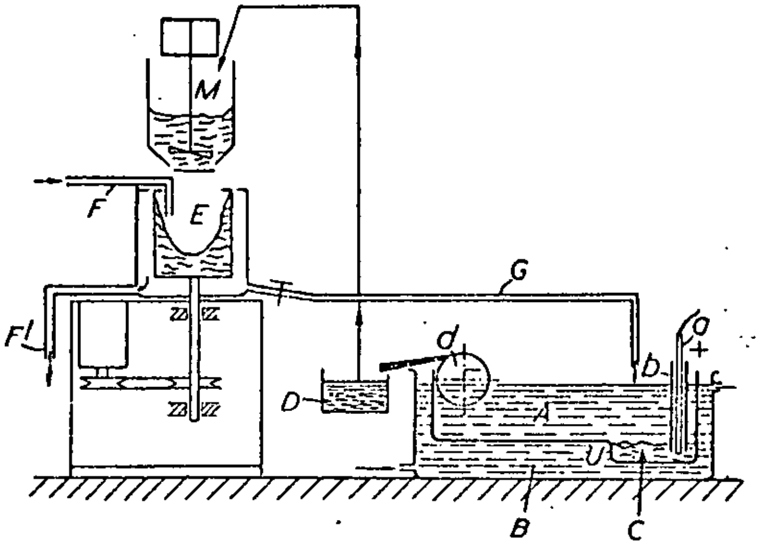
M
F
E
G
F
d
a
+
b
c
D
A
U
B
C

b)

FIG. 6.35 PATENTED ROTATING CYLINDER ELECTRODE for metal recovery (Prunet and Guillen, 1962)

a)

1. vessel/anode
2. anode connection
3. rotating cylinder cathode
4. drive shaft (insulating)
5. insulating end cap
6. scraper trough
7. cathode connection

b)

8. rotating cylinder anode
9. cell body/cathode
10. R.C.E. drive shaft

11.)
) scrapers
12.)
)
13.)

14. settling cone

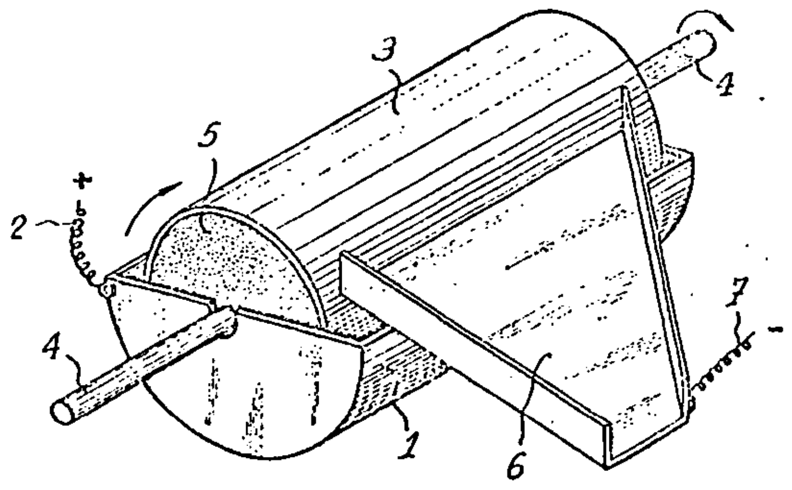

a)

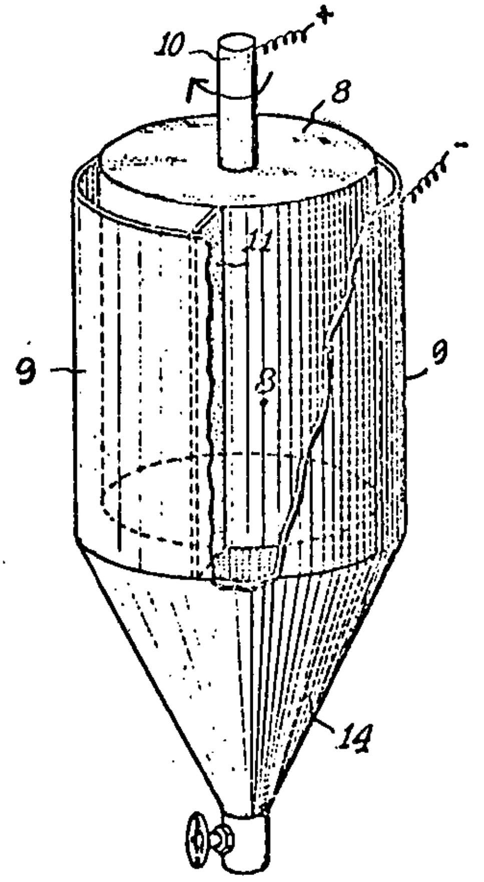
10
+
8
-
11
9
3
9
14

b)

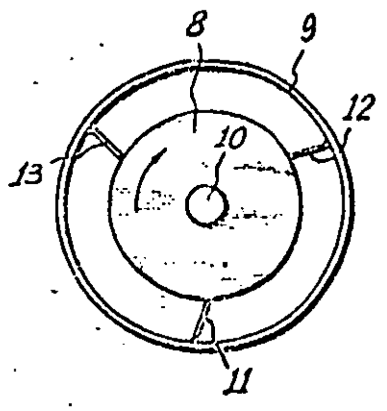
8
9
12
10
13
11

c)

FIG. 6.36 PATENTED ROTATING CYLINDER ELECTRODE for copper recovery from its ores (Gordy, 1970)

1. tank
2. anode chamber
3. anode
4. anode feeder
5. anode connection
6. anode chamber outlet
10. rotating cylinder cathode
11. drive shaft
12. scraper member
13. mounting for 12
14. tensioning spring
15. cathode connection
20. ore/electrolyte slurry hopper
21. catholyte inlet
22. catholyte

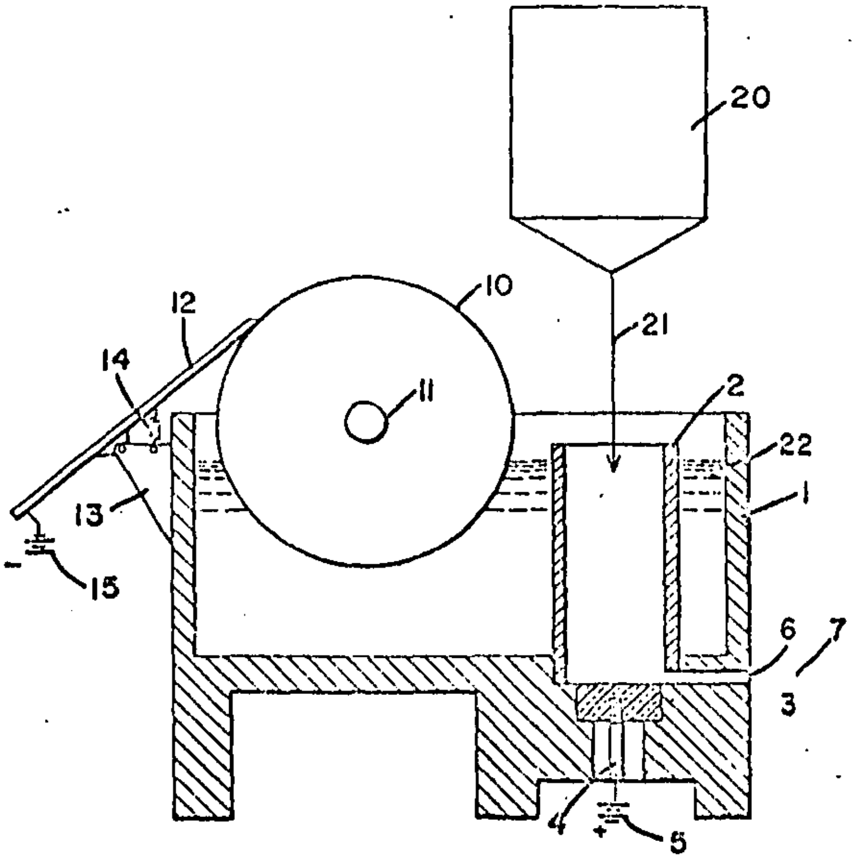
−
+

FIG. 6.37 PATENTED ROTATING CYLINDER ELECTRODE for the production of zinc dust
(Johnson, 1939)

1. vessel
2. inner cover
3. hollow shaft
4. rotating cylinder cathode
5. slip ring
6. cathode connecting rods
7. cooling medium inlet
8. " " outlet
9. " " groove
10. outer cover
11. anode aggregate
12. copper ring anode feeder
13. scrapers (rubber) secured to anodes
14. electrolyte inlet
15. " outlet
16. " " (optional)

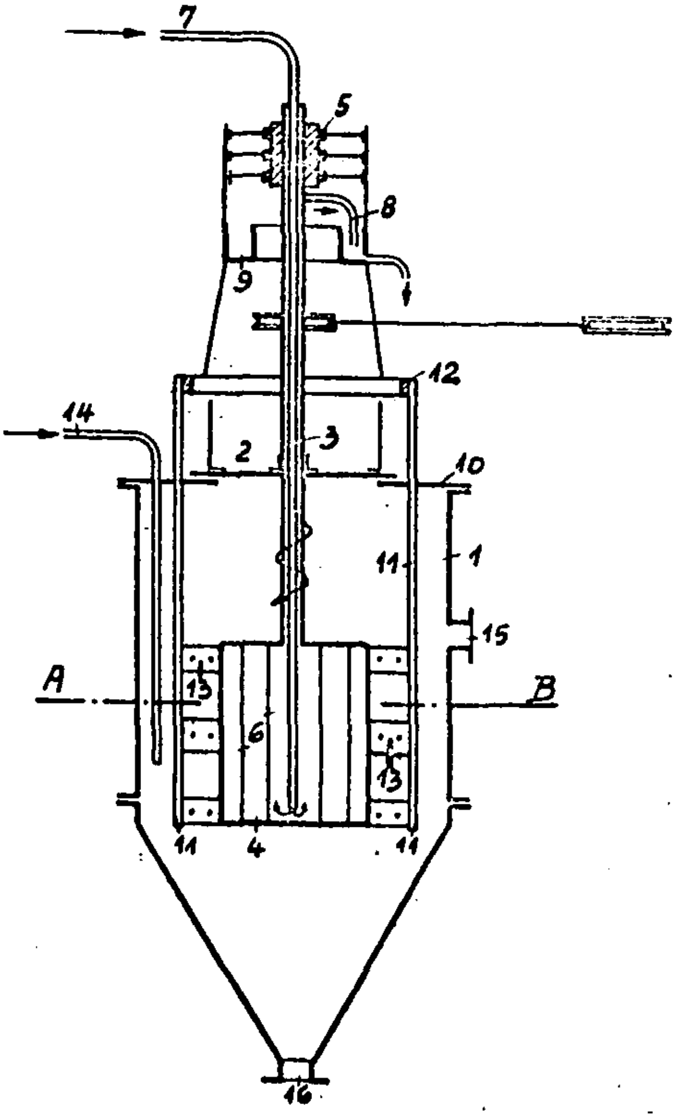
7
5
8
9
12
14
2
3
10
11
1
15
A
B
13
6
13
11
4
11
16

a)

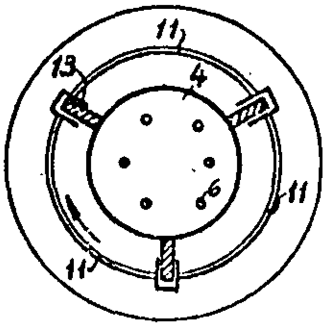
11
13
4
6
11
11

b)

FIG. 6.38 PATENTED ROTATING CYLINDER ELECTRODE for deposition of metals
(Cleave, 1925)

A. earthenware jar
C. anode plates
D. rotary cathode
E. drive shaft
F. scraper

For the meaning of other symbols, see the cited patent.

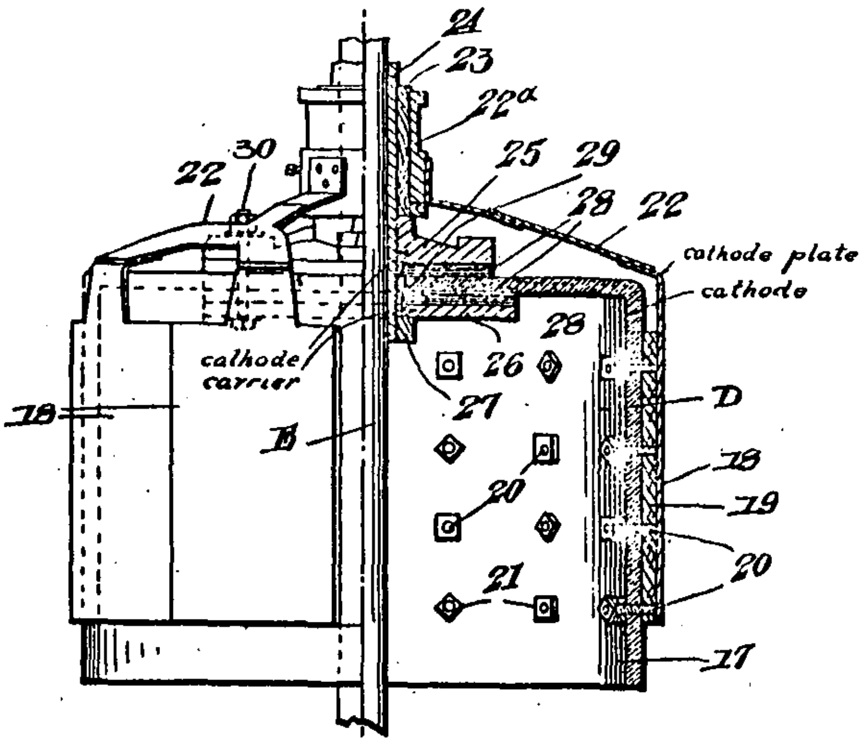
cathode plate
cathode
cathode carrier
E
D

a)

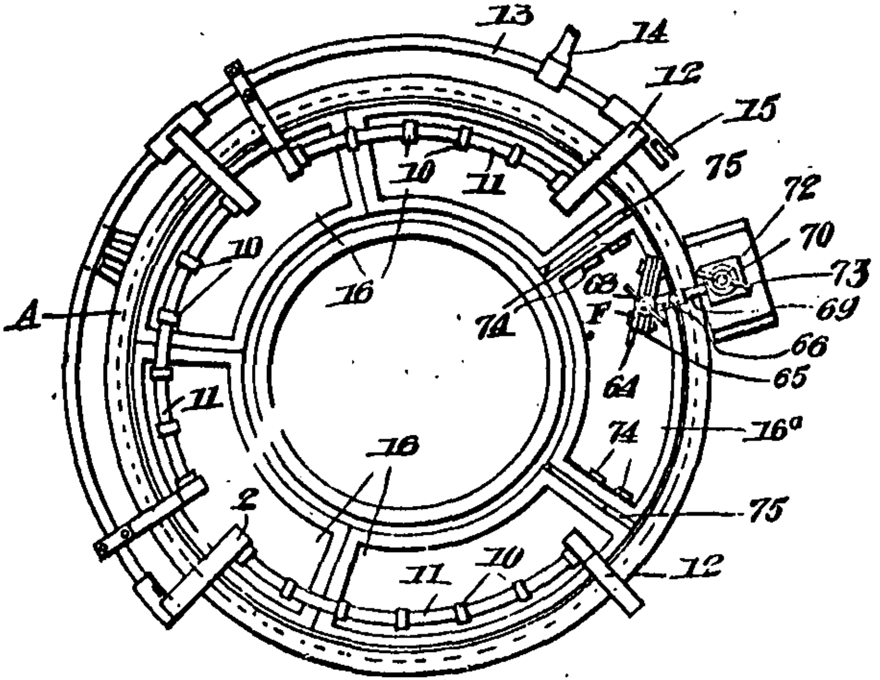
F
A

b)

FIG. 6.39 PATENTED ROTATING CYLINDER ELECTRODE for producing nickel flakes (Nordblom, 1968)

21. rotating cylinder cathode
22. non-conducting grid
23. electrolyte
24. anode
25. electrolyte jet (for metal removal)
26. pump
27. electrolyte jet (for gas removal)

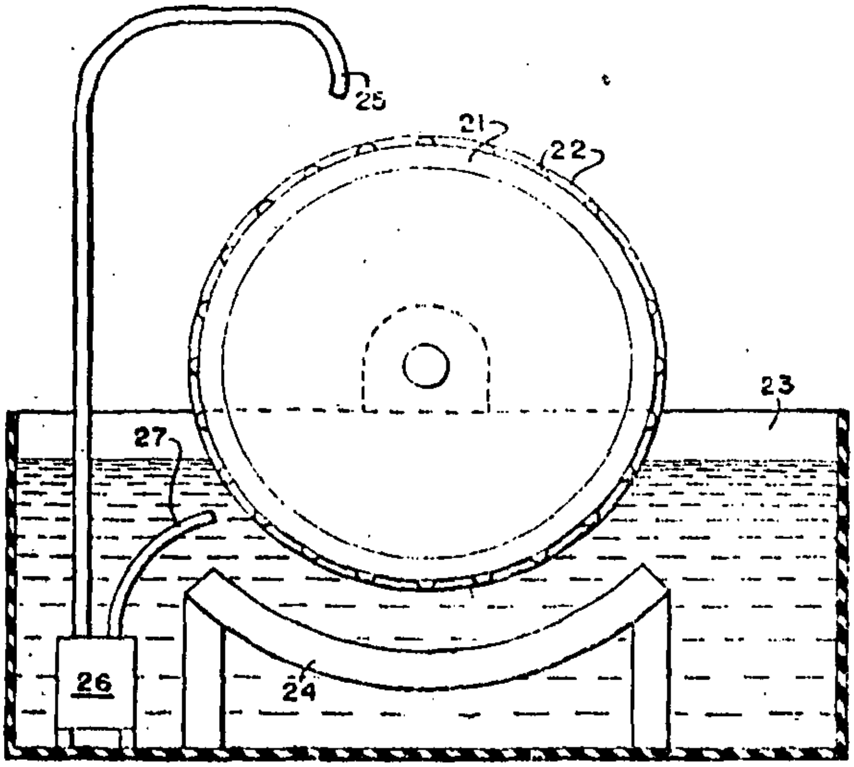

FIG. 6.40 PATENTED 'ECO-CELL' for recovery and production of metal as powder (Holland, 1977)

10. rotating cylinder cathode
13 anolyte inlet
14. anolyte outlet
15. catholyte inlet
16. catholyte outlet
17. " " (alternative)
18. scraper
19. gas vent

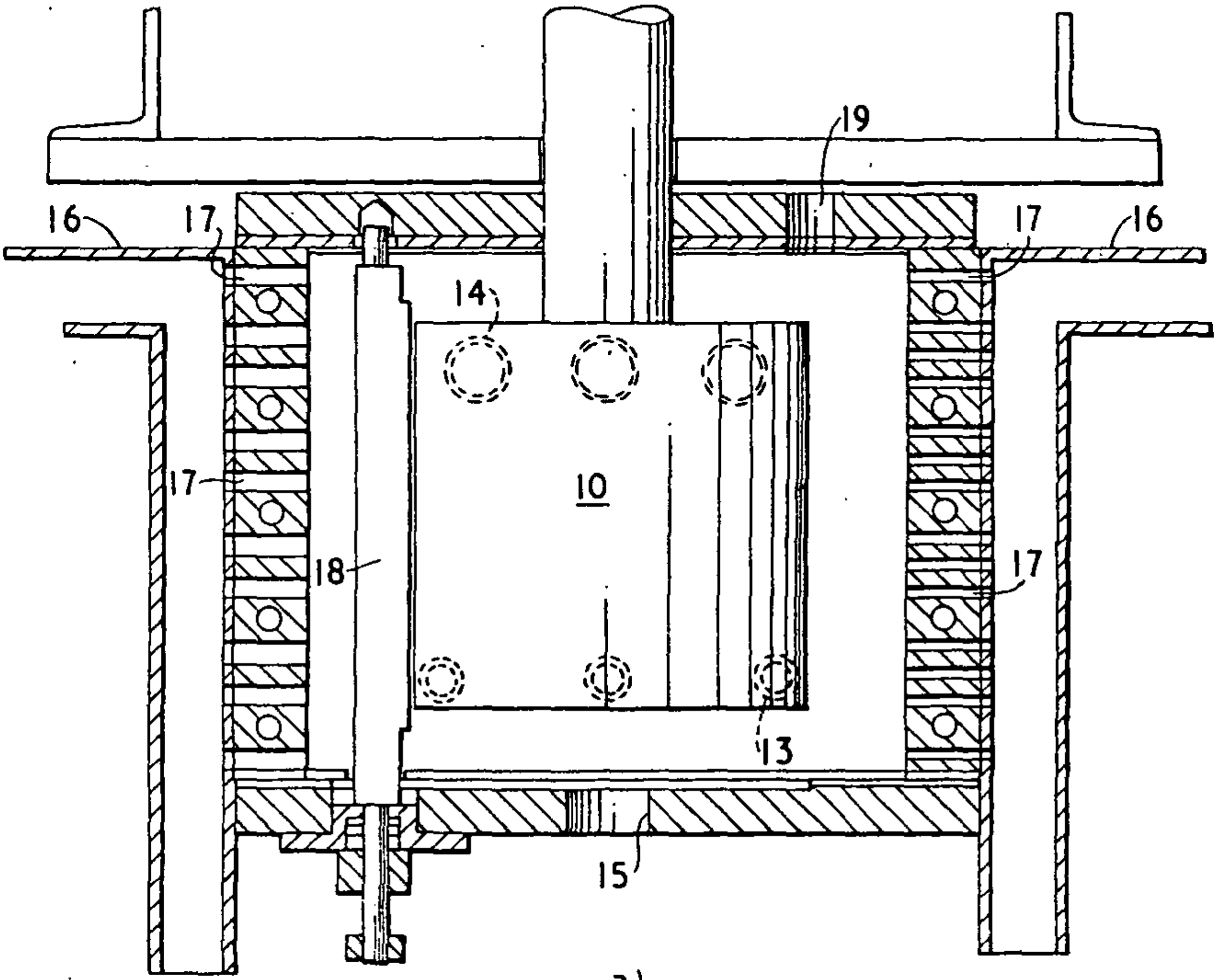

a)

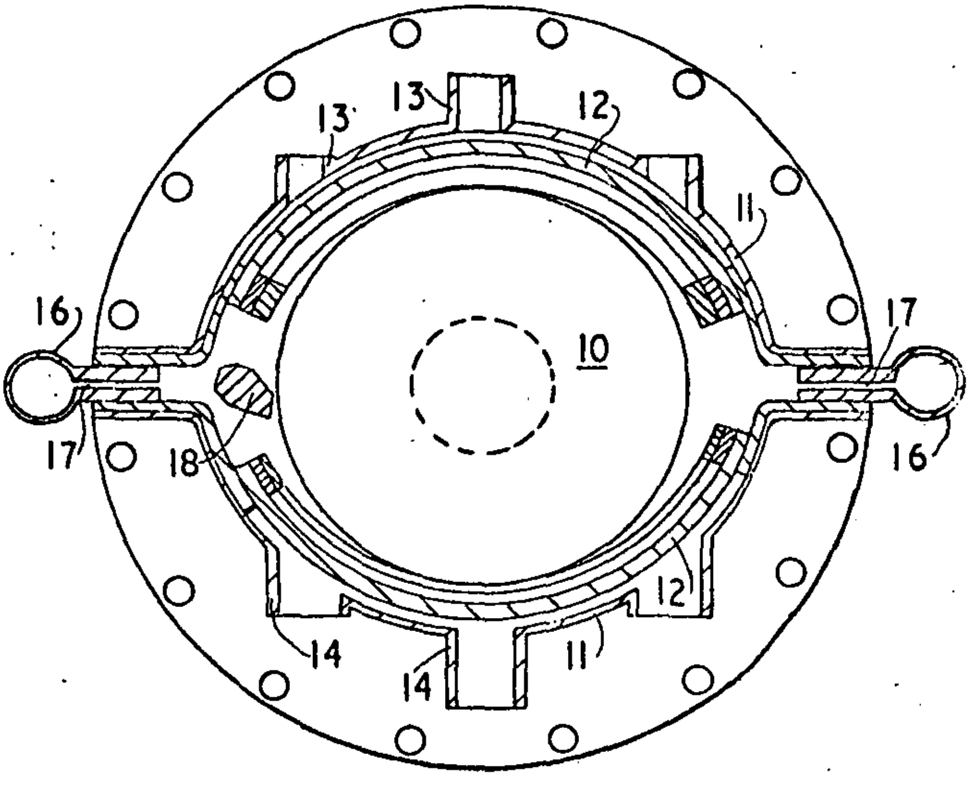

b)

FIG. 6.41 FLOW SCHEMATIC OF A TYPICAL'ECO-CELL' PROCESS

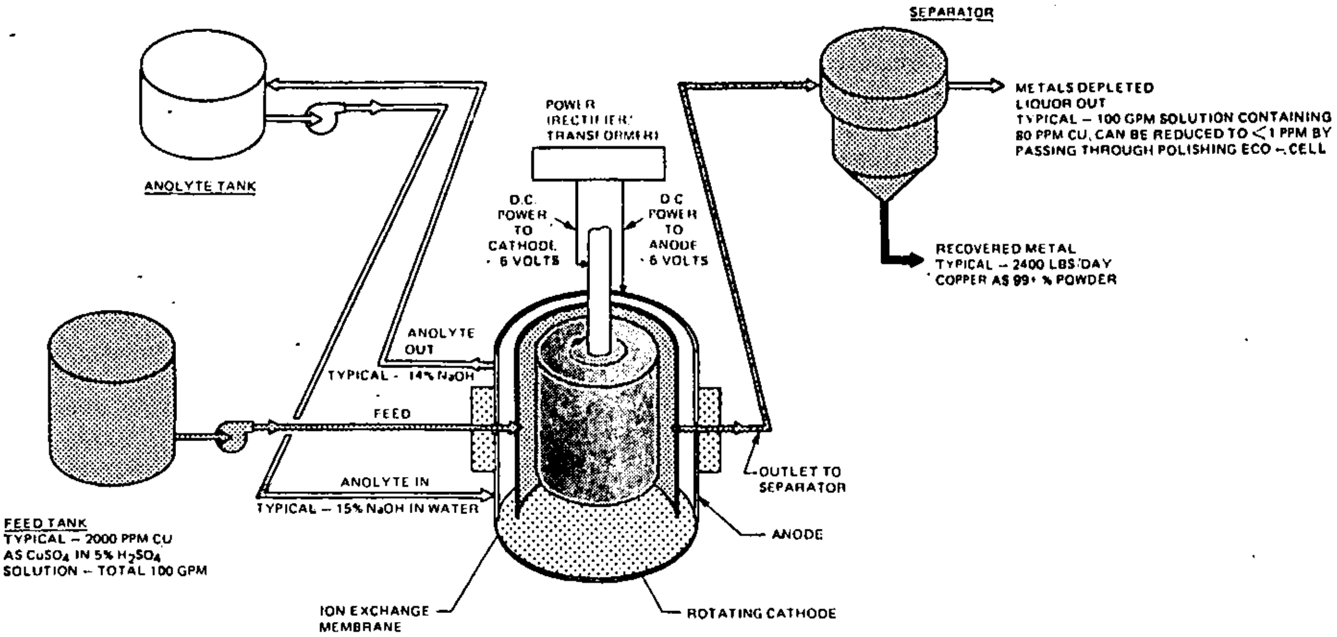
SEPARATOR
METALS DEPLETED
LIQUOR OUT
TYPICAL – 100 GPM SOLUTION CONTAINING
80 PPM CU, CAN BE REDUCED TO <1 PPM BY
PASSING THROUGH POLISHING ECO – CELL
RECOVERED METAL
TYPICAL – 2400 LBS/DAY
COPPER AS 99+ % POWDER
ANOLYTE TANK
POWER
(RECTIFIER/
TRANSFORMER)
D.C.
POWER
TO
CATHODE
- 6 VOLTS
D.C.
POWER
TO
ANODE
+ 6 VOLTS
ANOLYTE
OUT
TYPICAL – 14% NaOH
FEED
ANOLYTE IN
TYPICAL – 15% NaOH IN WATER
OUTLET TO
SEPARATOR
ANODE
FEED TANK
TYPICAL – 2000 PPM CU
AS CuSO4 IN 5% H2SO4
SOLUTION – TOTAL 100 GPM
ION EXCHANGE
MEMBRANE
ROTATING CATHODE

FIG. 6.42 A CASCADE OF R.C.E.R.'s IN HYDRAULIC SERIES

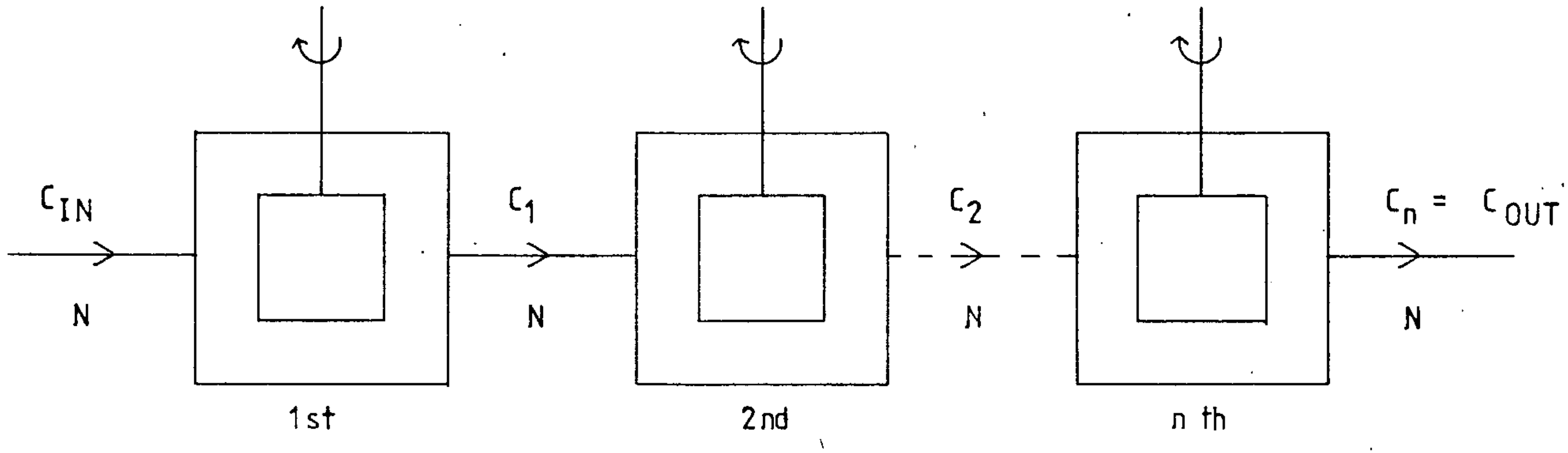
C_{IN}
N
1st
C_1
N
2nd
C_2
N
n th
$C_n = C_{OUT}$
N

FIG. 6.43 A SIX-ELEMENT 'CASCADE ECO-CELL'
(divided, with internal distribution
of current)

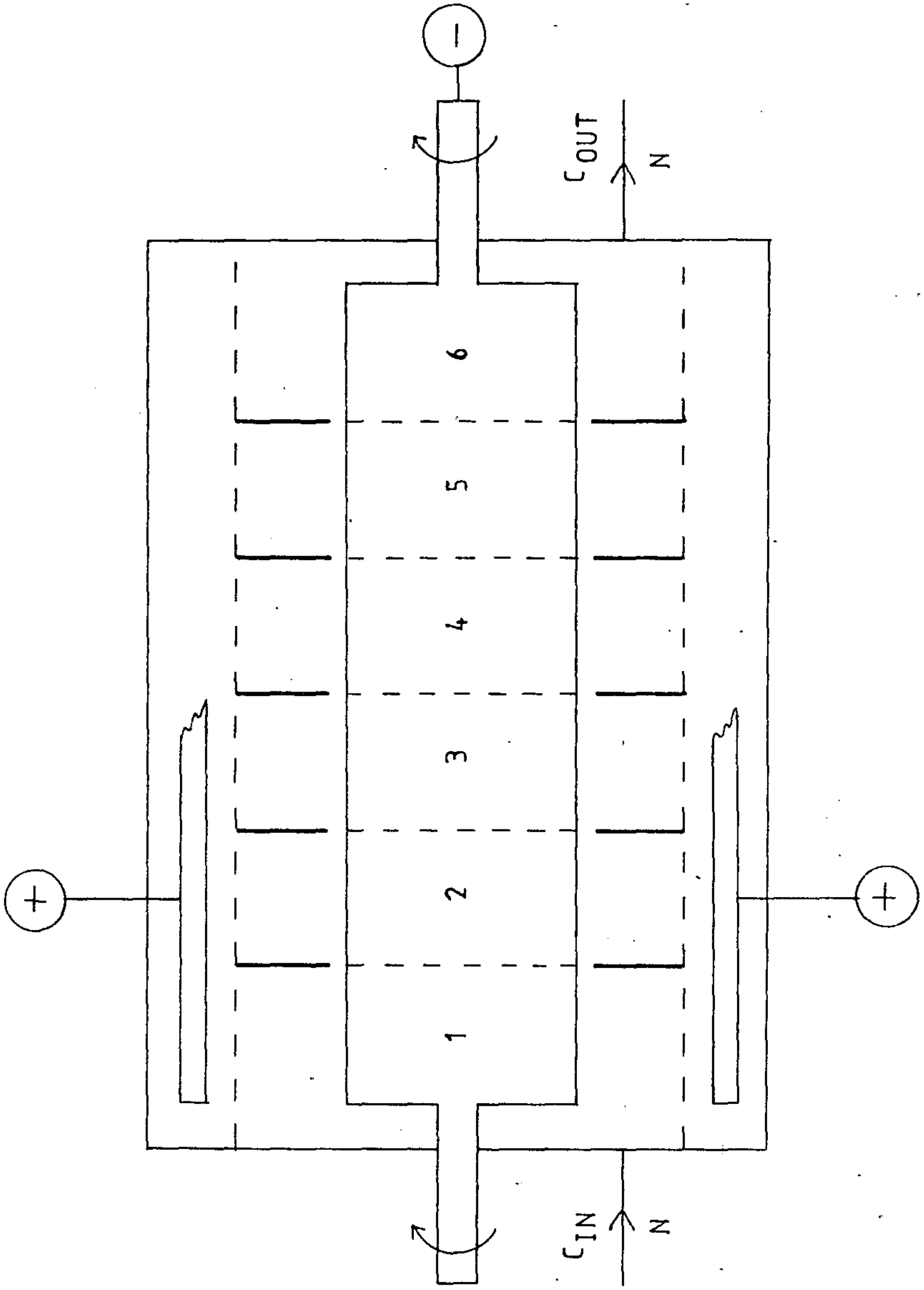
−
C_{OUT}
N
6
5
4
3
2
1
+
+
C_{IN}
N

FIG. 6.44 A SIX-ELEMENT 'CASCADE ECO-CELL'

(undivided with external resistive distribution of current)

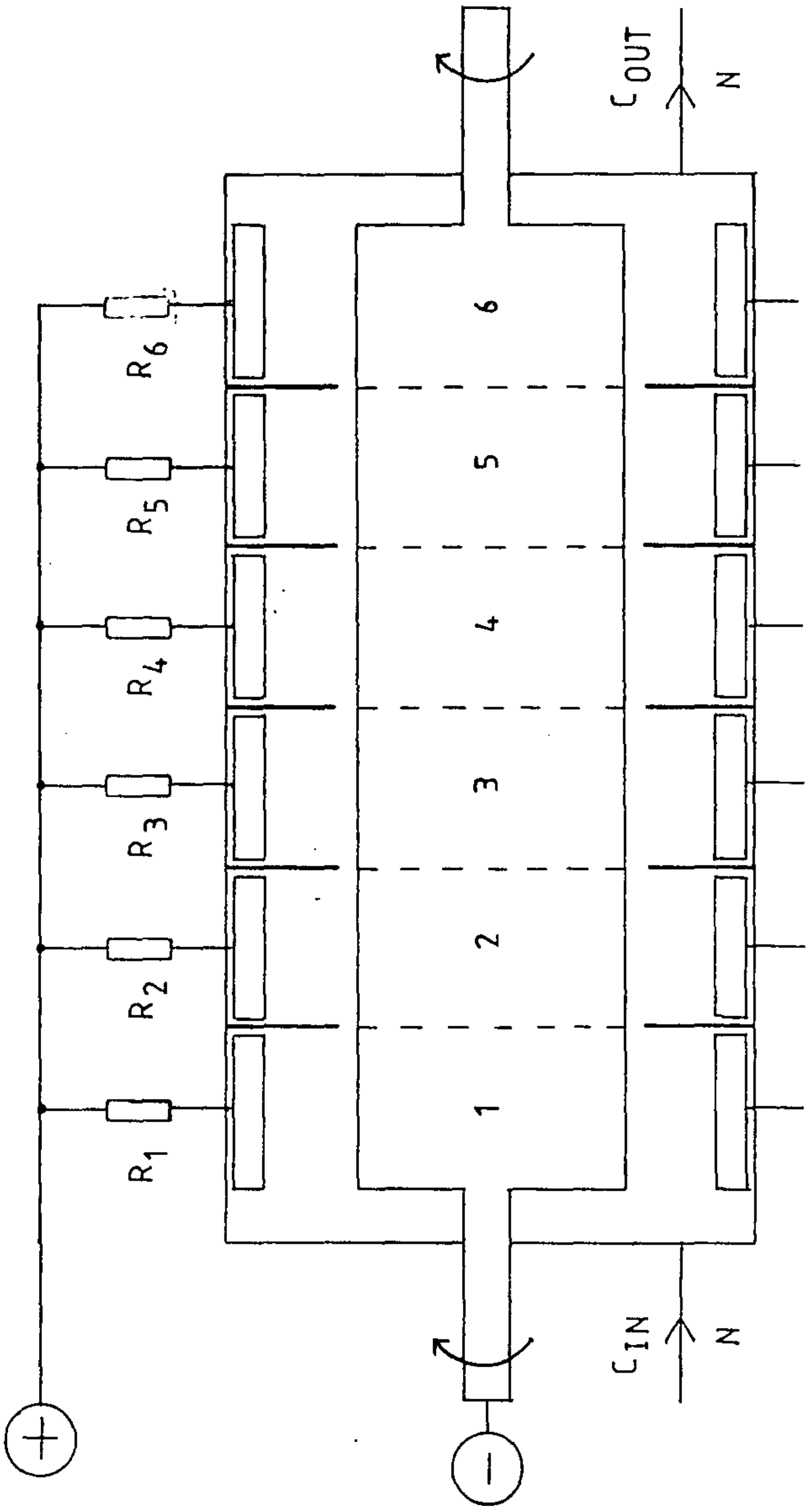
+
−
R1
R2
R3
R4
R5
R6
1
2
3
4
5
6
C_IN
N
C_OUT
N